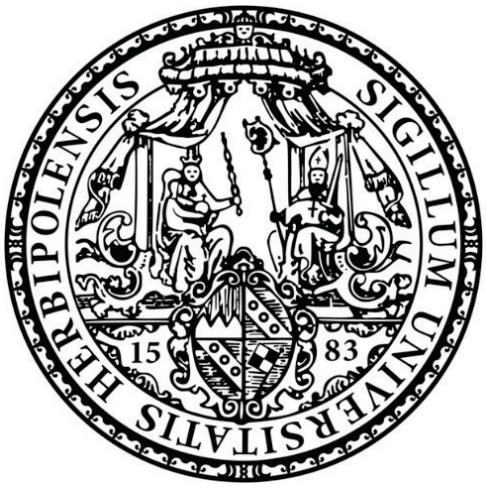

PRC1 serves as a microtubule-bundling protein and is a potential therapeutic target for lung cancer

PRC1 dient als ein Mikrotubuli-bündelndes Protein und ist ein potenzielles therapeutisches Target für Lungenkrebs

Doctoral thesis for a doctoral degree
at the Graduate School of Life Sciences,
Julius-Maximilians-Universität Würzburg,
Section Biomedicine
submitted by

Steffen Hanselmann

from

Schwäbisch Hall, Germany

Würzburg, 2021

Reverse page

Submitted on: ……..……..

Office stamp

Members of the *Promotionskomitee*:

Chairperson: Prof. Dr. Alexander Buchberger

Primary Supervisor: Prof. Dr. Stefan Gaubatz

Supervisor (Second): Prof. Dr. Svenja Meierjohann

Supervisor (Third): Dr. Markus Diefenbacher

Date of Public Defence: ……..……

Date of Receipt of Certificates: ……

Substantial parts of this thesis were published in the following article:

Steffen Hanselmann, Patrick Wolter, Jonas Malkmus and Stefan Gaubatz (2017): **The microtubule-associated protein PRC1 is a potential therapeutic target for lung cancer.** Oncotarget. 2017 Dec 22;9(4):4985-4997. doi: 10.18632/oncotarget.23577. eCollection 2018 Jan 12.

Table of Contents

Summary

Protein regulator of cytokinesis 1 (PRC1) is a microtubule-associated protein with essential roles in mitosis and cytokinesis. Furthermore, the protein is highly expressed in several cancer types which is correlated with aneuploidy and worse patient outcome. In this study it was investigated, whether PRC1 is a potential target for lung cancer as well as its possible nuclear role.

Elevated PRC1 expression was cell cycle-dependent with increasing levels from S-phase to G2/M-phase of the cell cycle. Thereby, PRC1 localized at the nucleus during interphase and at the central spindle and midbody during mitosis and cytokinesis. Genome-wide expression profiling by RNA sequencing of ectopically expressed PRC1 resulted in activation of the p53 pathway. A mutant version of PRC1, that is unable to enter the nucleus, induced the same gene sets as wildtype PRC1, suggesting that PRC1 has no nuclear-specific functions in lung cancer cells. Finally, PRC1 overexpression leads to proliferation defects, multi-nucleation, and enlargement of cells which was directly linked to microtubule-bundling within the cytoplasm.

For analysis of the requirement of PRC1 in lung cancer, different inducible cell lines were generated to deplete the protein by RNA interference (RNAi) *in vitro*. PRC1 depletion caused proliferation defects and cytokinesis failures with increased numbers of bi- and multi-nucleated cells compared to non-induced lung cancer cells. Importantly, effects in control cells were less severe as in lung cancer cells. Finally, p53 wildtype lung cancer cells became senescent, whereas p53 mutant cells became apoptotic upon PRC1 depletion. PRC1 is also required for tumorigenesis *in vivo*, which was shown by using a mouse model for non-small cell lung cancer driven by oncogenic K-RAS and loss of p53. Here, lung tumor area, tumor number, and high-grade tumors were significantly reduced in PRC1 depleted conditions by RNAi.

In this study, it is shown that PRC1 serves as a microtubule-bundling protein with essential roles in mitosis and cytokinesis. Expression of the protein needs to be tightly regulated to allow unperturbed proliferation of lung cancer cells. It is suggested that besides phosphorylation of PRC1, the nuclear localization might be a protective mechanism for the cells to prevent perinuclear microtubule-bundling. In conclusion, PRC1 could be a potential target of lung cancer as mono therapy or in combination with a chemotherapeutic agent, like cisplatin, which enhanced the negative effects on proliferation of lung cancer cells *in vitro*.

Zusammenfassung

Protein-Regulator der Zytokinese 1 (PRC1) ist ein Mikrotubuli-assoziierendes Protein mit wesentlicher Funktion bei der Mitose und Zytokinese. Die Expression des Proteins ist in verschiedenen Krebsarten stark erhöht, was mit Aneuploidie und schlechterer Lebenserwartung der Patienten korreliert. In dieser Untersuchung wurde erforscht, ob PRC1 ein potenzielles therapeutisches Target für die Behandlung von Lungenkrebs darstellt, sowie seine mögliche Zellkern-Funktion untersucht.

Die gesteigerte PRC1-Expression war Zellzyklus-abhängig, mit ansteigendem Expressionslevel von der S-Phase bis zur G2/M-Phase des Zellzyklus. Hierbei ist PRC1 während der Interphase im Zellkern lokalisiert und während der Mitose und Zytokinese an der zentralen Spindel und dem Mittelkörper lokalisiert. Genomweite Expressionsanalysen durch RNA-Sequenzierung nach ektopischer PRC1-Expression resultierte in einer Aktivierung des p53-Signalweges. Eine mutierte Version von PRC1, die nicht imstande ist in den Zellkern zu gelangen, hat dieselbe Gen-Zusammenstellung wie das Wildtyp-PRC1 induziert. Dies deutet auf keine Kern-spezifische Funktion von PRC1 im Lungenkrebs hin. Schlussendlich führt die Überexpression von PRC1 zu Proliferationsdefekten, mehreren Zellkernen und Vergrößerung der Zellen, was im direkten Zusammenhang mit der Mikrotubuli-Bündelung im Zytoplasma steht.

Zur Analyse des Bedarfs von PRC1 im Lungenkrebs wurden verschiedene induzierbare Zelllinien hergestellt, um die Expression des Proteins durch RNA-Interferenz (RNAi) im Zellkultursystem vermindern zu können. Die PRC1-Depletion durch RNAi führte bei Lungenkrebszellen zu Proliferationsdefekten und Zytokinese-Fehlern. Im Vergleich zu nicht-induzierten Lungenkrebszellen zeigte sich ein Anstieg von multinuklearen Zellen. Wichtig war hier, dass Effekte in Kontrollzellen weniger stark waren als in Lungenkrebszellen. Außerdem hat sich gezeigt, dass nach PRC1-Depletion, p53-Wildtyp Lungenkrebszellen seneszent und p53-mutierte Zellen apoptotisch wurden. PRC1 wird auch für die Tumorentstehung *in vivo* bei einem Mausmodell von nichtkleinzelligem Lungenkrebs, das durch Onkogenes K-RAS und Verlust von p53 getrieben ist, benötigt. Hierbei zeigte sich eine signifikante Reduzierung der Lungentumorfläche, Anzahl der Tumore und hochgradige Tumore durch Depletion von PRC1 durch RNAi.

In dieser Arbeit konnte gezeigt werden, dass PRC1 eine wichtige Funktion als Mikrotubuli-bündelndes Protein in der Mitose und Zytokinese hat. Die Expression des Proteins muss genau kontrolliert werden, um eine ungestörte Proliferation von Lungekrebszellen aufrecht zu erhalten. Es wird vorgeschlagen, dass neben der Phosphorylierung von PRC1, die Kern-Lokalisation ein Schutzmechanismus der Zellen vor perinukleärer Mikrotubuli-Bündelung darstellt. Schlussendlich könnte PRC1 ein potentielles therapeutisches Target für

Lungenkrebs sein, sowohl als Monotherapie oder auch in Kombination mit chemotherapeutischen Wirkstoffen, wie beispielsweise Cisplatin, was einen zusätzlichen negativen Effekt auf das Zellwachstum im Zellkultur System zeigte.

1 Introduction

1.1 Lung cancer

1.1.1 Lung cancer subtypes, incidence and survival rate

Lung cancer can be subdivided in non-small cell lung cancer (NSCLC), which are approximately up to 85% of all cases, and small cell lung cancer (SCLC), which makes up 15% of all cases. Further NSCLC subtypes are adenocarcinoma (~40%), squamous cell carcinoma (~25% to 30%) and large cell carcinoma (~10% to 15%) (Fig.1). Each subtype evolves from different types of lung cells. Adenocarcinomas starts in secretory cells and is usually found in outer parts of the lung. Squamous cell carcinoma evolves from squamous cells, which are flat cells that line the inside of the airways in the lungs. Large cell carcinoma can appear in any part of the lung and is suggested to grow and spread quickly (Niederhuber et al., 2013)

Lung cancer is one of the deadliest and most common type of cancer worldwide, with an estimate of more than 1.5 million deaths each year (Siegel et al., 2017, 2018). Also, the disease is still one of the leading causes accounting for cancer deaths in the United States with predicted 235,760 new cases in 2021 (American Cancer Society. Cancer Facts & Figures 2021). Lung cancer has the second highest prediction for new cases (13%) but the highest prediction for cancer deaths for both men (24%) and women (23%) of the top ten leading cancers in the United states (Siegel et al., 2019).

Even though improvements were made, the 5-year survival rate is still less than 20% (Siegel et al., 2019). The SEER database, which is maintained by the National Cancer Institute (NCI), tracks 5-year relative survival rates for NSCLC in the United States based on how far the cancer has spread. Localized cancer that has not spread out of the lungs shows a survival rate of 60%. NSCLC which has invaded regional and nearby structures or lymph nodes has a survival rate of 33%. Finally, lung cancer which has spread to distant parts of the body has a survival rate of 6% (Noone et al., 2018).

1.1.2 Oncogenic KRAS in lung cancer

Carcinogenic Kirsten rat sarcoma viral oncogene homolog (KRAS) mutations are found in approximately 30% of lung adenocarcinoma in western countries and thus is the most frequent driver mutation of this subtype (Dearden et al., 2013; Fig.1). It was found that KRAS mutations occur predominantly at codon 12 (>80%) and 13. The most common mutation variant at codon 12 of KRAS are G12C (~39%), G12V (18–21%) and G12D (17–18%) in NSCLC (Dogan et al., 2012; El Osta et al., 2017).

KRAS is a member of the human RAS gene family which encodes for GTPase membrane-bound proteins. The protein can switch between a GDP bound inactive state and a GTP bound active state upon extracellular stimuli. When active, GTP-RAS can transduce signals by interacting with downstream effectors which activate several signaling pathways (Barbacid, 1987; Malumbres & Barbacid, 2003). The switch is regulated by guanine nucleotide exchange factors (GEFs) and GTPase activating proteins (GAPs). RAS activation is enhanced by GEFs which leads to a replacement of GDP with GTP. Otherwise, GAPs increase the intrinsic GTPase activity of RAS and cause the conversion to the GDP bound state (Cox & Der, 2010; Karnoub & Weinberg, 2008).

Differently, mutated and oncogenic RAS is kept in a constitutively GTP-bound active state by preventing GAP from increasing the intrinsic catalytic rate of GTPase and thereby activates oncogenic pathways and cellular signal transduction (Gibbs et al., 1984; McGrath et al., 1984; Scheffzek et al., 1997, 1996). For instance, mitogen-activated protein kinase (MAPK) signaling pathway has been shown to plays an important role in RAS-mediated tumorigenesis. Here, RAF phosphorylates MEK, which in turn stimulates the extracellular signal-regulated kinase (ERK). Finally, ERK can activate cytosolic substrates and translocate to the nucleus where it promotes gene expression of genes involved in cell proliferation, survival, differentiation and cell cycle regulation (Khosravi-Far et al., 1995; Leevers et al., 1994; Stokoe et al., 1994). Another pathway which is essential for RAS-mediated oncogenesis is the phosphatidylinositol-4,5-bisphosphate 3 kinase (PI3K) pathway. PI3K can convert PIP2 to PIP3 by phosphorylation which activates phosphoinositide-dependent kinase 1 (PDK1) and in turn phosphorylates the serine/threonine-specific protein kinase AKT. Thus, AKT can further phosphorylate various substrates which stimulate cell cycle progression, metabolism, migration, survival and resistance to apoptosis. For example, substrates of AKT are nuclear factor (NF)-κB, forkhead box O (FOXO) or mammalian target of rapamycin (mTOR) (Ferrer et al., 2018; Gupta et al., 2007; Rodriguez-Viciana et al., 1997). Hence, KRAS mediated signaling represents several major characteristics of a cancer cell or hallmarks of cancer (Hanahan & Weinberg, 2011).

1.1.3 Tumor suppressor p53 and cancer

The tumor suppressor p53 is inactivated by mutation in many human cancer types and lung cancer is no exception. Mutations in p53 are found in about 90% in lung squamous carcinoma and in approximately 46% in lung adenocarcinoma (Fig.1). The prevalence of p53 mutations also depends on the developmental stage of the tumor and is more commonly observed with advanced grade of the tumor (Ahrendt et al., 2003; Herbst et al.,

2018; Leroy et al., 2014). Most cancer-associated mutations are located in the DNA-binding domain (DBD) (Leroy et al., 2014; Petitjean et al., 2007).

p53 plays an important role as a transcription factor (Lane & Levine, 2010). Upon cellular stress signals, like oncogenic stress or DNA damage, p53 is activated and causes expression of target genes which are involved in cell cycle arrest, DNA repair or apoptosis (Joerger & Fersht, 2016). Additionally, the p53 pathway has been linked to metabolic regulation, development and stem cell biology, as well as to mTOR signaling which is involved in senescence, angiogenesis and autophagy (Bieging et al., 2014; Vousden & Prives, 2009).

Importantly, p53 is under strict control of its negative regulator murine double-minute 2 (MDM2), which is a E3 ubiquitin ligase. During normal cell division, p53 levels are low and negatively regulated by MDM2. MDM2 binds to p53 together with its homolog MDMX (or MDM4), thereby reducing its activity and transporting the protein to the cytoplasm where it is degraded. For instance, when DNA damage occur, p53 gets activated through a cascade of phosphorylation events and other posttranslational modifications which increases the half-life and consequently the activity of the protein. Also, MDM2 gets phosphorylated and thus disrupts the MDM2-p53 interaction which is important for p53 activation (Gupta et al., 2019; Joerger & Fersht, 2016; Meek, 2015).

For cancers which retain p53 wildtype status, p53 pathway can be inactivated by high expression of negative regulators, such as MDM2. More than 17% of tumors show a gene amplification of MDM2 which is associated with poor prognosis and treatment failure in the presence of chemotherapeutics (Gupta et al., 2019).

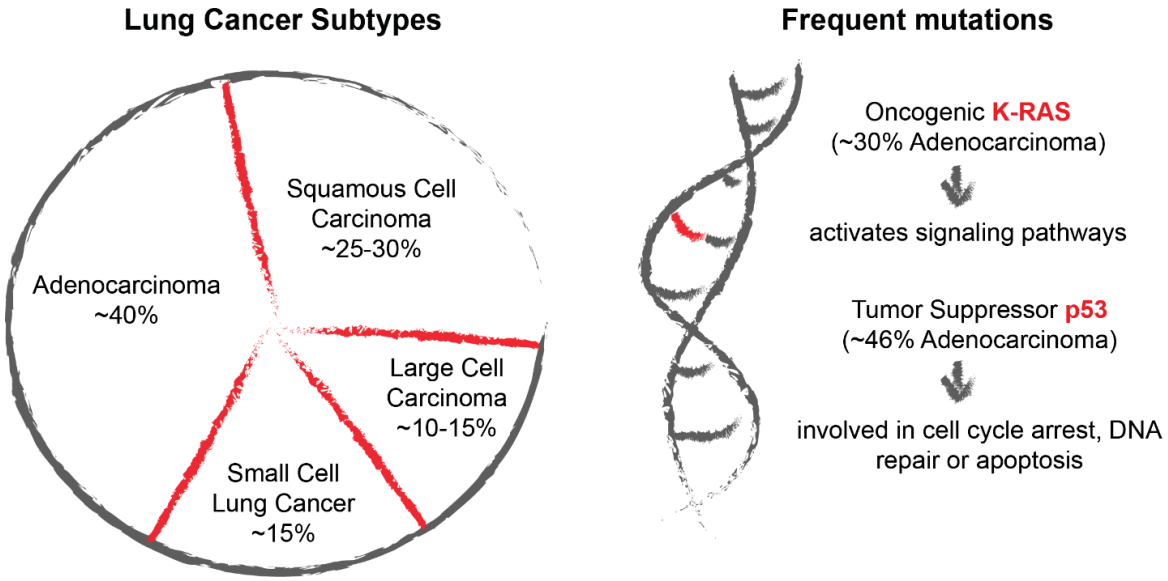

Figure 1: Lung Cancer.
Lung cancer can be subdivided into small cell lung cancer (SCLC) and non-small cell lung cancer (NSCLC). Main subtypes of NSCLC are adenocarcinoma, squamous cell carcinoma and large cell carcinoma. Frequent driver mutations are found in the KRAS oncogene and tumor suppressor p53.

1.2 Treatment strategies for NSCLC

Different treatment strategies are applied depending on the stage of lung cancer and typically include surgery, radiation therapy or chemotherapy (PDQ Adult Treatment Editorial Board, 2020). Chemotherapy is based on drugs that eliminate fast growing cells (see 1.2.1). In later stages of lung cancer, combinational treatment with chemotherapeutics, targeted therapy or immunotherapy is applied (PDQ Adult Treatment Editorial Board, 2020). Compared to chemotherapy, immunotherapy and targeted therapies can be more specific for cancer cells and less harmful to normal cells (see 1.2.2 and 1.2.3).

1.2.1 Chemotherapy

Chemotherapy is used to inhibit or destroy fast-growing cells in the body so as cancer cells by interfering with the proliferation process of the cells by chemical drugs. For instance, cisplatin is used as a platinum-based chemotherapy which induces DNA damage and interfere with DNA repair (Fennell et al., 2016). Even though side effects as emesis, nephrotoxicity, and neuropathy/ ototoxicity occur after cisplatin treatment, it remains standard care of NSCLC patients with no drug-targetable driver mutations. Resistances to cisplatin treatment are one of the significant limitations for improving long term outcome (Fennell et al., 2016; Sun et al., 2019). Over time cisplatin was combined with other chemotherapeutics as paclitaxel (interfere and stabilize microtubules) or gemcitabine (blocking new DNA synthesis) to improve and extent the survival of lung cancer patients (Alvarellos et al., 2014; Fennell et al., 2016; Jordan & Wilson, 2004; see Table 1).

1.2.2 Immunotherapy

Immunotherapy has been developed which focuses on several ligands and receptors that inhibit or stimulate the immune system in a wide range of cancer types as well as NSCLC. Possible immune checkpoint targets are the programmed cell death-1 (PD-1), programmed cell death ligand (PD-L1) and cytotoxic T lymphocyte-associated antigen-4 (CTLA-4). Anti-PD-1/PD-L1 antibodies have entered the clinic in 2015 and have shown impressive response rates but solely in a small percentage of cancer patients (Kim & Choi, 2020; Yuan et al., 2019; PDQ Adult Treatment Editorial Board, 2020). For instance, nivolumab is a human monoclonal antibody that inhibits PD-1 and atezolizumab is a PD-L1- blocking antibody which were used for therapy (PDQ Adult Treatment Editorial Board, 2020; see Table 1).

1.2.3 Targeted therapy

Advances in technologies for detection and knowledge of pathways as well as novel developed drugs to block the activities of the pathways improved the treatment options for

the patients (Herbst et al., 2018). Major targets for NSCLC are the RAS-MAPK, NTRK/ROS1, PI3K/AKT/mTOR or EGFR.

EGFR inhibitors gefitinib and erlotinib, NTRK/ROS1 inhibitors entrectinib, and PI3K/AKT/mTOR inhibitors everolimus, shows clinical benefits and replaced chemotherapy as the first line treatment pathways. Even though targeted therapy improved treatment strategy for NSCLC, a general problem is that many patients develop drug resistances (Yuan et al., 2019).

Direct inhibition of KRAS has been largely unsuccessful and therefore downstream effectors like RAF, MEK and mTOR have been investigated as potential targets in NSCLC (Cox et al., 2014; Yuan et al., 2019). Unfortunately, inhibitors targeting RAF , BRAF or MEK showed no efficiency and benefit in NSCLC (Ferrer et al., 2018; Yuan et al., 2019).

Table 1: Overview of three treatment strategies for NSCLC

Treatment	Target(s)	Agent/Inhibitor
Chemotherapy	fast-growing cells	cisplatin or in combination with paclitaxel or gemcitabine
Immunotherapy	PD-1 PD-L1	nivolumab atezolizumab
Targeted therapy	EGFR NTRK/ROS1 PI3K/AKT/mTOR	gefitinib and erlotinib entrectinib everolimus

1.3 Cell cycle as a cancer target

As cancer is characterized by aberrant cell cycle activity leading to uncontrolled proliferation, crucial cell cycle regulators are promising targets for cancer therapy. Compared to non-transformed cells, cancer cells are more likely dependent on these proteins and thus are more sensitive to their inhibition (Ingham & Schwartz, 2017; Otto & Sicinski, 2017).

Briefly, the cell cycle is the process during a cell divides into two identical daughter cells. During this highly ordered event, genetic information is duplicated and distributed equally to each daughter cell. The cell cycle is divided into four main phases and terms as gap-1 (G1, before S and after M phase), synthesis (S, DNA replication) phase, gap-2 (G2, after S and before M phase) and mitosis (M, cell division phase) phase. Additionally, a quiescent or resting cell in a temporal or permanent state is called G0 phase. G1, S and G2 phase of the cell cycle are commonly known as interphase (Malumbres & Barbacid, 2001; Molinari, 2000; Tessema et al., 2004; Weinberg, 2014). Mitosis can be further subdivided into

prophase, prometaphase, metaphase, anaphase and telophase. The final process when the cell is finally separated into two daughter cells is the so-called cytokinesis. Regulatory mechanisms and control checkpoints ensure that the cell proceeds in the cell cycle only after the prior phase is complete and DNA integrity is sustained (D'Avino et al., 2015; Green et al., 2012; Mitchison & Salmon, 2001; Scholey et al., 2003; Tessema et al., 2004).

The internal transition from one cell cycle phase to another is accomplished by a cascade of phosphorylation events mediated by cyclin-dependent kinases (CDKs), a class of serine/threonine protein kinases, in association with cyclins. These CDK/cyclin complexes are activated in a stage-specific manner and phosphorylate specific targets which in turn push the cell cycle forward. Specific cyclins are just expressed during distinct cell cycle phases or otherwise proteolytically degraded (Israels and Israels, 2001; Tessema et al., 2004). Moreover, CDK activity is also regulated by CDK-inhibitors (CKI) and by phosphorylation and dephosphorylation of specific residues (Tessema et al., 2004).

In the following parts, different cell cycle phases as potential targets for cancer therapy are explained in more detail.

1.3.1 G1 phase

In G0 or early to mid G1 phase, a cell is capable to respond to external stimuli, as mitogens or growth factors, to initiate cell cycle entry and progression. At the restriction point (R-point) near the end of G1 phase, a cell finally decides to proceed through the cell cycle until its completion and is then independent of extracellular signals (Israels and Israels, 2001; Tessema et al., 2004).

For progression through G1 phase, D-type cyclins (D1, D2, D3) are expressed and less proteolytically degraded. These D-type cyclins binding to cyclin-dependent kinase (CDK) 4 and 6 and form a CDK4/6-cyclin D complex, which becomes fully active upon phosphorylation by CDK-activating kinase (CAK) (Tessema et al., 2004). The active complex phosphorylates the retinoblastoma protein (pRB). pRB is a member of the pocket proteins (see 1.3.4 for other pocket proteins p107 and p130), which are cell cycle regulators through their regulation of E2F-responsive genes. pRB has a crucial role in G1 cell cycle progression by binding and inhibiting transcriptional activator E2Fs as E2F1, E2F2, and E2F3a (Cobrinik, 2005). Hypophosphorylated pRB prevents cell cycle progression through the restriction (R)-point. Further phosphorylation of pRB leads to hyperphosphorylation and release of E2F, which initiate transcription of many genes for S-phase entry as cyclin E (see Fig. 2). Together with CDK4/6-cyclin D, CDK2/cyclin E inactivate pRB completely and induce more E2F target genes to pass the cell through G1/S transition (Israels and Israels, 2001; Schafer, 1998 Tessema et al., 2004). Inhibitory factors as cyclin-dependent kinase

inhibitor (CKI) p27 are degraded and E2F transcriptional activity initiate more CDK2/cyclin E (Tessema et al., 2004).

Cancer cells need to overcome the cell cycle control by pRB for uncontrolled proliferation. One way is to constitutively activate CDK4/6-cyclin D complexes, for instance by deregulated transcription of the cyclin D1 gene. Alternatively, inactivation of CKIs, which inhibits CDK4 and 6 as cyclin-dependent kinase 4 (INK4) genes (e.g. $p16^{INK4a}$) are options for cancer cells. For therapy, three selective CDK4/6 inhibitors (palbociclib, ribociclib, abemaciclib) have been developed for pRB-positive tumor types including NSCLC (Vanarsdale et al., 2015). Palbociclib blocks pRB phosphorylation and prevents E2F release leading to a tumor growth suppression and G1 phase arrest (see Fig. 2; Liu, Liu, & Chen, 2018). It is been suggested that pRB-positive tumors are not able to bypass CDK4/6 inhibition and the vast majority of those tumors respond to CDK4/6 inhibitors. However, some data indicates resistances of CDK4/6 inhibitors in the presence of pRB so that there exist parallel or adaptive pathways for cell cycle progression (Knudsen et al., 2019). Combinational therapies of palbociclib and EGFR inhibitors gefitinib could be an option, which enhance effects *in vitro* and *in vivo* as single treatment (Liu, Liu, & Chen, 2018). Also, a combination of MEK inhibition (trametinib) and CDK4/6 inhibition by palbociclib showed reduced proliferation in KRAS-mutant NSCLCs that where initially resistant to MEK inhibitors (Tao et al., 2016). There are positive implications for the clinical use of palbociclib as a cancer target but some more research needs to be done to better understand resistance mechanism and combinational treatments (Liu, Liu, & Chen, 2018).

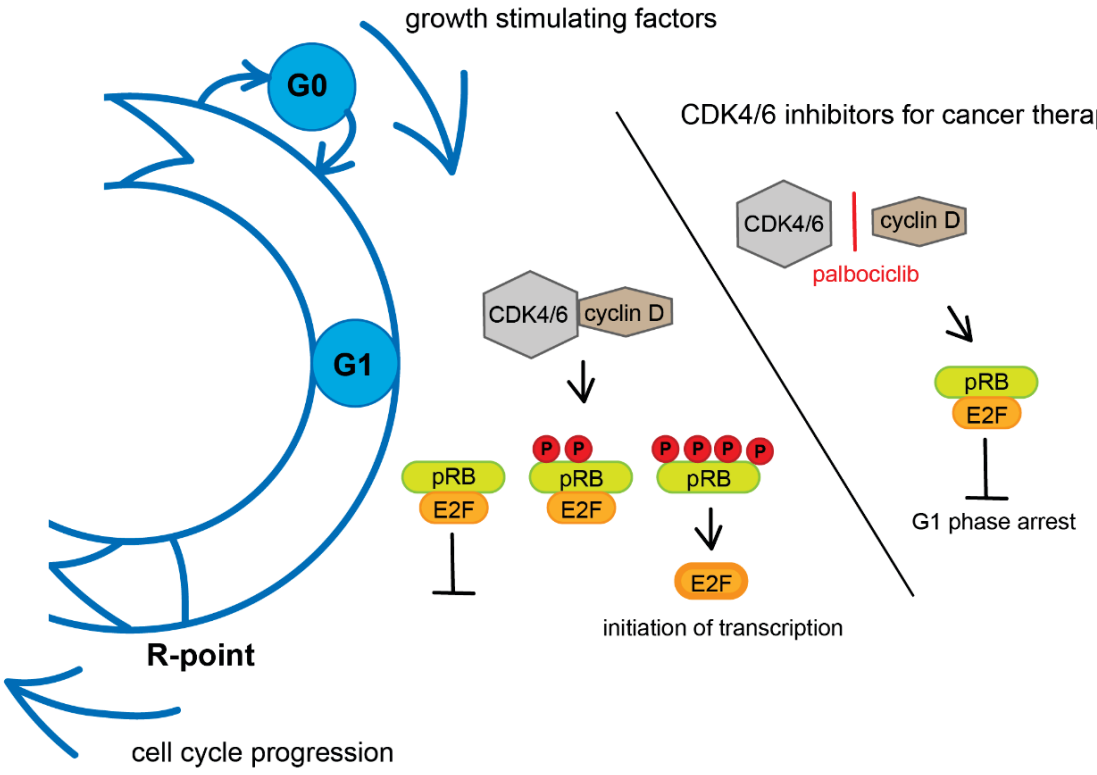

Figure 2: G1 cell cycle regulation and cancer target.
Cells receive growth stimulating factors to initiate cell cycle progression. Cyclin D is expressed and together with CDK4/6 phosphorylates retinoblastoma protein (pRB). pRB binds and inhibits transcritptional activator E2Fs. Hypophosphorylated pRB prevents cell cycle progression through the restriction (R)-point. Further phosphorylation of pRB leads to hyperphosphorylation and release of E2F, which initiate transcription of many genes for S-phase entry. For cancer therapy, selective CDK4/6 inhibitors (e.g. palbociclib) have been developed. Palbociclib are able to separate CDK4/6-cyclin D complexes which in turn blocks pRB phosphorylation and preventing E2F release leading to a tumor growth suppression and G1 phase arrest.

1.3.2 S/G2 phase

DNA damage during the replication process is a major cause of genomic instability. DNA damage can either be induced by exogenous factors as ultraviolet radiation, ionizing radiation, genotoxic chemicals or by endogenous factors as spontaneous or enzymatic reactions, chemical modifications, replication errors (Gourley et al., 2019). DNA damaging agents are used for chemotherapy (see 1.2.1). Cell cycle checkpoints get activated after errors in the replication process to repair and minimize DNA damage (Gourley et al., 2019; Otto & Sicinski, 2017). As mentioned in 1.1.3, the transcription factor p53 is a significant guardian of the genome and is activated upon DNA damage. If the DNA damage is too strong for the cell to repair, p53 can mediate apoptosis by inducing expression of pro-apoptotic proteins. On the other hand, incomplete DNA replication or DNA damage in G2 phase can activate checkpoint pathways to arrest the cell cycle (Tessema et al., 2004). Defective DNA activates ataxia telangiectasia mutated (ATM) and ATM and Rad3-related (ATR) protein kinases which phosphorylates and activates checkpoint kinase 1 (CHK1). ATM can also induce CHK2. These checkpoint kinases are involved in activation of p53, which in turn induces the expression of CKI $p21^{CIP1}$ and causing the inhibition of CDK2-cyclin E complexes. Also, CHK1 can inactivate cell division cycle 25A (CDC25A) for temporary S phase arrest or inactivate CDC25A, CDC25B and CDC25C for G2 arrest. CDC25 are protein tyrosine phosphatases which activates CDK2 and CDK1. CDK2 and CDK1 are important for G1/S transition and further progression through G2 phase together with cyclin A and B (Tessema et al., 2004; Otto & Sicinski, 2017). A serine/threonine kinase termed WEE1 gets also activated by CHK1, which causes inhibitory phosphorylations of CDK2 and CDK1 too. So, CHK1 is a crucial protein for cell cycle arrest in S and G2 phases upon DNA damage (Otto & Sicinski, 2017).

Targeting proteins of the DNA damage response (DDR) pathway might be new anti-cancer targets. Here, DDR molecules induces replication stress which could lead to apoptosis, when DNA damage is too strong or irreparable. For instance, ATM, ATR, CHK1, WEE1 and poly (ADP-ribose) polymerase 1 (PARP1) has been identified as cancer targets. PARP1 plays a role in DNA single strand breaks and homologous recombination repair (Burgess et al., 2020; Gourley et al., 2019). PARP inhibitors are more effective in tumors with

homologous recombination deficit, so as BRCA1/2 (breast cancer type 1 susceptibility protein) mutated breast, ovarien and pancreas cancer. BRCA1/2 mutations are only found in 5% of lung cancer patients but mutations in the DNA repair protein PTEN account for 4–8% of all NSCLCs, which are sensitive to PARP inhibitors and thus expand the group of patients which might benefit of the therapy (Burgess et al., 2020; Gourley et al., 2019). PARP inhibitors as veliparib are in clinical trials in lung cancer. CHK1/2 (CBP-501), WEE1 (AZD-1775), ATM (AZD-0156) and ATR (AZD-6738) inhibitors are also currently tested in clinical trials. CHK1/1, WEE1 and ATM inhibitors are used in combination with chemotherapy to enhance their efficiency. ATM inhibitors are tested together with PARP inhibitors and ATRi showed enhanced effects in combination with CHK1i. In the future, targeting DDR needs to be further studied as monotherapy, in combination with other inhibitors of DDR or with chemotherapeutics (Gourley et al., 2019; Matheson et al., 2016; Otto & Sicinski, 2017; Sanjiv et al., 2016).

1.3.3 Mitosis and mitotic exit as a target for therapy

1.3.3.1 DREAM and MMB complex

MuvB (multi-vulval class B) multiprotein complexes are highly conserved master regulators (its components are conserved in vertebrates, flies, worms and plants) of cell cycle-dependent gene expression. The MuvB core, consisting of LIN9, LIN54, LIN37, LIN52, and RBBP4, can bind to pocket protein p130 or p107 (see 1.3.1 for pocket protein pRB), E2F4 or E2F5, and dimerization partner 1/2, to build the DREAM complex (Fischer & Müller, 2017; Litovchick et al., 2007; Sadasivam & DeCaprio, 2013; Schmit et al., 2009; Schmit et al., 2007). The DREAM complex represses cell cycle-dependent gene expression in G0 by binding to E2F DNA binding sites and cell cycle gene homology regions (CHR) in promoter regions (Engeland, 2018; Fischer & Müller, 2017; Sadasivam & DeCaprio, 2013). It was shown that tumor suppressor p53 indirectly suppresses cell cycle gene expression by the formation of DREAM. Mechanistically, p53 upregulates a target gene, p21 (CDKN1A), which inhibits CDKs so that p107 and p130 are hypophosphorylated and can join other components of the DREAM complex (Engeland, 2018; Mannefeld et al., 2009). Target genes of the p53-DREAM pathway are involved in many cellular processes e.g. the G1/S checkpoint, the S phase, microtubule-organization, the G2/M checkpoint, Mitosis, spindle formation, spindle assembly checkpoint (SAC), Histone modification or DNA repair (Engeland, 2018).

When cells receive growth stimulatory factors and enter into the cell cycle, DREAM is disrupted. Now, activator E2Fs (E2F1-3) are recruited to E2F promoter sites and activate gene expression for G1/S phase transition (Fischer & Müller, 2017; Takahashi et al., 2000). Interestingly, in late S phase/early G2 phase the MuvB core interacts with the transcription

factor B-MYB (MYB-MuvB termed as MMB) and in late G2/M phase with the forkhead box protein M1 (FOXM1) to promote the second wave of cell cycle gene expression (see Fig. 3). Thus, MuvB can switch its function from a repressor to an activator of cell cycle genes (Engeland, 2018; Fischer & Müller, 2017; Osterloh et al., 2007; Schmit et al., 2007). Similar to DREAM, the MMB complex binds to CHR-elements, but now activates target gene expression (Engeland, 2018; Sadasivam & DeCaprio, 2013; Schmit et al., 2009).

Recently, it has been shown that in cancer cells another regulator of proliferation, the Hippo pathway and its downstream effector Yes-associated protein 1 (YAP1), activate mitotic gene expression by inducing the expression of B-MYB and promoting the binding of B-MYB to promoters of G2/M genes from distant enhancers (see Fig. 3; Pattschull et al., 2019). Pattschull et al. showed that MYBL2 (B-MYB)- and YAP-MMB-target genes are expressed in elevated levels in NSCLC, as compared to normal tissue. This high expression levels of YAP-MMB-target genes indicated a clinical relevance, as lung adenocarcinoma patients showed a significant shorter survival compared to patients with lower expression of these genes. Possibly, development of new therapeutics that target the YAP1-B-MYB interaction by specifically blocking the oncogenic, pro-proliferative functions of YAP1 would be a new approach for the future (see Fig. 3; Gründl et al., 2020; Pattschull et al., 2019; Weinstock & Gaubatz, 2019).

B-MYB and FOXM1, as well as many target genes including polo-like kinase 1 (PLK1), aurora kinase A (AURKA), DNA topoisomerase 2α (TOP2A) and protein regulator of cytokinesis 1 (PRC1), are frequently overexpressed in cancer (Sadasivam & DeCaprio, 2013; She et al., 2019; Wolter et al., 2017). High levels of B-MYB and FOXM1 are associated with poor outcomes in some types of cancers, including lung cancer (Iltzsche et al., 2016; Sadasivam & DeCaprio, 2013). A small molecule compound, Robert Costa Memorial drug-1 (RCM-1), has been identified as an inhibitor of FOXM1. Treatment of tumor cells with RCM-1 inhibited cell proliferation *in vitro* and also an inhibited growth of human H2122 lung adenocarcinoma *in vivo*, suggesting that RCM-1 could be candidate for anti-cancer therapy (see Fig. 3; Shukla et al., 2019). Iltzsche et al. showed that MMB is required for tumor formation in a mouse model for NSCLC (Iltzsche et al., 2016). However, targeting of MMB might be difficult to achieve as no enzymes have been identified in the MMB complex and complete inhibition of MMB could be difficult, as deletion of *B-Myb* or *Lin9* in mice results in lethality (Iltzsche et al., 2017; Reichert et al., 2010; Tanaka et al., 1999). Instead, it has been suggested to target downstream targets of MMB such as kinesin family member 23 (KIF23 or mitotic kinesin-like protein 1 (MKLP1)), which showed inhibited lung tumor formation *in vivo* and induced apoptosis in lung cancer cell lines (Iltzsche et al., 2016). In another study of the laboratory of Stefan Gaubatz, transcriptional targets of MMB and MMB-FOXM1 have been identified that are important for oncogenesis of breast cancer

cells. Here, it was demonstrated that at least six mitotic kinesins as well as centrosomal protein 55 (CEP55) and PRC1 are direct targets and the suppression of KIF23 and PRC1 strongly inhibited proliferation of breast cancer cells. Also, PRC1 and KIF23 expression levels correlated with the survival rate of breast cancer patients (Wolter et al., 2017). Taken together, target genes of MMB or MMB-FOXM1 could be potential therapeutic targets for the treatment of lung cancer (see Fig. 3). In the following parts, important regulators and proteins for mitosis and mitotic exit as well as possible strategies for targeting these components are explained in more detail.

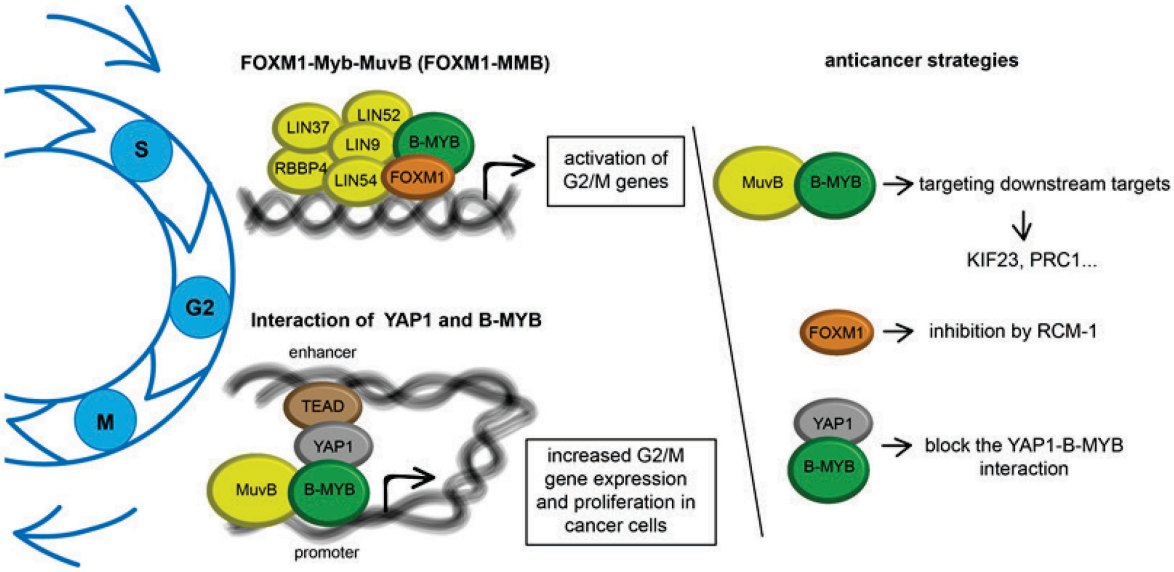

Figure 3: Activation of G2/M genes by the FOXM1-MMB complex, enhanced proliferation by the YAP1-B-MYB interaction and anticancer strategies.
Upon growth stimulatory signals, FOXM1-Myb-MuvB (FOXM1-MMB) is formed to activate cell cycle genes (G2/M genes) for proper mitosis and cytokinesis. In cancer cells, another regulator of proliferation, the Hippo pathway and its downstream effector Yes-associated protein 1 (YAP1), activate mitotic gene expression by inducing the expression of B-MYB and promoting the binding of B-MYB to promoters of G2/M genes from distant enhancers. Possible anticancer strategies are: targeting downstream targets of MMB as KIF23 or PRC1, inhibition of FOXM1 by RCM-1 or block the interaction between YAP1 and B-MYB.

1.3.3.2 Mitosis, SAC and APC/C

In prophase of mitosis duplicated centrosomes, containing two pairs of centrioles, thereby representing the major microtubule organization center, migrate to opposite poles and begins to form the spindle by polymerization of microtubules. Chromatin (DNA-protein complex) is further condensed by recruitment of condensin complexes (Antonin & Neumann, 2016; Rale et al., 2018). In prometaphase, the nuclear envelope breaks down and dynamic spindle microtubules search for connection with the kinetochores, a multiprotein structure that assembles at centromere regions, which are regions that join the two sister chromatids (identical copies of replicated DNA) of highly condensed chromatin

termed as chromosomes (Amin et al., 2019). Microtubules are growing from both poles of the spindle and start to pull chromosomes to opposite directions but sister chromatids are still connected by cohesion at their centromeres. In prometaphase and metaphase, pairs of sister chromatids are orientated between the two centrosomes by the mitotic spindle, a structure composed of microtubules, chromosomes, motor proteins and microtubule-associated proteins, at the middle of the cells and also called the metaphase plate or equatorial plane (Oriola et al., 2018; Scholey et al., 2003). After anaphase onset, cohesion between sister chromatids is lost by degradation of cohesin by the protease separase and the two identical chromatids are transported to opposite spindle poles. At the beginning anaphase, movement to the spindle poles is due to kinetochore-microtubule shortening and later through motor proteins that are connected to microtubules with opposite polarity. In telophase, the reassembly of the nuclear envelope starts at each cell pole while decondensation of the sister chromatids starts (Scholey et al., 2003).

A control system termed as spindle assembly checkpoint (SAC) machinery causes a mitotic arrest when failures during segregation of sister chromatids occurs (see Fig. 4). The anaphase-promoting complex or cyclosome (APC/C) plays a crucial role in the SAC. Before anaphase, APC/C binds to its cofactor CDC20 to generate an active E3 ubiquitin ligase that targets cyclin B and securin for proteasomal degradation. This allows separase to cleave cohesion inducing chromosome segregation and anaphase progression (see 1.3.4.3 for more information about cyclin B; Haschka et al., 2018; Liu et al., 2019). Unattached kinetochores activates the mitotic checkpoint complex (MCC), which in turn inhibits APC/C. MCC comprises of BUBR1 (budding uninhibited by benzimidazole-related-1), CDC20, BUB3 (budding uninhibited by benzimidazoles 3) and C-MAD2 (a natively folded state of mitotic arrest deficient 2 (MAD2)). Also, monopolar spindle (MPS) 1 kinase is crucial for MCC formation, recruitment of SAC proteins to unattached kinetochores, and is required for chromosome alignment and error correction. An important protein for disassembly of the MCC is p31 comet. The protein binds to C-MAD2 and regulate checkpoint homeostasis. Additional phosphatases PP1 (protein phosphatase 1) and PP2A (protein phosphatase 2A, see 1.3.4.3) at the kinetochore are required to efficiently terminate the SAC (Dominguez-Brauer et al., 2015; Haschka et al., 2018).

Mutations or post-translational modifications in APC/C subunit have been found that play a crucial role in cancer development and progression. Also, substrates of the APC/C as HEC1 (highly expressed in cancer 1) and ECT2 (epithelial cell transforming 2) play an important role in cancer progression. A high activity of APC/C and elevated expression level of CDC20 predicts a poor prognosis of patients with NSCLC (Liu et al., 2019). Anti-mitotic drugs such as vinca alkaloids and taxanes interfere with microtubule dynamics and activates the SAC (see Fig. 4). However, cells can escape from mitotic arrest by mitotic slippage or mitotic

checkpoint adaptation. Mitotic slippage occurs by slow degradation of cyclin B even when SAC is active. Upon a certain threshold of cyclin B, cells can exit mitosis, possibly resulting in polyploid interphase (Brito & Rieder, 2006; Yang et al., 2009). On the other hand, the SAC does not work in a bimodal fashion. Signaling strength can vary, as levels of intrinsic factors such as MAD2 or p31 comet (Haschka et al., 2018). Therefore, many cancer cells have a reduced but not absent SAC response which could lead to aneuploidy (Dominguez-Brauer et al., 2015). Aneuploidy is the result of chromosomal instability (CIN) and is defined by an increased rate of loss or gain of parts of chromosomes or even whole chromosomes during cell division. Aneuploidy might further contribute to cancer development (Holland & Cleveland, 2009; Lengauer et al., 1997; Potapova et al., 2013). However, aneuploid cancer cells may be more susceptible to chromosome mis-segregation as they need more time during metaphase to align their abnormal number of chromosomes. Complete inactivation of the SAC seems lethal for both non-transformed and malignant cells but non-transformed cells appear to be less sensitive than cancer cells to death caused by SAC inhibition (Dominguez-Brauer et al., 2015).

Two APC/C inhibitors, TAME (tosyl-L-arginine methyl ester) and apcin, have been developed. proTAME disrupts the interaction between APC/C and CDC20 which leads to increasing CDC20 auto-ubiquitination and stabilization of cyclin B. The action of proTAME caused an anaphase delay and finally blockage of mitotic exit in HeLa cells, an immortal cervical cancer cell line. Combination of APC/C inhibition with chemotherapeutic agents as paclitaxel or etoposide (DNA topoisomerase 2-alpha (Top2α) inhibitor) increases the sensitivity of cancer cells to these drugs which could lead to inhibition of mitotic exit and apoptosis in cancer cells (see Fig. 4; Liu et al., 2019). Another possible target with inhibitors under development or in clinics is MPS1 (empesertib, BAY 1217389,). MPS1 is highly expressed in several cancers and the elevated level correlates with worse prognosis. Inhibition of the protein causes to prematurely exit mitosis with unattached chromosomes, leading to aneuploidy and eventually cell death. Also, combinational treatment has shown that MPS1 inhibitors sensitize cancer cells to taxol treatment (Dominguez-Brauer et al., 2015; Janssen et al., 2009).

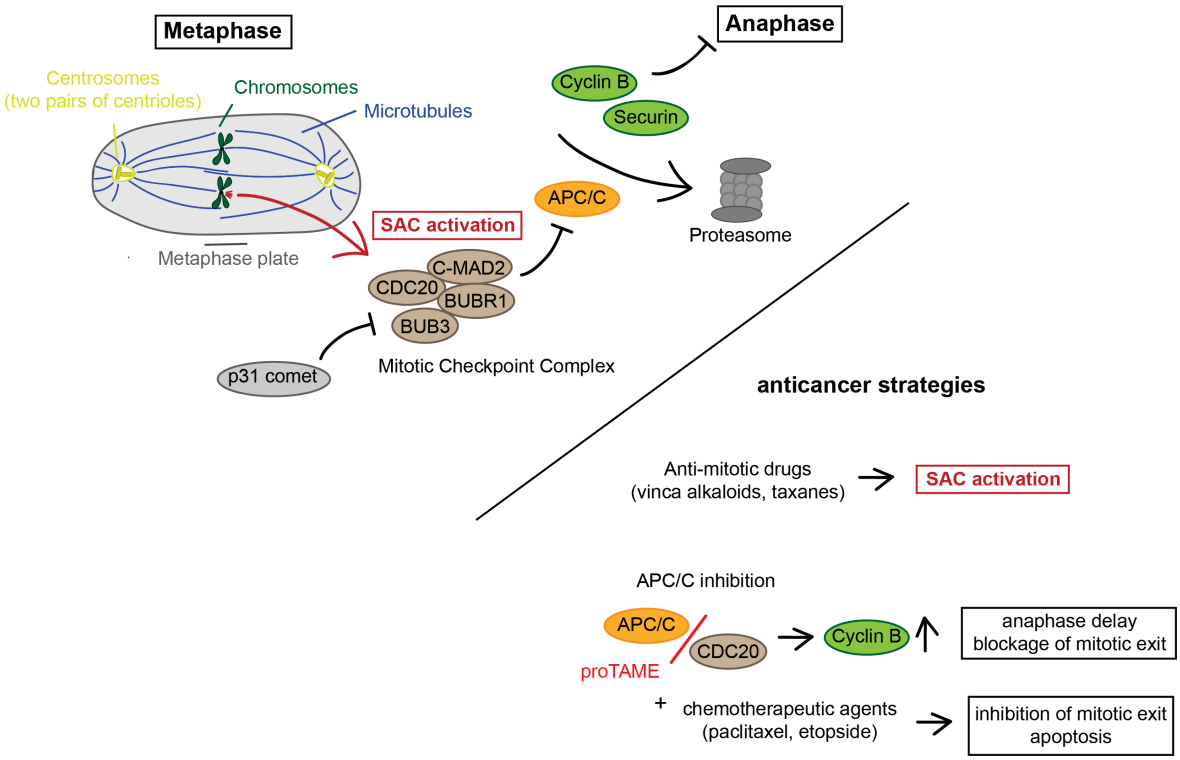

Figure 4: Spindle assembly checkpoint activation and anticancer strategies.
Unattached kinetochores can activate the SAC, which blocks the activity of the APC/C E3 ligase complex and leading to inhibition of metaphase to anaphase transition (mitotic arrest). Upon SAC activation, the mitotic checkpoint complex (MCC) inhibits CDC20, a cofactor for APC/C, which is needed for proteasomal degradation of cyclin B or securin and anaphase progression. MCC function can be antagonized by p31 comet. Anti-mitotic drugs interfere with microtubule dynamics and activates the SAC, which could be used for cancer therapy. Another anticancer strategy is inhibition of APC/C, which could lead to cyclin B stabilization and blockage of mitotic exit. In combination with chemotherapeutic drugs, sensitivity of cancer cells increases and could lead to apoptosis.

1.3.3.3 Mitosis promoting factor, mitotic kinases and phosphatases

Upon beginning of mitosis, CDK1/cyclin B activity increase and is also termed as mitosis promoting factor (MPF). MPF targets are for instance motor proteins and microtubule-binding proteins which have various important roles in nuclear envelope breakdown, centrosome separation, chromosome condensation and spindle assembly (Tessema et al., 2004). In late metaphase, cyclin B is rapidly degraded by APC/C and mitotic exit is initiated. Cyclin B is overexpressed in various cancers and correlated with poor prognosis. Upregulated cyclin B promotes G2/M transition. Targeting cyclin B for degradation might be an interesting cancer strategy but needs to be further researched (Liu et al., 2019). CDK inhibitors have been developed (see 1.3.1 for CDK4/6 inhibitors), as flavopiridol, which inhibits several CDKs including CDK1 and inhibits cell cycle arrest at both G1/S and G2/M transition. In NSCLC, flavopiridol plus paclitaxel and carboplatin showed a response in 66% of patients (Dominguez-Brauer et al., 2015).

Several kinases and phosphatases are involved in the process of mitosis and mitotic exit regulation, as Aurora kinases, Polo-like kinase 1 (PLK1), protein phosphatase 2A (PP2A), and could be potential targets for therapy.

Aurora kinases, including Aurora A, Aurora B and Aurora C are a serine/threonine kinase family that play crucial roles in centrosome/centromere function and spindle assembly during mitosis. Aurora A participates in establishing a bipolar mitotic spindle by regulating centrosome maturation and disjunction. Aurora B is a component of the chromosome passenger complex (CPC, see Table 2) and contributes to SAC function as well as cytokinesis. Abnormal Aurora kinase activity is linked to defects in cell division and aneuploidy. Aurora kinase A and B are overexpressed in several cancers, including lung cancer (Dominguez-Brauer et al., 2015). Targeting Aurora kinases might be an anti-cancer strategy and many inhibitors have been already reported. Aurora A inhibitor alisertib and Aurora B inhibitor barasertib have entered clinical trials. Treatment with alisertib produced mild to modest single-agent anti-tumor activity in phase II studies on various advanced solid tumors. However, patient response rate of alisertib was just 4-9% in NSCLC. It has been suggested that Aurora kinase inhibitors are more suitable for tumors with higher proliferation rates than solid tumors, as hematologic malignancies (Dominguez-Brauer et al., 2015; Liu et al., 2019).

Polo-like kinases are serine/threonine kinases that play important roles in many cellular processes, including cell cycle regulation. PLK1 is activated by Aurora kinase A and has regulatory roles in mitotic entry, spindle assembly, centrosome maturation, APC/C regulation, and cytokinesis. PLK1 is overexpressed in variety of cancers and often correlates with poor prognosis (Dominguez-Brauer et al., 2015; Liu et al., 2019). Selective inhibitors have been developed to target PLK1, such as BI 2536 and BI 6727, which clearly delay mitotic exit and trigger apoptosis of cancer cells. A few PLK1 inhibitors, such as rigosertib and volasertib, have entered to phase III trials to test anticancer efficacy. However, an optimized dosage of PLK1 inhibitors needs to be found to prevent mitotic slippage (Liu et al., 2019; Raab et al., 2015). Additionally, PLK1 inhibition enhances the antitumor activity of chemotherapeutic drugs (Liu et al., 2019).

Protein phosphatase 2A is a serine/threonine phosphatase which regulates a wide range of crucial cellular processes, including mitosis, proliferation, metabolism and apoptosis. PP2A is a heterotrimeric enzyme and its isoforms and subunits determine the substrate specificity and subcellular localization of the protein. During metaphase to anaphase transition, PP2A/B56 (B56 is a regulatory subunit) dephosphorylates and inactivates CDC25C, which causes CDK1 phosphorylation and cyclin B degradation and initiating mitotic exit. Another study described that PP2A/B56 enhances mitotic exit through dephosphorylation of CDC20, which promotes APC/CDC20 assembly (Forester et al., 2007; Lee et al., 2017; Liu et al.,

2019). It has been reported that PP2A functions as a tumor suppressor and attenuates the growth of cancer cells and induces apoptosis (Liu et al., 2019). A new regulatory mechanism has been described by which PP2A blocks mitotic exit. Here, a cell cycle kinase termed as MASTL acts as a regulator of mitotic progression by promoting the inactivation of PP2A/B55. It has been shown that MASTL depletion impairs proliferation of cancer cells through reactivation of PP2A/B55 *in vitro* and *in vivo* (Álvarez-Fernández et al., 2018). Activating tumor suppressor PP2A by suppressing its endogenous inhibitors in cancer cells might be a therapeutic strategy.

Inhibition of PP2A, by using small molecule inhibitor, as LB100, has been suggested as an anticancer strategy. Here, inhibition of PP2A should drive senescent cells, which is a protective mechanisms of cancer cell to generate resistance to chemotherapy and radiotherapy, into mitosis (Liu et al., 2019).

1.3.3.4 Central spindle, microtubule-binding proteins and kinesins

The central spindle emerges from the mitotic spindle after anaphase onset but is reorganized completely (see Fig. 5). Central spindle microtubules are arranged in a way that they are bundled at their overlapping plus ends and thus becomes an array of interdigitating and antiparallel microtubules. Also, de novo microtubule polymerization has been proposed to play a role in central spindle formation. The regulation of the overlapping regions is crucial for further cell division and positioning of the division plane as well as cleavage furrow ingression and abscission. During the process of anaphase and telophase, the central spindle becomes more and more compact and forms a dense structure called the midbody or Flemming body whereas the cleavage furrow further ingresses (see Fig. 5). Important factors or proteins that play a crucial role in central spindle formation can be divided in microtubule-associated proteins (MAPs) and motor proteins. Several of those major components of central spindle formation have been suggested as potential targets for cancer (see Table 2; Carter et al., 2006; D'Avino et al., 2015; Douglas & Mishima, 2010; Glotzer, 2009; Iltzsche et al., 2016; Jeffery et al., 2016; Kitagawa & Lee (2015); Labrière et al., 2016; Li et al., 2018; Liu et al., 2019; Liu, Li, Zhang, et al., 2018; Martínez-García et al., 2019; Oriola et al., 2018; Rath & Kozielski, 2012; Wolter et al., 2017).

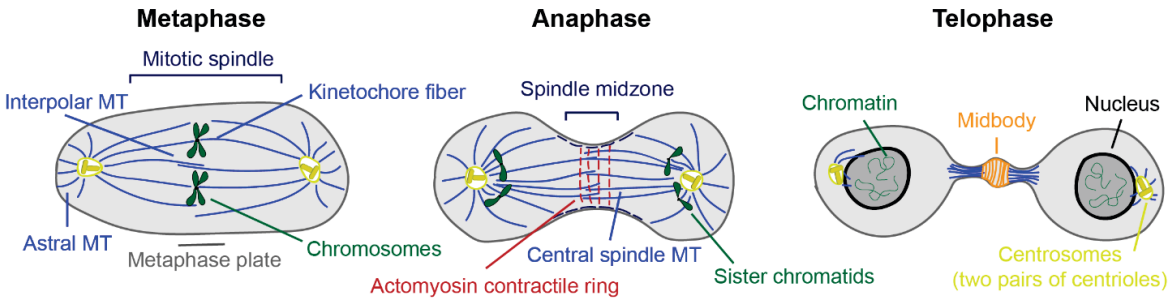

Figure 5: Different stages of cell division and distribution of microtubules (MT).
In metaphase, chromosomes (pairs of sister chromatids) are orientated between the two centrosomes by the mitotic spindle. In anaphase the two identical chromatids are transported to opposite spindle poles and furrow ingression starts at the central spindle or spindle midzone. In telophase, the reassembly of the nuclear envelope begins at each cell pole while decondensation of the sister chromatids starts. After furrow ingression is accomplished by the actomyosin contractile ring, an organelle at the center evolves and termed as midbody.

One core microtubule organizer is protein regulator of cytokinesis 1 (PRC1, see 1.4), a member of the MAP65 protein family and a highly conserved protein found in metazoans, plants and yeasts. PRC1 forms a homodimer and binds microtubules through a conserved spectrin fold and thereby cross-linking antiparallel microtubules at an average distance of 35 nm (Jiang et al., 1998; Kellogg et al., 2016; She et al., 2019; Subramanian et al., 2010). Distinct phosphorylations of PRC1 are proposed to be important for the spatiotemporal regulation and activation of the protein. More recently, the spatiotemporal regulation is suggested by upstream regulator PLK1, rather than CDK1 (Hu et al., 2012; Neef et al., 2007; Zhu et al., 2006; Zhu and Jiang 2005). Here, it was proposed that PRC1, PLK1 and microtubules built homeostatic model that regulates microtubule-bundling during cell division. Moreover, the binding of PRC1 and PLK1 seems to be crucial through further cytokinesis (Hu et al., 2012; Neef et al., 2007). Upon PRC1 activation, the protein interacts with a kinesin family member 4A (KIF4A) which contains a motor domain and translocate PRC1 along microtubules (Kurasawa et al., 2004; Zhu and Jiang, 2005). Two *in vitro* studies showed that a minimal two protein system of PRC1 and KIF4 is needed to promote antiparallel microtubule crosslinking which also controlling the plus-end dynamics of microtubules (Hannabuss et al., 2019; Bieling et al., 2010). PRC1 recruits KIF4 to antiparallel overlap regions where KIF4 has an inhibitory effect on microtubule growth suggesting a mechanism in controlling the elongation of plus-ends in the central spindle (Bieling et al., 2010). Similarly, it's shown that the PRC1/KIF4 ratio is important for the length of central antiparallel overlaps (Hannabuss et al., 2019).

In cancer cells, KIF4A and PRC1 are found to be overexpressed and their elevated expression correlated with short survival for patients (Hou et al., 2017; Kanehira et al., 2007; Luo et al., 2016; Shimo et al., 2007; Taniwaki et al., 2007; Zhang et al., 2017). Loss of KIF4 is described to cause abnormal elongated spindle midzones with unfocused overlapping

regions (Hu et al., 2011). Knockdown of PRC1 results in great disorganization of the spindle midzone which leads to remarkable mitotic defects and cytokinesis failure. As an outcome, microtubule spindle fails to bundle resulting in the absence of a clear midzone as well as abnormal chromosome misalignment and segregation (Li et al., 2018; Maton et al., 2015; Mollinari et al., 2002; Zhu et al., 2006). KIF4A and PRC1 are suggested as a possible target for cancer, including lung cancer, but so far no specific inhibitors has been developed (Li et al., 2018; Liu et al., 2019; Rath & Kozielski, 2012; Taniwaki et al., 2007).

Table 2: Important factors for central spindle assembly and potential anticancer targets

Name	Function	Cancer
PRC1	Microtubule bundling protein and important factor for central spindle formation and cytokinesis. Crucial interaction partner for several proteins, as KIF4A, centralspindlin, CLASP, KIF14, PLK1.	Overexpressed in many cancer types and elevated levels are correlated with aneuploidy and worse patient expectations.
Centralspindlin (2:2 heterotetrametric complex consisting of KIF23 dimer and RacGAP1 dimer)	KIF23: function in proper microtubule bundle formation with its plus-end directed motor activity. RacGAP1: recruits a downstream effector ECT2, which play a role in Rho A activation and further initiation of cytokinesis.	KIF23 is found to be upregulated in breast cancer and its expression is linked to poor outcome in breast cancer patients. Also, KIF23 is required for lung tumorigenesis and depletion inhibited lung tumor formation *in vivo* and *in vitro*.
Chromosome passenger complex (CPC consisting of Aurora B kinase, INCENP, survivin and borealin)	Important for central spindle assembly and phosphorylates several central spindle components including MKLP1 which facilitates recruitment of centralspindlin to the midzone.	Aurora B as a cancer target is described in part 1.3.3.3. Survivin (BIRC5) has also been suggested to be a promising target for cancer. Survivin overexpression has been correlated with a negative clinical outcome and drug resistance in many cancers.
KIF20A (MKLP2)	Essential for the relocation of CPC from the centromere to the central spindle as well as for the localization of PLK1 at the spindle midzone.	Overexpressed in cancer and inhibition leads to binucleated cells due to cytokinesis failures. Selective inhibitors (paprotrain, MKLP2 inhibitor 9a) has been found.
KIF20B (MPP1)	Localizes to the spindle midzone and is needed for correct cytokinesis.	Elevated expression in cancer and its expression is associated with poor prognosis of patients.

CEP55	Localizes at the central spindle and midbody where it can promote membrane fusion during final stages of cytokinesis.	High expression in cancer is associated with poor prognosis of patients

Out of the 45 different kinesins which found in the human genome, 16 have been implicated in coordinating mitosis and cytokinesis. For two of them, KIF11 (EG5) and centromere-associated protein E (CENPE), specific inhibitors (e.g. litronesib, MK0731 or ispinesib for EG5 and GSK923295 or syntelin for CENPE) have been developed and are in clinical trials to treat cancer cells (Liu et al., 2019; Rath & Kozielski, 2012).

CENPE is a kinesin which is required for progression from metaphase to anaphase. Here, it plays a role in microtubule kinetochore capture which is important for chromosome congression and alignment. Inhibition of CENPE by GSK923295 leads to failures of metaphase chromosome alignment and induces mitotic arrest in cultured cells and tumor xenografts. Treatment with GSK923295 leads to a significant delay on hepatocellular carcinoma growth and CENPE inhibition is also suggested to be a therapeutic strategy for medulloblastoma. Phase I clinical studies showed a dose-proportional pharmacokinetic with mild adverse effects (Chung et al., 2012; Iegiani et al., 2021; Rath & Kozielski, 2012; Tang et al., 2019; Wood et al., 2010).

EG5 is suggested to form a homotetramer with two antiparallel dimers and play a role in bipolar spindle formation by crosslinking and pushing two antiparallel spindle microtubules apart through its plus end-directed motility. Knockdown of EG5 is described to activate the spindle checkpoint, mitotic arrest and cell death in certain tumor cell lines. Preclinical studies with agents targeting EG5 showed high efficacy and regression of tumor mouse xenografts. However, agents targeting EG5 were moderately successful in clinical trials when used as a monotherapy. So, combination of KIF inhibitors with other chemotherapeutic drugs might be an option for clinical studies (Liu et al., 2019, 2013; Rath & Kozielski, 2012).

1.4 Protein regulator of cytokinesis 1 (PRC1)

PRC1, the mammalian homolog of MAP65/AseI, is a mitotic spindle-associated CDK substrate which plays various important roles during mitosis and cytokinesis (Jiang et al., 1998; Mollinari et al., 2002; Zhu & Jiang, 2005). PRC1 is required for spindle integrity, midzone microtubule bundle formation, and the completion of cell cleavage (She et al., 2019).

Expression levels of PRC1 are cell cycle dependent with high level during S phase and G2/M phase and low levels when cells enter the G1 phase of the cell cycle (see Fig. 6A; Jiang et al., 1998; Pellman et al., 1995). It has been shown that PRC1 is a direct target gene

of the DREAM and MMB complex, a master regulator of cell cycle dependent gene expression, and described in more detail in 1.3.3.1. During interphase, PRC1 is mainly nuclear (see Fig. 6A; Jiang et al., 1998; Mollinari et al., 2002). However, little is known about the potential nuclear role of the protein. The functions of PRC1 during cell division have been investigated in more detail (see 1.3.3.4).

PRC1 consists of a N-terminal coiled-coil domain, a central region and a C-terminal regulatory region (see Fig. 6B; Gaillard et al., 2008; Kellogg et al., 2016; She et al., 2019; Subramanian et al., 2013; 2010). The N-terminal region contains a dimerization domain within the first amino acids (1-66) so that the protein can build a homodimer out of two monomers (Subramanian et al., 2013). The following region is termed as rod domain (amino acids 67-340) and consists of α-helices with many coiled-coil motifs, which seems to be important for its midzone localization (see Fig. 6B; Mollinari et al., 2002; Subramanian et al., 2013). Furthermore, the rod domain of PRC1 is flexible when it attaches to a single microtubule but acquires a rigid conformation when it crosslinks two antiparallel microtubules at an average distance of 35 nm (see Fig. 6C; Kellogg et al., 2016; Subramanian et al., 2013; 2010). Microtubule-binding is mediated through a structural domain with a spectrin-fold (amino acid 341 to 466) and an unstructured Lys/Arg-rich region at the C-terminus (amino acid 466 to 620) which contributes to the long-lived association to microtubules. A conserved basic region of the spectrin domain is needed for electrostatic interactions with acidic microtubules and is evolutionarily conserved within the protein family (Kellogg et al., 2016; Mollinari et al., 2002; Subramanian et al., 2013, 2010). Here, the spectrin domain forms a fixed ~70° angle with microtubules towards the minus end of microtubules and as a dimer, PRC1 selectively cross-links antiparallel microtubules (see Fig. 6C; Kellogg et al., 2016). The C-terminal region of PRC1 is unstructured and consists of β-sheets/turns with low complexity (Mollinari et al., 2002; Zhu et al., 2006). Within the C-terminal part, PRC1 has two cyclin-dependent kinase (Cdk) phosphorylation sites (Thr-470 and Thr-481) which are important for its regulation, activation, and proper spindle organization (Fu et al., 2007; Jiang et al., 1998; Mollinari et al., 2002). Additionally, Polo-like kinase 1 (PLK1) phosphorylation sites have been found at Thr-578 and Thr-602 and seem to be essential for the spatiotemporal regulation of PRC1 (Hu et al., 2012; Neef et al., 2007; Zhu & Jiang, 2005). Furthermore, the C-terminal region of PRC1 consists of several consensus motifs for ubiquitin-mediated proteolysis and cell cycle-dependent degradation like two destruction boxes (D boxes) and Ken box (Lysine-Glutamic acid-Asparagine box) (Glotzer et al., 1991; Pfleger & Kirschner, 2000). Finally, PRC1 has two nuclear localization signals (NLS) within amino acid 470-500 of the C-terminal domain (see Fig. 6B; Jiang et al., 1998; Mollinari et al., 2002). As mentioned above, whether PRC1 functions in the interphase of the cell cycle is still unclear (She et al., 2019).

PRC1 is highly expressed in several cancer types as for instance in lung, breast, hepatocellular, bladder, ovarian and gastric cancer (Bu et al., 2020; Chen et al., 2016; Kanehira et al., 2007; Shimo et al., 2007; Wang et al., 2017; Wolter et al., 2017; Zhan, Xi et al., 2017; Zhan, Zhang, et al., 2017; Zhang et al., 2017). Alterations in PRC1 expression are most likely due to copy number gains, amplifications or transcriptional dysregulation as seen in cancer cells (Li et al., 2018). A signature of chromosomal instability (CIN) was identified, in which PRC1 is the second-highest ranked gene out of 10,151 genes and is also listed in the top-ranked gene signature (CIN25) whose high expression is correlated with aneuploidy and worse patient expectations (Carter et al., 2006). Distinct outcomes of tumors are connected to PRC1 overexpression such as early recurrence of hepatocellular carcinoma (HCC; Chen et al., 2016), poor differentiation and large tumor size as well as high clinical grade in oral squamous cell carcinomas (Wu et al., 2018), lymph node metastasis and poor prognosis in lung adenocarcinoma patients (Zhan, Zhang et al., 2017), chemoresistance to 5-florouracil and taxol, and lower survival rate of hepatocellular carcinoma patients (Liu, Li, Meng et al., 2018; Wang et al., 2017).

In HCC, PRC1 was identified as a novel Wnt target. Here, PRC1 promotes the membrane sequestration of the destruction complex, inhibits APC stability and causes active β-catenin release from the APC complex to positively influence HCC metastasis and proliferation (Chen et al., 2016). PRC1 depletion of lung adenocarcinoma cells revealed that the expression of the protein significantly correlated with the Wnt signaling pathway. Moreover, PRC1 depletion impaired the proliferation of lung adenocarcinoma cells by a G2/M phase cell cycle arrest and apoptosis (Zhan, Zhang, et al., 2017). Thus, PRC1 might be a potential target for NSCLC (see Fig. 6D).

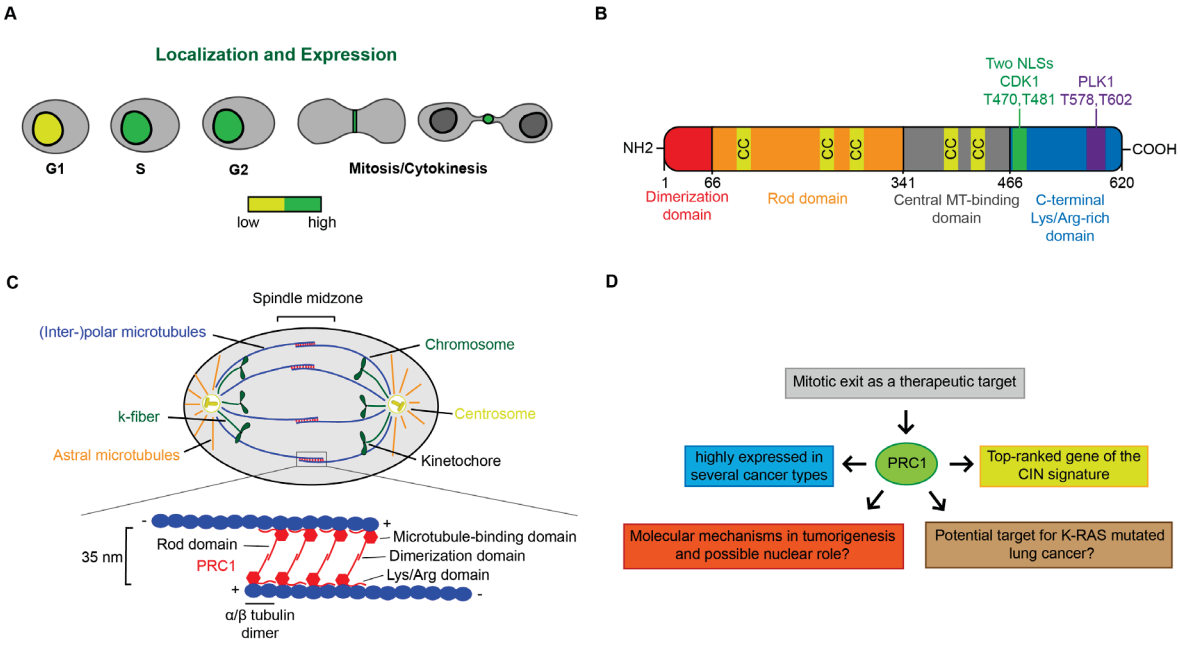

Figure 6: PRC1: Expression and localization, structural motifs, microtubule cross-linking and potential cancer target.
(A) Expression levels of PRC1 are cell cycle dependent with high level during S phase and G2/M phase and low levels when cells enter the G1 phase of the cell cycle. The protein localizes at the nucleus during interphase and then at the central spindle and midbody during mitosis and cytokinesis. (B) Schematic representation of the structural motifs of PRC1. CC, coiled coil; CDK1, cyclin-dependent kinase 1; NLS, nuclear localization signal; PLK1, Polo-like kinase 1. (C) Illustration of a mitotic cell. The spindle midzone is magnified, which highlights the cross-linking of two antiparallel microtubules by PRC1. (D) Scheme of PRC1 in the context of cancer.

1.5 Aim of the doctoral project

MMB, a key regulator of mitotic and late cell cycle genes, is required for lung tumor development. It was suggested to target downstream targets of MMB, which might have less side-effects, as a putative treatment strategy for lung cancer. Accordingly Iltzsche et al. reported that the depletion of MMB-target KIF23 inhibits lung tumor formation *in vivo* and induced apoptosis in lung cancer cell lines *in vitro* (Iltzsche et al., 2016).

The aim of the doctoral project was to characterize PRC1 in lung cancer, an additional MMB target gene that is involved in mitosis and cytokinesis. The role of PRC1 in tumorigenesis is not consistent over the studies and its putative nuclear function has not been described clearly. So, two main questions arise: Is PRC1 a potential therapeutic target for lung cancer? Has PRC1 additional functions besides its role during cell division, possibly in the nucleus during interphase?

To address those questions, one aim of this thesis was to generate lung cancer cell lines with different inducible expression constructs of PRC1, including a mutant version that is unable to enter the nucleus. A second aim was to obtain genome-wide expression data by RNA sequencing after ectopic expression PRC1 to better understand its possible nuclear functions. Another aim was to investigating PRC1 as a possible lung cancer target by determining the impact of PRC1 depletion *in vitro and in vivo* in a mouse model of lung cancer.

2 Material and Methods

2.1 Material

2.1.1 Chemical stocks and reagents

The following chemicals and reagents were used in this thesis. Enzymes, antibiotics, transfection reagents, protein and DNA markers, cell culture medium, buffers and solutions were listed separately in following tables. Chemicals and reagents from Table 3 were purchased from Sigma Aldrich, Merck, AppliChem, Thermo Fisher Scientific and Roth if not otherwise named.

Table 3: Chemical stocks and reagents

Chemical/reagent	Stock concentration
Acetic acid (CH_3COOH)	N/A
Agarose	N/A
Amonium persulfate (APS)	10% in ddH_2O
Ammonium sulfate ($(NH_4)_2SO_4$)	N/A
AMPure XP Beads (Beckman Coulter)	N/A
Bradford reagent	Ready to use
5-bromo-4-chloro-3-indolyl-β-D-galactopyranoside (X-Gal)	40 mg/ml in DMF
Bromphenol blue	N/A
Bovine serum albumin (BSA)	N/A
β-Mercaptoethanol, 14.3 M	Ready to use
Calcium chloride ($CaCl_2$)	2.5 M in ddH_2O
Cisplatin (AG Diefenbacher, Selleckchem)	1 mM in DMF
Citric acid ($C_6H_8O_7$)	N/A
Coomassie Brilliant Blue G250	N/A
Crystal violet	1% in ddH_2O
D-glucose	N/A
Diethyl pyrocarbonate (DEPC)	Ready to use
Dimethyl sulfoxide (DMSO)	Ready to use
Dithiothreitol (DTT)	1 M in ddH_2O
Deoxynucleotide Triphosphates (dNTPs)	2 mM in ddH_2O

HEPES	N/A
Ethylenediaminetetraacetic acid (EDTA)	N/A
Ethanol	N/A
Ethidium bromide, 10 mg/ml	Ready to use
Ficoll	N/A
Formaldehyde, 37%	N/A
Glycerol	N/A
Glycine	N/A
Hydrogen peroxide (H_2O_2), 30%	N/A
Hemalum solution acid acc. to Mayer	Ready to use
Hoechst 33258	10 mg/ml in ddH_2O
Isopropanol	N/A
Luminol	250 mM in DMSO
Luria Bertani (LB) Agar	40 g powder in 1 l H_2O, autoclaved
Low melting agarose	N/A
Magnesium chloride ($MgCl_2$)	1 M in ddH_2O
Magnesium sulfate ($MgSO_4$)	N/A
Methanol	N/A
Milk powder	N/A
Nutlin-3	4.3 mM in DMSO
Nocodazole	1 mg/ml in DMSO
Nonyl phenoxypolyethoxylethanol (NP-40)	N/A
Paraffin wax	N/A
Paraformaldehyde (PFA)	N/A
p-Coumaric acid	90 mM in DMSO
peqGOLD TriFast (Trizol; Peqlab)	Ready to use
Phenylmethylsulfonyl fluoride (PMSF)	100 mM in isopropanol
Polyethylene glycol (PEG) 6000	50% in ddH_2O (sterilized by autoclaving for cell culture use)
Polybrene (Hexadimethrine bromide)	4 mg/ml in ddH_2O
Potassium acetate (KH_3COO)	N/A
Potassium chloride (KCl)	N/A
Potassium dihydrogenphosphate (KH_2PO_4)	N/A

Potassium ferrocyanide ($K_4[Fe(CN)_6]$)	500 mM in ddH_2O
Potassium ferricyanide ($K_3[Fe(CN)_6]$)	500 mM in ddH_2O
Propidium iodide (PI)	1 mg/ml in ddH_2O
Protease inhibitor cocktail (PIC, P8340 from Sigma Aldrich)	Ready to use
Proteinase K	10 mg/ml in 50 mM Tris pH 8.0, 1 mM $CaCl_2$
ProtoGel (30%; Acrylamide) (national diagnostics)	Ready to use
Random primer (Roche)	500 µg/ml in ddH_2O
Shandon Immu-Mount	Ready to use
Sodium bicarbonat	1 M in ddH_2O
Sodium chloride (NaCl)	4 M in ddH_2O
Sodium dodecyl sulfate (SDS)	N/A
Sodium fluoride (NaF)	N/A
Sodium hydrogen phosphate (Na_2HPO_4)	N/A
Sodium hydroxide (NaOH)	N/A
Sodium orthovanadate (Na_3VO_4)	N/A
Sucrose	N/A
Tetramethylethylenediamine (TEMED)	Ready to use
Tetrasodium pyrophosphate ($Na_4P_2O_7$)	N/A
Tris(hydroxymethyl)aminomethan (TRIS)	N/A
Triton X-100	Ready to use
Thymidine	200 mM in ddH_2O
Tween-20	Ready to use
Xylene cyanol	N/A
Xylol	N/A

2.1.2 Enzymes

Table 4: Enzymes, reverse transcription buffer and SYBR mater mix

Enzyme/buffer	**Company**
His-Taq DNA Polymerase (15 U/µl)	Provided by the working group of Prof. Dr. Gessler
5x RT reaction buffer (for Reverse Transcriptase)	Thermo Fisher

Phusion Hot Start II DNA Polymerase [2 U/µl]	Thermo Fisher
RevertAid Reverse Transcriptase (RT) [200 U/µl]	Thermo Fisher
RiboLock RNase Inhibitor (RI) [40 U/µl]	Thermo Fisher
SYBR Select Master Mix	Thermo Fisher
SYBR Green Master Mix (SYBR Green I nucleic acid gel stain [S9430] 10,000 x in DMSO was diluted 1:10 in DMSO and then 1:200 in ddH_2O. 0.75 µl of the diluted SYBR Green was mixed with 3.5 µl of dNTPs (2 mM), 2.5 µl of 10x ReproFast buffer and 11.45 µl of ddH_2O and stored at -20°C)	Sigma Aldrich
T4 DNA Ligase	New England Biolabs
RNAse A (10 mg/ml in 10 mM Tris pH 7.4, 150 mM NaCl)	AppliChem
Restriction endonucleases (XhoI/EcoRI/BamHI) (10 U/µl)	Thermo Fisher/ New England Biolabs

2.1.3 Antibiotics

Table 5: Antibiotics for selection and induction

Antibiotic	Stock concentration	Final concentration	Application
Ampicillin	100 mg/ml	100 µg/ml	Selection of transformed bacteria
Blasticidin	10 mg/ml	5-6 µg/ml	Selection of cell lines
Doxycycline	1 mg/ml	see 2.2.2.1	Induction of shRNA or expression constructs of stable cell lines
Kanamycin	50 mg/ml	50 µg/ml	Selection of transformed bacteria
Neomycin	200 mg/ml	300-800 µg/ml	Selection of cell lines

2.1.4 Buffers and solutions

Table 6: General buffers

Buffer	Ingredients/formulation
1x Phosphate buffered saline (PBS)	13.7 mM NaCl
	0.3 mM KCl
	0.64 mM Na_2HPO_4
	0.15 mM KH_2PO_4
	Adjust pH to 7.4 with HCl

1x TAE buffer	40 mM Tris base
	5 mM CH_3COOH
	10 mM EDTA, pH 8.0
1x TE buffer	10 mM Tris/HCl, pH 7.5
	1 mM EDTA
1x Tris buffered saline (TBS)	50 mM Tris/HCl, pH 7.4
	150 mM NaCl
50 mM Tris-HCl pH 7.4	In ddH_2O, autoclaved for cell culture
2x HEPES buffered saline (HBS) pH 7.05	280 mM NaCl
	50 mM HEPES
	1.5 mM Na_2HPO_4
	Adjust pH with 5 M NaOH to 7.05, sterile filtered
Citric acid/sodium phosphate buffer	0.1 M Citric acid
	0.2 M sodium phosphate
	Mix both buffers
	Adjust to pH 6.0 and autoclaved
0.1% Crystal violet staining solution	1% Crystal violet dissolved in ddH_2O is diluted 1:10 in 20% ethanol
10% Acetic acid (CH_3COOH)	100% Acetic acid (CH_3COOH) is diluted 1:10 in ddH_2O
4% Paraformaldehyde (PFA)	4% PFA (40 g)
	100 ml 10x PBS (DEPC)
	3.5 ml 2 M NaOH (DEPC)
	Warm up to approx. 68 °C; adjust pH with 1 M HCl to 7.0; add to 1 l DEPC-H_2O
0.1% Eosin Y solution	Dilute 0.5% Eosin Y solution (Roth) in ddH_2O to 0.1% and add 1-2 drops CH_3COOH
Sodium citrate	38 mM in 1x PBS

Table 7: Buffers and solutions used for molecular biology

Buffer	**Ingredients/formulation**
Mini-preparation solution S1	25 mM Tris/HCl, pH 8.0
	10 mM EDTA
	100 µg/ml RNAse A

Mini-preparation solution S2	200 mM NaOH
	1% SDS
Mini-preparation solution S3	7.5 M KCH_3COO
	11.5 ml CH_3COOH
	28.5 ml H_2O
Luria Bertani (LB) liquid medium	25 g powder in 1 l H_2O, autoclaved
10x ReproFast buffer	100 mM $(NH_4)_2SO_4$
	200 mM Tris-HCl, pH 8.8
	100 mM KCl
	20 mM $MgSO_4$
	1% BSA
	1% Triton X-100
	Sterile filtered
5x Loading buffer	15% Ficoll
	0.05% Bromophenol blue
	0.05% Xylene cyanol
	0.05 M EDTA
DEPC water	1 ml DEPC is added per 1000 ml of ddH_2O to a final concentration of 0.1%, stirred until completely dissolved, and autoclaved earliest after 1 hour stay at room temperature
Base buffer	25 mM NaOH
	0.2 mM EDTA, pH 8.0
	Adjust pH to 12.0 with NaOH
Neutralization buffer	40 mM Tris-HCl, pH 5.0
Ear punching buffer	100 mM Tris-HCl pH 8.5
	5 mM EDTA
	0.2% SDS
	200 mM NaCl

Table 8: Buffers and solutions for protein biochemistry, SDS-PAGE and immunoblotting

Buffer	Ingredients/formulation
TNN lysis buffer	50 mM TrisHCl, pH 7.5
	120 mM NaCl
	5 mM EDTA
	0.5% NP-40
	10 mM $Na_4P_2O_7$
	2 mM Na_3VO_4
	100 mM NaF
	Adjust pH with 37% HCl to 7.5
Bradford solution	0.12 mM Coomassie Brilliant Blue G250
	23.75 ml ethanol
	50 ml 85% (v/v) H_3PO_4
	Add to 500 ml ddH_2O, twice filtered
0.5 M Tris, pH 6.8	0.5 M Tris base in ddH_2O
	Adjust pH with 37% HCl to 6.8
1.5 M Tris, pH 8.8	1.5 M Tris base in ddH_2O
	Adjust pH with 37% HCl to 8.8
10x SDS running buffer	1.9 M Glycine
	0.25 M Tris
	35 mM SDS
5x Blotting buffer	124 mM Tris
	0.75 M Glycine
	Autoclaved
3x ESB	300 mM Tris-HCl pH 6.8
	15 mM EDTA
	150 mM DTT
	12% (w/v) SDS
	15% (w/v) Glycerol
	0.03% Bromophenol blue
Ponceau S solution	0.1% Ponceau S
	5% CH_3COOH
20x TBS	1 M Tris-HCl
	3 M NaCl
	Adjust pH with 37% HCl to 7.4
TBS-T	1x TBS with 0.1% Tween 20

Enhanced chemiluminescence solution (ECL)	10 ml 100 mM Tris-HCl pH 8.5
	50 µl 250 mM Luminol
	22 µl 90 mM p-Coumaric acid
	3 µl 30% H_2O_2
Blocking solution	3% milk powder or BSA in TBS-T (w/v)

Table 9: Buffers and solutions for immunostaining and β-galactosidase assay

Buffer	**Ingredients/formulation**
PSP	3% paraformaldehyde
	2% sucrose
	Add to 500 ml in 1x PBS
PBS-T	0.1-0.2% Triton-X in 1x PBS (v/v)
Blocking solution	3% BSA in PBS-T (w/v)
X-gal staining solution	1 mg/ml X-Gal, 40 mM citric acid/sodium phosphate buffer (dibasic, each 200 mM), 5mM potassium ferrocyanide ($K_4Fe(CN)_6$), 5 mM potassium ferricyanide ($K_3Fe(CN)_6$), 150 mM NaCl, 2 mM $MgCl_2$

2.1.5 Kits and Protein/DNA markers

Table 10: Kits used for molecular biology and next-generation sequencing

Name	**Company**
PureLink™ HiPure Plasmid Filter Midi- or Maxiprep Kits	Thermo Fisher
QIAquick PCR Purification Kit	Qiagen
GeneJET Gel Extraction Kit	Thermo Scientific
RNeasy Mini Kit	Qiagen
NEBNext Multiplex Oligos for Illumina (Dual Index Primers Set 1)	NEB
NEBNext Poly(A) mRNA Magnetic Isolation Module	NEB
NEBNext Ultra II DNA library Prep Kit for Illumina	NEB

Table 11: Protein and DNA markers

Name	**Company**
DNA Ladder 100 bp	Thermo Fisher
GeneRuler 1 kb DNA Ladder	Thermo Fisher
PageRuler Prestained Protein Ladder, 10 to 180 kDa	Thermo Fisher

2.1.6 Transfection reagent, AnnexinV-FITC staining and cell culture media

Table 12: Transfection reagent and AnnexinV-FITC detection Kit

Reagent	Company
Lipofectamine 3000	Thermo Fisher
Lipofectamine RNAiMAX	Thermo Fisher
Opti-MEM (1X) + GlutaMAX	Thermo Fisher
eBioscience™ Annexin V-FITC Apoptosis Detection Kit	Thermo Fisher

Table 13: Cell culture media

Reagent	Company or Ingredients/formulation
DMEM (1x) + GlutaMAX	Thermo Fisher
RPMI Medium 1640 (1x) + GlutaMAX	Thermo Fisher
FBS	Thermo Fisher
Penicillin-Streptomycin (10,000 U/ml)	Thermo Fisher
Trypsin-EDTA (0.05%), phenol red	Thermo Fisher
RPMI freezing media	50% RPMI, 40% FBS, 10% DMSO
DMEM freezing media	50% DMEM, 40% FBS, 10% DMSO
2x DMEM soft agar medium	10x concentrated DMEM dilute to final concentration of 2x DMEM
	3,7% 1 M sodium bicarbonate
	20% FBS
	20 mM GlutaMAX
	9 mg/ml D-Glucose
	1% Pen-Strep
	Add H_2O to final volume

2.1.7 Bacteria strains, mouse strains and cell lines

Table 14: Bacteria strains, mouse strains and cell lines

Type	Name	Information	Reference
Bacteria strain	DH5α	genotype: F– Φ80lacZΔM15 Δ(lacZYA-argF) U169 recA1 endA1 hsdR17 (rK–, mK+) phoA supE44 λ– thi-1 gyrA96 relA1	Thermo Fisher
Bacteria strain	XL1-Blue	genotype: recA1 endA1 gyrA96 thi-1 hsdR17 supE44 relA1 lac [F´ proAB lacIqZΔM15 Tn10 (Tetr)].	Agilent Technologies

Mouse strain	C57BL/6	$Kras^{tm4Tyj}$ (K-$Ras^{LSL-G12D/+}$) mice were crossed with $Trp53^{tm1Brn}$ ($p53^{fl/fl}$) to get K-$Ras^{LSL-G12D/+}$; $p53^{fl/fl}$ mice	Marino et al. 2000; Jackson et al. 2001
Human cell line	HEK293TN	human embryonic kidney cells with constitutive expression of SV40 large T antigen and neomycin resistance gene	SBI Cat.-no.: LV900A-1
Mouse cell line	NIH/3T3-pZ/EG	embryonic fibroblasts (NIH/3T3) stably transfected with the GFP-reporter plasmid pZ/EG	Novak et al. (2000) Iltzsche et al. (2016)
Mouse cell line	NIH/3T3	embryonic fibroblasts	ATCC® CRL-1658™
Human cell line	A549	epithelial lung carcinoma cell line	ATCC® CCL-185™
Human cell line	BJ-hTERT	fibroblast immortalized, containing a human telomerase reverse transcriptase (hTERT) construct	ATCC® CRL-4001™
Human cell line	H460	large cell lung cancer cell line, epithelial	ATCC® HTB-177™
Human cell line	HOP62	lung adenocarcinoma cell line, epithelial	Mclemore et al., 1989
Human cell line	HOP92	lung adenocarcinoma cell line, epithelial	Mclemore et al., 1989
Human cell line	H23	lung adenocarcinoma cell line, NSCLC, epithelial	ATCC® CRL-5800™

2.1.8 Antibodies

Table 15: Primary antibodies

Name	Lab ID	Origin & Clonality	Application and dilution	Company	Catalog number
acetylated- α Tubulin	#315	Mouse monoclonal	Immunofluorescence 1: 200	Santa Cruz Biotechnology	sc-23950
α-Tubulin	#295	Mouse monoclonal	Immuno-blotting/ fluorescence 1:5000/ 1:200	Santa Cruz Biotechnology	sc-23948

β-actin	#196	Mouse monoclonal	Immunoblotting 1:5000	Santa Cruz Biotechnology	sc-47778
Cleaved Caspase-3	#184	Rabbit polyclonal	Immunoblotting 1:1000	Cell Signaling	9661
anti-Flag	#94	Rabbit polyclonal	Immunofluorescence 1: 100	Sigma-Aldrich	F7425
anti-Flag	#93	Mouse monoclonal	Immunoblotting 1:1000	Sigma-Aldrich	F3165
Cleaved PARP	-	Rabbit monoclonal	Immunoblotting 1:1000	Cell Signaling	5625
PRC1	#258	Rabbit polyclonal	Immuno-blotting/ fluorescence 1:1000/ 1:100	Santa Cruz Biotechnology	sc8356
p53	#239	Mouse monoclonal	Immunoblotting 1:1000	Santa Cruz Biotechnology	sc-126
p21	#146	Mouse monoclonal	Immunoblotting 1:1000	Calbiochem	OP64

Table 16: Secondary antibodies

Name	**Species Reactivity**	**Application and dilution**	**Company**	**Catalog number**
Alexa Fluor 488 anti-rabbit IgG (H+L)	Rabbit	Immunofluorescence 1: 500	Thermo Fisher	A-21206
Alexa Fluor 594 anti-mouse IgG (H+L)	Mouse	Immunofluorescence 1: 500	Thermo Fisher	A-11032
Alexa Fluor 700 anti-mouse IgG (H+L)	Mouse	Immunofluorescence 1: 500	Kind gift from Prof. Dr. S. Meierjohann	
anti-mouse HRP conjugated	Mouse	Immunoblotting 1:5000	GE Healthcare	NXA931
anti-rabbit HRP conjugated	Rabbit	Immunoblotting 1:5000	Thermo Fisher	656120
HRP Protein A	Rabbit	Immunoblotting 1:5000	BD Biosciences	610438

2.1.9 siRNAs, Oligos, Primers and Plasmids

Table 17: siRNA sequences

Name	Species	Stock concentration	Sequence (5' to 3')	Company
siControl #1	-	75 µM	UGGUUUACAUGUCGACUAA	Dharmacon
siControl #2	-	75 µM	UAGCGACUAAACACAUCAA	Eurofins Genomics
sip53	human	75 µM	GAGGUUGGCUCUGACUGUATdT	Eurofins Genomics
siPRC1	human	75 µM	ACGACCAUCUUGCAACUAG	Eurofins Genomics

Table 18: Oligos for cloning and sequencing

Name	Internal number	Sequence (5' to 3')
shPRC1-oligo	SG1728	TGCTGTTGACAGTGAGCGCGACGACCATCTTGCAACTAGATAGTGAAGCCACAGATGTATCTAGTTGCAAGATGGTCGTCTTGCCTACTGCCTCGGA
shLuc-oligo	SG1992	TGCTGTTGACAGTGAGCGCCCGCCTGAAGTCTCTGATTAATAGTGAAGCCACAGATGTATTAATCAGAGACTTCAGGCGGTTGCCTACTGCCTCGGA
Flag-PRC1 Forward gateway cloning	SG2475	AGGCTCCTGCAGGACCATGGATTACAAGGATGACGACGATAAGAGGAGAAGTGAGGTGCTGGC
PRC1 Reverse gateway cloning	SG2476	GAAAGCTGGGTCTCGAGCTATCAGGACTGGATGTTGGTTGAATTG
Flag-ΔN78 mutant_PRC1 Forward gateway cloning	SG2525	AGGCTCCTGCAGGACCATGGATTACAAGGATGACGACGATAAGCTGTGCAGCGAGTTACATGTTGAG
PRC1-siRNA_resistent Forward	SG2291	GGAGAGACGACCATCTTGCAGTTAGAAAAAGATTTGCGCAC
PRC1-siRNA_resistent Reverse	SG2292	GTGCGCAAATCTTTTTCTAACTGCAAGATGGTCGTCTCTCC

Mutagenesis PRC1 (R377A) Forward	SG2627	GAGAAAAGCTTCAGATCCAAATGCATTTACAAACCGAGGAGGAAATC
Mutagenesis PRC1 (R377A) Reverse	SG2628	GATTTCCTCCTCGGTTTGTAAATGCATTTGGATCTGAAGCTTTTCTC
Gateway cloning- attL1-T1	SG2437	CCCCGATGAGCAATGCTTTTTTATAATGCCAACTTTGTACAAAAAAGCAGGCTCCTGCAGGACCATG
Gateway cloning- attL2-T1	SG2438	GGGGGATAAGCAATGCTTTCTTATAATGCCAACTTTGTACAAGAAAGCTGGGTCTCGAGCTA
PRC1-oligo mouse (shRNA #19)	SG2198	TGCTGTTGACAGTGAGCGCCACATATATGTTGTTTTTAAATAGTGAAGCCACAGATGTATTTAAAAACAACATATATGTGTTGCCTACTGCCTCGGA
PRC1-oligo mouse (shRNA #16, #1560, #1570)	SG2200	TGCTGTTGACAGTGAGCGACCCAAGAAGTCTGGCAAAGTATAGTGAAGCCACAGATGTATACTTTGCCAGACTTCTTGGGCTGCCTACTGCCTCGGA
PRC1-oligo mouse (shRNA #14)	SG2199	TGCTGTTGACAGTGAGCGACCGAGATTGTACGGTTAAGAATAGTGAAGCCACAGATGTATTCTTAACCGTACAATCTCGGCTGCCTACTGCCTCGGA
shRNA-Oligo amplification Primers Forward	SG2052	TGAACTCGAGAAGGTATATTGCTGTTGACAGTGAGCG
shRNA-Oligo amplification Primers Reverse	SG2053	TCTCGAATTCTAGCCCCTTGAAGTCCGAGGCAGTAGGC
pINDUCER20-sequencing	SG2462	GGACGTCGTATGGGTATTCG
pINDUCER10/Ubc-shRNA-pgk-Cre-sequencing	SG1162	GCTTCGGCAGCACATATACTA
siRNA resistent-sequencing	SG2305	TTCAAGGAGGACGGCAACATCCTG
PRC1-R377A mutation sequencing	SG1891	TCGTGCCTTCAACTCTTCTTC

Table 19: Plasmids

Name	Internal number	Reference	Description
pInducer10-Blasti	#1369	Meerbrey et al., 2011 and subcloned by Dr. Marc Fackler	Lentiviral expression construct, inducible shRNA expression by doxycycline, blasticidin selection
pInducer20 (ORF-UN)	#1343	Meerbrey et al., 2011, Addgene#44012	Lentiviral expression construct, inducible cDNA expression by doxycycline, neomycin selection
pInducer20-Flag_PRC1_WT	#1591	Subcloned from #1343 by Steffen Hanselmann	See #1343 and #1564/1553, N-terminal flag-tagged wildtype PRC1 (620 amino acids) expression
pInducer20-Flag_PRC1_NLS3A	#1592	Subcloned from #1343 by Steffen Hanselmann	See #1343 and #1569/1554, expression of N-terminal flag-tagged NLS3A mutant version of PRC1
pInducer20-Flag_PRC1_ΔN78	#1602	Subcloned from #1343 by Steffen Hanselmann	See #1343, expression of N-terminal flag-tagged ΔN78 mutant version of PRC1 (lacks the first 78 amino acids of the 620 amino acids wildtype PRC1)
pInducer20-Flag_PRC1_WT_R377A	#1616	Subcloned from #1591 by Steffen Hanselmann	See #1591, mutation in the microtubule-bundling domain (Arg to Ala on position 377)

pInducer20-Flag_PRC1_NLS3A_R377A	#1617	Subcloned from #1592 by Steffen Hanselmann	See #1592, mutation in the microtubule-bundling domain (Arg to Ala on position 377)
pCMV-VSV-G	#1348	Stewart et al., 2003, Addgene#8454	Lentiviral envelope plasmid
psPAX2	#1386	Addgene#12259	Lentiviral packaging plasmid
Ubc-shRNA-pgk-Cre	#1492	Subcloned from pInducer backbone by Dr. Sabine Stopp	Cre-expressing lentiviral construct for intratracheal infection of K-Ras$^{LSL-G12D/+;}$ p53$^{fl/fl}$ mice
Ubc-shLuc-pgk-Cre	#1558	Subcloned from #1492 backbone by Dr. Sabine Stopp	See #1492, control shRNA against Luciferase
Ubc-shPRC1-pgk-Cre	#1560	Subcloned from #1492 backbone by Steffen Hanselmann	See #1492, shRNA against PRC1 (mouse)
pInd10-Blasti-shPRC1	#1471	Subcloned from #1369 by Dr. Patrick Wolter	See #1369, shRNA against PRC1
pInd10-Blasti-sLuc	#1449	Subcloned from #1369 by Dr. Sabine Stopp	See #1369, shRNA against Luciferase
pInd10-Blasti-shPRC1 (mouse)	#1570	Subcloned from #1369 by Steffen Hanselmann	See #1369, shRNA against PRC1 (mouse)
pEGFP-c2 -PRC1_WT	#1564	Chen et al., 2016	Mammalian expression vector, N-terminal EGFP sequence followed by PRC1 full-length (620aa)

			construct (wildtype), CMV promoter control
pEGFP-c2-PRC1_NLS3A	#1569	Chen et al., 2016	See #1564, PRC1 full-length construct but with mutation in the NLS (470-488, KR to AA and K to A, no nuclear localization
pEGFP-c2-PRC1_WT (siRNA-resistant)	#1553	Subcloned from #1564 by Steffen Hanselmann	See #1564, change in nucleotide sequence of PRC1 but same amino acid sequence (amino acid 98/99- nucleotide sequence 5'-3' caacta to cagtta)
pEGFP-c2-PRC1_NLS3A (siRNA-resistant)	#1554	Subcloned from #1569 by Steffen Hanselmann	See #1569, change in nucleotide sequence of PRC1 but same amino acid sequence (amino acid 98/99- nucleotide sequence 5'-3' caacta to cagtta)
pBABE-H2B-GFP	#746	pBABE vector backbone (Addgene#1764) and H2B-GFP (Addgene#11680) subcloned by Zsolt Magyari	GFP expression vector used to determine transfection efficiency

Table 20: PCR and qPCR Primers

Gene	**Internal number**	**Direction** Forward (FW) Reverse (RV)	**Primer sequence (5' > 3')**
PRC1 (qPCR)	SG1890	FW	TTTACAAACCGAGGAGGAAATC
	SG1891	RV	TCGTGCCTTCAACTCTTCTTC

GAPDH (qPCR)	SG645	FW	GCCCAATACGACCAAATCC
	SG646	RV	AGCCACATCGCTCAGACAC
p53 (qPCR)	SG771	FW	AGGCCTTGGAACTCAAGGAT
	SG772	RV	CCCTTTTTGGACTTCAGGTG
p21 (qPCR)	SG628	FW	TCACTGTCTTGTACCCTTGTGC
	SG629	RV	GGCGTTTGGAGTGGTAGAAA
LSL-K-RAS (genotyping)	SG2031	FW	GTCTTTCCCCAGCACAGTGC
	SG2032	RV	CTCTTGCCTACGCCACCAGCTC
	SG2033	FW	AGCTAGCCACCATGGCTTGAGTAAGTC TGCA
p53 (genotyping)	SG1556	FW	GGTTAAACCCAGCTTGACCA
	SG1557	RV	GGAGGCAGAGACAGTTGGAG

2.1.10 Devices

Table 21: Devices

Name	**Company**
Agarose gel electrophoresis system	Peqlab
Axio Vert.A1 FL-LED	Leica Microsystems
BP-310S Balance	Sartorius
Centrifuge 5415C	Eppendorf
Centrifuge 5415D	Eppendorf
Centrifuge 5417R	Eppendorf
Centrifuge Megafuge 1.0R	Heraeus
Clean Air CA/RE4 laminar flow cabinet	Clean Air
Cytomics FC 500 flow cytometer	Beckman Coulter
DynaMag-2 magnet	Thermo Fisher
Electrophoresis power supply E835	Consort
Experion automated electrophoresis station	Bio-Rad
Galaxy S incubator	Nunc
HERAcell incubator	Heraeus
Heraeus LaminAir HB 2448 S	Heraeus
Hyrax M 40	Carl Zeiss
KL 1500 LCD	Leica Microsystems
Laboratory water bath	GFL
Leica DFC350 FX digital camera	Leica Microsystems

Leica DMI 6000B inverted microscope	Leica Microsystems
Leica MC170 HD	Leica Microsystems
Min-PROTEAN 3 cell system	Bio-Rad
Mini Trans-Blot cell system	Bio-Rad
Multiskan Ascent plate reader	Labsystems
Mx3000P qPCR system	Stratagene
NanoDrop 2000 spectral photometer	Peqlab
Neubauer chamber	BRAND
NextSeq 500	Illumina
Nikon Eclipse TS100	Nikon
Nikon SMZ 1500	Nikon
PowerPac HC High-Current power supply	Bio-Rad
RNA fragment analyzer	Advanced Analytical Technologies
T1 Thermocycler	Biometra
Thermomixer compact	Eppendorf
Ultrospec 2100 pro spectrophotometer	Amersham Biosciences
VHX Multi Scan	Keyence
VH-Z20R 0x-200x	Keyence
Vortex-Genie 2 mixer	Scientific Industries

2.1.11 Software

Table 22: Software

Name	**Company/Reference**
ApE (v2.0.49.10)	A plasmid Editor by M. Wayne Davis https://jorgensen.biology.utah.edu/wayned/ape/
Adobe Illustrator (version 2017.0.2)	Adobe
Microsoft Office (2016)	Microsoft
CXP Acquisition and Analysis (Cytomics FC 500)	Beckman Coulter
Image J (1.49v)	https://imagej.nih.gov/ij/index.html
KM-plotter (see 2.5.9)	(Gyorffy et al., 2013) http://kmplot.com/analysis/
Leica Application Suite (LAS) 3.7	Leica Microsystems
Prism 5 (version 5.0)	GraphPad Software, Inc
Oncomine (see 2.5.9)	(Rhodes et al., 2004)

	www.oncomine.org
cBioPortal (see 2.5.9)	https://www.cbioportal.org/ (Cerami et al., 2012; Gao et al., 2013)
Galaxy	https://usegalaxy.org
HISAT2	(Kim et al., 2015)
FeatureCounts and limma	(Law et al., 2014; Liao et al., 2014; Liu et al., 2015)
Metascape	(Zhou et al., 2019)

2.2 Methods

2.2.1 Basic mammalian cell culture techniques

2.2.1.1 Cultivation of adherent cells

Human and mouse cell lines were cultured at 37°C with 5% CO_2. A549, H460. H23, HOP62 and HOP92 cell lines were cultured in GIBCO Roswell Park Memorial Institute (RPMI) 1640 medium containing 10% (v/v) fetal bovine serum (FBS) and 1% (v/v) penicillin-streptomycin. HEK293TN, NIH3T3 and immortalized BJ cell line were cultured in GIBCO Dulbecco's Modified Eagle Medium (DMEM) medium containing 10% FBS and 1% penicillin-streptomycin. Medium was changed after every two to four days.

2.2.1.2 Passaging and seeding of adherent cells

Confluent cell culture dishes or wells were washed once with 1x PBS followed by incubation with 0.05% Trypsin/EDTA for 5-15 min to detach adherent cells from culturing dishes or wells. Detachment was verified by light microscopy. Trypsinization was stopped by resuspension of the cells with medium containing FBS and penicillin-streptomycin. Cells were then seeded with lower densities depending on their proliferation rate into a new dish or well. For experiments cells were seeded with a defined cell number and is described in the methods part for each individual assay. Counting cells is described in 2.2.1.4.

2.2.1.3 Thawing and freezing cells

For freezing, cells were detached from cell culture dish by trypsinization as described above. Then, cells were resuspended with 9 ml fresh medium and transferred to a 15 ml reaction tube. Afterwards cells were centrifuged for 5 min at 300 x g at room temperature. The medium was discarded and the cell pellet was resuspended with 1 ml of freezing medium and transferred to a cryotube. Freezing medium contains 50% of either RPMI or DMEM or 25% DMEM and 25% Hams F12, 40 % FBS or horse serum and 10% DMSO depending of the used cell lines (see 2.2.1.1). Cryotubes were kept on ice shortly and then

placed at - 80°C for at least 24 hours up to 6 months. For long term storage, cells were kept in liquid nitrogen tanks.

Cells were thawed quickly in a 37°C water bath. Once the cells were thawed completely, they were transferred to a 15 ml reaction tube containing 9 ml fresh medium. The reaction tube was inverted and centrifuged for 5 min at 300 x g at room temperature. The cell pellet was resuspended with fresh medium and plated in a new cell culture dish or well.

2.2.1.4 Counting and seeding of cells

Cells were counted in a Neubauer chamber. Firstly, cells were detached from cell culture dishes by trypsinization as described above. Afterwards, cells were resuspended with 4 to 8 ml of medium depending on their cell density and then transferred to a 15-ml reaction tube. First, the tube was inverted, then 10 µl of the cell suspension was used to load on a Neubauer chamber between a cover slip. A Neubauer chamber is a glass plate with defined areas of squares. Cell numbers of four different squares were counted whereby cells were magnified by a light microscope. To get the cell numbers per milliliter, the mean of four squares was multiplied with 10,000 to get the cell number per milliliter.

Defined cell numbers were seeded in new dishes or wells for experiments and are summarized in Table 23.

Table 23: Seeded cell numbers for 4- or 8 days cultivation

	24-well	6-well	6-cm dish	10-cm dish	15-cm dish
A549	- 8d: 1500	4d: 1.5-6x 10^4 8d: 2.5-6x 10^3	4d: 5.5x 10^4 -	4d: 1.6x 10^5 -	- -
H460	- 8d: 1000	4d: 1.5-6x 10^4 8d: 2.5-6x 10^3	4d: 5-8x 10^4 8d: 1-3x 10^4	4d: 1-1.2x 10^5 -	4d: 3x 10^5 -
H23	- 8d: 1500	4d: 4-5x 10^4 -	4d: 1.2-2,5x 10^5 8d: 4-8x 10^4	4d: 2.5-5x 10^5 -	4d: 6x 10^5 -
HOP62	- 8d: 2000	4d: 1.8-4x 10^4 -	4d: 4-10x 10^4 8d: 2-4x 10^4	4d: 1.1x 10^5 -	4d: 3.04x 10^5 -
HOP92	- 8d: 1000	4d: 1.5-50x 10^4 -	4d: 4.5-6x 10^4 8d: 1-3x 10^4	4d: 0.9-1.25x 10^5 -	- -

NIH3T3	- 8d: 500	4d: 2x 10^4 -	4d: 2x 10^4 -	- -	- -
BJ hTERT	- 8d: 5000	4d: 3x 10^4 8d: 1.5x 104	- -	4d: 2.5x 10^5 -	- -

2.2.2 Experimental cell culture techniques

2.2.2.1 Treatment of cells with reagents

Table 24: Treatment of cells with reagents

reagent	usage	Description/concentrations
Doxycycline	Induction of PRC1-expressing constructs or shRNA	Cells were induced with 0.25-1 µg/ml doxycycline for 4 days and with 0.5 µg/ml doxycycline for 8 days. For proliferation assay concentrations of either 0.05-; 0.1-; 0.25-; 0.5-; 1 µg/ml of doxycycline or 0.01-; 0.025-; 0.05-; 0.1-; 0.25-; 0.5 µg/ml of doxycycline were used to induce the constructs or shRNA.
Neomycin	Selection	To select for stable integrated pInducer20 construct, 300-800 µg/ml of Neomycin were used for selection of cell lines.
Blasticidin	Selection	To select for stable integrated pInducer10 construct, 5-6 µg/ml of Blasticidin were used for selection of cell lines.
Cisplatin	Chemotherapeutic drug: treatment of lung cancer cells	A549 cells were treated with 0.5- or 1 µM of cisplatin for 6 days.
Thymidine	Cell synchronization	A549 cells were synchronized by 2 mM thymidine (24 hours thymidine incubation- 8 hours release- 16 hours second thymidine incubation).
Nutlin-3	Stabilization of p53	Cells were treated with 2.5 µM of Nutlin-3 for 4 days.

Nocodazole	Microtubule depolymerization	Cells were treated with 1 µg/ml of nocodazole for 1.5 hours

2.2.2.2 Transient transfection methods

2.2.2.2.1 Calcium phosphate transfection for lentivirus production

HEK293TN cells were used for lentivirus production. Cells were seeded one day before transfection. For a 6-cm dish 1.2-1.4x 10^6, for a 10-cm dish 2.5-3x 10^6 and for a 15-cm dish 10x 10^6 cells were seeded. Before transfection old medium was replaced by 2 ml (6-cm dish) or 6-7 ml (10-cm dish) or 12-14 ml (15-cm dish) of fresh medium. First, DNA was mixed in a sterile tube and 25 µl (6-cm dish) or 50 µl (10-cm dish) or 125 µl (15-cm dish) 2.5 M $CaCl_2$ was added. Then, the volume was filled up with sterile ddH_2O to 250 µl (6-cm dish) or 500 µl (10-cm dish) or 1250 µl (15-cm dish). The same volume of 2x HBS was added to a sterile tube. A pipette aid and a Pasteur-pipette were used to keep 2x HBS solution under constant bubbling and meanwhile the DNA/$CaCl_2$/ddH_2O mixture was added dropwise to 2x HBS solution. Finally, 500 µl (6-cm dish), 1000 µl (10-cm dish) or 2500 µl (15-cm dish) of the solution were added dropwise to the adherent cells in a way that whole dish was covered. Cells were gently shaken and then directly brought to the (BSL2) cell culture. As a control for transfection efficiency, one dish was transfected with a construct expressing a green fluorescent protein (GFP, pBABE-H2B-GFP, #746).

2.2.2.2.2 RNAi MAX transfection

1-2x 10^5 (6-well) or 1-5x 10^5 (6-cm) cells were seeded one day before transfection. Medium was replaced by 1.5 ml or 2 ml of medium containing 10% FBS but without penicillin-streptomycin for 6-well or 6-cm dish. Solution A and B were prepared as described in Table 25. Solution A contained siRNA (for siRNA list see Table 17) in Opti-MEM medium and solution B contained Lipofectamine RNAiMAX in Opti-MEM medium. Solutions were incubated separately for 5 min at room temperature and then solution A was transferred and gently mixed with solution B. After an incubation time of 15 min at room temperature, the cells were transfected by pipetting 0,5 ml (6-well) or 1 ml (6-cm) of the mixture dropwise to the cells so that the total area of the well was covered. After 4- to 5 hours or at the latest on the next day, the medium was replaced by fresh medium containing 10% FBS and 1% penicillin-streptomycin or the cells were re-seeded for experiments.

Table 25: RNAiMax transfection solutions

	6-well	6-cm
Solution A	15- or 30 nM siRNA added to final volume of 300 µl Opti-MEM	15- or 30 nM siRNA added to final volume of 600 µl Opti-MEM
Solution B	3- to 6 µl of Lipofectamine RNAiMAX added to final volume of 300 µl Opti-MEM	6- to 12 µl of Lipofectamine RNAiMAX added to final volume of 600 µl Opti-MEM

2.2.2.3 Lentivirus production

HEK293TN cells were transfected for lentivirus production by the calcium phosphate method described in 2.2.2.2.1. The following DNA amounts were used for transfection:

Table 26: DNA amount for transfection and lentiviral production

	6-cm dish	10-cm dish	15-cm dish
Lentiviral construct (see Table 19)	3 µg	6 µg	24 µg
CMV-VSVg (#1348)	1,5 µg	3 µg	8 µg
psPAX2 (#1386)	2,25 µg	4,5 µg	16 µg

As a control of transfection efficiency, a GFP-encoding vector (pBABE-H2B-GFP, #746) was transfected (same DNA amount). Cells for lentivirus production were cultured under biosafety level 2 (BSL2) conditions. On the next day, the medium of the transfected cells was changed (2.5 ml- 6-cm dish; 7.5-8 ml- 10-cm dish; 15 ml- 15-cm dish). 48- and 72 hours after transfection, virus-containing medium was collected and filtered through a 0.45 µm pore size filter. The virus-containing medium was stored up to 1 week at 4°C or at -80°C for longer storage.

2.2.2.4 Lentivirus concentration using PEG precipitation

Lentivirus was produced as described in 2.2.2.3. Per milliliter virus-containing medium, 106.4 µl of 4 M NaCl, 114.2 µl of 1x PBS and at last 250 µl of 50% polyethylene glycol 6000 (PEG_{6000}) were added as published before (Kutner et al., 2009). This mixture was inverted every 20- to 30 min for a total time of 1.5 hours and kept at 4°C the whole time. Lentiviruses were pelleted by a centrifugation step at 4500 rcf for 30 min at 4°C. The supernatant was aspirated completely and 5.88 µl of 50 mM Tris HCl (pH 7,4) was used per milliliter of original supernatant to resuspend the virus-containing pellet. The virus was aliquoted and stored at -80°C.

2.2.2.5 Lentivirus titration using flow cytometry

To determine the titer of lentiviruses expressing Cre recombinase, a reporter cell line NIH/3T3-pZ/EG was used (Novak et al., 2000). This cell line expresses a GFP signal upon Cre-mediated recombination.15,000 cells were seeded in a 24-well plate 24 hours before infection. Just before infection of the cells, the cell numbers of three wells were determined. Medium was replaced by one milliliter of fresh medium without penicillin-streptomycin. Then, a serial dilution of the virus was prepared (see Table 27). A negative control was also performed. The cells were infected with 10 µl of different dilutions in duplicates.

Table 27: Serial dilution of lentivirus for titer determination

	dilution factor	volume of lentivirus	Volume of medium
1	-	-	-
2	1:40	1 µl of concentrated lentivirus	39 µl medium
3	1:80	20 µl of 2	20 µl medium
4	1:160	20 µl of 3	20 µl medium
5	1:320	20 µl of 4	20 µl medium
6	1:640	20 µl of 5	20 µl medium

On the next day, the medium was replaced by fresh medium. Two days post-infection, GFP-positive cells were determined by flow cytometry. Transducing units (TU) were calculated by the following formula:

TU/ml = [(%GFP-positive cells/100) x cell number just before infection x dilution factor]/ volume

Dilutions with 1- to 40% GFP positive cells were used for titer calculation.

2.2.2.6 Generation of stable cell lines

For generating stable cell lines, 3-15x 10^4 cells of parental cell lines were seeded one day before infection in 6-well plates. Lentivirus was produced according 2.2.2.3. However, 48 hours after transfection of HEK293TN cells, virus-containing medium was filtered through a 0.45 µm pore size filter. Then, virus-containing medium was mixed 1:1 with fresh medium (depending on the cell line, see 2.2.1.1) and 4 µg/ml of Polybrene was added. The medium of the parental cells was replaced by virus-containing medium for infection of the cells. After 24 hours of infection, the cells were washed several times with 1x PBS and afterwards fresh medium was added. Depending on their confluency, the cells were seeded either on a larger cell culture dish after around 8 hours or left in the 6-well plates. On the next day, the selection process started to get cells which successfully integrated and expresses the

lentiviral construct (see Table 24 for selection). As a control for the selection process, non-infected cells were treated with the same amount of antibiotics.

2.2.2.7 tRFP measurement by flow cytometry

Cell lines, which were lentivirally transduced with pInducer10 vector (Meerbrey et al., 2011), express turbo red fluorescence protein (tRFP)-shRNA cassette upon addition of doxycycline. The cell lines were seeded in 6-cm dishes (see Table 23) and shRNA directed against PRC1 or luciferase control were induced (see Table 24) about 5 hours post-seeding. After 2 days, the medium was replaced by fresh medium and the cells were cultured for 4 days in total. Then, the cells were detached from the cell culture dishes and washed once with 1x PBS. tRFP expression was determined by flow cytometry. Non-induced cells were used as a reference.

2.2.2.8 Proliferation assay

The cells were seeded in 24-well plates (see Table 23) in triplicates for treatment with different doxycycline concentrations (see Table 24). The cells were fixed after 2-, 4-, 6-, and 8 days. As a reference, cells were also fixed at day 0. Before fixation, the cells were washed once with 1x PBS and then fixed by 3.7% paraformaldehyde in ddH_2O for 10 min. Afterwards, the cells were washed twice with ddH_2O and then dried overnight (O/N) at room temperature. The cells were stained by 0.1% crystal violet in 20% ethanol for 30 min and afterwards washed twice with ddH_2O and dried O/N at room temperature. The proliferation was documented by scanning the plates and for quantification, crystal violet was extracted by 500 µl of 10% acetic acid while shaking for at least 30 min. Then, 100 µl were transferred to a 96-well plate. The different densities of crystal violet were determined by photometric measurements at 595 nm with Multiskan Ascent plate reader.

2.2.2.9 Cell cycle analysis by flow cytometry

Cells were seeded in 6-cm dishes for 4- or 8 days of cultivation (see Table 23). For cell cycle analysis, cells were detached from the cell culture dishes and centrifuged together with collected supernatant for 5 min at 1200 rpm at 4°C. Then, cells were washed with 5 ml ice cold 1x PBS once. Afterwards, cells were fixed by dropwise adding of 1 ml ice cold 80% ethanol while vortexing the reaction tube. The cells were kept at 4°C O/N or for several hours at -20°C. Then, cells were centrifuged for 10 min at 1500 rpm at 4°C and washed once with 1x PBS. The cells were resuspended in 525 µl 38 mM sodium citrate and 500 µg/ml RNase A. After an incubation time of 30 min at 37°C, 15 µl of propidium iodide (1 mg/ml) were added and cells were transferred to flow cytometric tubes. The cell cycle profile was determined by flow cytometry.

2.2.2.10 Cell synchronization- Double thymidine block

A549 cells were seeded in 6-well dishes, 6-cm dishes or 15-cm dishes one day before starting the thymidine block. For cells, which were not synchronized, 30,000 (6-well), 100,000- (6-cm) or 720,000 (15-cm) cells were seeded. Cells, which were used for synchronization, were seeded twice as much as asynchronous cells. On the next day, the cells were synchronized by adding 2 mM thymidine to the cell culture medium for 24 hours. Then, the cells were released for 8 hours by washing twice with 1x PBS and adding complete medium to the cells, followed by a second thymidine block for 16 hours. The cells were fixed directly after second thymidine block or released for 3-, 6- and 8 hours for immunofluorescence staining (see 2.2.3.1), flow cytometry (see 2.2.2.9), RNA isolation (see 2.2.4.1) or protein extraction (see 2.5.6.1).

2.2.2.11 Soft agar assay

The soft agar assay is used to analyze colony formation in an anchorage independent growth assay. A549 and HOP92 cells were able to grow under these culturing condition and 10,000 cells were seeded in each single 6-well in the top layer. First a base layer of 1.4% low melting agarose was mixed 1:1 with 2x DMEM soft agar medium (see Table 13) and 2 ml were added to each well. After the base layer was solid, 2 ml of the top layer consisting of a mixture (1:1) of 0.7% low melting agarose and 2x DMEM soft agar medium was added on the base layer. Before, the top layer was resuspended with a defined cell number. For the induction of the shRNA, 0.5 µg/ml of doxycycline were added directly to the soft agar medium. The cells were cultivated for 14- or 18 days and fed every 3 days. Colony formation was analyzed by microscopy.

2.2.3 Staining of cells for microscopy

2.2.3.1 Immunofluorescence staining

Cells were seeded in 6-well dishes (see Table 23) on cover slips. For immunofluorescence staining, the cells were first washed once with 1x PBS and then fixed with PSP (3% paraformaldehyde, 2% sucrose in 1x PBS) for 10 min. The cells were washed three times with 1x PBS. Afterwards, cell membranes were permeabilized by incubation with 1x PBS and 0.2% Triton X-100 for 5 min. Then, the cells were washed twice with 1x PBS/0.1% Triton X-100 (PBS-T) and blocked for 20 min with 3% BSA in PBS-T. The cells were incubated with first antibody diluted in blocking solution (see Table 15) for 1 hour at room temperature (RT) in a humidified chamber. The cells were washed three times with PBS-T and then incubated with secondary antibody (see Table 16) diluted 1:500 in blocking solution together with Hoechst 33258 for 30 min at RT in a light protected in a humidified chamber. The Hoechst solution was diluted between 1:500 and 1:1000. Afterwards, the

cells were washed three times with PBS-T or 1x PBS followed by mounting on a glass slide using ImmuMount. Finally, cover slips were sealed with nail polish and stored at 4°C in the dark. Slides were analyzed at the fluorescence microscope (Leica DMI 6000B microscope).

2.2.3.2 Annexin V-FITC staining

Cells were seeded in 24-well dishes (see Table 23) for 8 days or re-seeded after siRNA transfection (see 2.2.2.2.2) for 3 days. The cells were washed twice with 1x PBS and incubated with Annexin V-FITC in 1x binding buffer (1:40-1:50) for 10 min according to manufactures protocol. Samples were protected from light. After the incubation step, the samples were washed twice with 1x binding buffer. Apoptotic cells were determined by fluorescence microscopy.

2.2.3.3 Senescence-associated β-galactosidase assay

This cytochemical assay has been described to detect β-galactosidase activity and is based on the production of a blue-dyed precipitate by cleavage of chromogenic substrate X-Gal specific in senescent cells (Dimri et al., 1995). Cells were seeded for 4- and 8 days in a 6-well (see Table 23). Cells were fixed with 3.7% formaldehyde in 1x PBS for 5 min and then washed twice with 1x PBS. X-gal staining solution (see Table 9) was added to the cells. An incubation step followed at 37°C and 5% CO_2 for 12-16 h protected from light. Afterwards cells were washed twice with 1x PBS. Samples were analyzed by microscopy.

2.2.4 Molecular biological methods part 1- RNA and cDNA

2.2.4.1 RNA isolation

Cells were seeded in a 6-well or a 6-cm dish for RNA isolation (see Table 23). peqGOLD TriFast from Peqlab was used for whole RNA isolation. The medium was removed completely before 1 ml of TriFast was added. Cells were lysed and detached from wells or dishes by pipetting several times up and down while gently shaking. Lysed cells were transferred to a 1.5 ml tube and stored at -80°C or incubated for 5 min at room temperature. Then, 200 µl of Chloroform were added and the tube was vortexed for 15 s and incubated for 3 min at room temperature. After a centrifugation step at 11,400 rpm for 10 min at 4°C, the aqueous phase was transferred to a fresh tube. Afterwards, 500 µl of isopropanol was added and the RNA was pelleted after 10 min incubation at 4°C. The RNA pellet was washed twice with 75% ethanol (9,000 rpm centrifugation). After a 5-10 min air drying step, the RNA pellet was dissolved in 20-25 µl of DEPC-H_2O. The RNA concentration and purity were determined by the NanoDrop 2000 spectrophotometer. The RNA was stored at -80°C.

2.2.4.2 cDNA synthesis

1-2.5 µg of RNA was used for reverse transcription of the RNA into complementary DNA (cDNA). The RNA was mixed with 0.5 µl of random primers (0.5 mg/ml) and adjusted to 10 µl of volume with DEPC-H_2O on ice. This mix was incubated for 5 min at 70°C and then kept at 4°C. A second mix, containing 5 µl of 5x RT reaction buffer, 6.25 µl of dNTPs (2 mM), 0.5 µl of RiboLock RNase Inhibitor, 0.5 µl of RevertAid Reverse Transcriptase and 2.75 µl of DEPC-H_2O were gently mixed and kept on ice. Both, RNA mix and reverse transcriptase mix were mixed together and placed into the thermocycler. cDNA synthesis took place at 37°C for 1 h followed by a 15 min step at 70°C. The cDNA was kept at 4°C or stored at -20°C.

2.2.4.3 Quantitative real-time PCR

Quantitative real-time PCR (qRT-PCR) was used to analyze the relative expression of specific genes compared to another sample (reference) after normalization to the expression of a housekeeping gene (GAPDH).

For preparing the individual qRT-PCR master mix, 18.2 µl of SYBR Green Master Mix was mixed with 0.75 µl of forward primer (10 µM), 0.75 µl of reverse primer (10 µM) and 0.3 µl of His Taq polymerase (HisTaq16 [5 U/µl]) to a final volume of 20 µl. 20 µl of the qRT-PCR master mix and 5 µl of 1:16 diluted cDNA (see 2.2.4.2) was pipetted into a 96-well plate in triplicates. A negative control without cDNA was pipetted for each master mix. The 96-well plate was sealed with a transparent foil and centrifuged shortly at 4°C. qRT-PCR was measured using the Stratagene Mx3000P qPCR cycler with the cycling program showed in Table 28.

Table 28: Normal 3 Step qRT-PCR program

Temperature [°C]	Time [s]	Cycles	Description
95	120	1	initialization
95	15	40	amplification
60	30		
72	30		
95	15	1	melting curve
60	15		
95	15		

The relative expression of a sample was calculated as the comparative C_t method and is described below:

$$2^{-\Delta\Delta Ct}$$

$$\Delta Ct = Ct \text{ (gene of interest)} - Ct \text{ (housekeeping gene)}$$

$$\Delta\Delta Ct = \Delta Ct \text{ (sample)} - \Delta Ct \text{ (reference)}$$

The standard deviation was calculated according the formula below:

$$s = \sqrt{s_1^2 + s_2^2}$$

s1 = standard deviation of gene of interest
s2 = standard deviation of housekeeping gene

The error of $2^{-\Delta\Delta Ct}$ used for error bars was calculated as followed using the error margin:

$$(2^{-\Delta\Delta Ct + s}) - (2^{-\Delta\Delta Ct})$$

2.2.5 Molecular biological methods part 2- Cloning and DNA

2.2.5.1 Cloning of mouse shRNA sequences of PRC1 into lentiviral vectors

First, murine shRNA oligonucleotides were cloned into pInducer10_Blasti (#1369, see Table 19) vector (Meerbrey et al., 2011) and the knockdown efficiency was tested in a cell culture system. shRNA sequences which showed the best depletion were used for cloning into the hUbc_shRNA_pgk-cre (#1492, see Table 19) vector for lentivirus production and infection of mice (see 2.2.2.3-2.2.2.5; 2.5.8). Murine shRNA sequences are from Fellmann et a., 2013 and shown in Table 18 (Fellmann et al., 2013). Primers for PCR amplification contained XhoI and EcoRI overhangs. PCR was performed as shown in Table 29.

Table 29: PCR composition and PCR program for shRNA-oligo amplification

PCR composition	Volume	PCR program	Time	Cycles
shRNA-oligo (100 µM) (see Table 18)	1 µl	95°C	3 min	1x
His-Taq polymerase (15 U/µl)	0.5 µl	95°C	45 sec	29x
10x ReproFast buffer	5 µl	54°C	30 sec	
dNTPs (2mM)	5 µl	72°C	1 min	
Primer SG2052 (10 µM)	2 µl	72°C	10 min	1x
Primer SG2053 (10 µM)	2 µl	10°C	holding	
H_2O	34.5 µl			

After PCR amplification, the PCR product was purified by a preparative 2.5% agarose gel electrophoresis (see 2.2.5.7) using the GeneJet Gel Extraction Kit (Thermo Scientific) according the manufacturers` protocol. The purified PCR product and vector (see Table 19) were digested with XhoI and EcoRI as described in Table 30.

Table 30: Digestion of PCR product and pInducer10 vector for cloning

Compound	Amount/Volume	Temperature	Time
DNA	5 µg vector/total PCR product	37°C	4 hours
NEB4 buffer	5 µl		
BSA (10 mg/ml)	0.5 µl		
XhoI	1 µl		
EcoRI-HF	0.5 µl		
H_2O	add to 50 µl final volume		

After digestion, the vector was purified on a 0.8% agarose gel as described above. The PCR product was purified by the GeneJet Gel Extraction Kit (Thermo Scientific) (adding 150 µl of binding buffer and then 100 µl of isopropanol and then following the protocol) or by using a PCR Purification Kit from Qiagen, following the manufacturer's protocol. The DNA concentration was determined by a NanoDrop 2000 spectral photometer (Peqlab). Then, a ligation reaction was set up according Table 31.

Table 31: Ligation reaction and conditions for shRNA cloning

Compound	Amount/Volume	Conditions
Vector	25-100 ng or 1µl	16°C overnight
PCR product	4 ng or 2 µl	
T4 DNA Ligase	0.5 µl	
10x Ligase buffer	1 µl	
H_2O	Add to 10 µl final volume	

The ligation reaction was heat inactivated for 10 min at 65°C and then the reaction mixture was stored at -20°C or was used for transformation into chemically competent bacteria as explained in 2.2.5.4. Afterwards, a Mini plasmid DNA purification (see 2.2.5.5) was performed and the isolated DNA was used for a control digest (see Table 32).

Table 32: Control digestion of cloned mouse KIF4 and PRC1 into lentiviral vectors

Mix 1	Mix2	Volume	Conditions
Mini-DNA	Mini-DNA	3 µl	37°C, 1.5 hours
BamHI buffer	NEB 1 buffer	2 µl	
BamHI	KpnI	0.2 µl	
H_2O	H_2O	14.8 µl	

Then, the DNA was separated by a 1% agarose gel electrophoresis (see 2.2.5.7) and checked for the correct size. A plasmid editor program (ApE) was used for *in silico* cloning

and comparing sequences from plasmid maps and analyzing results from sequencing. Mini-DNA, which had the correct size, was purified by agarose gel electrophoresis by the GeneJet Gel Extraction Kit (Thermo Scientific). Here, the DNA was filled up to a volume of 200 µl with TE buffer and then 200 µl binding buffer from the GeneJet Gel Extraction Kit (Thermo Scientific) as well as 200 µl H_2O were added and mixed. Further purification was performed according the manufacturer's protocol. 1 µg of the purified plasmid DNA was diluted in 15 µl of H_2O and 2 pmol of a sequencing primer (SG1162) was added and the mixture was sent for sequencing to Eurofins.

2.2.5.2 Cloning strategy and cloning of vectors for ectopically expression of PRC1 and mutational versions of PRC1 in human cell lines

The different expressing constructs of PRC1 were cloned into pInducer20 (Meerbrey et al., 2011) backbone by direct gateway cloning according to Gateway Technology from Thermo Fisher Scientific. The concept in this approach was to design primers of the gene of interest with overhangs which could be further used after amplification for a second PCR. Then, the product of the second PCR amplification could be used for the LR reaction. As a source for amplification of the PRC1 constructs, plasmids from 2.2.5.3 were used which had nucleotide changes in the PRC1 sequence so that they are resistant to siRNA treatment without a change in the amino acid sequence. Three different primer constructs of PRC1 were designed by using plasmid editor program (ApE) (see Table 33) and used for the first-round PCR amplification (see Table 34).

Table 33: First round Primers with overhangs for gateway cloning

Forward Primer for amplification of PRC1 product (SG2475)	Part of attL1/Kozak/Start-Codon/Flag-tag/PRC1 start
	AGGCTcctgcagg/ACC/ATG/gattacaaggatgacgacgataag/aggagaagtgaggtgctggc
Forward Primer for amplification of -ΔN78 mutant of PRC1 (SG2525)	Part of attL1/Kozak/Start-Codon/Flag-tag/PRC1 start at position 234
	AGGCTcctgcagg/ACC/ATG/gattacaaggatgacgacgataag/ctgtgcagcgagttacatgttgag
Reverse Primer for amplification of PRC1 product (SG2476)	Part of attL2/Stopp-Codon/ Stopp-Codon/PRC1 end
	GAAAGCTGGGTctcgag/CTA/tca/ggactggatgttggttgaattg

Table 34: First round PCR reaction for gateway cloning

PCR composition	Amount/Volume	PCR program	Time	Cycles
Template DNA (#1553 for WT/ΔN78 or #1554 for NLS3A)	15 ng	98°C	30 sec	1x
FW Primer SG2475 or SG2525 (10 µM)	1 µl	98°C	10 sec	30x
RV Primer SG2476 (10 µM)	1 µl	66.3°C for Wt and NLS3A 69.8°C for ΔN78	30 sec	
5x Phusion Buffer HF	10 µl	72°C	60 sec for WT and NLS3A 30 sec for ΔN78	
dNTPs (2 mM)	5 µl	72°C	10 min	1x
ddH_2O	add to 50 µl	10°C	holding	
Phusion Polymerase (2 U/µl)	0.5 µl			

After the first round of PCR amplification, the PCR product was purified by 0.9% agarose gel electrophoresis and gel extraction using the GeneJet Gel Extraction Kit (Thermo Scientific) according to the manufacturers` protocol. Second, a PCR was performed by using the same PCR conditions as in Table 34 and using primer pairs SG2437/SG2438 (see Table 18) with an annealing temperature of 63.1°C. The second PCR product was purified as described for the first PCR product and was then used for gateway cloning shown in Table 35.

Table 35: Gateway cloning of PCR fragments into pInducer20 backbone

Compound	Amount/Volume
PCR fragment (second PCR reaction)	150 ng
pInducer20 (#1343, see table 19)	300 ng
TE buffer	add to 8 µl
mix	
Clonase II mix	2 µl
18 hours at 25°C	
Proteinkinase K	1 µl
10 min at 37°C	
Storage at -20°C or 3 µl for transformation into competent bacteria	

After transformation into competent bacteria and Mini-DNA purification, the DNA was used for a control digestion with BamHI as described in Table 32. Then, the DNA was purified with the GeneJet Gel Extraction Kit (Thermo Scientific) as described above and sent for sequencing by using the primer SG2462 (10 µM, see Table 18).

2.2.5.3 Mutagenesis of the PRC1 sequence

Mutagenesis of the PRC1 sequence was performed according the QuikChange Site-Directed Mutagenesis Kit instruction manual (Agilent). A plasmid editor program (ApE) was used for *in silico* cloning. As a source of the PRC1 sequence, Chen et al., 2016 provided us pEGFP-c2-PRC1-FL- and pEGFP-c2-NLS-3A- constructs which were explained in Supplementary Figure 6 in their publication (Chen et al., 2016) (internal number #1564 and #1569). The siRNA sequence against PRC1 (see Table 17) was designed which additionally had overlaps to our shRNA sequence (plasmid number #1471, 97-oligo SG1728). Primers were designed containing the desired mutations (see Table 18; SG2291/SG2292 or SG2627/SG2628) and were used for a PCR reaction (see Table 36). To generate a siRNA resistant sequence, the nucleotide sequence of amino acid (AA) 98 and 99 of the 620 AA protein was changed in a way that the same AA sequences were kept (5'-3' caacta -> caGTta). For PRC1 mutagenesis in the microtubule binding (MTB) domain, AA Arginine was changed at position 377 to Alanine (5'-3' cga -> GCa). This AA change was suggested to weaken the binding of PRC1 to microtubules and in a biochemical assay the binding was reduced to about 50% (Kellogg et al., 2016; Subramanian et al., 2010).

Table 36:PCR reaction for mutagenesis of nucleotides in the siRNA recognition site and microtubule-binding domain of PRC1

PCR composition	Amount/Volume	PCR program	Time	Cycles
DNA template **- siRNA resistant:** **#1564 or #1569** **- R377A mutagenesis:** **#1616 or #1617**	50 ng (1 µl)	98°C	30 sec	1x
Forward Primer (10 µM) **- siRNA resistant: SG2291** **- R377A mutagenesis: SG2627**	1 µl	98°C	15 sec	15x
Reverse Primer (10 µM) **- siRNA resistant: SG2292** **- R377A mutagenesis: SG2628**	1 µl	55°C	1 min	
5x Phusion Buffer HF	10 µl	72°C	4 min	
dNTPs (2 mM)	5 µl	72°C	10 min	1x
Phusion Polymerase	1 µl	10°C	holding	
ddH_2O	31 µl			

After the PCR reaction, the non-mutated parental strand DNA template was digested with DpnI. 1 µl of DpnI were added directly to the PCR tube and incubated for 2 hours at 37°C. Then, 5 µl of the plasmid DNA were transformed into XL1-Blue supercompetent bacteria. 0.85 µl of β-Mercaptoethanol was added to 50 µl of XL1-Blue bacteria suspension and gently shaken every 2 min for 10 min in total. Then, 5 µl of the plasmid DNA was added to the bacteria suspension and mixed gently. After an incubation time of 30 min on ice, a heat shock was performed at 42°C for 45 sec. Subsequently, the bacteria were placed on ice for 2 min and then resuspended with pre-warmed LB medium. After 1 hour of shaking at 37°C, the bacteria were plated on a LB-Kanamycin plate (#1564, #1569) or LB-Ampicillin plate (#1616, #1617) and incubated upside down at 37°C overnight. The next day bacteria

colonies were picked for a Mini DNA purification (see 2.2.5.5) and sequenced by Eurofins (sequencing primer for siRNA resistance: SG2305; sequencing primer for R377A: SG1891) after purification. Positive colonies were then used for a Midi DNA purification (2.2.5.5).

2.2.5.4 Transformation of chemically competent DH5α *E. coli* bacteria

Chemically competent DH5α *E. coli* bacteria were thawed on ice. 5 µl of the ligation reaction (containing plasmid DNA) was added to 45 µl of competent bacteria and incubated for 10 min on ice. A heat shock took place for 45 s at 42°C and immediately thereafter, cells were placed on ice. Then, 400 µl of pre-warmed LB medium were added to the mix and incubated for 1 h at 37°C while gently shaking. Afterwards, the bacteria were pelleted and resuspended in a small amount of LB medium. The bacteria suspension was spread onto pre-warmed LB agar plates containing the appropriate antibiotics. For bacteria growth, the LB agar plates were incubated upside down at 37°C overnight.

2.2.5.5 Mini, Midi and Maxi plasmid DNA preparation from bacteria

Mini DNA plasmid preparation was performed from 1.5 ml of bacteria suspensions which were grown overnight at 37°C with the appropriate antibiotics. Previously, LB medium was inoculated by a bacteria colony, picked from a LB agar plate with the appropriate antibiotics. The bacteria were pelleted by 2 min centrifugation at full speed. They were resuspended with 150 µl of a S1 buffer containing 100 µg/ml RNase A. Afterwards 150 µl of buffer S2 were added and the reaction tubes were inverted for several times. After an incubation step for 5 min at room temperature, 150 µl of buffer S3 was added and the tubes were inverted again. Lysed bacteria suspension was centrifuged for 5 min at 4°C at full speed. The supernatant was transferred into a new tube and 800 µl of 100% EtOH were added and vortexed. After a centrifugation step of 10 min at 4°C at full speed, the DNA was washed with 500 µl 70% EtOH. The pellet was then air dried and depending on the pellet size either resuspended with 20 µl or 30 µl of TE buffer.

For Midi and Maxi plasmid DNA purification, PureLink™ HiPure Plasmid Midiprep Kit and PureLink™ HiPure Plasmid Filter Maxiprep Kit from ThermoFisher Scientific were used. Up to 100 ml of bacteria suspension were used for Midi plasmid DNA purification and up to 500 ml of bacteria suspension were used for Maxi plasmid DNA purification and following the manufacturers` instruction. Plasmid DNA was stored at -20°C.

2.2.5.6 Genomic DNA isolation from mouse ear-punching and genotyping PCR

A genotyping PCR was performed to determine the correct genotype of mice. Mouse ear biopsis were incubated at 95°C for 30 min in 75 µl of base buffer. Then, 75 µl of neutralization buffer was added and samples were mixed. 1 µl or 3 µl of the supernatant were used for the genotyping PCR and termed as DNA template. Samples were stored at

4°C. The PCR reactions were set up with primers specific for K-Ras or p53. The size of wildtype (WT) p53 is 270 bp and of floxed p53 is 390 bp. The size of WT K-Ras is 622 bp, of LSL K-Ras is 500 bp and of ∆LSL is 650 bp. The PCR products were separated in a 2% agarose gel.

Table 37: Genotyping PCR for K-RAS and p53

	LSL-Ras [µl]	PCR conditions LSL-Ras	p53fl [µl]	PCR conditions p53
DNA template	3	95°C- 2 min 1x	1	95°C- 5 min 1x
Primer 1 (10 µM)	SG2031-1	95°C- 30 s 61°C- 30 s 35x 72°C- 45 s	SG1556-1	95°C- 30 s 56°C- 1 min 30x 72°C- 1 min
Primer 2 (10 µM)	SG2032-1		SG1557-1	
Primer 3 (10 µM)	SG2033- 1		-	
dNTPs (2 mM)	2.5	72°C- 10 min 1x	2.5	72°C- 3 min 1x
10x ReproFast	2.5	10°C- hold	2.5	10°C- hold
His-Taq 16 (5 U/µl)	0.2		0.2	
ddH_20	13.8		16.8	

2.2.5.7 Agarose gel electrophorese

Agarose gel electrophoresis was used to separate or verify PCR products or plasmid DNA after restriction digestion according to their size. The appropriate amount of agarose was dissolved in 1x TAE buffer by boiling the solution in the microwave. For instance, for a 1% agarose gel, 1 g agarose was solved in 100 ml 1x TAE buffer. After cooling down the solution to about 50°C, 0.2-0.5 µg/ml of ethidium bromide was added and the solution was mixed. Then, the agarose solution was poured into a gel tray with inserted well comb. After further cooling, the agarose gel was solidified and was placed in a gel chamber filled with 1x TAE buffer. DNA samples were mixed with 5x loading dye and then pipetted into the gel wells. Additionally, a 1 kb or a 100 bp molecular weight ladder was pipetted into a well as a reference for the DNA size. DNA was separated in an electric field with 80 V to 100 V for 45 min to 1.5 h. For visualization of the DNA bands, a UV transilluminator was used.

2.2.5.8 Isolation of PCR products or vector DNA from agarose gels

The PCR product or vector DNA was separated according to agarose gel electrophoresis. Bands were cut under UV light with a scalpel and transferred into a 1.5 ml reaction tube.

DNA was isolated using the sing the GeneJET Gel Extraction Kit (ThermoFisher Scientific) following the manufacturers' protocol.

2.5.6 Protein biochemistry

2.5.6.1 Whole cell lysates

Cells were washed once with ice cold 1x PBS and were kept on ice. 1 ml of 1x PBS was added to the dishes. Cells were scraped from the cell culture dishes and transferred to a reaction tube. For analysis of apoptosis, the supernatant was collected together with the cells. Cells were pelleted for 5 min at 3,000 x rpm at 4°C and then resuspended in TNN lysis buffer containing a protease inhibitor cocktail (PIC, 1:1000), 1 mM DTT and 1 mM PMSF. After an incubation time of 20 min on ice, the lysate was briefly vortexed and centrifuged for 10 min at 14,000 x rpm (4°C). The supernatant was transferred to a fresh tube and the protein concentration was determined by Bradford assay (2.5.6.2). The lysate was mixed with 0.5x of the volume of 3x electrophoresis sample buffer (ESB) and boiled at 95°C for 5 min. Samples were stored at -20°C.

2.5.6.2 Determination of the protein concentration by Bradford assay

The Bradford assay was established by Bradford (Bradford, 1976) and was used to determine protein concentrations. 1 µl of the whole cell lysate or for generation of a reference standard curve, 1 µl of a generated BSA dilution series were added to a disposable semi-micro cuvette together with 100 µl of 0.15 M NaCl solution. Afterwards, 1 ml of a Bradford solution was added and mixed. After around 5 min of incubation time, the samples were measured at a spectrophotometer with an extinction of 595 nm. The samples were measured in duplicates and the protein concentration was calculated according the formula calculated from the standard curve.

2.5.6.3 SDS polyacrylamide gel electrophoresis

Sodium dodecyl sulfate polyacrylamide gel electrophoresis (SDS-PAGE) was used to separate denatured proteins generated by whole protein lysate (2.5.6.1) according to their molecular mass. A system from Bio-Rad named Mini-PROTEAN 3 Cell system was used for gel electrophoresis. Depending on the molecular sizes of the proteins of interest, between 8% to 15% of SDS separation gels were prepared (see Table 38) and poured between a fixed 1.5 mm spacer plate and a short plate according to the Bio-Rad instruction manual. The gel was overlaid by water and left for complete polymerization. The water was removed and a stacking gel was prepared (see Table 38) and poured on top of the separation gel and a 10-well or 15-well comp was inserted. The Mini-PROTEAN 3 Cell was assembled according to the instruction manual with the polymerized SDS-gels. The inner

and the outer chamber were filled with 1x SDS running buffer. The comb was removed and the pockets were rinsed with buffer. 30-100 µg of protein lysate were loaded onto the gel. The proteins were separated by 35 mA per gel for 1-2 hours and were used for immunoblotting (2.5.6.4).

Table 38: Composition of stacking gel and separation gel for SDS-PAGE

Reagents	Stacking gel	Separation gel					
Acrylamide percentage	5%	8%	10%	12%	13%	14%	15%
ddH2O	3 ml	4.6 ml	3.8 ml	3.2 ml	2.9 ml	2.6 ml	2.2 ml
1.5 M Tris pH 8.8	-	2.6 ml	2.6 ml	2.6 ml	2.6 ml	2.6 ml	2.6 ml
0.5 M Tris pH 6.8	1.25 ml	-	-	-	-	-	-
30% Acrylamide/Protogel	0.67 ml	2.6 ml	3.4 ml	4 ml	4.3 ml	4.6 ml	5 ml
20% (w/v) SDS	25 µl	50 µl	50 µl	50 µl	50 µl	50 µl	50 µl
10% APS	50 µl	100 µl	100 µl	100 µl	100 µl	100 µl	100 µl
TEMED	5 µl	10 µl	10 µl	10 µl	10 µl	10 µl	10 µl

2.5.6.4 Immunoblotting

The proteins, separated by SDS-PAGE (2.5.6.3), were transferred to a polyvinylidene fluoride (PVDF) membrane by using a Mini Trans-Blot wet transfer apparatus from BioRad. The PVDF membrane was incubated for 1 min in 100% methanol and then placed together with the Whatman paper, sponges and gel cassette holder in ice cold blotting buffer. All these components were assembled according to the manufacturers` protocol. The transfer of proteins from the gel to the PVDF membrane was performed at 270 mA for 1.5 hours in the Mini Trans-Blot. For validation of the protein transfer, the PVDF membrane was stained with Ponceau S solution for several seconds and then washed with ddH_2O. Afterwards, the PVDF membrane was incubated for 1 hour in a blocking solution (5% milk in 1x TBS-T or 5% BSA in 1x TBS-T) while gently shaking. The first antibody (see Table 15) was diluted in blocking solution and incubated with the PVDF membrane over night at 4°C while gently shaking. The membrane was washed 3x with 1x TBS-T for 10 min at RT while gently shaking. The secondary antibody (see Table 16), coupled to HRP, was diluted in blocking solution and incubated for 30 min at RT while gently shaking. Then, the PVDF membrane was washed 3x with TBS-T for 10 min at RT while gently shaking. Next, the enhanced chemiluminescence (ECL) components were mixed together in 1 M Tris (pH 8.5) and

activated by H_2O_2. The membrane was incubated for 1 min in the development solution and then transferred to a cassette, where the membrane was wrapped in a plastic foil and exposed to X-ray films in a dark room.

2.2.7 RNA sequencing

2.2.7.1 Sample preparation for high throughput sequencing

1.25x 10^5 A549 cells were seeded in triplicates in a 6-cm dish. The next day PRC1-Wildtype or PRC1-NLS3A constructs were induced by treatment of the cells with 0.25 µg/ml of doxycycline. After two days, RNA was isolated by using the RNAeasy Mini Kit from Qiagen according to the manufacturers' protocol. RNA quality and concentration was determined by an RNA fragment analyzer (Advanced Analytical Technologies). 1 µg of RNA was used for isolating the mRNA by using the NEBNext Poly(A) mRNA Magnetic Isolation Module (New England Biolabs). A cDNA library was generated by using the NEBNext Ultra II RNA Library Prep Kit for Illumina (New England Biolabs). For purification, AMPure XP Beads were used (Beckman Coulter). For adaptor ligated PCR, NEBNext Multiplex Oligos for Illumina (Dual Index Primers) were used (New England Biolabs). Seven PCR cycles were used for amplification. The quality of the cDNA library was determined by an RNA fragment analyzer (Advanced Analytical Technologies). Finally, all samples were mixed together with equal molarities. The library was sequenced on the HiSeq500 platform (Illumina). Dr. Carsten Ade (University of Würzburg, Germany) performed the sequencing on the HiSeq500 platform.

2.2.7.2 Data analysis after RNA seq

Galaxy was used to analyze the RNA seq data (https://usegalaxy.org). HISAT2 was used to align RNA-seq reads against the human genome hg19 (Kim et al., 2015). FeatureCounts and limma were used to analyze differential expression (Law et al., 2014; Liao et al., 2014; Liu et al., 2015). Metascape (www.metascape.org) was used for identification of enriched pathways (Zhou et al., 2019). Gene Set Enrichment Analysis (GSEA) (Subramanian et al., 2005) with FGSEA (Sergushichev, 2016) was used to determine whether a set of genes is enriched or downregulated in a list of differentially expressed genes (ranked list of genes). The molecular signatures database (MSigDB) was used to download gene set collections for FGSEA or gene group analysis. The RNA-sequencing datasets are available at the NCBI's Gene Expression Omnibus with the accession number GEO: GSE137940. The analysis of RNA seq data was performed by Prof. Dr. Stefan Gaubatz (University of Würzburg, Germany) and Steffen Hanselmann.

2.5.8 Mouse experimental methods

2.5.8.1 Mouse model for lung cancer (NSCLC)

The mouse experiments were performed according to German law and were approved by an institutional committee (Tierschutzkommission der Regierung von Unterfranken).
The genetically modified C57BL/6 inbred mouse strain was used for animal experiments and has been described before (Jackson et al., 2001; Marino et al., 2000). Mice were obtained from the NCI Mouse Repository, Bethesda, MD, USA. K-Ras$^{LSL-G12D/+}$; p53$^{fl/fl}$ mice contain an oncogenic mutation of K-Ras by changing of a glycine to aspartic acid at codon 12 in the genes` endogenous locus of one allele. Expression of the K-Ras-G12D is prevented by an LSL cassette (Lox-Stop-Lox, transcriptional and translational stop elements) that was engineered into the first intron of the K-Ras gene and flanked by LoxP sites (Jackson et al., 2001; Lakso et al., 1992). Additionally, exon two to ten of both alleles of the tumor suppressor protein p53 are flanked by LoxP sites (Jackson et al., 2005; Johnson et al., 1997). Before Cre-mediated recombination, the p53 locus is kept in a wildtype state. Upon Cre-mediated recombination, tumors are driven by oncogenic K-Ras and loss of p53.

2.5.8.2 Intratracheal infection

Lentiviral Cre-expressing vectors containing either a shRNA directed against murine PRC1 or luciferase control were cloned as described in 2.2.5.1. Lentivirus was produced (2.2.2.3), concentrated (2.2.2.4) and transducing units (TU) were determined as described in 2.2.2.5. Twenty 9-15 -week-old female and male mice were intratracheally infected with 1x10^6 TU per mouse as previously described (DuPage et al., 2009). Mice were anesthetized by injecting them intraperitoneally with 7 µl per gram of body weight of a mixture of 150 µl Xylazine/450 µl Ketamine in 1.8 ml 0.9% NaCl. An anesthetized mouse was placed on a platform by their front teeth so that their chest hangs vertically beneath them. The mouth was opened using a catheter and the tongue was gently pulled out using the flat forceps. A light was directed on the mouse upper chest so that the white light was emitted from the trachea. The catheter was slid into the trachea and the needle was removed immediately. The mouse was moved into a biosafety hood, where the virus was dispensed into the opening catheter. The virus was inhaled by the mouse. Then, the catheter was removed after a few seconds, when the virus was not visible anymore. The mouse was placed back into the cage. Lung tumorigenesis was analyzed by histopathology in the following sections.

2.5.8.3 Preparation of lung paraffin sections

Mice were sacrificed 16 weeks after infection by exposure to carbon dioxide gas followed by cervical dislocation. The lungs were washed with 1x PBS by perfusion and filled with 4%

PFA. Then, the lungs were excised and fixed in 4% PFA over night at 4°C. The lungs were washed twice in 1x PBS for 10 min at RT on a rotating wheel. Afterwards, the lungs were washed in 0.9% $NaCl_2$ for 10 min at RT on a rotation wheel. The lungs were documented by digital microscope (Keyence VHX Multi Scan). Then, the lungs were dehydrated and embedded in paraffin according to the following protocol:

Table 39: Dehydration and embedding of mouse lungs

	Solution	Time [hours]	Temperature	Storage/incubation
1	**50% ethanol**	1	RT	
2	**70% ethanol**	1	RT	at 4°C for several days/weeks
3	**80% ethanol**	1	RT	
4	**90% ethanol**	1	RT	
5	**95% ethanol**	1	RT	overnight at 4°C
6	**100% ethanol**	2x 1	RT	
7	**Ethanol/Xylol (1:1)**	1	RT	
8	**Xylol**	2x 1	RT	
9	**Xylol/Paraffin (1:1)**	1	60°C	
10	**Paraffin**	overnight 2-3x change	60°C	

The lungs were placed in paraffin-filled molds which were kept at 60°C on a hotplate. A cassette with the specimen identification details was placed on the top of the mold and was attached by adding further paraffin. This composition was slid onto a cold surface to solidify. After complete solidification of the paraffin at 4°C, the mold was removed and the paraffin block with the cassette was used for clamping in the microtome. The paraffin-embedded lung tissues were cut by Susanne Spahr (University of Würzburg, Germany) in 5 µm sections using a Hyrax M 40 rotary microtome (Carl Zeiss). Subsequently, the sections were fixed on glass slides at 42°C overnight and then stored at 4°C.

2.5.8.4 Hematoxylin and Eosin (H/E) staining of paraffin sections

Before the tissue sections were stained by H/E, they were equilibrated to RT. The stepwise procedure for H/E staining is explained in Table 40.

Table 40: Hematoxylin and Eosin staining of paraffin sections

Procedure	Solution	Time [min]
Deparaffinization	Xylol I	10
	Xylol II	10
Rehydration	100% ethanol	3
	95% ethanol	3
	80% ethanol	3
	70% ethanol	3
	50% ethanol	3
	Demineralized-H_2O	5
Nuclei staining with Hematoxylin	Hemalum solution acid according to Mayer (Roth)	8
	Demineralized-H_2O	shortly
	Running tap water	15
	Demineralized-H_2O	several seconds
Counterstaining with Eosin	0.1% Eosin Y solution supplemented with 1-2 drops of glacial acetic acid	3
	Running tap water	5
	95% ethanol	3
	100% ethanol	3
	Xylol I	10
	Xylol II	10
Embedding	Sections were mounted with Roti-Histokitt	

The tissue sections were analyzed at the Keyence VHX Multi Scan with 30x, 50x or 200x magnification with the objective VH-Z20R. Further analysis of the tumor area was performed with Image J software (https://imagej.nih.gov/ij/index.html).

2.5.9 Database analysis of PRC1

Oncomine database was used to analyze the expression of PRC1 in different lung cancer tissue types compared to control lung tissue. Information of a published microarray dataset from Hou et al. (Hou et al., 2010) was selected for the analysis.

cBioPortal database (Cerami et al., 2012; Gao et al., 2013) was used to analyze the mutation frequency and copy number alterations of the PRC1 sequence. Information from TCGA, PanCancer Atlas of 566 patient samples, was used for analysis of the mutation

frequency of PRC1. Information of 507 patients' samples with copy number alterations were available from the TCGA Pan Cancer Atlas and were used for the analysis.
Kaplan-Meier plotter (Gyorffy et al., 2013; Nagy et al., 2018) was used to analyze the expression of PRC1 linked to clinical outcome of lung adenocarcinoma patients. Database uses mRNA gene chip expression data (lung cancer) and overall survival data information downloaded from GEO, EGA and TCGA.

2.5.10 Statistical analysis

Data were analyzed and presented as mean ± standard deviation (SD) or standard error of the mean (SEM). The performed statistical tests are provided in the figure legends. Usually, differences between two experimental groups were determined by Student's t-test (two-tailed, unpaired). Statistical significance was distinguished according to their p-value and indicated with asterisks ($p \leq 0.05$ *; $p \leq 0.01$ **; $p \leq 0.001$ ***; $p \leq 0.0001$ ****). P-values >0.05 considered as not significant (ns) if not indicated differently. Statistical analysis was performed with GraphPad Prism 5 software (GraphPad Software, Inc., La Jolla, CA, USA).

3 Results

3.1 PRC1 is highly expressed in NSCLC and the expression level of the protein correlates with the survival rate of lung adenocarcinoma patients

Protein regulator of cytokinesis 1 (PRC1) is highly expressed in several cancer types for instance in bladder, breast, liver, gastric, prostate and lung cancer (Li et al., 2018; She et al., 2019). However, molecular mechanisms and functions of PRC1 in tumorigenesis are not sufficiently well-known or consistent among the studies. Therefore, further analysis and clarification of the role of PRC1 in lung cancer, one of the leading causes of cancer deaths (Siegel et al., 2019), is necessary.

A genome-wide expression analysis, using biopsies from 91 patients with 91 non-small cell lung cancer (NSCLC) tissue samples and 65 adjacent normal lung tissue samples, was performed by Hou et al. (Hou et al., 2010). Using this dataset, PRC1 expression of different NSCLC subtypes and normal lung tissue was analyzed by using the Oncomine database (Fig. 6A). Compared to normal lung tissue, PRC1 expression was increased about 9-fold in large cell carcinoma and squamous cell carcinoma (Fig. 7A). In lung adenocarcinoma, PRC1 expression was enhanced around 4-fold compared to control lung tissue (Fig. 7A). Analysis of the overexpression gene rank revealed that PRC1 belonged to the top 1% (lung adenocarcinoma, squamous cell carcinoma) and 2% (large cell carcinoma) expressed genes in those NSCLC subtypes (Fig. 7A). This database analysis confirmed enhanced PRC1 expression in lung cancer which has been described before (Li et al., 2018; She et al., 2019).

Besides higher expression of PRC1 in lung cancer, I asked whether the gene is often mutated in lung cancer and might have some beneficial features for the tumor which could contribute to tumorigenesis. Therefore, a cBioPortal database analysis of PRC1 was performed by using 507 patient's samples with mutation data and somatic copy alteration (CNA) data from the cancer genome atlas programme (TCGA) for lung adenocarcinoma (Cerami et al., 2012; Gao et al., 2013). Analysis of the PRC1 sequence revealed a low mutation frequency of slightly above 1% (Fig. 7B). It seems that PRC1 is rarely mutated in lung adenocarcinoma and the wildtype version is needed for proliferation of the cells.

Next, I asked whether the protein has a high proportion of copy number alterations in lung cancer which could contribute to the high expression level of the protein. Therefore, cBioPortal database analysis was performed by using the same patient's samples as described above and by choosing copy number alteration from GISTIC (TCGA, PanCancer Atlas). GISTIC stands for Genomic Identification of Significant Targets in Cancer and is an algorithm which attempt to identify significantly altered regions of amplification or deletion and calculate a statistical score. The output is categorized into deep deletion (deep loss,

possibly homozygous deletion), shallow deletion (shallow loss, possibly heterozygous deletion), diploid, gain (low level gain, a few additional copies) and amplification (high level amplification, more copies). The biological relevance is mainly considered to be deep deletions and amplifications.

Analysis of the 507 lung adenocarcinoma patients revealed that just one samples contained a deep deletion event (0.2%) and 3 samples had amplification events (0.6%) (Fig. 7B). Thus, 99.2% belonged to the normal (diploid, 46.6%) or less severe (shallow deletions, 41.4%; copy number gain, 11.2%) group (Fig. 7B). In Figure 7B, copy number alterations are also subdivided into not mutated, missense mutation or truncating version of PRC1 (Fig. 7B). One truncating version and three missense mutations of PRC1 belonged to the diploid group as well as one version of the missense mutation belonged to shallow deletion and copy number gain group (Fig. 7B). Taken together, high PRC1 expression in lung adenocarcinoma might not be due to amplification events, consistent with published data where the PRC1 sequence was rarely altered by mutations (1% missense mutations) (Li et al., 2018). Also, the putative copy number alterations which might be relevant were low with 1% amplification events and even 0% deep deletions (Li et al., 2018).

Next, I asked whether the expression of PRC1 correlates with the survival rate of human lung adenocarcinoma patients. For this analysis, the Kaplan-Meier plotter database was used (Gyorffy et al., 2013). Information of gene expression data and overall survival of lung adenocarcinoma were downloaded from GEO, EGA and TCGA by the database. Obviously, lung adenocarcinoma patients with tumors in which PRC1 expression is elevated (259 patients) showed a significantly shorter survival compared to patients with lower (460 patients) PRC1 expression (Fig. 7C). The median survival of the low expression cohort was about 126 months and of the high expression cohort was approximately 48 months (Fig. 7C). This result indicates a clinical significance of PRC1 expression and survival of human lung adenocarcinoma patients.

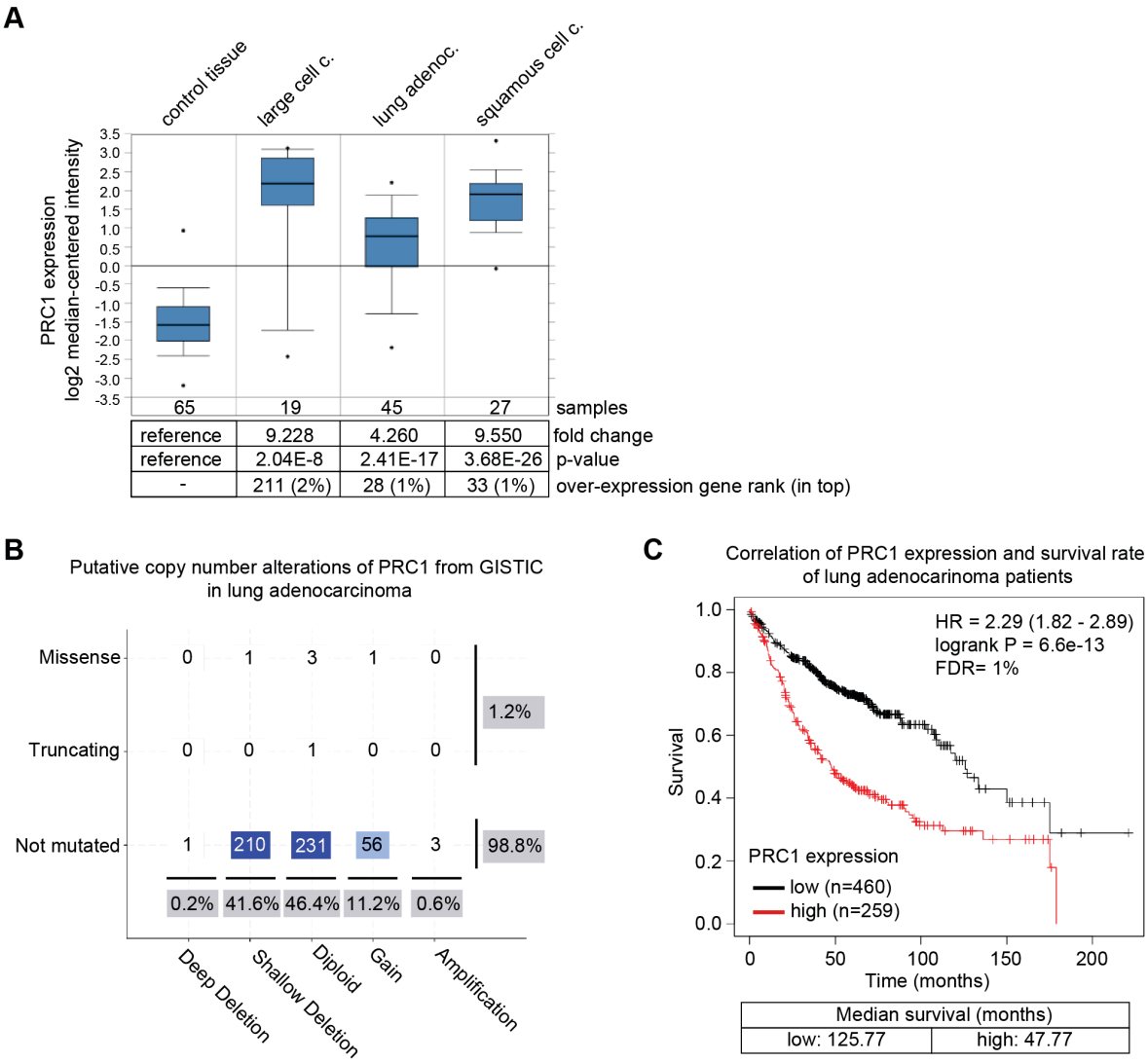

Figure 7: PRC1 is highly expressed in NSCLC and the survival rate of lung adenocarcinoma patients correlates negatively with the expression level of the PRC1 mRNA.
(A) Oncomine data analysis from (Hou et al., 2010). A genome-wide expression analysis of 91 patients with NSCLC was performed and different lung cancer tissues were distinguished by histology. Differences in PRC1 expression between lung cancer tissue and adjacent control tissue are shown. Fold change, p-value and over-expression gene rank (in top percentage of genes) are in comparison of each cancer type with the control lung tissue. Abbreviation: c., carcinoma. (B) cBioPortal database analysis (https://www.cbioportal.org/; Cerami et al., 2012; Gao et al., 2013) of PRC1 mutation data and copy number alteration data from GISTIC of lung adenocarcinoma from TCGA, PanCancer Atlas, were performed. 507 Samples were categorized into mutations (missense, truncating) and not mutated group as well as in the different copy number alterations (deep deletion, shallow deletion, diploid, gain, amplification) and shown in a table. Percentages of the different categories (mutated-not mutated, copy number alterations) were calculated and shown in grey boxes. (C) Expression of PRC1 linked to clinical outcome of lung cancer patients. Kaplan-Meier plot (Gyorffy et al., 2013) showing overall survival of lung adenocarcinoma patients based on expression of PRC1. An algorithm was used by the Kaplan-Meier plotter which includes the use of all percentiles between the lower and upper quartile to identify the best performing cutoff. In addition, median survival rate in months of the low and high expression group are shown. n: number of patients with available clinical data, HR: hazard ratio, FDR: false discovery rate.

3.2 Depletion of PRC1 inhibits lung tumorigenesis *in vivo*

Database analysis from 3.1 showed that PRC1 is highly expressed in NSCLC and expression level correlated with the survival rate of lung adenocarcinoma patients. It has been suggested that targeting mitotic exit can be a strategy to treat cancer cells (Liu et al., 2019). Based on those findings, PRC1 depletion might be a potential strategy to inhibit lung tumor growth. To support this hypothesis and test whether lung tumorigenesis could be reduced by PRC1 depletion, a mouse model was chosen which reflects the genetic and histopathological features of the human disease.

An oncogenic K-RAS mutation at codon 12 (change of glycine to aspartic acid) was used as a tumor driver and activating mutation. Oncogenic K-RAS mutations, especially at codon 12, have been found frequently in NSCLC, especially in lung adenocarcinomas (Dearden et al., 2013; Dogan et al., 2012; El Osta et al., 2017). In addition, tumor suppressor p53 function was inactivated which has also been often found in NSCLC (Ahrendt et al., 2003; Herbst et al., 2018; Leroy et al., 2014). The mouse model was engineered in a way that the expression of K-RAS^{G12D} was controlled by a lox-stop-lox cassette (LSL) which consists of transcriptional and translational stop elements flanked by LoxP sites in the first intron of the K-RAS gene (Jackson et al. 2001). To mimic the loss of tumor suppressor p53, a mouse strain with LoxP sites flanking exons two through ten of p53 was used (Marino et al. 2000). For K-RAS, one allele-maintained wildtype statues, whereas both alleles of p53 were flanked by LoxP sites. Intratracheal intubation of lentivirus ensured specific infection of the lungs (DuPage et al., 2009). Finally, upon expression and activity of the Cre recombinase, stop elements of K-RAS^{G12D} will be removed as well as exon two through ten of p53, which results in initiation of lung tumors. In parallel to tumor initiation, a shRNA directed at PRC1 or a control shRNA was delivered to virus-infected lung cells (Fig. 8A).

First, to test the knockdown efficiency, several shRNAs directed against mouse PRC1 were designed and cloned into an inducible lentiviral vector. Then, stable NIH-3T3 cells were generated by lentiviral infection and selection (see 2.2.2.6). PRC1 depletion was evaluated by immunoblotting (Fig. 8B). Two shRNA sequences (#14, #16) led to knockdown of PRC1 in murine cells whereas one shRNA directed against PRC1 as well as a shRNA directed at luciferase and used as a control showed unchanged PRC1 level (Fig. 8B). shRNA #16 was cloned into a bifunctional lentiviral vector shown in Figure 8C. Lentiviral particles were produced as described in 2.2.2.3-2.2.2.5. Afterwards, ten K-RAS^{G12D};p53$^{fl/fl}$ mice were infected by intratracheal intubation with a lentivirus that simultaneously activate K-RAS and delete p53 by Cre recombinase and deplete PRC1 by RNAi.

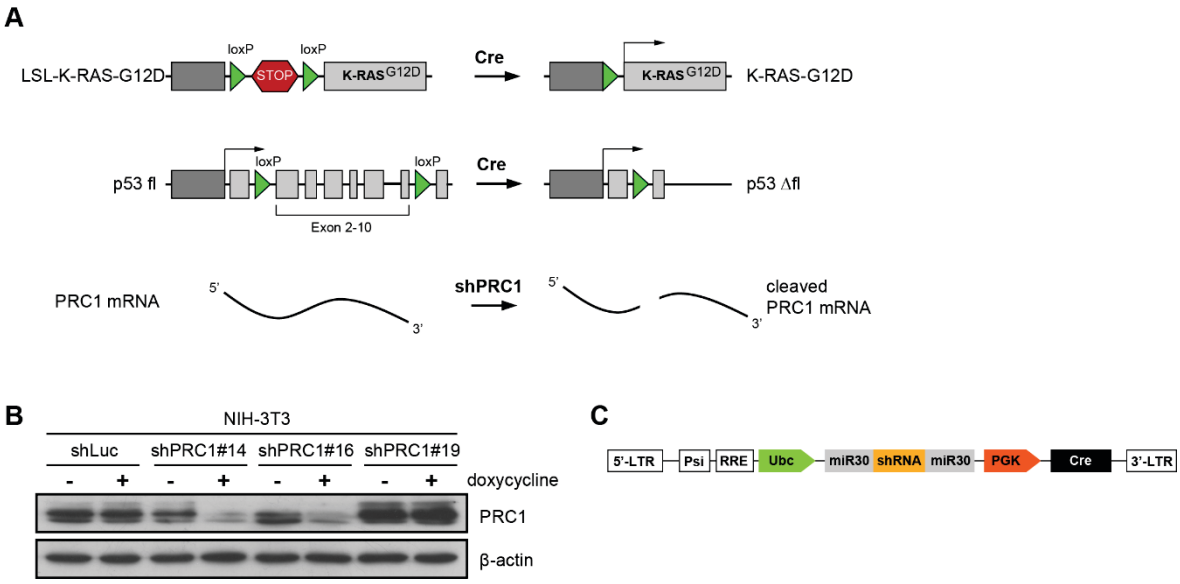

Figure 8: PRC1 depletion *in vitro* and strategy for *in vivo* knockdown of PRC1.
(A) Strategy to activate K-RAS and delete p53 by Cre and deplete PRC1 by RNAi in a lung-specific manner by intratracheal infection of LSL-K-Ras^{G12D}, p53$^{fl/fl}$ mice with the lentivirus. (B) Lentiviral constructs encoding shRNAs directed against murine PRC1 or luciferase control were introduced into NIH-3T3 cells. The depletion of PRC1 after addition of 1 µg/ml doxycycline for 4 days was analyzed by immunoblotting. shPRC1 #16 sequence was used for the *in vivo*. experiment (C) Scheme of the lentiviral Cre/ shRNA vector to deliver a mir30 based shRNA and Cre recombinase *in vivo*.

As a control, ten K-RAS^{G12D};p53$^{fl/fl}$ mice were infected in parallel with a lentivirus expressing a non-specific shRNA (shLuc). Mice were sacrificed 16 weeks after tumor induction, their lungs were fixed and paraffin sections were prepared (Fig. 9A). Afterwards, lung paraffin sections were stained by Hematoxylin and Eosin (H/E) (Fig. 9B). Lung tumorigenesis was evaluated by histopathology. Tumor area of mice infected with the lentivirus expressing the PRC1-specific shRNA was strongly reduced compared to mice infected with the control shRNA (Fig. 9B). Quantification showed a significantly smaller lung tumor area in mice which were infected with the PRC1-specific shRNA lentivirus compared to mice infected with the control lentivirus (Fig. 9C, Table 41-44). The mean of the relative tumor area of shLuc infected mice was 12.4%, whereas in shPRC1 infected mice, the relative tumor area was only 4.5% (Fig. 9C).

Next to the tumor area, the number of tumors per mouse were counted. Tumor numbers of mice infected with the lentivirus expressing the PRC1-specific shRNA were significantly lower compared to mice infected with the control shRNA (Fig. 9D, Table 45,46). On average of 25.5 tumors were present in shLuc infected mice, whereas 13.3 tumors were present in shPRC1 infected mice (Fig. 9D). In addition to tumor number, tumors were categorized depending on their heterogeneity and progression according the four-stage grading system of the used NSCLC model (DuPage et al., 2009). The earliest lesion starting with an atypical adenomatous hyperplasia (AAH) and designated as grade 1. The next stage, grade 2 tumors, were adenomas with uniform nuclei but larger than AAH. Grade 3 tumors were

adenocarcinomas, which had a great degree of pleomorphic nuclei and displaying mixed cellular phenotypes. Further tumor progression led to invasive adenocarcinomas, grade 4, with glandular/acinar architecture and desmoplasia. Representative images of all four stages are shown in Fig. 9E. Quantification of the tumor grades revealed that highest proportion of tumors were grade 1 and 2 with about 35 to 50% (Fig. 9F, Table 45,46). The proportion of grade 1 tumors grade 2 tumors were similar in mice infected with the PRC1-shRNA compared to the Luc-shRNA (Fig. 9F, Table 45,46). However, the fraction of more aggressive and higher-grade tumors was reduced in shPRC1 infected mice compared to shLuc infected mice. Especially, significant less grade 4 tumors were found mice upon depletion of PRC1 (Fig. 9F, Table 45,46).

Taken together, PRC1 depletion significantly reduced the relative tumor area, tumor numbers, as well as the proportion of high-grade tumors compared to the control group. This result indicated a requirement of PRC1 in K-RAS-driven non-small cell lung cancer *in vivo*.

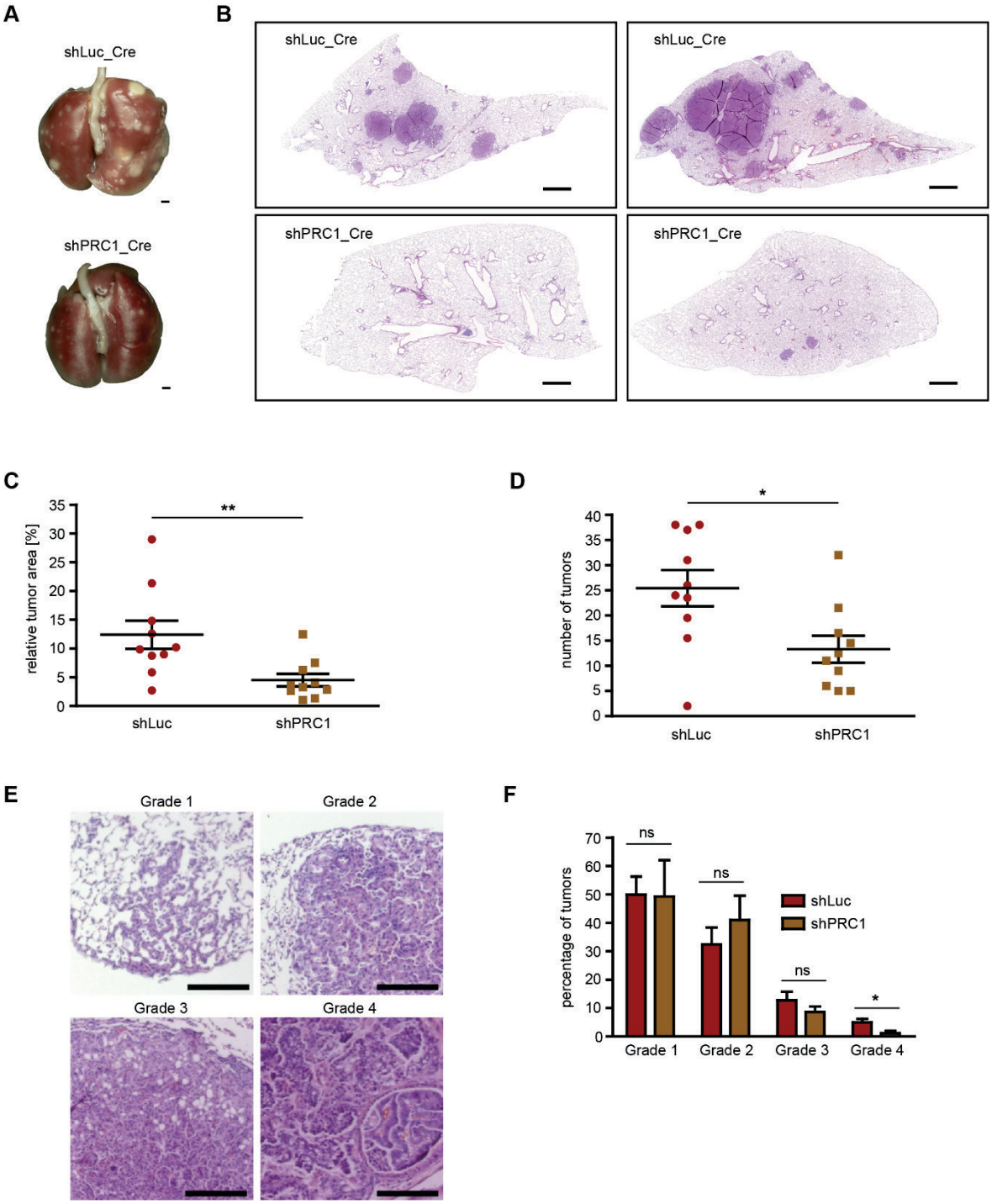
A
shLuc_Cre
shPRC1_Cre
B
shLuc_Cre
shLuc_Cre
shPRC1_Cre
shPRC1_Cre
C
relative tumor area [%]
**
shLuc
shPRC1
D
number of tumors
*
shLuc
shPRC1
E
Grade 1
Grade 2
Grade 3
Grade 4
F
percentage of tumors
ns
ns
ns
*
shLuc
shPRC1
Grade 1
Grade 2
Grade 3
Grade 4

Figure 9: PRC1 is required for lung tumorigesnesis *in vivo*.
LSL-KRAS-G12D;p53fl/fl mice were infected with a bifunctional lentivirus encoding Cre and a control shRNA (n=10) or with a virus encoding Cre and a shRNA specific for PRC1 (n=10). Mice were sacrificed after 16 weeks post infection (A,B) Representative lungs (A) and H&E stained lung sections are shown (B). Bar: 1 mm. (C) Quantification of tumor area to total lung area. Each symbol represents the analysis of an individual animal. The tumor area was obtained by measuring all tumors from two sections from each mouse. Mean and SEM. **p < 0.01 (Student's t-test.). Raw data are shown in Table 41-44. (D) Numbers of tumors of two sections were counted. Each symbol represents the mean value of an individual mouse. SEM is shown. *p < 0.05 (Student's t-test.). Raw data are shown in Table 45-46. (E) Lung tumors were categorized according their histopathological phenotype and tumor progression. Grade 1: atypical adenomatous hyperplasia (AAH), Grade 2: adenoma, Grade 3: adenocarcinoma, Grade 4: invasive adenocarcinoma. Representative pictures are shown. Bar: 125 µm. (F) Distribution of tumor grades. Mean value was calculated of two lung sections per mouse (shLuc: n=254.5 tumors, shPRC1: n=133 tumors). The error bar represents SEM. ns: not significant, *p < 0.05 (Student's t-test.). Raw data are shown in Table 45-46.

3.3 PRC1 depletion leads to a proliferation deficit, inhibits anchorage-independent growth and results in multi-nucleation in a panel of lung cancer cell lines

PRC1 is required for lung tumorigenesis *in vivo* as shown in a mouse model of NSCLC previously. In this part of the thesis, the consequences of depleting PRC1 in a panel of human lung cancer cell lines was analyzed in more detail.

First, human lung cancer cell lines (H23, HOP92, HOP62, H460, A549) were generated which express a doxycycline-inducible small hairpin RNA (shRNA) directed at PRC1 to deplete the protein (Fig. 10A). As a control cell line, immortalized BJ skin fibroblasts were used. Apart from shRNA expression upon doxycycline treatment, turbo red fluorescence protein (tRFP) is expressed at the same time as it is under control of the same promoter. tRFP expression indicates whether the shRNA is expressed and also how many cells of the population are expressing the construct strongly. Microscopic analysis of HOP62 shPRC1 cells showed that tRFP was expressed upon doxycycline treatment of the cells compared to non-induced cells (Fig. 10B). Flow cytometry analysis revealed a range of tRFP expression of about 40% to more than 90% depending on the cell line (Fig. 10C). To test whether PRC1 was depleted, immunoblotting with a specific PRC1 antibody was performed. A knockdown on protein level was shown for all cell lines after treatment with doxycycline (Fig. 10D). As an additional control, cell lines were generated that express a shRNA directed against luciferase to exclude possible non-specific effects of doxycycline. shLuc expressing cells showed comparable levels of PRC1 and no change in the levels of the PRC1 protein upon treatment with doxycycline (Fig. 10D).

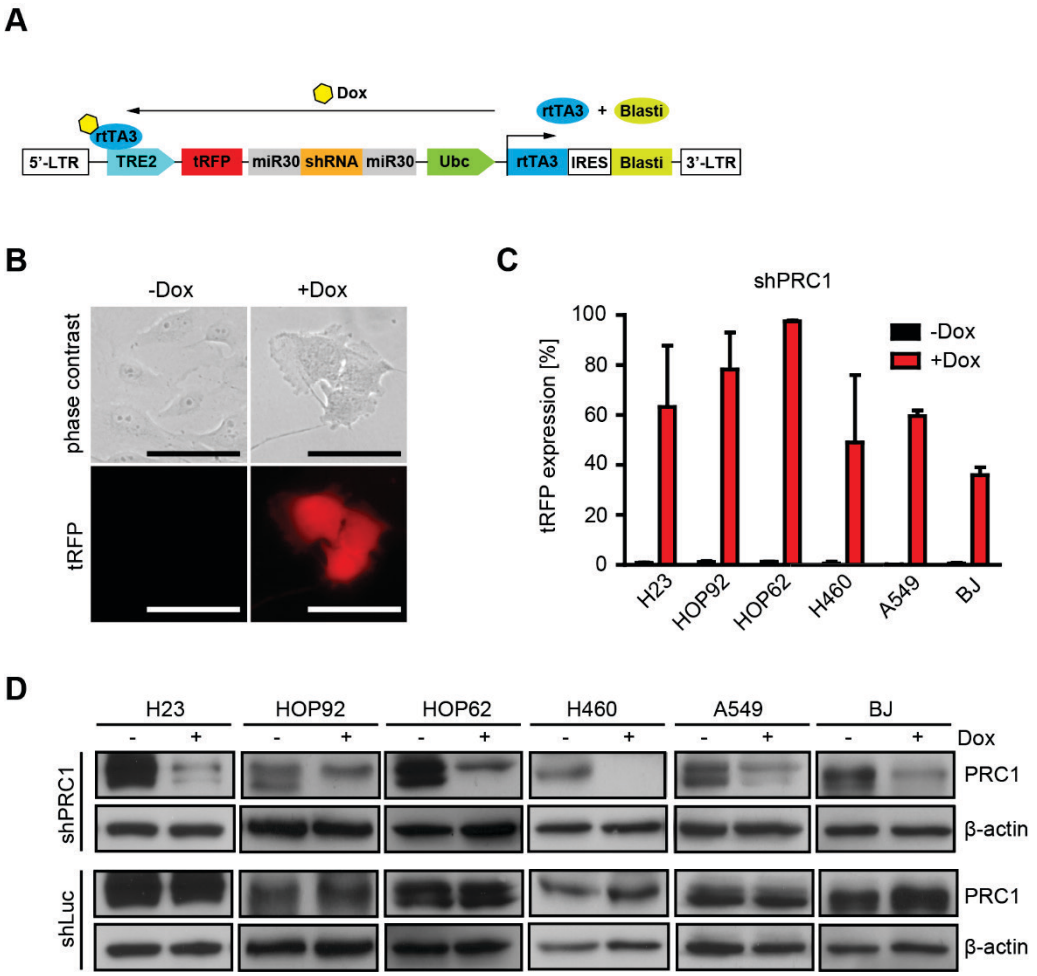

Figure 10: PRC1 depletion in a panel of lung cancer cell lines and BJ control cells.
(A) Scheme of the pINDUCER vector for shRNA-mediated depletion of PRC1. (B) HOP62 shPRC1 cells were induced (+) with 1 µg/ml of doxycycline (Dox) for 4 days. Microscopic analysis of the tRFP expression. Non-induced (-) cells were used as a control. tRFP expression is under same promoter control as the shRNA (see A) and indicates the expression of the shRNA. Bar: 75 µm. (C) Quantification of the tRFP expression by flow cytometry are shown. Cancer cell lines were treated with 1 µg/ml doxycycline for 4 days to induce the shRNA. BJ cells were treated for three days with the same amount of doxycycline. n=2 experiments (D) PRC1 depletion after induction (+; not induced, -) of the shRNA with doxycycline (Dox) was determined by immunoblotting. Control cell lines were stably infected with a shRNA directed against luciferase and served as a control to exclude possible non-specific effects of doxycycline.

As PRC1 knockdown was achieved, I next asked whether this knockdown has an effect on proliferation of the cells. Therefore, cell lines were seeded in low densities and cultured over 8 days with or without different concentrations of doxycycline and were then fixed and stained by crystal violet. PRC1 depletion caused a dose-dependent proliferation defect of all five lung cancer cell lines (Fig. 11A,C). Quantification revealed a significant negative effect on proliferation in all lung cancer cell lines upon 8 days of PRC1 depletion (Fig. 11C). HOP62 and HOP92 cells started to show proliferation defects upon PRC1 depletion between day 2 and 4 and the other cancer cell lines from day 4 on with further increases after 6 to 8 days in all cell lines (Fig. 11C). BJ control cells were less sensitive to PRC1 depletion than lung cancer cell lines (Fig. 11C). Additionally, doxycycline treatment just

showed minor effects on proliferation of lung cancer cell lines stably infected with the control shRNA (Fig. 11B,D).

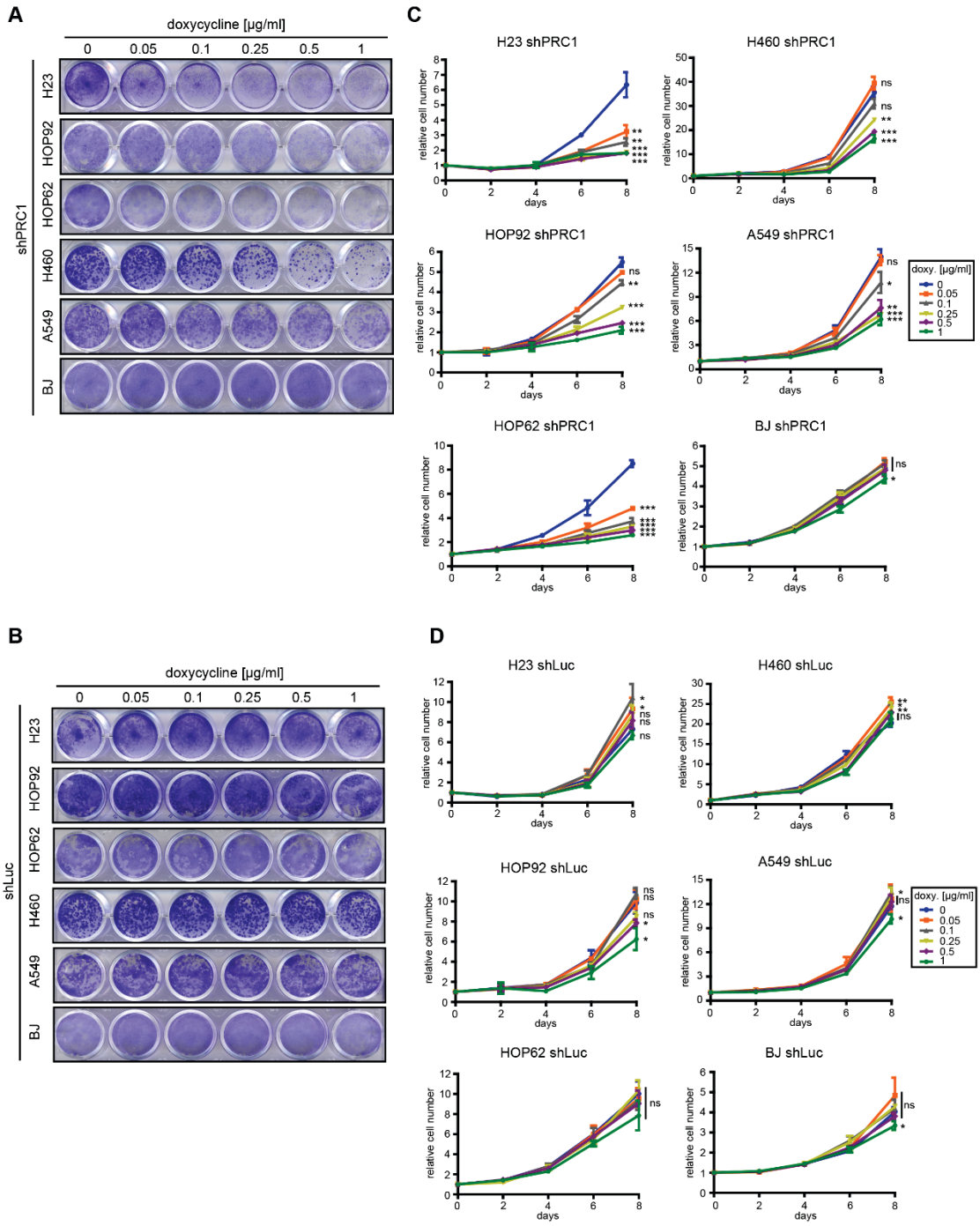

Figure 11: PRC1 depletion leads to a proliferation deficit in a panel of lung cancer cell lines. (A,B) Cell lines expressing the PRC1-specific shRNA or a control shRNA directed against luciferase were cultured for a period of 8 days with the indicated concentrations of doxycycline. Colonies were stained with crystal violet. (C,D) Quantification of growth of lung cancer cell lines and BJ cells stably expressing the PRC1-specific shRNAs or luciferase-specific shRNAs in the presence of the indicated concentrations of doxycycline was analyzed over 8 days. n=3 replicates. For clarity, statistical significance (Student's t-test) is only shown for day 8. *p<0.05; **p<0.01; ***p<0.001; ns: not significant. (A-D) Experiments of H23 and H460 cells were performed by Jonas Malkmus.

Next, I asked whether PRC1 knockdown also inhibits oncogenic transformation of lung cancer cells. Therefore, a soft agar colony formation assay was performed to analyze the anchorage-independent growth ability of cells. HOP92 and A549 lung cancer cell were able to grow under those conditions and were seeded in low densities. After 14 days, colonies of HOP92 cells with and without PRC1 depletion were analyzed by microscopy (Fig. 12A). Also, A549 cells were analyzed by microscopy after 18 days of treatment. (Fig. 12A). Significantly less colonies were observed when PRC1 was depleted compared to non-induced cells (Fig. 12B). Additionally, colonies were smaller in PRC1 depleted conditions compared non-treated cells (Fig. 12A). Taken together these data indicate that PRC1 is required for anchorage-independent growth which is an indicator of the malignancy of tumor cells.

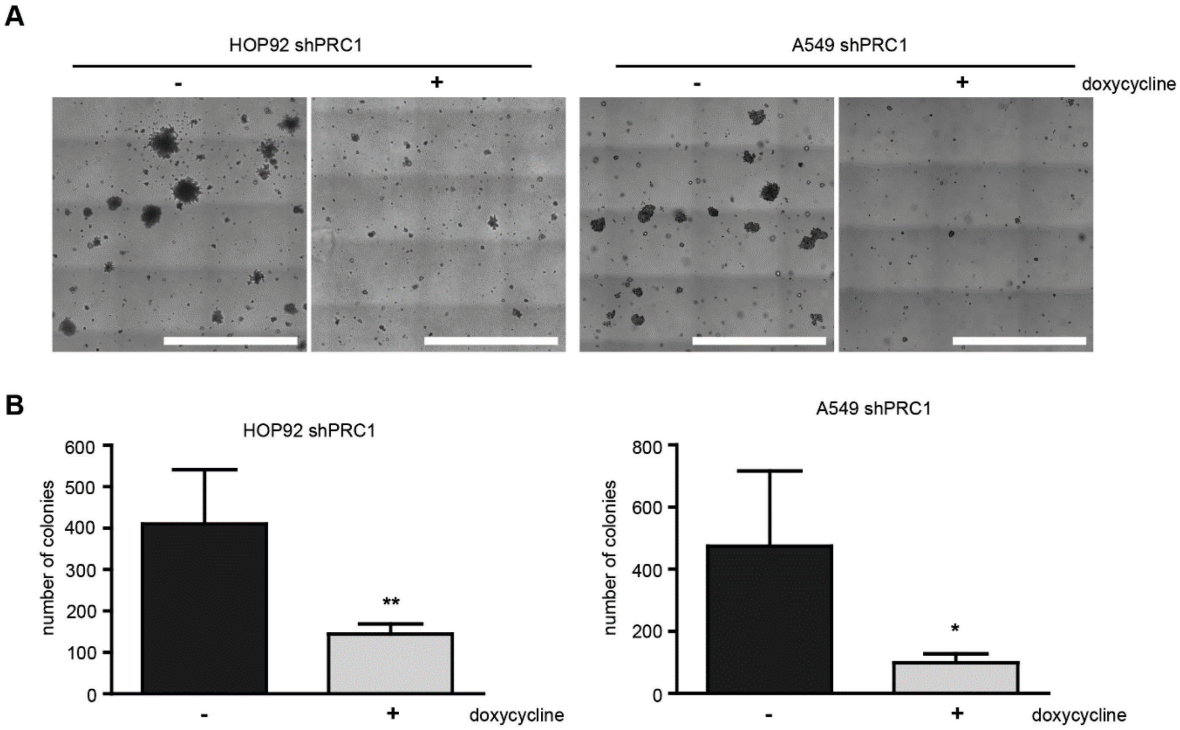

Figure 12: PRC1 is required for anchorage-independent growth *in vitro*.
(A) HOP92 and A549 cells stably expressing the inducible shRNA directed against PRC1 were left untreated (-) or treated (+) with 0.5 µg/ml doxycycline for 14 (HOP92) and 18 (A549) days. Anchorage-independent growth in soft agar was analyzed. Example images of non-induced and induced HOP92 shPRC1 and A549 shPRC1 cells are shown. Bar: 2.5 mm. (B) Quantification of colonies from (A). n=4 experiments for HOP92 and n=3 experiments for A549. *p < 0.05, **p < 0.01. Student's t-test.

PRC1 has been described as a cytokinesis protein and has been linked to CIN in cancer (Carter et al., 2006; Jiang et al., 1998; Mollinari et al., 2002; Zhu & Jiang, 2005). Hence, I asked whether the inhibitory effects on proliferation upon PRC1 depletion are due to increased cytokinesis defects in lung cancer. Therefore, lung cancer cells and BJ control cells were treated for four days with 1 µg/ml of doxycycline to deplete PRC1 or to induce

the shRNA directed against luciferase and were then fixed and investigated by microscopy (Fig. 13A,B). A significant increase in the fraction of multi-nucleated cells of approximately 15% to 50% after PRC1 depletion was observed in all lung cancer cells but not in BJ control cells (Fig. 13B). H23 and H460 lung cancer cells showed only an increased level of multi-nucleated cells and decreased level of mono-nucleated cells but not a significant change in bi-nucleated cells (Fig. 13B). The fraction of bi-nucleated cells increased in HOP92, HOP62, A549 and in BJ cells (Fig. 13B). However, compared to BJ control cells, the effects in lung cancer cells upon PRC1 depletion were more severe as cells with two nuclei increased from around 35% to 55% (Fig. 13B). In BJ cells, cells with two nuclei increased to roughly 10% (Fig. 13B). Importantly, the shRNA directed against luciferase showed no significant change in nucleation of lung cancer cells (Fig. 13B).

In conclusion, PRC1 is required for proliferation as well as cytokinesis of lung cancer cells.

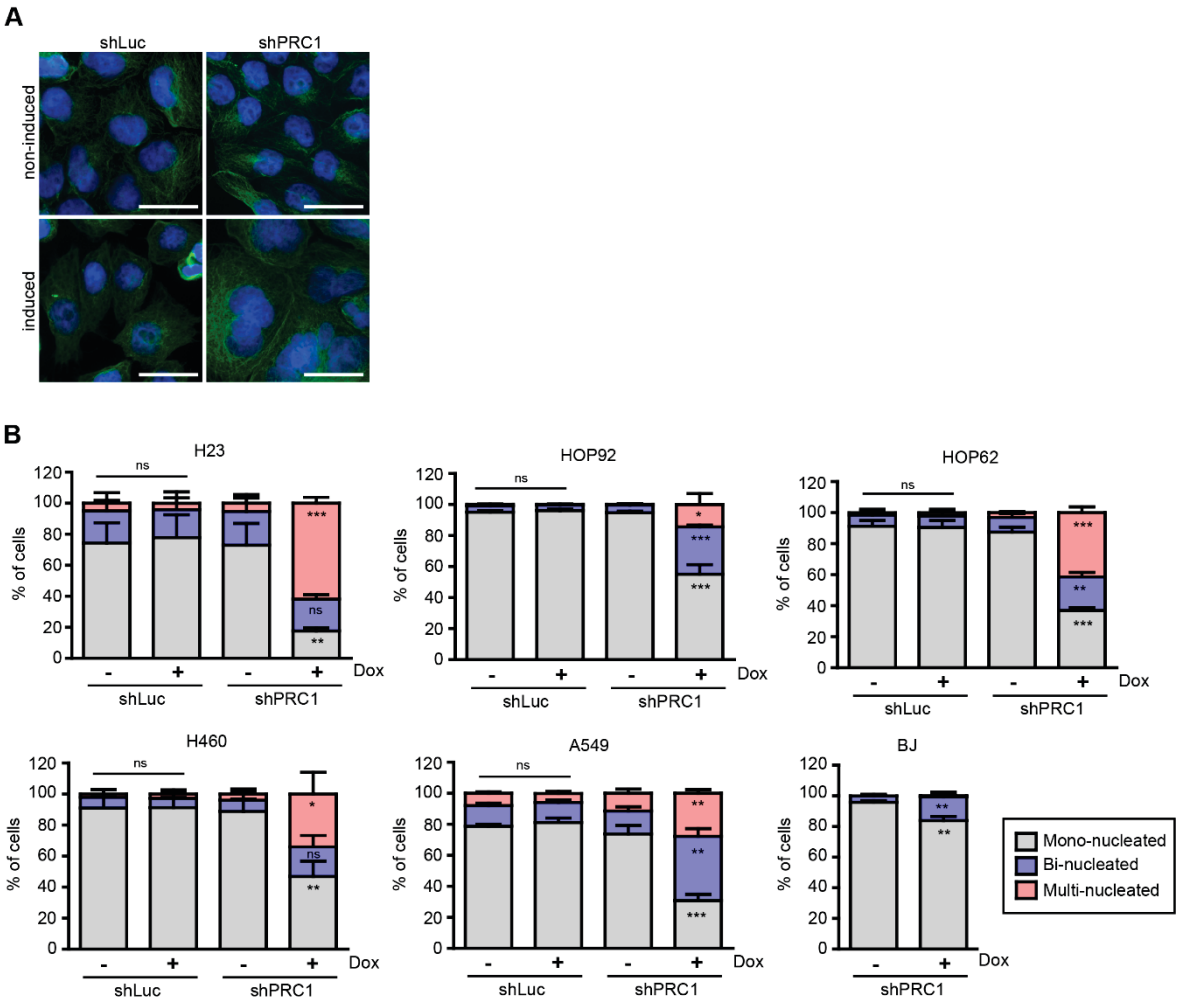

Figure 13: PRC1 depletion causes cytokinesis defects in lung cancer cell lines.
(A) H460 lung cancer cell lines either expressing an inducible control shRNAs (shLuc) or a shRNA directed against PRC1 (shPRC1) were treated with or without doxycycline for 4 days. Subsequently, cells were fixed and immunostained with tubulin (green) and Hoechst (blue) and investigated by fluorescence microscopy. Bar: 25 µm. (B) H23, HOP92, HOP62, H460 and A549 lung cancer cells expressing either a control shRNA (shLuc) or a PRC1-specific shRNA (shPRC1) were treated without (-) or with (+) 1 µg/ml doxycycline (Dox) for 4 days. BJ control cells expressing a PRC1-specific shRNA were treated in the same way as the lung cancer cells. Cells were fixed and investigated by microscopy. Quantification of mono-, bi- and multinucleated cells were shown. n=3 biological replicates. Statistical significance was determined by Student's t-test. *p<0.05; **p<0.01; ***p<0.001; ns: not significant.

3.4 Depletion of PRC1 results in apoptosis of p53-mutant lung cancer cell lines and in senescence of p53-wildtype lung cancer cell lines

PRC1 depletion leads to a proliferation deficit and multi-nucleation of different lung cancer cell lines as described above. To follow up effects in lung cancer cells upon PRC1 knockdown, I first performed a flow cytometry analysis after PRC1 depletion. Cell cycle analysis after 8 days of PRC1 depletion revealed a strong increase in the percentage of subG1 cells from around 4% to approximately 20% in H23 cells and over 30% in HOP62 cells (Fig. 14A). The subG1 population is indicative of degraded DNA which is a hallmark of apoptosis. The subG1 population was also significantly higher in HOP92 cells (Fig. 14A). Remarkably, an increase in the subG1 population correlated with the p53 mutant status of the cells, whereas p53 wildtype cells showed almost no effect upon PRC1 depletion (Fig. 14A). To independently confirm the flow cytometry results, immunoblotting was performed using a specific antibody against cleaved caspase-3, which is the effector caspase downstream of intrinsic and extrinsic apoptosis stimuli. As expected, apoptosis was observed after PRC1 depletion in H23, HOP62 and HOP92 cells but not in H460 and A549 cells (Fig. 14B). Apoptosis after PRC1 depletion was independently confirmed by Annexin V-FITC staining of H23, HOP62, and HOP92 cells and by fluorescence microscopy (Fig. 14C). BJ control cells served as a negative control and showed no apoptosis upon PRC1 depletion as determined by Annexin V-FITC staining (Fig. 14C).

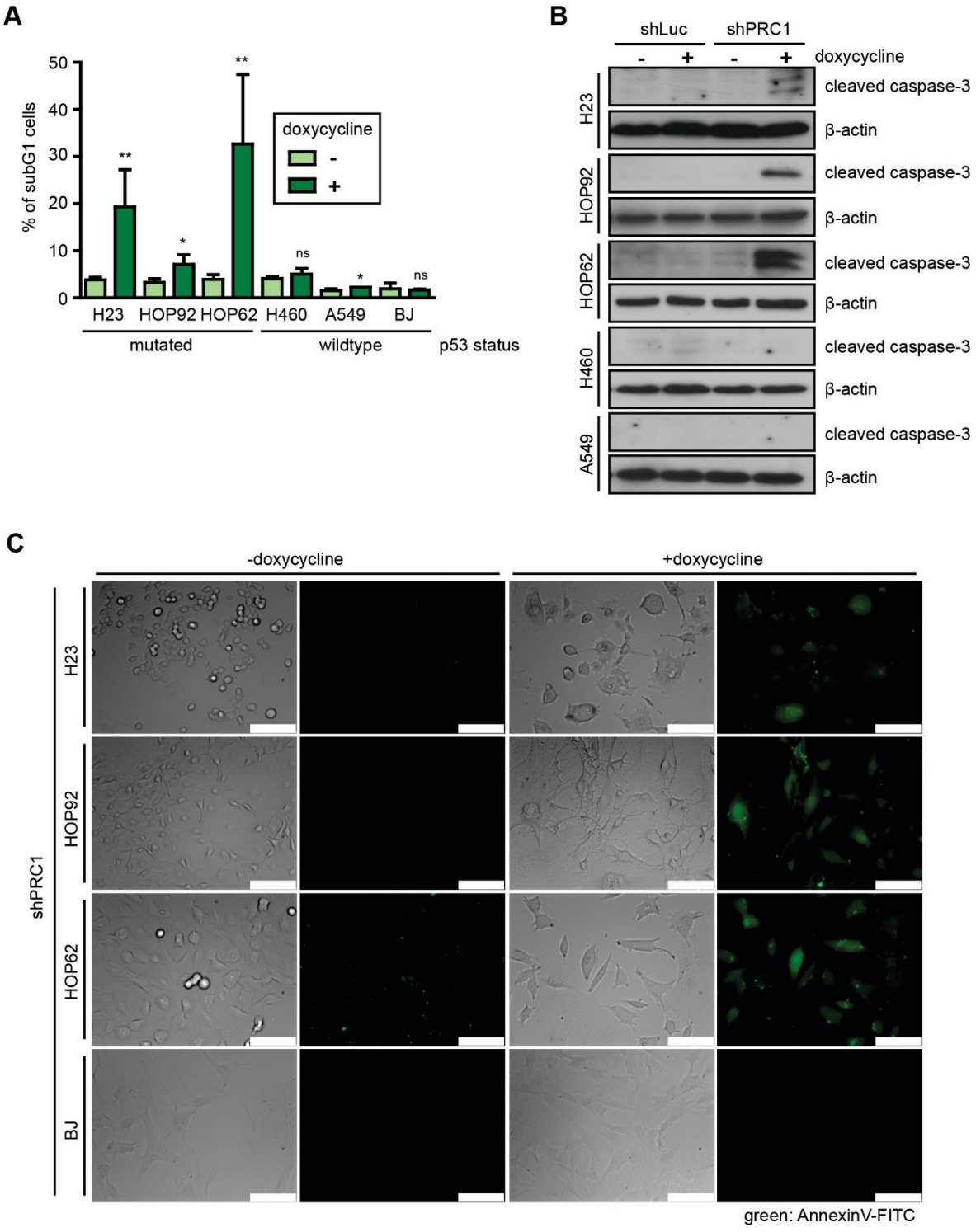

Figure 14: PRC1 depletion results in apoptosis in p53 mutant lung cancer cells.
(A) The indicated cell lines stably expressing the inducible shRNA directed against PRC1 were treated with 0.5 µg/ml doxycycline for 8 days. The fraction of apoptotic subG1 cells after depletion of PRC1 was determined by flow cytometry (n=3 experiments for HOP92, H460, A549, BJ; n=4 experiments for H23 and HOP62). **p < 0.01, *p< 0.05. Student's t-test. (B) Immunoblotting for cleaved caspase-3 confirmed the induction of apoptosis in HOP62, HOP92 and H23 cells upon depletion of PRC1 with 0.5 µg/ml doxycycline for 8 days. (C) Apoptotic cells were detected with Annexin V-FITC staining by fluorescence microscopy after same treatment as in (B). Bar: 100 µM.

Interestingly, p53 wildtype lung cancer cells showed no induction of apoptosis after PRC1 depletion. Therefore, growth inhibition upon PRC1 knockdown might be due to senescence of the cells. To test whether p53 wildtype lung cancer cells became senescent after PRC1 depletion, cells were stained for ß-galactosidase, a marker of senescent cells. A549 and H460 lung cancer cell became indeed senescent upon PRC1 depletion (Fig. 15A). A positive β-galactosidase staining was observed after 4 days and the staining was even stronger after 8 days of PRC1 depletion in H460 and A549 cells (Fig. 15A). Lung cancer cells expressing a luciferase control shRNA showed no senescence phenotype (Fig. 15A). Next, to investigate molecular mechanisms underlying the growth arrest by PRC1 knockdown, immunoblotting was performed. Both, H460 and A549 lung cancer cells stabilized the tumor suppressor protein p53 on protein level after PRC1 depletion (Fig. 15B). Stabilization of p53 also resulted in the activation of the protein, as it induced its bona-fide downstream target p21, a cyclin dependent kinase inhibitor, on protein level too (Fig. 15B).

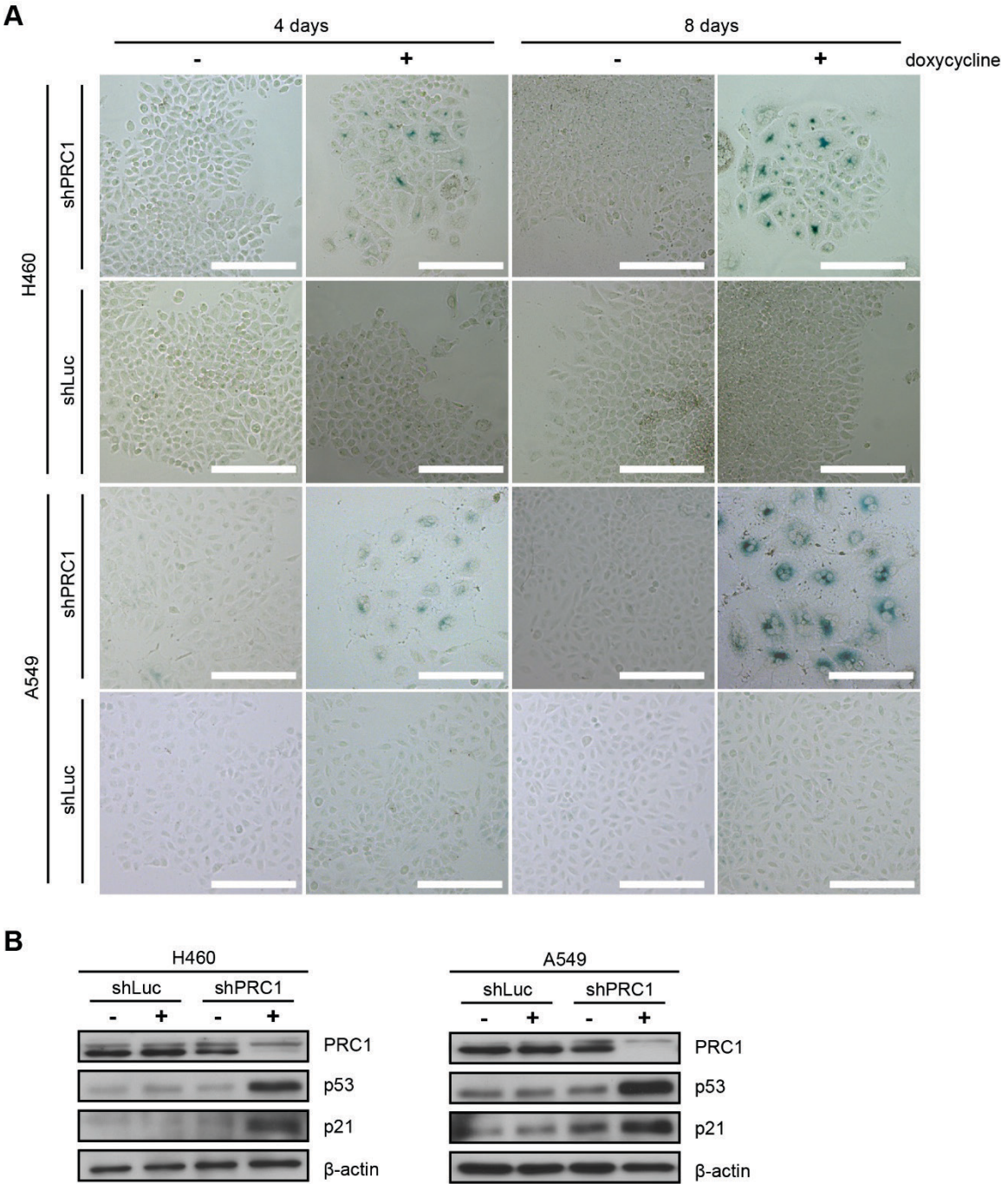

Figure 15: PRC1 depletion leads to senescence in p53 wildtype lung cancer cells.
(A) H460 and A549 cells stably expressing an inducible shRNA directed against PRC1 (shPRC1) or against luciferase (shLuc) were treated with 1 µg/ml doxycycline for 4 days or with 0.5 µg/ml doxycycline 8 days. Senescent cells were detected by staining for ß galactosidase. Bar: 200 µM. (B) Immunoblotting indicates that p53 and p21 are induced in H460 and A549 cells upon depletion of PRC1 with 1 µg/ml doxycycline for 4 days. β-actin was used as a loading control.

Next, A549 cells were treated with a compound called Nutlin-3 which inhibits the MDM2-p53 interaction and thus activates the p53 pathway (Tovar et al., 2006). A549 shPRC1 cells showed a significant proliferation deficit upon Nutlin-3 treatment next to PRC1 depletion (Fig. 16A). Moreover, p53 was strongly stabilized, p21 activated and proliferation was arrested due to senescence after 2.5 µM Nutlin-3 treatment for 4 days (Fig. 16B,C,E). These

results indicate that the p53 pathway is functional in A549 cells. Nutlin-3 treatment also caused a downregulation of PRC1 which might be due to the formation of DREAM by p53 through p21 (Fig. 16B,C) (Engeland, 2018). In contrast to depletion of PRC1, p53 stabilization by Nutlin-3 resulted in G1 cell cycle arrest and not in polyploidization or more cells in G2/M (Fig. 16D).

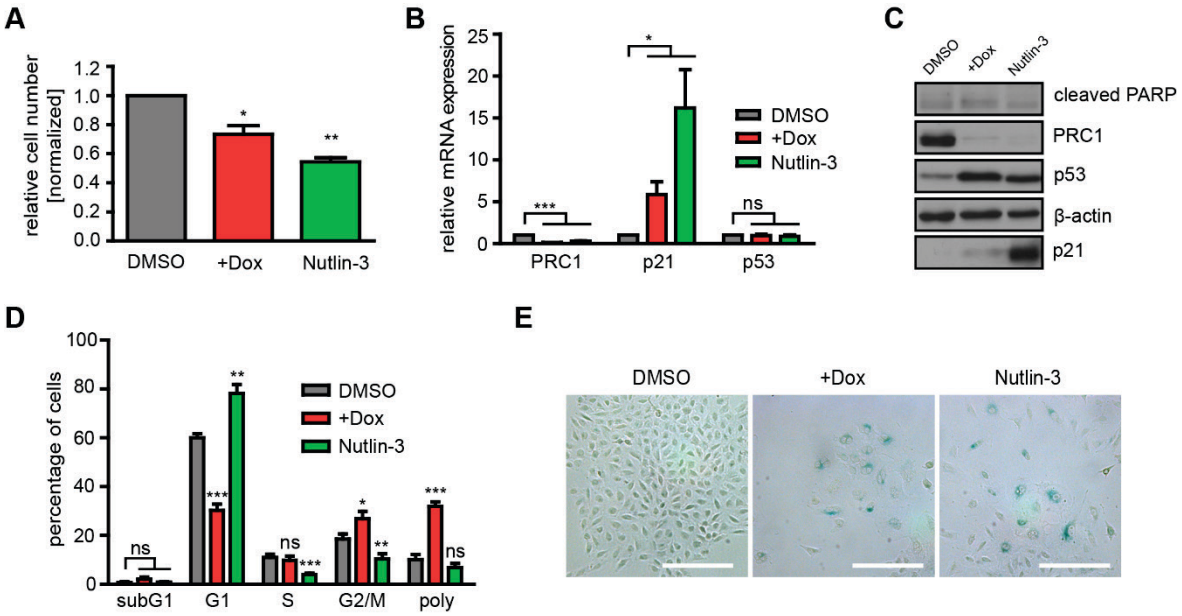

Figure 16: The p53 pathway is functional in A549 lung cancer cells.
(A) A549 shPRC1 cells were induced with 1 µg/ml doxycycline (Dox) or treated with 2.5 µM Nutlin-3 for 4 days. DMSO treated and non-induced cells served as a control. Cells were fixed and stained by crystal violet. Quantification of growth is shown. n=3 biological replicates. Student's t-test was used to determine statistical significance. *p<0.05; **p<0.01. (B,C) qRT-PCR and immunoblotting analysis of p53 and p21 after same treatment as in (A). mRNA expression of the different genes was calculated relative to the housekeeping gene GAPDH and normalized to the DMSO condition. As a marker for apoptosis cleaved PARP was used for immunoblotting. β-actin was used as a loading control for immunoblotting. qPCR analysis was done in n=3 biological replicates. Student's t-test. *p<0.05; ***p<0.001; ns: not significant. (D) A549 shPRC1 cells were treated as in (A). The fraction of cells in the different cell cycle phases were determined by flow cytometry. n=3 biological replicates. Student's t-test was used to determine statistical significance. *p<0.05; **p<0.01; ***p<0.001; ns: not significant. (E) Cells were treated as in (A). Senescent cells were detected by staining for ß-galactosidase. Bar: 200 µm.

Next, to test whether p53 is required for the induction of p21 and for senescence upon PRC1 depletion, I additionally performed a siRNA knockdown of p53 in PRC1 depleted cells. Immunoblotting showed that a p53 knockdown was achieved (Fig. 17B). The combined depletion of PRC1 and p53 prevented senescence and instead A549 cells became apoptotic (Fig. 17A,B,C). Apoptosis was detected by immunoblotting of cleaved caspase-3 and cleaved PARP as well as staining the cells with Annexin V-FITC for fluorescence microscopy (Fig. 17B,C). Importantly, A549 cells transfected with a control siRNA showed senescence and no apoptosis upon PRC1 depletion (Fig. 17A,B,C).

Additionally, I asked whether PRC1 depletion has an influence on the response to treatment with chemotherapeutics. Combinational treatment may enhance the effect of a single PRC1 depletion in p53-wildtype cells. Therefore, A549 lung cancer cells were treated with low concentrations of cisplatin together with PRC1 depletion for 6 days. Analysis of the proliferation of A549 cells showed a significantly enhanced inhibition of proliferation of cells with combined treatment compared to cells only depleted of PRC1 or treated with cisplatin (Fig. 17D). Moreover, p21 was induced when A549 cells were treated with cisplatin alone or treated with cisplatin and PRC1 was depleted in parallel (Fig. 17E). No apoptosis was detectable by 1 µM cisplatin treatment with or without PRC1 depletion (Fig. 17E). Instead, A549 cells were stained positive for senescence by combined treatment of cisplatin and PRC1 depletion (Fig. 17F). Also, cells after PRC1 knockdown or cisplatin treatment showed a senescence phenotype (Fig. 17F).

Taken together, PRC1 depletion causes apoptosis of p53 mutant cells and senescence of p53 wildtype cells.

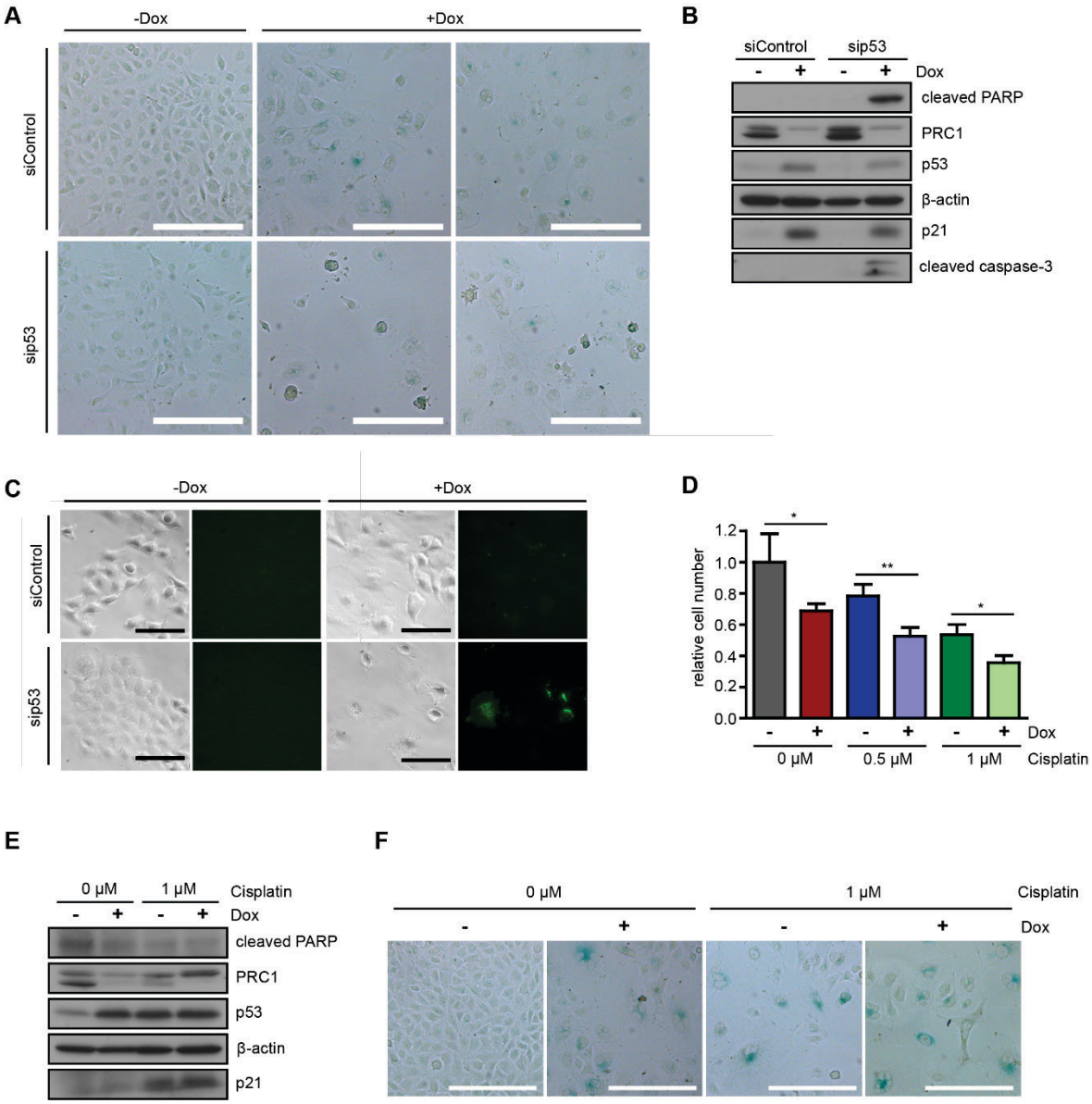

Figure 17: siRNA mediated knockdown of p53 and PRC1 depletion results in apoptosis of p53 wildtype cells, whereas cisplatin treatment leads to senescence of the cells.
(A) A549 shPRC1 cells were transfected with a siRNA specific for p53 or with a control siRNA. The expression of the shRNA directed against PRC1 was induced with 1 µg/ml of doxycycline (Dox) for 3 days. Senescent cells were detected by staining for ß-galactosidase. Bar: 200 µm. (B) Cell were treated as in (A) and induction of doxycycline were illustrated with – (non-induced) and + (induced). p53 and p21 were analyzed by immunoblotting. As markers of apoptosis, cleaved PARP and cleaved caspase-3 were analyzed by immunoblotting. β-actin was used as a loading control. (C) A549 shPRC1 cells were treated as in (A). Cells were fixed and stained for Annexin V-FITC. Apoptotic cells (green) were determined by fluorescence microscopy. Bar: 100 µm. (D) A549 cells were treated for 6 days with 0.5 µM or 1 µM cisplatin in combination with shRNA mediated depletion of PRC1, which was induced (+) by 0.5 µg/ml doxycycline (Dox). Non-induced cells were illustrated with -. As a control, cells were treated with DMF. Cells were fixed and stained by crystal violet and quantified. n=3 replicates. Student's t-test. *p<0.05; **p<0.01. (E) p53, p21 and cleaved PARP were analyzed by immunoblotting. β-actin served as a loading control. Indicated cell lines were treated for 6 days with 1 µM cisplatin and PRC1 depletion was induced (+) with 0.5 µg/ml of doxycycline. Non-induced cells were illustrated with -. (F) Cells were treated as described in (E). Senescent cells were detected by staining for ß-galactosidase. Bar: 200 µm.

3.5 PRC1 expression increases from S phase to G2/M phase of the cell cycle and localizes in the nucleus during interphase and at the central spindle and midbody during mitosis and cytokinesis in A549 lung cancer cells

PRC1 was first described as a mitotic spindle-associated CDK substrate which plays various important roles during mitosis and cytokinesis (Jiang et al., 1998; Mollinari et al., 2002; Zhu & Jiang, 2005). Furthermore, PRC1 contains two nuclear localization signals (NLS) in its C-terminal domain (Kellogg et al., 2016). To follow-up the enhanced expression of PRC1 in lung cancer, I was interested in the localization of the protein within the cell which might be helpful to understand its role in tumorigenesis.

A549 cells were fixed and stained for endogenous PRC1 and were investigated by fluorescence microscopy (Fig. 18A). Examples of a cell in mitosis and cytokinesis are shown in Fig. 18A. PRC1 is localized between dividing cells at the central spindle during mitosis and at the midbody during cytokinesis (Fig. 18A). Moreover, PRC1 was detected in the nucleus during interphase (Fig. 18A). Nuclear PRC1 staining was specific as shRNA-mediated depletion of PRC1 led to a loss of the signal (Fig. 18A).

Next, I was interested in the expression levels of PRC1 during different phases of cell cycle. Therefore, A549 lung cancer cells were synchronized at G1/S-border, before DNA replication, by a double thymidine block (Chen & Deng, 2018) and afterwards released for 3, 6, and 8 hours. Cell cycle synchronization was monitored by flow cytometry as shown in Fig. 17B. In parallel PRC1 protein levels were analyzed by immunoblotting (Fig. 18C). PRC1 amount was slightly enhanced after the thymidine block compared to asynchronous cells (Fig. 18C). After release of the cells back into the cell cycle the levels of PRC1 increased continuously as cells progressed from S phase to G2/M (Fig. 18C). The highest PRC1 protein levels were observed when cells were in late G2 phase or in mitosis (Fig. 18C). High levels of PRC1 during S phase and G2/M and low levels of PRC1 in G1 is consistent with previous results (Jiang et al., 1998; Pellman et al., 1995). It was also described that PRC1 localizes to the nucleus during interphase (Jiang et al., 1998; Mollinari et al., 2002). However, so far, the function of nuclear PRC1 during interphase remains largely unknown.

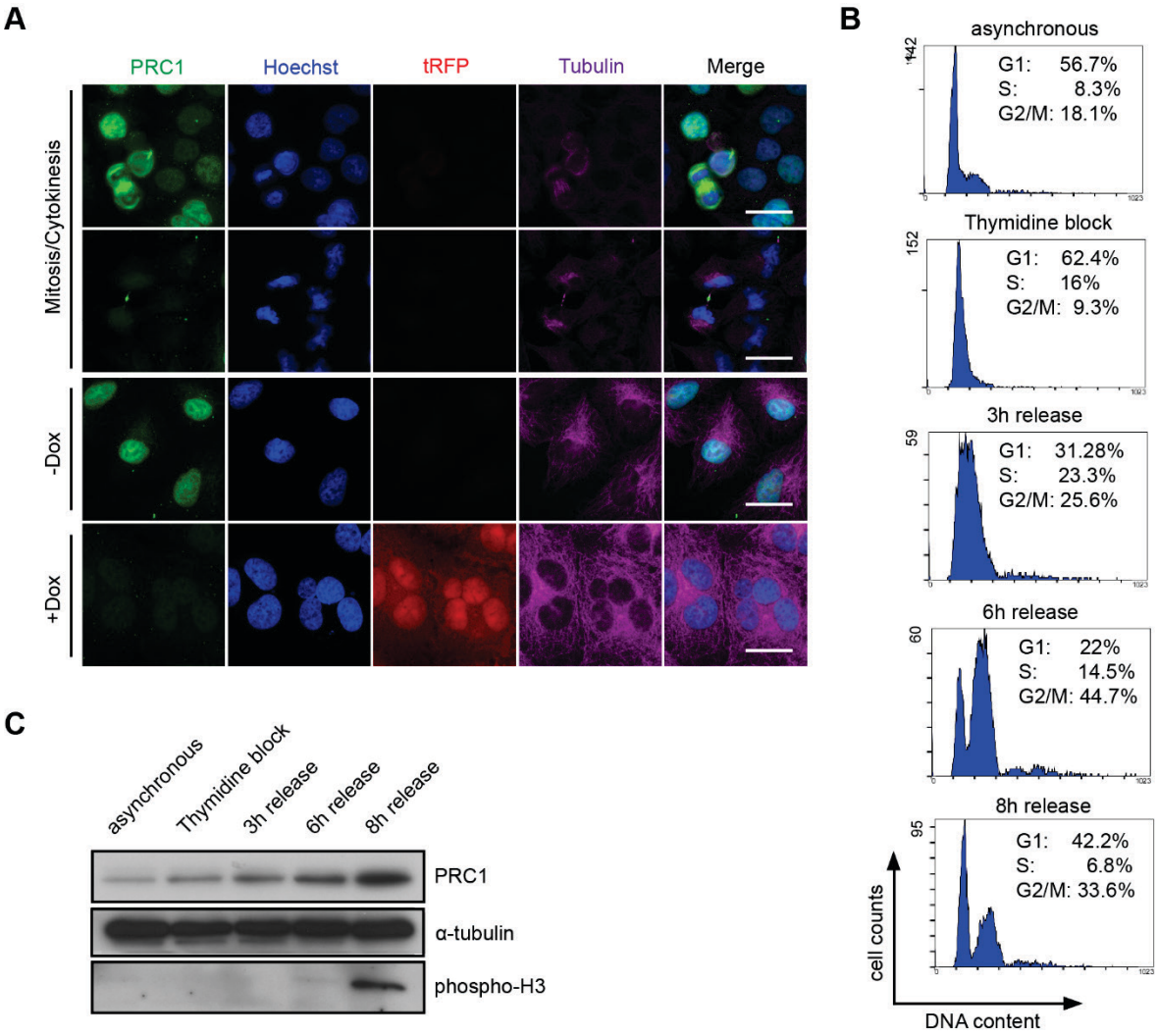

Figure 18: Subcellular localization of PRC1 and expression during the cell cycle in A549 lung cancer cells.
(A) A549 cells expressing an inducible shRNA directed against PRC1 (shPRC1) were treated without (-Dox, no tRFP signal) or with 1 µg/ml doxycycline (+Dox) for 3 days. Cells were fixed and stained for PRC1 (green), Hoechst (blue) and α-tubulin (purple) and investigated by fluorescence microscopy. tRFP is co-expressed with the shRNA. Bar: 25 µm. (B) A549 lung cancer cells were synchronized at the G1/S-border by a double thymidine block and then released for 3, 6 and 8 hours. The fraction of cells in the different cell cycle phases was measured by flow cytometry. (C) The protein expression of PRC1 was analyzed in synchronized A549 cells as described in (B) by immunoblotting. α-tubulin served as a loading control and phospho-H3 was used as a marker of cells in late G2 phase or mitosis.

3.6 Overexpression of PRC1-WT and PRC1-NLS3A mutant leads to a proliferation deficit, strong microtubule-bundling, multi-nucleation and enlargement of the cells

Besides the well-established role of PRC1 in cytokinesis, Chen et al. linked the protein to the Wnt signalling pathway in hepatocellular carcinoma (Chen et al., 2016). More recently, PRC1 has also been linked to Wnt/β-catenin signalling in lung adenocarcinoma but its molecular function remains unclear (Zhan, Zhang, et al., 2017). It has been hypothesized that PRC1 has additional functions besides its role in mitosis and cytokinesis also due to its localization in the nucleus and expression before mitosis and cytokinesis (see 3.5).

To begin to address the putative nuclear function of PRC1, A549 lung cancer cell lines which stably express doxycycline-inducible versions of flag-tagged PRC1 were generated (Fig. 19A). A549 cells were also used by Zhan et al. for their study of PRC1 in lung cancer (Zhan, Zhang, et al., 2017). For analysis of the possible nuclear function, a version of PRC1 with mutations in the nuclear localization sequence (NLS) were generated and named NLS3A (Fig. 19A). The NLS3A mutant of PRC1 has been described before by Chen et al. (Chen et al., 2016). Additionally, a mutant lacking the first 78 amino acids at the N-terminus and failing to associate with the spindle midzone in mitosis was generated (Fig. 19A). The N-terminal domain is essential for the function of PRC1 in mitosis and cytokinesis (Kurasawa et al., 2004; Mollinari et al., 2002).

Dose-dependent expression of the different constructs was achieved by doxycycline as analyzed by immunoblotting using an anti-flag antibody to distinguish them from endogenous PRC1 (Fig. 19B). PRC1-WT and PRC1-NLS3A expression plateaued at about 0.05 µg/ml of doxycycline whereas maximum levels of PRC1-ΔN78 were reached with 0.025µg/ml of doxycycline with little increase with higher concentrations (Fig. 19B).

Next, localization of the different PRC1 constructs was analyzed by immunostaining using an anti-flag antibody. Non-induced cells only showed a background signal compared to doxycycline-induced cells (Fig. 19C-E). PRC1-WT and PRC1-NLS3A were localized at the midbody between dividing cells, whereas PRC1-ΔN78 was absent from the midbody (Fig. 19C-E). Moreover, PRC1-WT and PRC1-ΔN78 were detected in the nuclei of interphase cells (Fig. 19C,E). As expected, PRC1-NLS3A mutant was not detectable in the nuclei of interphase cells (Fig. 19D). Instead, PRC1-NLS3A mutant was detected in the cytoplasm where it co-localized with bundled perinuclear microtubules (Fig. 19D). Similar effects of strong microtubule-bundling and colocalization within the cytoplasm were also observed in PRC1-WT expressing cells but not for PRC1-ΔN78 which is explained in more detail in the following parts (Fig. 19C,E).

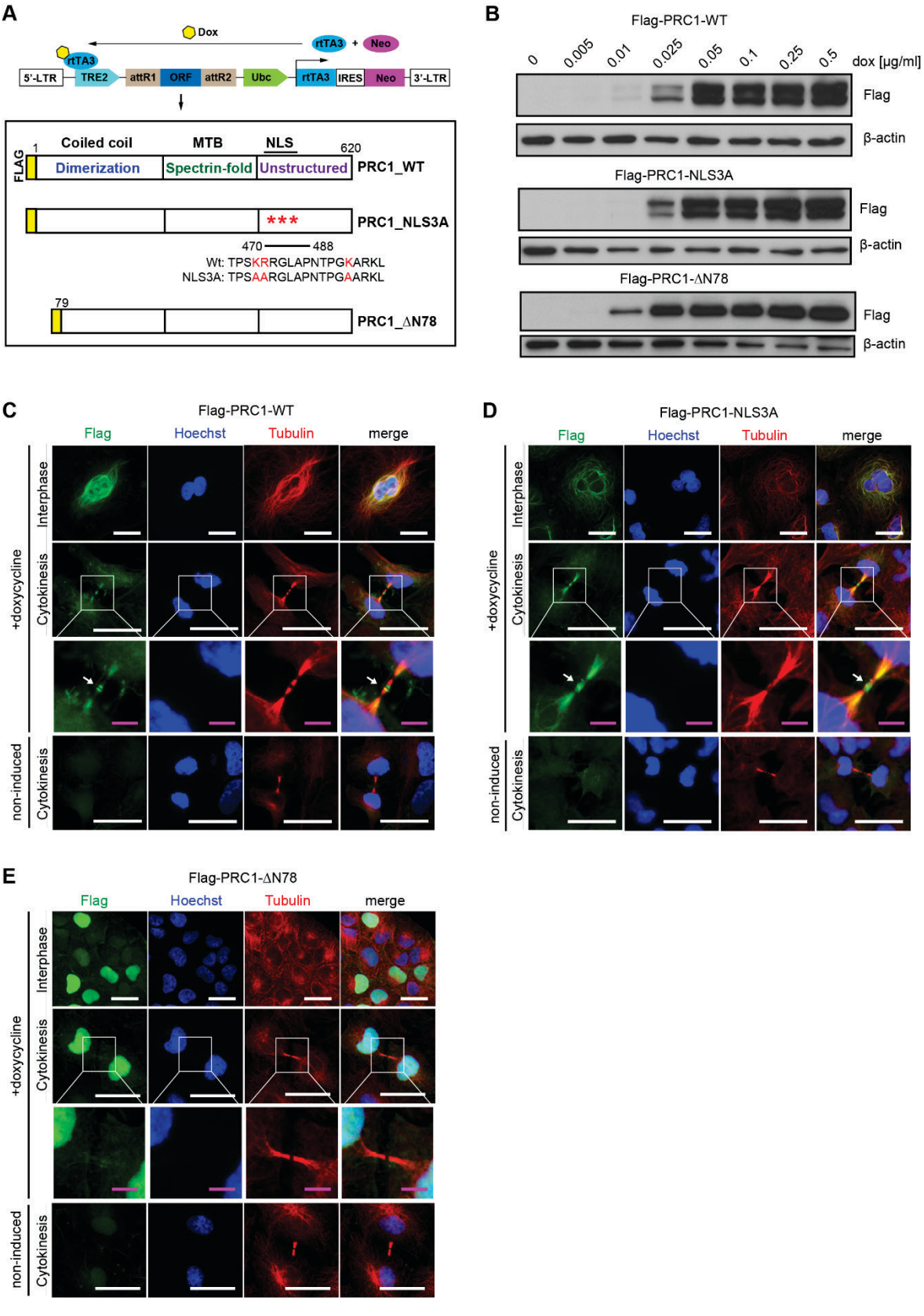
A
Dox
rtTA3
rtTA3 + Neo
5'-LTR
TRE2
attR1
ORF
attR2
Ubc
rtTA3
IRES
Neo
3'-LTR
FLAG
1
Coiled coil
MTB
NLS
620
Dimerization
Spectrin-fold
Unstructured
PRC1_WT
***
PRC1_NLS3A
470
488
Wt: TPSKRRGLAPNTPGKARKL
NLS3A: TPSAARGLAPNTPGAARKL
79
PRC1_ΔN78
B
Flag-PRC1-WT
0
0.005
0.01
0.025
0.05
0.1
0.25
0.5
dox [µg/ml]
Flag
β-actin
Flag-PRC1-NLS3A
Flag
β-actin
Flag-PRC1-ΔN78
Flag
β-actin
C
Flag-PRC1-WT
Flag
Hoechst
Tubulin
merge
+doxycycline
Interphase
Cytokinesis
non-induced
Cytokinesis
D
Flag-PRC1-NLS3A
Flag
Hoechst
Tubulin
merge
+doxycycline
Interphase
Cytokinesis
non-induced
Cytokinesis
E
Flag-PRC1-ΔN78
Flag
Hoechst
Tubulin
merge
+doxycycline
Interphase
Cytokinesis
non-induced
Cytokinesis

Figure 19: Expression and localization of PRC1, PRC1-NLS3A and PRC1-ΔN78 in A549 lung cancer cells.
(A) Scheme of the pINDUCER vector for inducible cDNA expression. Scheme of the different PRC1 constructs are shown below. The NLS3A mutant contains three amino acid changes in the NLS sequence. PRC1-ΔN78 lacks the first 78 amino acids from the N-terminus. All three constructs were generated with an N-terminal flag-tag. Dox: doxycycline; rtTA3: reverse tet-transactivator 3; TRE2: tetracycline response element 2; attR1/2: recombination sites for cloning; ORF: open reading frame; Ubc: Ubiquitin C promoter; IRES: internal ribosomal entry site; Neo: Neomycin resistance; LTR: long terminal repeat; MTB: microtubule-binding; NLS: nuclear localization signal; WT: wildtype. (B) PRC1 wildtype, NLS3A mutant and -ΔN78 mutant were induced with increasing doxycycline concentrations for 4 days in A549 cells. PRC1 expression was determined by immunoblotting using a flag antibody. ß-actin served as a loading control. Dox: doxycycline. (C-E) A549 cells either expressing PRC1-WT (C), or PRC1-NLS3A (D) or PRC1-ΔN78 (E) were treated with or without 0.5 µg/ml doxycycline. Four days later, cells were fixed and immunostained for flag (green), Hoechst (blue) and tubulin (red) and investigated by fluorescence microscopy. Example of a cell in interphase and cytokinesis are shown. Arrow: midbody. White bar: 25 µm; Magenta bar: 5 µm.

Next, I was interested in whether expression of the different PRC1-construct has any effect on proliferation of A549 cells. To address this, PRC1-WT, PRC1-NLS3A or PRC1-ΔN78 A549 cells were seeded in low densities and expression of the constructs was induced with different doxycycline concentrations for up to 8 days. Afterwards cells were fixed and stained with crystal violet every two days. Crystal violet staining after 8 days revealed that proliferation was inhibited by wildtype and NLS3A PRC1 but not by ΔN78-PRC1 which was surprising as PRC1 is highly expressed in cancer cells (Fig. 20A). Analysis of the kinetics illustrated a dose-dependent negative effect on proliferation by PRC1-WT and PRC1-NLS3A starting from day two by 0.025 µg/ml and higher concentrations of doxycycline (Fig. 20B).

As mentioned above, expression of PRC1-WT and PRC1-NLS3A expression leads to perinuclear microtubule-bundling. This effect may cause a change in cell size upon expression of PRC1-WT and PRC1-NLS3A. To analyse the cell size, A549 cells were cultured for four days with and without 0.5 µg/ml of doxycycline and then the cells were fixed and immunostained (Fig. 20C; Shin, 2018). The diameter of the cells was measured by fluorescence microscopy. Quantification revealed that the cell size was significantly enlarged from around 30 µM to more than 90 µM after expression of PRC1-WT or PRC1-NLS3A (Fig. 20D; Shin, 2018). In contrast, PRC1-ΔN78 only caused a slight increase in cell size (Fig. 20D; Shin, 2018).

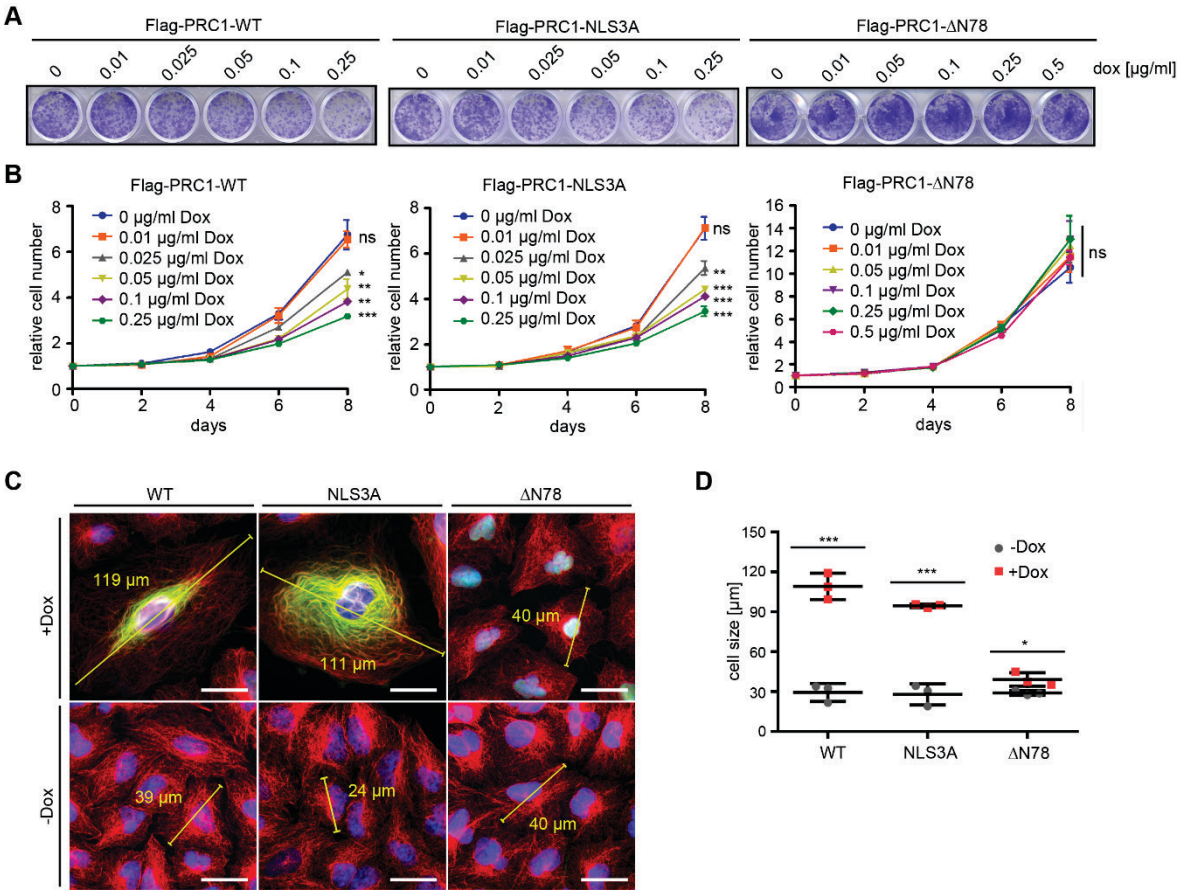

Figure 20: Ectopical expression of PRC1-WT or PRC1-NLS3A causes a proliferation deficit and enlargement of A549 cells.
(A) A549 lung cancer cell lines expressing inducible PRC1-WT, PRC1-NLS3A or PRC1-ΔN78 were cultured for a period of 8 days with the indicated concentrations of doxycycline (Dox). Every two days, cells were fixed and colonies were stained with crystal violet. Crystal violet staining after 8 days of culture is shown. (B) Quantification of the cell growth from (A) by measuring the density of crystal violet relative to day 0. n=3 biological replicates. Student's t-test was used for statistical analysis. For clarity, statistical significance is only shown for day 8. *p<0.05; **p<0.001; ***p<0.0001; ns: not significant. (C) A549 cells either expressing PRC1-WT, or PRC1-NLS3A or PRC1-ΔN78 were treated with or without 0.5 µg/ml doxycycline (Dox) for four days. Subsequently, cells were fixed and immunostained for flag (green), Hoechst (blue) and tubulin (red) and investigated by fluorescence microscopy. The diameter of the cells was measured at the fluorescence microscope. Bar: 25 µm. The experiment was performed by Shin, 2018 (D) Quantification of the cell size from (C) is shown. Each dot and square represent one experiment. n=3 biological replicates. The experiment was performed by Shin, 2018. Student's t-test. *p<0.05; ***p<0.0001. Dox: doxycycline

Next, I asked whether microtubule-bundling correlates with expression of the different PRC1 constructs and with their localization. To do so, A549 cells were cultured for four days and PRC1-WT, PRC1-NLS3A and PRC1-ΔN78 were induced with 0.25 µg/ml of doxycycline and then cells were fixed and immunostained (Fig. 21A). Quantification revealed that 80-90% of the cells stained flag-positive upon induction of PRC1-WT, PRC1-NLS3A and PRC1-ΔN78 in A549 cells (Fig. 21B). PRC1 wildtype was detected in around 40% of the cells in the nucleus, in 20% only in the cytoplasm and in about 20% in the cytoplasm and in the nucleus (Fig. 21B). PRC1-NLS3A was exclusively detectable in the cytoplasm, whereas PRC1-ΔN78 mutant was only detectable in the nucleus (Fig. 21B). Microtubule-bundling was observed in around 50% of flag-positive A549 cells expressing wildtype PRC1 in the

cytoplasm or in the cytoplasm and nucleus (Fig. 21C). When wildtype PRC1 was only detected in the nucleus, no microtubule-bundling was observed (Fig. 20C). Almost all flag-positive stained cells expressing cytoplasmic NLS3A-PRC1 also exhibited microtubule-bundling (Fig. 21C). In contrast PRC1-ΔN78 was only detected in the nucleus and no microtubule-bundling was observed (Fig. 21C).

Next, I asked whether expression of PRC1-WT and PRC1-NLS3A results in multi-nucleation, an indication of cytokinesis failure. To analyze also the alteration over time, PRC1-WT, PRC1-NLS3A and PRC1-ΔN78 were induced for 1, 2, 3 and 4 days with 0.25 µg/ml of doxycycline and then PRC1 expression and microtubule-bundling was investigated by immunostaining (Fig. 21A, Supplementary Fig. 1). After one day of induction of PRC1-WT and PRC1-NLS3A, cytoplasmic microtubule-bundling was already observed (Supplementary Fig. 1). After two days the perinuclear microtubule-bundling has further increased, especially upon PRC1-NLS3A expression (Supplementary Fig. 1). Quantification of mono-nucleated cells revealed a reduction of about 15% upon PRC1-WT and PRC1-NLS3A induction after one day (Fig. 21D,E). Mono-nucleated cells decreased further by around 30-40% after two days with no enhancement by longer expression of PRC1-WT and PRC1-NLS3A (Fig. 21D,E). Whereas mono-nucleated cells decreased, bi- and multi-nucleated cells increased together to more than 10% after one day and up to 40% after two through four days upon PRC1-WT and PRC1-NLS3A expression (Fig. 21D,E). PRC1-ΔN78 expression had minor effects on the status of mono-, bi-, and mutli-nucleated cells over four days of cultivation (Fig. 21F).

In conclusion, expression of PRC1-WT and PRC1-NLS3A in A149 cells leads to a proliferation deficit, microtubule-bundling, multi-nucleation and enlargement of the cells.

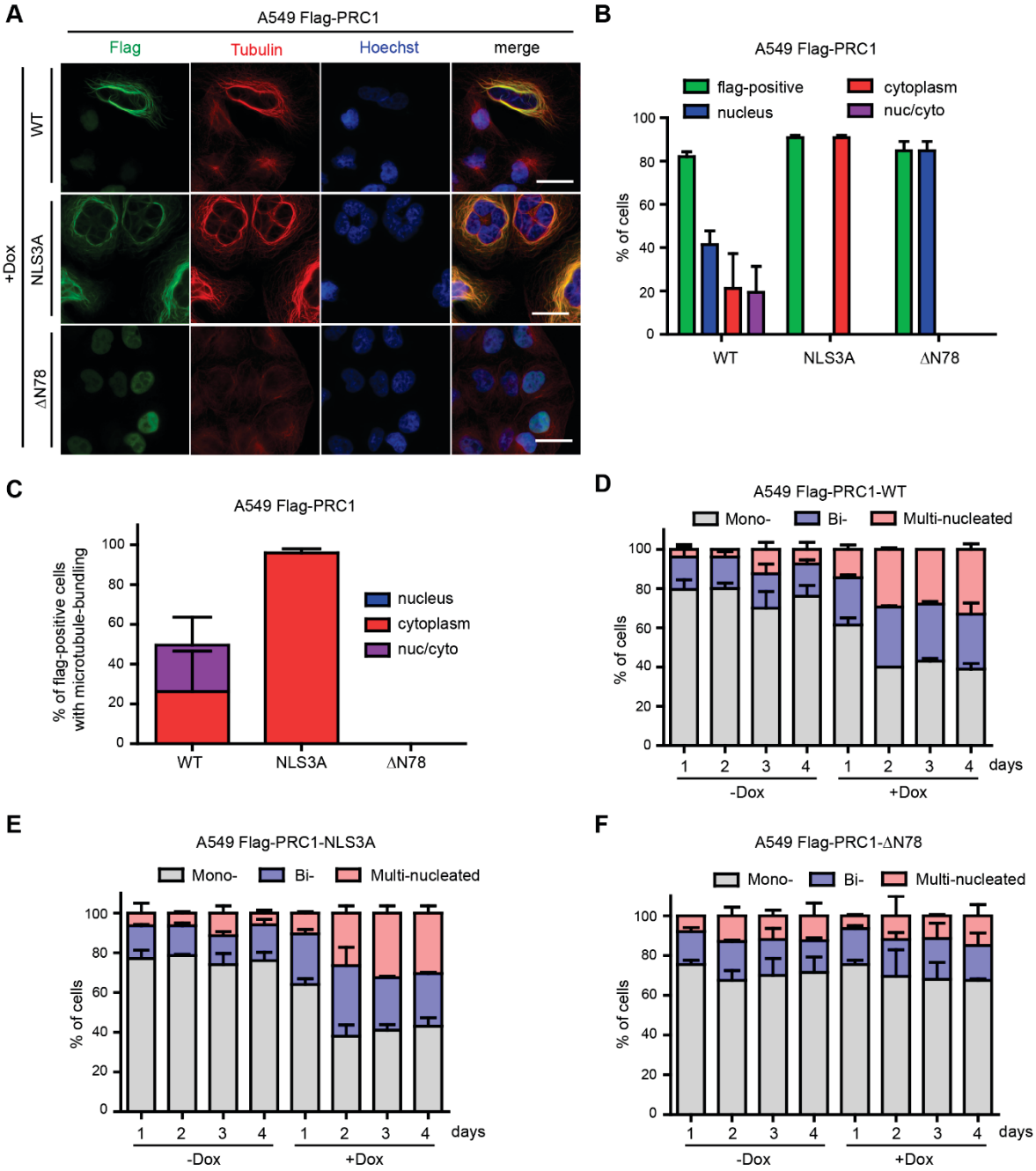

Figure 21: PRC1-WT and PRC1-NLS3A overexpression leads to strong microtubule-bundling and multi-nucleation in A549 lung cancer cells.
(A) A549 cells either expressing PRC1-WT, PRC1-NLS3A or PRC1-ΔN78 were treated with (+) or without (-) 0.25 µg/ml doxycycline (Dox) for 4 days. Subsequently, cells were fixed and immunostained for flag (green), tubulin (red), and Hoechst (blue) and investigated by fluorescence microscopy. Non-induced cells are shown in Supplementary Figure 1. Bar: 25 µm. (B) Quantification of cells from (A) in following categories are shown: flag-positive cells and localization of the constructs (nucleus, cytoplasm or nuc/cyto). Mean of n=2 biological replicates. nuc/cyto, nucleus/cytoplasm (C) Quantification of flag-positive A549 cells with a microtubule-bundling phenotype after 4 days of doxycycline treatment from (A) is shown. Mean of n=2 biological replicates. (D-F) A549 cells either expressing PRC1-WT, PRC1-NLS3A or PRC1-ΔN78 were treated with (+) or without (-) 0.25 µg/ml doxycycline (Dox) for 1-, 2-, 3-, and 4 days. Example images are shown in (A) or supplementary figure 1. Quantification of mono-, bi- and multi-nucleated cells are shown. Flag-positive cells were counted for the induced condition. Mean of n=2 biological independent experiments are shown.

Next, PRC1-WT, PRC1-NLS3A and PRC1-ΔN78 were expressed in H460 cells to confirm the effects of microtubule-bundling, multi-nucleation and cell enlargement in a second cell line. Expression of the different PRC1 constructs in H460 cells was determined by immunoblotting using an anti-flag antibody (Fig. 22A). Like in A549 cells, expression of PRC1-WT or PRC1-NLS3A but not PRC1-ΔN78 caused perinuclear bundling of the microtubules (Fig. 22B). Quantification of the number of nuclei of flag-positive cells revealed a reduction in mono-nucleated cells from nearly 90% to around 55% after expression of PRC1-WT or PRC1-NLS3A (Fig. 22C). Bi-nucleated cells were only slightly increased, whereas multi-nucleated cells increased about 30% after PRC1-WT and PRC1-NLS3A expression (Fig. 22C). Expression of PRC1-ΔN78 had only minor effects on the proportion of multi-nucleated cells (Fig.22C). For analysis of cell size, H460 cells were treated for four days with 0.5 µg/ml of doxycycline and then fixed and immunostained. Microscopic measurement of the diameter of the cells revealed a significant enlargement of H460 cells from around 20 µM to more than 60 µM in diameter upon expression of PRC1-WT and PRC1-NLS3A. Expression of PRC1-ΔN78 had a minor effect on cell size (Fig. 22D, Shin, 2018).

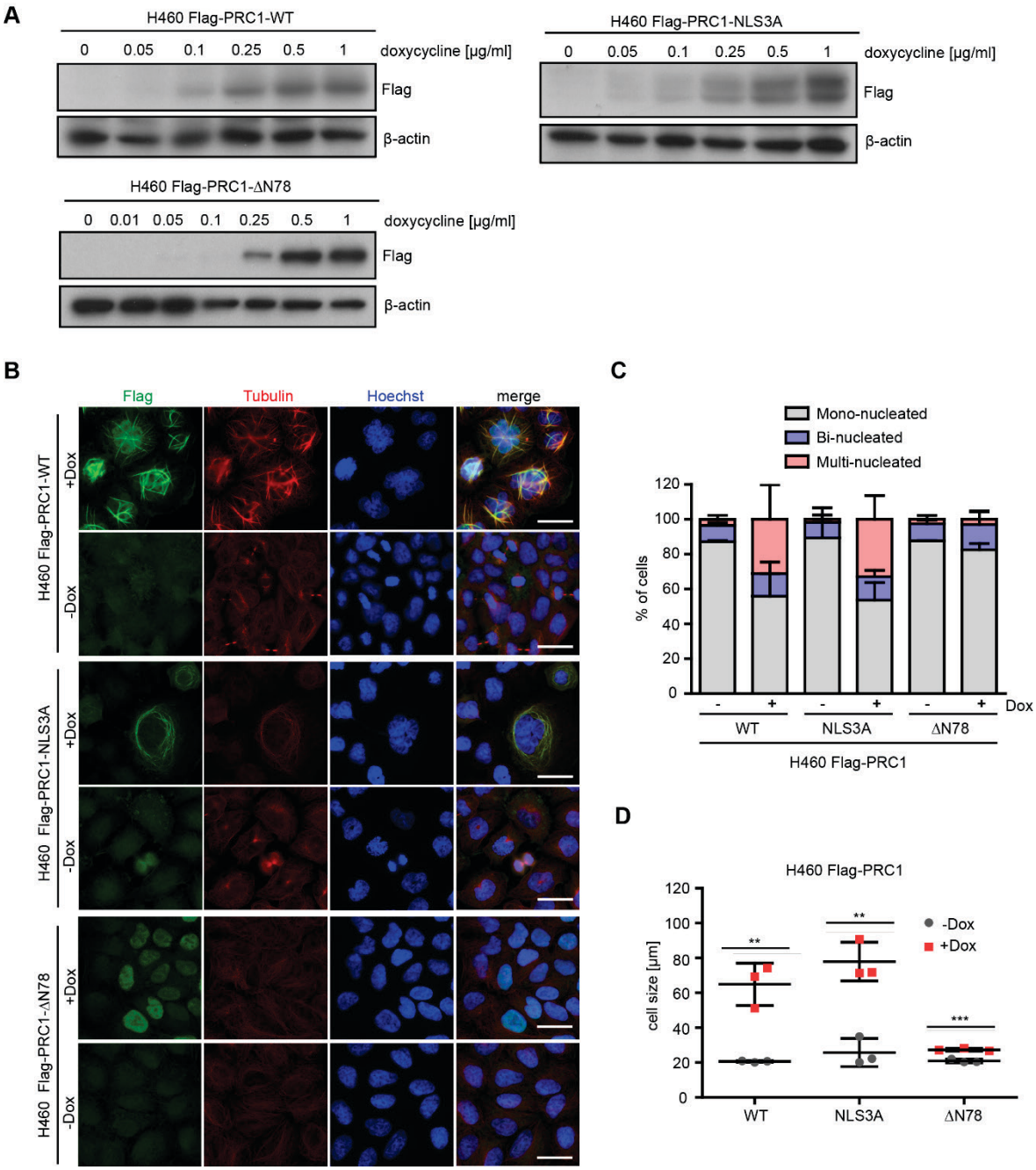

Figure 22: PRC1-WT and PRC1-NLS3A expression in H460 lung cancer cells leads to microtubule-bundling, multi-nucleation and enlargement of the cells.
(A) The expression of Flag-PRC1-WT, Flag-NLS3A or Flag-PRC1-ΔN78 was induced in H460 cells with the indicated doxycycline concentrations. Cells were fixed and the expression of PRC1 was determined by immunoblotting by using an anti-Flag antibody. As a loading control β-actin was used. (B) Indicated cell lines were treated without (-) or with (+) 0.5 µg/ml doxycycline (Dox) for 4 days. Subsequently, cells were fixed and immunostained for PRC1 by using an anti-Flag antibody (green), tubulin (red) and Hoechst (blue) and investigated by fluorescence microscopy. Bar: 25 µm. (C) Flag-PRC1-WT, Flag-NLS3A or Flag-PRC1-ΔN78 constructs were induced with (+) 0.5 µg/ml doxycycline (Dox) for 4 days. Non-induced (-) cells served as a control. Cells were fixed and immunostained as in (B). Quantification of mono, bi and multi-nucleated cells is shown. Just flag-positive cells were counted for the induced condition. Mean of n=2 biological independent experiments are shown. (D) H460 cells either expressing PRC1-WT, PRC1-NLS3A or PRC1-ΔN78 were treated as in (C). Quantification of the cell size is shown. Each dot and square represent one experiment. n=3 biological replicates. The experiment was performed by Shin, 2018. Student's t-test. *p<0.05; ***p<0.0001.

3.7 PRC1 overexpression stabilizes microtubules and its ability to bind to microtubules is involved in the inhibition of proliferation

PRC1 overexpression causes strong perinuclear microtubule-bundling as described before. Based on this observed phenotype, I asked whether the enhanced PRC1 expression caused microtubule stabilization within the cytoplasm. To address this question, A549 PRC1-WT, PRC1-NLS3A and PRC1-ΔN78 expressing cells were stained with an antibody directed at acetylated α-tubulin. Acetylation of α-tubulin is associated with microtubule-stabilization (Al-Bassam & Corbett, 2012). As expected, PRC1-WT and PRC1-NLS3A expression resulted in an enhanced stabilization of microtubules that co-localized with PRC1 (Fig. 23). PRC1-ΔN78 was unable to stabilize microtubules (Fig. 23).

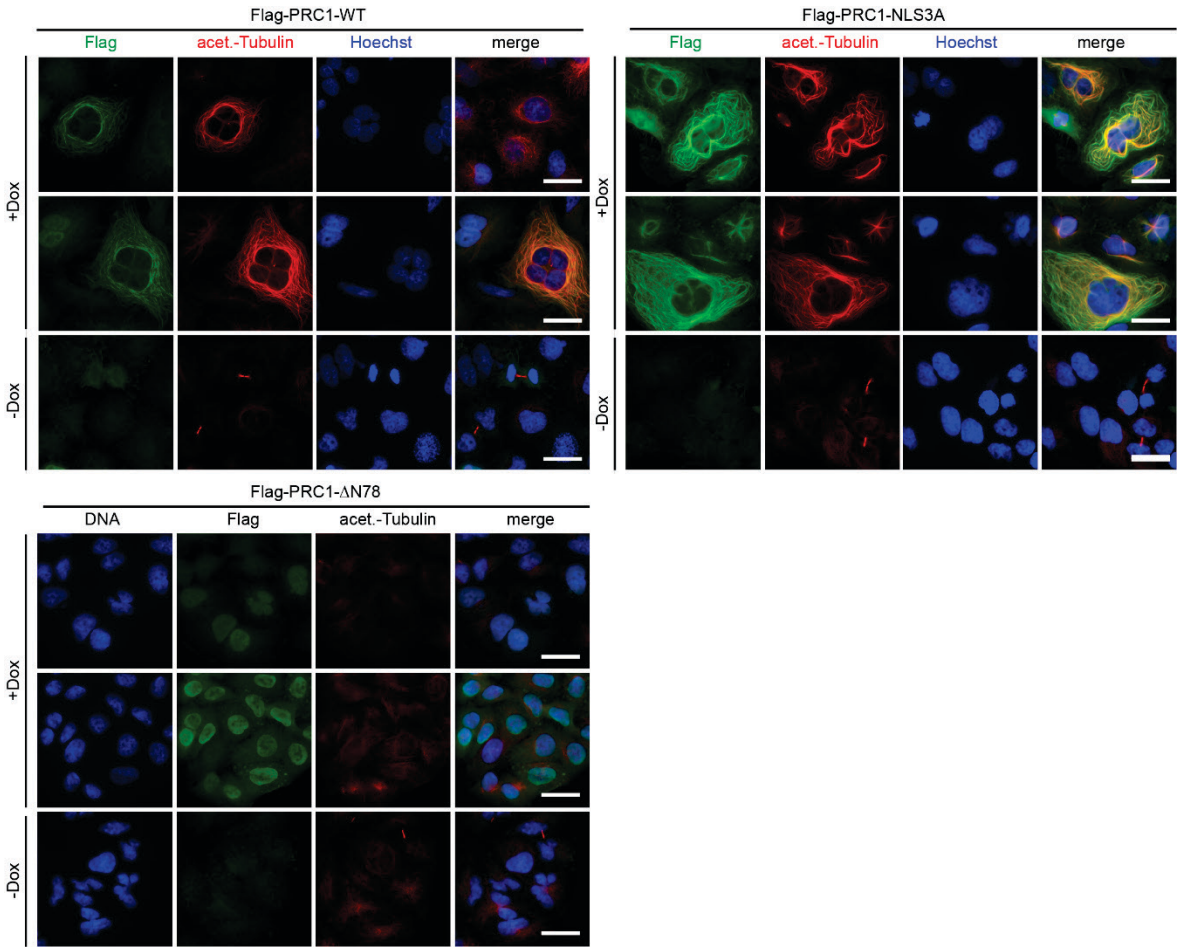

Figure 23: Enhanced microtubule stability due to PRC1 overexpression.
PRC1-WT, PRC1-NLS3A and PRC1-ΔN78 were induced for 3 days with 0.5 µg/ml doxycycline. Afterwards, the cells were fixed and immunostained for flag (green), acetylated α-tubulin (red) and Hoechst (blue) and investigated by fluorescence microscopy. α-tubulin K40 acetylation is associated with stabilized microtubules and used here to show stabilized microtubules after PRC1 overexpression. Bar: 25 µm.

Next, to further confirm the enhanced microtubule stability upon PRC1 expression, A549 or H460 cells expressing PRC1-NLS3A were treated with 1 µg/ml nocodazole, a microtubule

depolymerization drug, for 1.5 hours. Nocodazole treatment in the absence of PRC1 overexpression resulted in a disperse distribution of tubulin within the cytoplasm, while non-treated cells showed microtubule fibers (Suppl. Fig. 2, Shin, 2018). When PRC1-NLS3A was induced for 2 days, microtubule fibers were then protected from degradation by nocodazole (Supplementary Fig. 2, Shin, 2018).

To directly test whether the inhibition of proliferation by PRC1 overexpression is linked to its ability to bind to microtubule, arginine 377 located within the spectrin-fold of the PRC1 microtubule binding domain was mutated to an alanine. Arginine 377 plays an important role in binding to microtubules and biochemical assays indicate that the ability to bind to microtubule is reduced about 50% when arginine 377 is changed to an alanine (Kellogg et al., 2016; Subramanian et al., 2010). A549 cells stably expressing either inducible PRC1-R377A or PRC1-NLS3A-R377A (doubly mutated in the NLS and in arginine 377) containing an N-terminal Flag-tag were generated (Fig. 24A). Immunoblotting showed a strong overexpression of the constructs compared to endogenous PRC1 (Fig. 24B). Immunostaining with an anti-flag antibody illustrated that both, PRC1-R377A and PRC1-NLS3A-R377A, did not co-localize with or bundle microtubules at all (Fig. 24C). Instead, PRC1-R377A or PRC1-NLS3A-R377A were diffusely localized in nucleus or cytoplasm and were absent from the central spindle and midbody between dividing cells (Fig. 24C). Furthermore, PRC1-R377A and PRC1-NLS3A-R377A expression had only minor effects on proliferation (Fig. 24D,E). Analysis of cell cycle profiles revealed no obvious differences in the cell cycle distribution after induction of PRC1-R377A or PRC1-NLS3A-R377A (Fig. 24F). Thus, the ability of PRC1 to inhibit proliferation correlates with its ability to bind to microtubule.

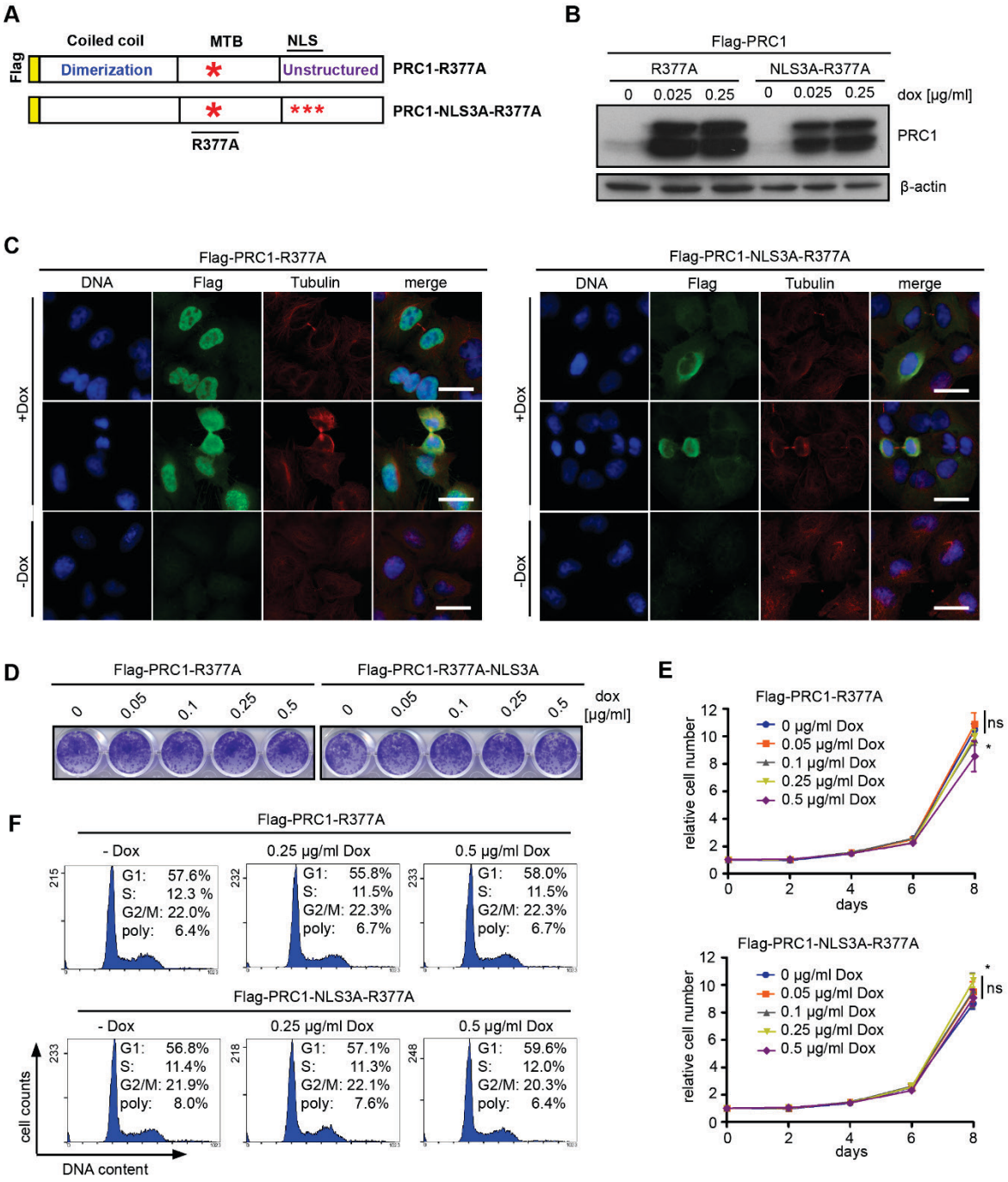
A
Coiled coil
MTB
NLS
Flag
Dimerization
Unstructured
PRC1-R377A
PRC1-NLS3A-R377A
R377A
B
Flag-PRC1
R377A
NLS3A-R377A
0 0.025 0.25 0 0.025 0.25
dox [µg/ml]
PRC1
β-actin
C
Flag-PRC1-R377A
Flag-PRC1-NLS3A-R377A
DNA
Flag
Tubulin
merge
+Dox
-Dox
D
Flag-PRC1-R377A
Flag-PRC1-R377A-NLS3A
0 0.05 0.1 0.25 0.5
dox [µg/ml]
E
Flag-PRC1-R377A
0 µg/ml Dox
0.05 µg/ml Dox
0.1 µg/ml Dox
0.25 µg/ml Dox
0.5 µg/ml Dox
relative cell number
days
ns
*
Flag-PRC1-NLS3A-R377A
F
Flag-PRC1-R377A
- Dox
0.25 µg/ml Dox
0.5 µg/ml Dox
G1: 57.6%
S: 12.3 %
G2/M: 22.0%
poly: 6.4%
G1: 55.8%
S: 11.5%
G2/M: 22.3%
poly: 6.7%
G1: 58.0%
S: 11.5%
G2/M: 22.3%
poly: 6.7%
Flag-PRC1-NLS3A-R377A
G1: 56.8%
S: 11.4%
G2/M: 21.9%
poly: 8.0%
G1: 57.1%
S: 11.3%
G2/M: 22.1%
poly: 7.6%
G1: 59.6%
S: 12.0%
G2/M: 20.3%
poly: 6.4%
cell counts
DNA content

Figure 24: Growth inhibition by PRC1 expression correlates with its ability to bind to microtubules.
(A) Scheme of the PRC1 constructs with the R377A mutation in the MTB domain and a N-terminal flag tag. R377A-NLS3A additionally contains three amino acid changes in the NLS sequence. (B) Expression of PRC1-R377A and PRC1-NLS3A-R377A was induced by the addition of 0.025 µg/ml and 0.25 µg/ml doxycycline for 3 days and investigated by immunoblotting. Actin was used as a loading control. (C) PRC1-R377A and PRC1-NLS3A-R377A were induced by 0.25 µg/ml doxycycline for 3 days. Cells were fixed and immunostained with anti-flag (green), anti-tubulin (red) and Hoechst (blue) and investigated by fluorescence microscopy. Bar 25 µm. (D) A549 lung cancer cell lines expressing the R377A constructs of PRC1 were cultured for a period of 8 days with the indicated concentrations of doxycycline. Cells were stained with crystal violet. (E) Quantification of growth of lung cancer cell lines stably expressing the PRC1-R377A and PRC1-NLS3A-R377A mutants in the presence of the indicated concentrations of doxycycline was analyzed over 8 days. n=3 biological replicates. For clarity, statistical significance (Student's t-test) is only shown for day 8. *p<0.05; ns: not significant. (F) A549 cells expressing PRC1-R377A or PRC1-NLS3A-R377A were treated with 0.25 µg/ml doxycycline or without doxycycline for 3 days. The cell cycle profile was determined by flow cytometry.

3.8 PRC1-WT and PRC1-NLS3A overexpression results in p53-mediated cellular senescence

To investigate the involvement of PRC1 in signalling pathways or its possible nuclear role, I determined genome-wide changes in gene expression after expression of PRC1-WT or PRC1-NLS3A in A549 cells by RNA-seq. PRC1 was induced for 2 days with 0.25 µg/ml of doxycycline and then RNA was isolated. Non-induced cells served as controls. 370 genes were downregulated and 351 genes were upregulated by PRC1 (adjusted p-value < 0.01) (Fig. 25A). Fewer genes were downregulated (130) and upregulated (145) in PRC1-NLS3A expressing A549 cells compared to control cells by using the same threshold of adjusted p-value (<0.01) (Fig. 25B). However, gene ontology analysis showed that the p53 signalling pathway was strongly enriched upon both, PRC1-WT and PRC1-NLS3A expression, among the upregulated genes (Fig. 25C,D). On the other hand, the most significantly downregulated gene sets for both, PRC1-WT and PRC1-NLS3A expressing A549 cells compared to control cells, are related to the cell cycle, including genes regulated by the pro-proliferative transcription factors E2F (Fig. 25E,F).

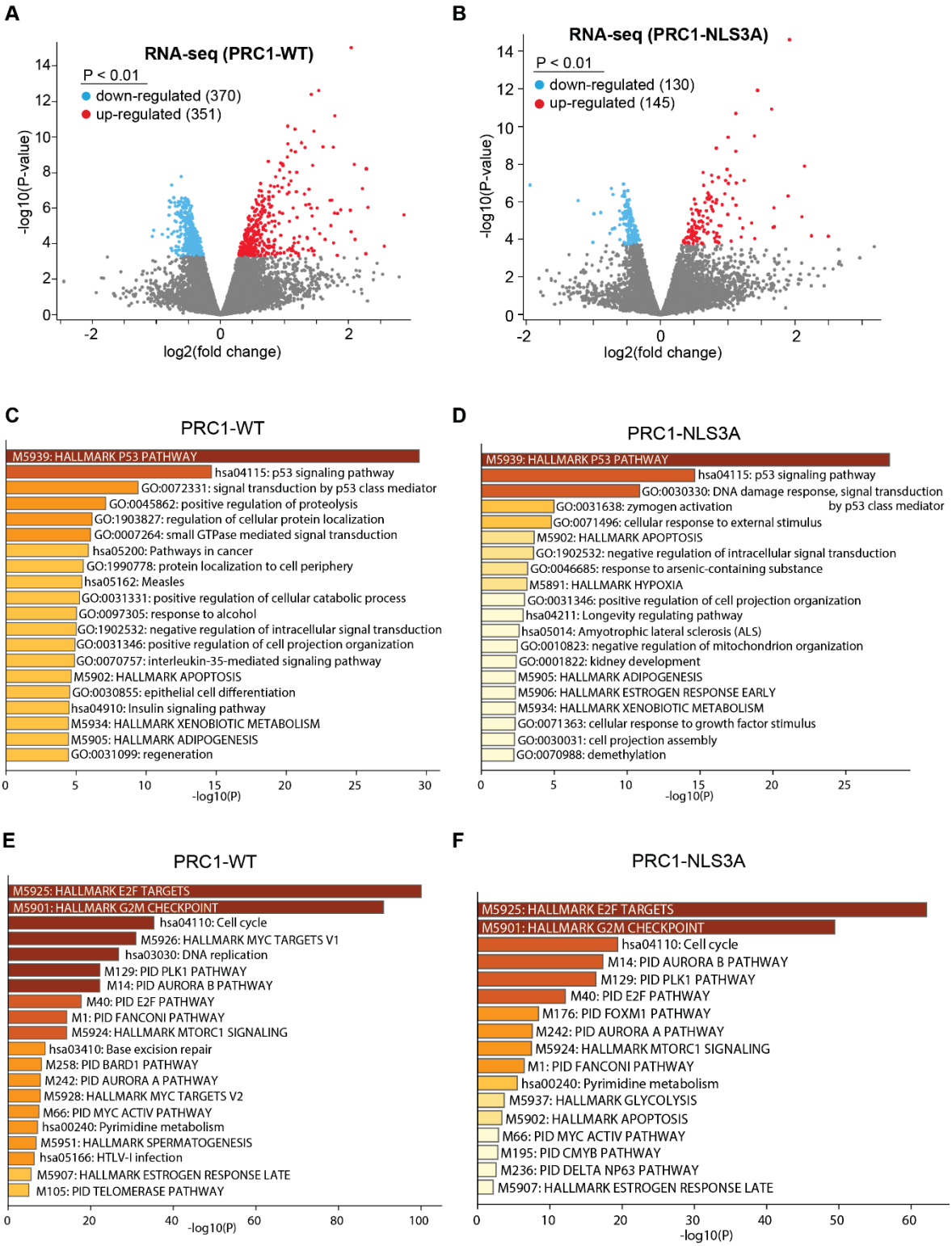

Figure 25: Overexpression of PRC1-WT and PRC1-NLS3A results in activation of the p53 pathway and downregulation of cell cycle genes.
(A,B) A549 PRC1-WT and PRC1-NLS3A cells were induced for 2 day with 0.25 µg/ml of doxycycline and then harvested for RNA-seq. Volcano plot of RNA-seq data- by adjusted p-value and fold change. Significantly up-regulated genes (< 0.01) are shown with red dots and significantly downregulated genes (< 0.01) with blue dots. (C,D) Enriched pathways and gene ontologies in genes upregulated after PRC1-WT or PRC1-NLS3A overexpression. (E,F) Enriched pathways and gene ontologies in genes downregulated after PRC1-WT or PRC1-NLS3A overexpression.

As described in 3.6, PRC1 has been linked to the Wnt signaling pathway in hepatocellular carcinoma and lung adenocarcinoma (Chen et al., 2016; Zhan, Zhang, et al., 2017). To analyze possible changes of the Wnt signaling pathway upon PRC1 overexpression, gene set enrichment analysis with FGSEA (fast preranked gene set enrichment analysis) was performed by using the human hallmark gene sets from MSigDB (Molecular Signatures Database) and the RNA-seq data from Figure 25. FGSEA analysis revealed that Wnt/β-catenin signaling was not significantly altered after PRC1-WT or PRC1-NLS3A expression (Fig. 26A). Further, analysis of the Wnt/β-catenin signaling gene group showed no significant differences between all genes and Wnt/β-catenin signaling genes after PRC1-WT and PRC1-NLS3A expression (Fig. 26B). In Figure 25C, 22 Wnt signaling pathway genes are shown in a heatmap. There is no specific pattern of differently expressed genes detectable upon PRC1 expression (Fig. 26C,D).

A

Hallmark: Wnt/beta-catenin signaling

PRC1	NES	p-value	adj. p-value
WT	0.67	0.93	0.93
NLS3A	-0.89	0.61	0.7

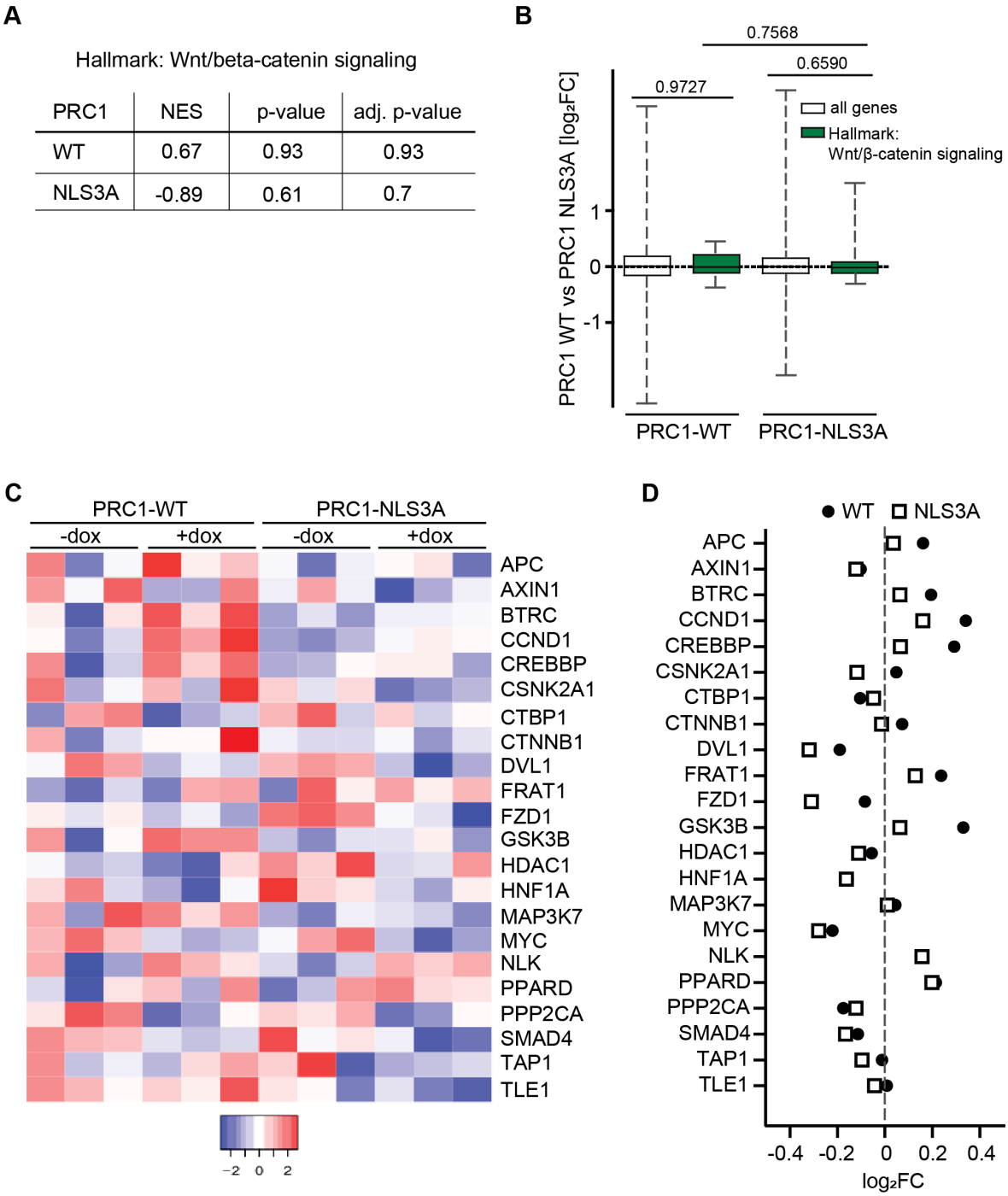

Figure 26: No alteration of Wnt/β-catenin signaling by ectopically PRC1 expression.
(A) FGSEA analysis of RNA-seq data from Figure 25 was done using the human hallmark gene sets from MSigDB. Ranked lists of differently expressed genes after PRC1-WT or PRC1-NLS3A expression were used. A table of Hallmark Wnt/β-catenin signaling is shown. NES, normalized enrichment score; p-val, p-value; p-adj., adjusted p-value. (B) Boxplots comparing differences in gene expression of the Wnt/β-catenin signaling pathway between PRC1-WT and PRC1-NLS3A expression. Boxplots showing log2 fold changes (FC). All genes: n=14.880, Wnt/β-catenin singaling: n=36. p-values were calculated with a two-tailed Wilcoxon rank sum test (unpaired samples). (C, D) RNA-seq data from Figure 25 was used to analyze the Wnt signaling pathway gene set. (C) Differently expression of 22 genes of the Wnt signaling pathway by PRC1-WT and PRC1-NLS3A expression is shown in a heatmap. (D) Log 2 fold changes (FC) of the genes from (C) in comparison of PRC1-WT and PRC1-NLS3A expression are shown.

Next, a FGSEA analysis was performed as described before and a list of the top 10 enriched and down regulated hallmark gene sets are shown in Table 47. Similar to gene ontology analysis, the top enriched hallmark gene set was the p53 pathway after ectopically PRC1 expression (Fig. 27A, Table 47). Here, PRC1-WT and PRC1-NLS3A expression showed a comparable normalized enrichment score (NES) of 2.86 (WT) and 2.93 (NLS3A) and indicates a similar impact on A549 lung cancer cells (Fig. 27A, Table 47). The top downregulated hallmark gene set was E2F targets upon PRC1 expression (Fig. 27A, Table 47). A negative and comparable NES of -3.79 (WT) and -3.75 (NLS3A) was also shown for the top down regulated gene set after PRC1-WT or PRC1-NLS3A expression in A549 cells (Fig. 27A, Table 47).

Next, to further compare the impact of PRC1-WT and PRC1-NLS3A expression on the p53 and E2F pathway, the different gene groups were analyzed (Fig. 27B,C). In comparison to all genes, the p53 pathway gene set was significantly upregulated after PRC1-WT and PRC1-NLS3A expression (Fig. 27B). p53 pathway genes were not differently expressed between PRC1-WT or PRC1-NLS3A expression in A549 cells (Fig. 27B). E2F targets were significantly down regulated in comparison to all genes after PRC1-WT or PRC1-NLS3A expression (Fig. 27C). Expression of wildtype PRC1 resulted in slightly stronger downregulation of E2F targets with a median $\log_2$ fold change (FC) of -0.36 compared to PRC1-NLS3A with a median log2 FC of -0.31(Fig. 27C).

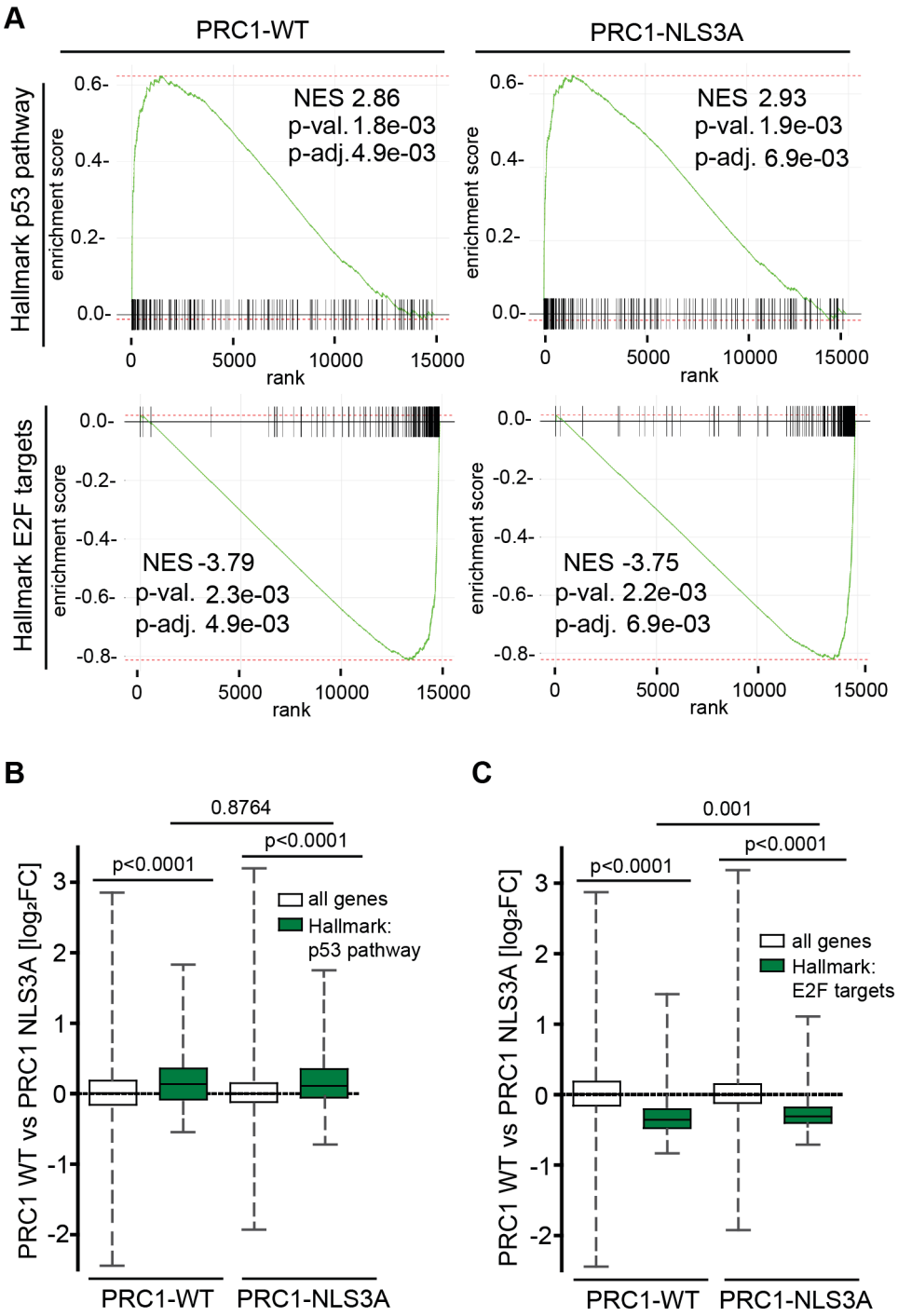

Figure 27: Similar impact of PRC1-WT and PRC1-NLS3A expression on the top upregulated and downregulated hallmark gene set.
(A) FGSEA analysis was performed using the human hallmark gene sets from MSigDB and RNA-seq data from Figure 25. Ranked lists of differently expressed genes after PRC1-WT or PRC1-NLS3A expression were used. Enrichment plots of hallmark p53 pathway and E2F targets are shown. NES, normalized enrichment score; p-val, p-value; p-adj., adjusted p-value. (B,C) Boxplots comparing differences in p53 pathway (B) and E2F target (C) gene expression between PRC1-WT and PRC1-NLS3A expression is shown. Log2 fold changes (FC) of the specific gene group is shown. All genes: n=14.880, p53 pathway: n=176, E2F targets: n=195. p-values were calculated with a two-tailed Wilcoxon rank sum test (unpaired samples).

In Figure 28A, the top 20 differentially expressed genes are listed in a heatmap. As expected, the top expressed gene is PRC1 confirming the overexpression of the protein (Fig. 28A). Interestingly, 10 out of the 20 genes are bona-fide p53-target genes (Fig. 28A,B). Examples for upregulated p53-target genes are the antiproliferative protein BTG2, the cyclin-dependent kinase inhibitor CDKN1A (p21), the E3 ubiquitin ligase MDM2, the proapoptotic receptor FAS and SESN1, which mediates p53 inhibition of cell growth. Analysis of the log_2 fold changes of the top 20 differently expressed genes showed slightly higher values for the most genes after PRC1-WT expression in comparison to PRC1-NLS3A expression (Fig. 28B, Table 48). However, there were no fundamental differences in genes activated or repressed by PRC1-WT or PRC1-NLS3A and no pathways were selectively regulated by wildtype PRC1.

Taken together, genome-wide expression analysis suggests no involvement of PRC1 in Wnt-signaling or an exclusive nuclear role. The data rather suggest that PRC1 overexpression in A549 cells activates a stress response mediated by the tumor suppressor p53.

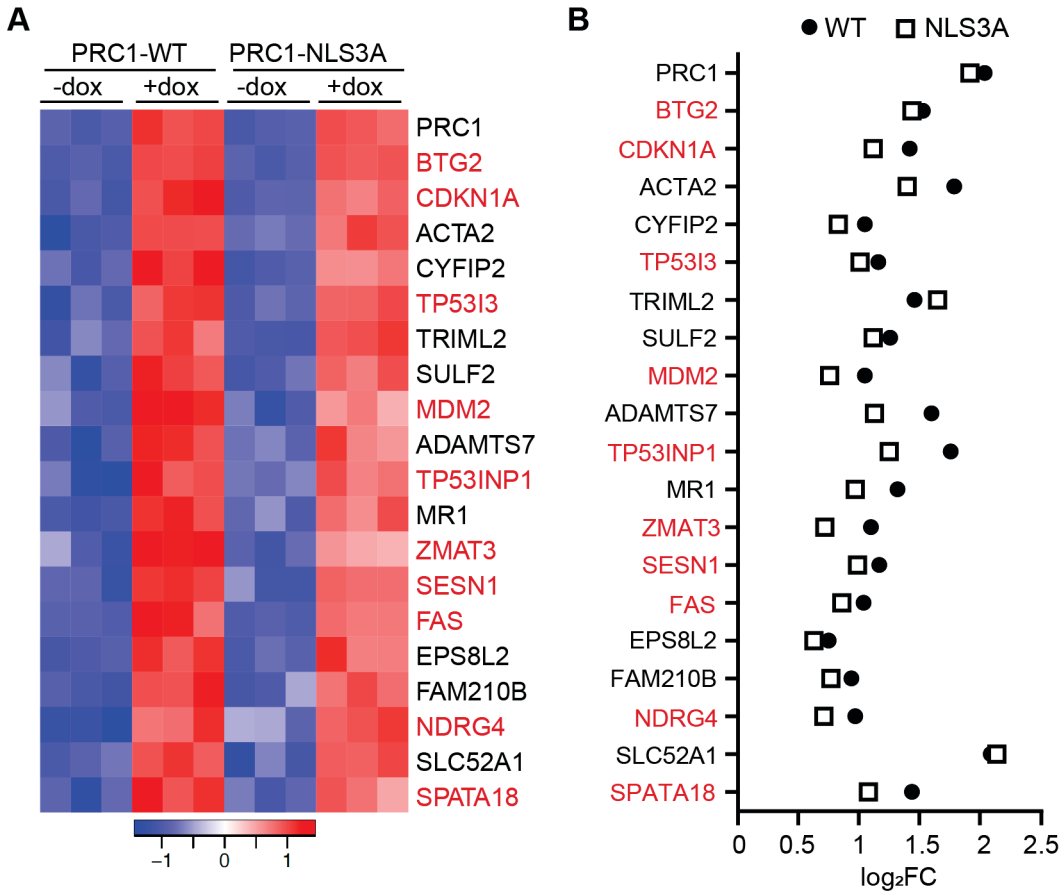

Figure 28: Activation of p53-target genes by PRC1 overexpression.
(A, B) A549 PRC1-WT and PRC1-NLS3A cells were induced for 2 day with 0.25 µg/ml of doxycycline and then harvested for RNA-seq. (A) Heatmap of the top 20 differentially expressed genes. 10 out of 20 genes are bona-fide p53-target genes and highlighted in red. (B) Log 2 fold changes (FC) of the top differentially expressed genes in comparison to PRC1-WT and PRC1-NLS3A expression are shown. Raw data is shown in Table 48.

Next, to confirm the p53 stabilization and the target gene expression of p21, A549 cells were treated with 0.25 µg/ml or without doxycycline for 4 days and then harvested for immunoblotting analysis. PRC1-WT and PRC1-NLS3A expression led to an induction of p21 and p53 on protein level in A549 cells (Fig. 29A). p53 stabilization and p21 induction were not seen upon PRC1-ΔN78 expression in A549 cells, as expected (Fig. 29A).

One of the top differently expressed genes after PRC1 overexpression found by RNA-seq was FAS, a pro-apoptotic receptor. Therefore, one outcome of the p53-response might be apoptosis. However, immunoblotting for cleaved PARP and cleaved caspase-3, markers for apoptotic cells, indicated that expression of PRC1-WT or PRC1-NLS3A does not result in apoptosis (Fig. 29A). To test if cellular senescence contributes to the growth inhibition of A549 cells upon PRC1 overexpression, I induced PRC1-WT or PRC1-NLS3A for 4 and 8 days and then stained cells for β-galactosidase, a marker for senescent cells. Compared to untreated A549 cells, cells which expressed PRC1-WT or PRC1-NLS3A but not cells expressing PRC1-ΔN78, stained positive for β-galactosidase, indicating that they became senescent (Fig. 29B-D).

Taken together, PRC1 overexpression in A549 cells caused the stabilization of p53, activation of p21 and induction of senescence.

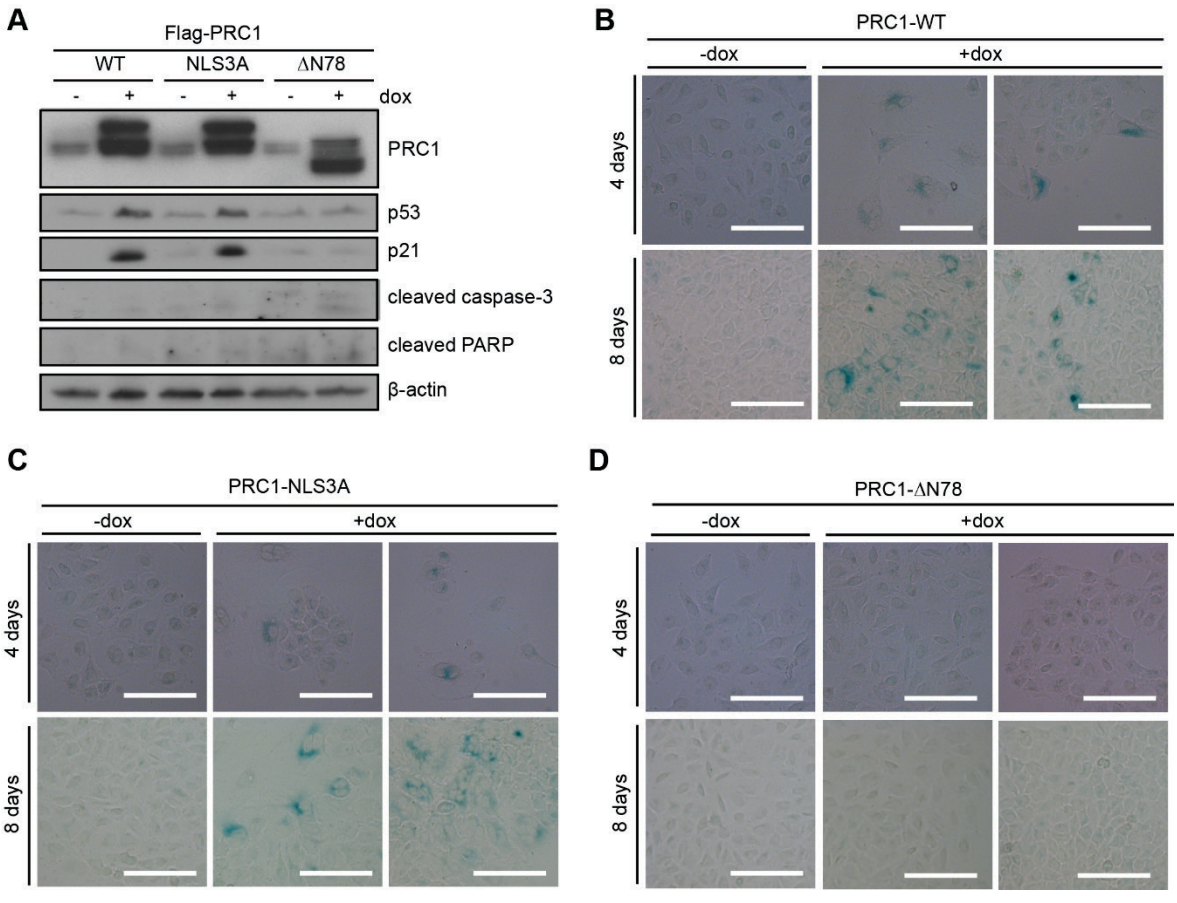

Figure 29: Overexpression of PRC1-WT and PRC1-NLS3A leads to stabilization of p53 and induction of p21 and finally to senescence in A549 cells.
(A) A549 PRC1-WT, PRC1-NLS3A or PRC1-ΔN78 cells were treated with (+) 0.25 µg/ml or without (-) doxycycline (dox) for 4 days and analyzed by immunoblotting indicating that p53 is stabilized by PRC1-WT and PRC1-NLS3A. As markers for apoptosis, cleaved PARP and cleaved caspase-3 were used. (B-D) The indicated cell lines were treated with (+) 0.5 µg/ml doxycycline (dox) for 4 days and with (+) 0.25 µg/ml dox for 8 days to induce the expression of the PRC1 constructs. As a control non-induced (-) cells were used. Senescent cells were detected by staining for ß-galactosidase. Bar: 100 µm.

4 Discussion

4.1 Expression and localization of PRC1 in lung cancer

A screen of potential DREAM/MMB target genes, which are involved in late stages of mitosis and cytokinesis, revealed that protein regulator of cytokinesis 1 (PRC1) might be a candidate as a therapeutical target for lung cancer. PRC1 is a core microtubule organizer with essential roles in central spindle formation and cytokinesis due to its ability to cross-link antiparallel microtubules (Bieling et al., 2010; Jiang et al., 1998; Kellogg et al., 2016; Kurasawa et al., 2004; Mollinari et al., 2002; Subramanian et al., 2010; Zhu & Jiang, 2005). However, the role of PRC1 in tumorigenesis is not clear and consistent over the studies. One part of the thesis focused on the expression and localization of PRC1 in lung cancer to test the hypothesis that PRC1 could be used as a biomarker for lung cancer.

PRC1 was highly expressed on RNA level in non-small cell lung cancer (NSCLC) tissue samples, which was examined by database analysis. The elevated expression of PRC1 in lung cancer as well as in ovarian, gastric, hepatocellular, breast, and bladder cancer has also been described by others and suggests that PRC1 could be important in different types of tumors (Bu et al., 2020; Chen et al., 2016; Kanehira et al., 2007; Shimo et al., 2007; Wang et al., 2017; Wolter et al., 2017; Zhan, Xi et al., 2017; Zhan, Zhang, et al., 2017; Zhang et al., 2017). In addition, cBioPortal database analysis of lung adenocarcinoma samples confirmed the findings that the PRC1 sequence was rarely mutated in NSCLC as previously concluded by Li et al. (Li et al., 2018). A low mutational burden suggests that alteration in PRC1 protein function do not contribute to tumorigenesis. Although enhanced expression of the protein could be a consequence of copy-number gains (Li et al., 2018), database analysis of amplification events were very low with 0.6%.

This raises the question, which pathways and transcription factors contribute to the increased expression of PRC1 in lung cancer? One prime candidate is DREAM/MMB as PRC1 is a bona-fide target gene of the this complex, which is a master regulator of cell cycle-dependent gene expression (Esterlechner et al., 2013; Musa et al., 2017; Sadasivam & DeCaprio, 2013; Schmit et al., 2007; Wolter et al., 2017). Consistent with this notion, components of the MMB complex, such as B-MYB, LIN9 and FOXM1 as well as their target genes are frequently expressed at elevated levels in human tumors (Sadasivam & DeCaprio, 2013). High expression of MYBL2 (encoding B-MYB) is linked to deregulation of DREAM/MMB-mediated gene expression in cancer cells (Iness et al., 2021). Thus, elevated PRC1 expression could be due to highly expressed upstream regulators, as MMB, in cancer cells. Also, tumor suppressor p53 could influence the expression of PRC1, as p53 plays a role in the p53-p21-DREAM-CDE/CHR signaling pathway (Fischer et al., 2016). Mutations

of p53 in tumor cells could lead to de-repression of oncogenic DREAM target genes (Cancer Genome Atlas Research Network 2011; Fischer et al., 2013; 2015). It's been shown that compared to p53 wildtype cells, p53 negative cancer cells have an increased G2/M gene expression in response to DNA damage, which is linked to stable association of B-MYB to the complex. Moreover, high levels of B-MYB correlate with a p53 mutant status and a progressed tumor stage in primary human breast cancer (Mannefeld et al., 2009). This data suggests that p53 could indirectly influence the PRC1 expression levels through regulation of DREAM/MMB.

Furthermore, the Hippo pathway and its downstream effector YAP have been suggested to enhance mitotic gene expression by interactions with MMB from distal enhancers and could possibly contribute to increased levels of G2/M genes, including PRC1 in cancer (Pattschull et al., 2019). YAP has been found to be overexpressed in NSCLC and is suggested to function as an oncogene in lung cancer (Wang et al., 2010; Yeung et al., 2016). A constitutively activated form of YAP (YAP-S127A) was able to drive lung tumor progression *in vivo* (Lau et al., 2014). Clinical data supported the significant role of YAP in lung cancer too. High YAP levels in NSCLC patients correlated with lymph node metastasis, pathological tumor-node-metastasis stage and shorter survival (Kim et al., 2011; Su et al., 2012; Wang et al., 2010). So, MMB and/or YAP could contribute to the elevated expression of PRC1 in lung cancer.

PRC1 might be expressed in higher levels during G2/M phase compared to G1/S phase of the cell cycle, as it is a target gene of MMB. I found that PRC1 was expressed in a cell cycle-dependent manner in A549 lung cancer cells with increasing expression levels from S-phase to G2/M phase. The highest level of PRC1 was detected in late G2 and M phase. Jiang et al. could show that the levels of PRC1 protein were high during S to G2/M and dropped dramatically after cells exited mitosis and entered the G1 phase of the cell cycle in HeLa cells (Jiang et al.,1998). Those expression patterns have initially been suggested in *Saccharomyces cerevisiae* for Asel, a PRC1 homolog in yeast, with low levels of Asel in G1 and maximal levels after S phase that then drop as cells exit mitosis (Pellman et al., 1995). These results are consistent with our observations in A549 lung cancer cells and thus indicate that PRC1 might have a function during cell cycle progression before central spindle formation and cytokinesis.

Apart from transcriptional regulation, PRC1 can be degraded as it contains several consensus motifs for ubiquitin-mediated proteolysis in the C-terminal region and cell cycle-dependent degradation could be a possible regulatory mechanism. The protein could be degraded by the anaphase-promoting complex/cyclosome (APC/C), an E3 ubiquitin ligase that targets cell cycle proteins for degradation and could recognize D boxes and Ken boxes, which have been found in the PRC1 sequence (Glotzer et al., 1991; Morgan, 2013; Pfleger

& Kirschner, 2000; Yamano, 2019). As shown for AseI in budding yeast, the D box is a substrate of the anaphase-promoting complex/cyclosome (APC/C) (Juang et al., 1997). These findings suggest that degradation of the protein could be involved in the observed drop of PRC1 protein levels after mitosis.

Consistent with what was found by others (Jiang et al., 1998; Kieserman et al., 2008; Kurasawa et al., 2004; Mollinari et al., 2002; Zhu & Jiang, 2005), PRC1 localized at the central spindle and midbody during mitosis and cytokinesis but also to the nucleus during interphase in A549 lung cancer cells. PRC1 seems to be important for central spindle formation and cytokinesis by cross-linking antiparallel microtubules as described in literature (Jiang et al., 1998; Kellogg et al., 2016; Kurasawa et al., 2004; Mollinari et al., 2002; Subramanian et al., 2010). However, less is known about the potential function of PRC1 during interphase or its nuclear role. The nuclear localization of PRC1 can be explained by the two nuclear localization signals (NLS) in the C-terminal domain but so far has not been linked to any function (Jiang et al.,1998; Mollinari et al., 2002).

4.2 PRC1 and lung cancer- more than a cytokinesis protein?

As discussed before, PRC1 might play a role during cell cycle progression before central spindle formation and cytokinesis because of its expression during interphase and nuclear localization. Indeed, another microtubule-bundling protein which plays a role in cytokinesis, termed as CEP55, was linked to additional functions and was found to be overexpressed in several cancers, which correlated with poor prognosis (Jeffery et al., 2016). For example, CEP55 activated the nuclear factor κB (NF-κB)/IκBα signalling pathway and this contributed to pancreatic cancer cell aggressiveness (Peng et al., 2017), potentially indicating a similar situation in the case of PRC1.

Another suggestion why PRC1 might have more functions in tumorigenesis was shown by Chen et al., which linked PRC1 to Wnt signaling in hepatocellular carcinoma (HCC) (Chen et al., 2016). In this study, Wnt3a signaling promoted the expression of PRC1 as a direct target gene which further induced the membrane sequestration of the destruction complex, led to suppression of adenomatous polyposis coli (APC) stability, and the release of β-catenin from the APC complex. Thus, PRC1 promotes proliferation, stemness, metastasis and tumorigenesis in HCC (Chen et al., 2016). These findings indicate a cytoplasmic function of the protein in Wnt signaling in HCC. However, nuclear localization of PRC1 during interphase instead of cytoplasmic localization was dominant in A549 lung cancer cells. In my study, ectopically expression of PRC1 showed no significant alteration of Wnt/β-

catenin signaling or differently expressed gene pattern of the Wnt signaling pathway in A549 lung cancer cells. Instead, genome-wide expression analysis by RNA-seq revealed that overexpression of PRC1 leads to activation of the p53 pathway and downregulation of E2F target genes. These observations are differently from Zhan et al. who observed an enhanced proliferation of A549 cells upon PRC1 overexpression (Zhan, Zhang, et al., 2017). Methodically, they used a mammalian expression vector for PRC1 expression under CMV promoter control in A549 cells (Zhan, Zhang, et al., 2017). Unfortunately, they provided no exact details about their methods or experimental setup as information about their transfection or time points for RNA and protein extraction, except of the duration of the colony formation assay, which was 14 days. Possibly, cells with strong PRC1 expression died within the first days and cells with less or no amount of the PRC1 construct grow out of the cell population. Zhan et al. provided no further data of PRC1 overexpression in A549 cells which could be used to compare with my findings (Zhan, Zhang, et al., 2017).

Does PRC1 have any function in the nucleus? The NLS3A mutant version of PRC1 which were absent in the nucleus, induced the same top enriched and down regulated hallmark gene sets in a comparable impact as PRC1 wildtype in A549 cells. Also, no fundamental differences in genes activated or repressed by PRC1-WT or PRC1-NLS3A were observed. This result indicates no exclusive role of PRC1 in the nucleus. Furthermore, overexpression of PRC1-WT and PRC1-NLS3A but not PRC1-ΔN78 (failing to associate with the spindle midzone) resulted in a proliferation deficit, an increased number of bi- and multi-nucleated cells, enlargement of the cells, and finally caused p53-mediated cellular senescence in A549 lung cancer cells.

This leads to the further question: What causes the activation of the p53 pathway and the cellular stress response upon PRC1 overexpression in A549 lung cancer cells? Immunofluorescence staining revealed a strong perinuclear microtubule-bundling phenotype within the cytoplasm of A549 and H460 lung cancer cells in the interphase. PRC1 co-localizes with microtubules, stabilizes them and further protects microtubules from degradation when the cells were treated with nocodazole, a microtubule depolymerization drug. Similar effects of interphase microtubule-bundling into perinuclear rings upon PRC1 overexpression has also been reported in HeLa cells (Mollinari et al., 2002; Perchey et al., 2018). Possibly, PRC1 overexpression might thus have a similar consequence as treatment of cells with Taxol (paclitaxel), a microtubule-stabilizing drug. Concentration-dependent treatment of Taxol was described to induce mitotic arrest, which causes cell death or to lead to multipolar divisions followed by partial cytokinesis failures which resulted in aneuploid daughter cells (Weaver, 2014). Tumor cells may develop resistances to overcome the mitotic and cytokinesis failures by severe microtubule-bundling. One possibility for cancer

cells would be to express proteins which inhibits the microtubule-bundling activity. Perchey et al. found that p27Kip (p27) is a novel binding partner of PRC1 which interfered with the microtubule binding ability of PRC1 (Perchey et al., 2018). Co-expression of p27 inhibited the strong microtubule-binding phenotype during interphase by PRC1 as well as cytokinesis failures shown by significant reduced bi-nucleated HeLa cells (Perchey et al., 2018).
To directly link the stress response and proliferation deficit of lung cancer cells to strong microtubule-bundling mediated by PRC1, PRC1 R377A was expressed in A549 cells. R377A carries a mutation in the microtubule-binding (MTB) domain of PRC1 resulting in reduced microtubule binding as predicted by biochemical assays (Kellogg et al., 2016; Subramanian et al., 2010). PRC1 R377A did not co-localization or bundle microtubules within the cytoplasm. Furthermore, both PRC1-WT-R377A and PRC1-NLS3A-R377A (double mutant) were diffusely localized in the nucleus or cytoplasm and were absent from the central spindle and midbody between dividing cells. Expression of these constructs showed just minor effects on proliferation and no obvious differences of the cell cycle phases. Taken together these observations link the proliferation deficit upon PRC1 overexpression to the ability of PRC1 to bind and bundle microtubules.

During cell division, strong bundling activity of PRC1 could be controlled by phosphorylation events. In early mitosis, it's been suggested that CDK1/Cyclin B phosphorylation of PRC1 on T470 and T481 sites prevents the microtubule-bundling activity of the protein (Cundell et al., 2013; Jiang et al., 1998; Mollinari et al., 2002; Zhu & Jiang, 2005; Zhu et al., 2006). CDK1 inhibition results in fatal sister chromatid alignment errors and mitotic arrest in the spindle checkpoint activation, which is linked to insufficient repression of PRC1 and KIF4 during prometaphase (Voets et al., 2015). Hu et al. proposed a model in which the activity of PRC1 was regulated by PLK1 (Hu et al., 2012). In this model, PRC1 activity is inhibited by microtubule-stimulated PLK1 phosphorylation on Thr-602 in high microtubule density conditions in pre-anaphase (Hu et al., 2012). However, the regulation of the protein during interphase is not well described.
Recently, Hernández-Ortega et al. found that PRC1 is the first *bona fide* substrate of the CDK16/CCNY complex, which has been implicated in cancer pathogenesis, and demonstrated that the proliferative function of CDK16 is mediated by PRC1 phosphorylation. Here, the complex phosphorylates PRC1 at T481, similar like CDK1/Cyclin B, which contributes to the localization of the protein. T481 is located within the NLS of PRC1 and inhibition of CDK16 leads to PRC1 delocalization into the nucleus (Hernández-Ortega et al., 2019). However, it's not clear why the increased nuclear localization of PRC1 by CDK16 inhibition should negatively affect the proliferation of the cells. One possibility is that CDK16/CCNY phosphorylation of PRC1 on T481 during S and G2 phase inhibits the

microtubule bundling activity of PRC1 before mitosis. My studies provide no evidence for a role of PRC1 in the nucleus that would suppress the proliferation of cancer cells. Rather, the microtubule bundling activity of the protein appears to be responsible for the antiproliferative effects. Apart from phosphorylation of PRC1, nuclear localization could therefore be a mechanism which protects cells from perinuclear microtubule-bundling.

Taken together, I found no additional function of the protein besides its known role as a microtubule-bundling protein for central spindle formation and cytokinesis. It seems that elevated PRC1 expression in cancer needs to be regulated, in a cell cycle-dependent manner, by factors that could influence the ability of PRC1 to bundle microtubules, or by maintaining its nuclear localization.

4.3 PRC1- a potential therapeutic target for lung cancer

A signature of CIN was identified, in which PRC1 is the second-highest ranked gene out of 10,151 genes and also listed in the top-ranked gene signature (CIN25), whose high expression is correlated with aneuploidy and worse patient expectations (Carter et al., 2006). Additionally, a database analysis showed that the expression levels of PRC1 correlated with the survival rate of lung adenocarcinoma patients. These results indicate a clinical significance of PRC1 expression and survival of human lung cancer patients.

Five different lung cancer cell lines and a control cell line were generated which express a doxycycline-inducible small hairpin RNA (shRNA) directed against PRC1 to deplete the protein. Suppression of PRC1 resulted in significant and dose-dependent proliferation defects of all five lung cancer cell lines. Importantly, immortalized skin fibroblasts had minor effects on proliferation upon PRC1 depletion and served as control cells. Also, PRC1 knockdown inhibits the anchorage-independent growth ability of two lung cancer cell lines determined by soft agar colony formation assay. Inhibited proliferation of lung cancer cell lines by PRC1 knockdown has also been observed by Zhan et al. (Zhan, Zhang, et al., 2017). PRC1 depletion causes proliferation defects also in other cancer types, as ovarian, breast, bladder and hepatocellular carcinoma (Bu et al., 2020; Chen et al., 2016; Kanehira et al., 2007; Wolter et al., 2017). Taken together, PRC1 is required for proliferation and anchorage-independent growth of lung cancer cells *in vitro* and indicated that PRC1 might be good target for lung cancer but also other cancer types.

PRC1 has been described to be important for spindle integrity and midzone microtubule bundle formation and the completion of cell cleavage (She et al., 2019). In the literature, suppression of the protein is suggested to cause a greatly disorganized spindle midzone

which leads to remarkable mitotic defects and cytokinesis failure. As an outcome, the microtubule spindle fails to bundle and an absence of a clear midzone is shown as well as abnormal chromosome alignment and segregation (Maton et al., 2015; Mollinari et al., 2002; Zhu et al., 2006). Depletion of PRC1 results in bi- and multi-nucleated cells and indicates that the protein is required for proper cytokinesis in lung cancer cells. Additionally, compared to BJ control cells, the effects in lung cancer cell lines upon PRC1 depletion were more severe. Possibly, PRC1 knockdown can cause failures in cleavage furrow ingression and thus leads to multiple nuclei (Lens & Medema, 2019).

In this study, I could show that p53 wildtype lung cancer cells stabilize p53 and induces its *bona fide* target gene p21 after PRC1 depletion which finally leads to senescence of the cells. So similar to knockdown of PRC1, also overexpression of PRC1 caused a p53-mediated cellular senescence of the lung cancer cells. The activation of p53 by depletion or overexpression of PRC1 is consistent with the observation that p53 block cell proliferation of tetraploid cells (Laffin et al., 1989). This was confirmed by studies which showed that cytokinesis failures resulted into an G1 arrest in p53-proficient tetraploid cells, whereas p53-deficient tetraploid cells can continue in cell division (Andreassen et al., 2001; Kuffer et al., 2013; Lanni & Jacks, 1998). Treatment of lung cancer cells by a drug, Nutlin-3, which inhibits the MDM2-p53 interaction and thus activates the p53 pathway (Tovar et al., 2006), also resulted in the suppression of proliferation and the induction of senescence. In contrast to PRC1-depleted cells or PRC1-overexpressing cells, Nutlin-3 treated lung cancer cells showed a G1 cell cycle arrest and no elevated multi-nucleation. Also, Nutlin-3 treatment downregulated the level of PRC1 which might be indirectly due to p53 stabilization and DREAM formation as discussed above.

In many human cancers, as well as lung cancer, tumor suppressor p53 is frequently inactivated by mutation (Ahrendt et al., 2003; Herbst et al., 2018; Leroy et al., 2014). Three lung cancer cell lines which are mutated in p53 were also used in this study. PRC1 depletion leads to apoptosis in p53-mutant lung cancer cells. So, it seems that lung cancer cells behave differently depending on the status of p53. Direct proof for the role of p53 comes from the observation that a siRNA mediated knockdown of p53 in p53-wildtype lung cancer cells and together with PRC1 depletion resulted in apoptosis, instead of senescence. This directly links the role of p53 to the induction of p21 that finally leads to senescence of the cells. So, if this guardian of the cell, p53, is missing or mutated, lung cancer cells die upon apoptosis in a p53-independent way.

Targeting mitotic exit might be a good strategy to target lung cancer. However, one big risk is the possibility to induce CIN or aneuploidy upon treatment which could further drive cancer progression (Sansregret et al., 2018). It was also suggested that increased CIN

above a certain limit might negatively affect the viability of cancer cells (McKenzie & D'Avino, 2016). Moreover, mitotic exit inhibitors affect not only cancer cells but also normal dividing cells. In my experiments, control cells showed weaker effects on PRC1 knockdown than cancer cells. However, highly proliferative cells in the body might be affected by PRC1 depletion. It was shown that these adverse effects can be reduced by applying lower dosages or treatment in combination with other drugs (Cormie et al., 2017; Dominguez-Brauer et al., 2015; Liu et al., 2013; Mokhtari et al., 2017). For example, loss of PI3K-C2α in breast cancer cells or decrease of KIF20B or PRC1 in HCC showed that cancer cells with CIN or aneuploidy are more sensitive to certain chemotherapeutic drugs (Gulluni et al., 2017; Liu, Li, Zhang, et al., 2018; Liu et al., 2014). Consequently, I asked whether a combinational treatment of p53 wildtype lung cancer cells with a commonly used chemotherapeutic drug, cisplatin, may enhance the proliferation defects upon PRC1 depletion. Indeed, suppression of proliferation was significantly increased by PRC1 depletion in combination with cisplatin treatment of lung cancer cells. However, the cells did not switch from their senescence phenotype to apoptosis by treatment of the cells with low concentrations of cisplatin. Nevertheless, combinational treatment could improve the treatment strategies of lung cancer. For instance, for NSCLC patients who do not have drug targetable driver mutations, platinum-based chemotherapy remains the first-line treatment which confers the most clinical benefit for patients with advanced NSCLC (Fennell et al., 2016). Potentially, their treatment outcome could be improved by additionally targeting PRC1.

One of the most common oncogenic driver mutations in lung adenocarcinoma concern KRAS (Dearden et al., 2013). Direct inhibition of KRAS has been largely unsuccessful and therefore downstream receptors as RAF, MEK and mTOR have been investigated as potential targets in NSCLC (Cox et al., 2014; Li et al., 2017; Wilhelm et al., 2004). Unfortunately, inhibition of RAF or MEK showed no efficiency and benefit in NSCLC (Blumenschein et al., 2013, 2015; Ferrer et al., 2018; Miller et al., 2012; Papadimitrakopoulou et al., 2016; Wilhelm et al., 2004). Also, KRAS mutations have implicated to be a factor in EGFR tyrosine kinase inhibitor (TKI) resistance to targeted therapy in NSCLC (Massarelli et al., 2007). To address whether PRC1 is a potential target in KRAS-driven lung tumors *in vivo*, a genetically engineered mouse model of NSCLC that mimics the genetic and histopathological features of the human disease was used (DuPage et al., 2009). Lung tumors were driven by oncogenic KRAS and loss of p53 and simultaneously PRC1 was depleted. Compared to control infected mice, the lung tumor area was significantly reduced when was PRC1 depleted. Also, tumor numbers and higher-grade tumors were reduced in mice infected with the shRNA directed against PRC1 compared to

the control group. This result indicated a requirement of PRC1 in KRAS-driven non-small cell lung cancer *in vivo*. However, this mouse model does not fully reflect the situation in patients, as in patients lung tumors are developing first, and then treatment strategies are applied. In the future, a different mouse model of lung cancer could be used where tumors are initiated first and then PRC1 should be depleted.

Importantly, the question raises, how PRC1 could be targeted or be influenced as an option for therapy? So far, no drugs are available to target PRC1, and direct targeting of PRC1 might be difficult to achieve as the protein contains no enzymatic activity. Possibly, a structure-based drug design which blocks for instance the dimerization domain and binding to KIF4A might be a strategy. Alternatively, blocking the microtubule-binding domain could be a strategy but could also have more side effects as it may influence several microtubule binding proteins. The PRC1 structure has been analyzed with special focus on the interaction of PRC1 with microtubules which could be used for drug development (Kellogg et al., 2016; Subramanian et al., 2010). Alternatively, RNA interference (RNAi)-based therapeutic approaches might be an option as PRC1 is very infrequently mutated. However, some challenges have to be overcome for a clinically suitable, safe, and effective drug delivery system, such as instability under physiological condition, poor cellular uptake, possible immunogenicity and off target effects (Singh et al., 2018).
As mentioned above, stabilization of p53 by Nutlin-3 is another option to treat lung cancer cells with a wildtype status of p53 and also influences the PRC1 level. It's been shown that Nutlin-3 treatment has a good efficacy against tumors with normal MDM2 expression, suggesting that many of the patients with wild-type p53 tumors may benefit from antagonists of the p53–MDM2 interaction (Tovar et al., 2006).
YAP1-B-MYB interaction was also suggested to play an important role for increased G2/M target gene expression in lung cancer which could be blocked and thereby influence the PRC1 level (Gründl et al., 2020; Pattschull et al., 2019; Weinstock & Gaubatz, 2019).
Also, post-transcriptional deregulation and abnormal activation of PRC1 in cancer might be an option. PRC1 becomes phosphorylated by CDK1/Cyclin B and later by PLK1, which is important for the activation and correct spatio-temporal regulation of the protein (Hu et al., 2012; Jiang et al., 1998; Mollinari et al., 2002; Neef et al., 2007; Zhu & Jiang, 2005; Zhu et al., 2006). Effects of CDK1 inhibition, as chromosome alignment defects, were connected to insufficient repression of PRC1 and KIF4 during prometaphase (Voets et al., 2015). It was shown that targeting PLK1 in cancer by novel inhibitors directed against its Polo box domain could have strong anticancer effects. Also, cancer cells with activated KRAS mutation and inactivated p53 appear to be more sensitive to PLK1 inhibition and might be an option for patients with both mutations (Lee & Bae, 2015).

Taken together, PRC1 depletion in a direct way or through components that influences the level or its activation could be a treatment option for lung cancer. In addition, combinational treatment with a chemotherapeutic drug, like cisplatin, could enhance the effects of PRC1 depletion and might be an option for therapy.

4.4 Conclusion and outlook

PRC1 is highly expressed in NSCLC as well as in other cancer types and is linked to a bad prognosis for cancer patients. Here I show that the elevated expression of PRC1 seems to be cell cycle regulated with increasing protein levels from S-phase to G2/M-phase of the cell cycle. PRC1 is a target gene of the DREAM/MMB complex, a master regulator of cell cycle-dependent gene expression, which could contribute to its expression pattern. Furthermore, the Hippo pathway and its downstream effector YAP may enhance G2/M gene expression in cancer by interaction with MMB from distal enhancers. Although PRC1 is located in the nucleus during interphase, my data do not support an additional function of the protein in lung cancer besides its well-established role as a microtubule-bundling protein for central spindle formation and cytokinesis. One can speculate that the nuclear localization of PRC1 during interphase might be a protective mechanism for the cells to prevent cytoplasmic microtubule-bundling. In addition, published studies demonstrate that coordinated phosphorylation events by CDK1/cyclin B and PLK1 are crucial for proper regulation of PRC1 activity during mitosis.

In the future, phosphorylation and dephosphorylation events of PRC1 should be further analyzed which seems to be a key event for its function. Here, the role of CDK16/CCNY complex in PRC1 phosphorylation was recently found and could be investigated in more detail. Besides, the interaction of PRC1 with p27, a cyclin-CDK inhibitor, that causes cell cycle arrest in G1 but also plays a role in regulation of G2/M progression and cytokinesis as well as actin and microtubule cytoskeleton dynamics, left open questions (see 4.2), which could be addressed in the future.

My data support the notion that PRC1 is a potential therapeutic target for lung cancer although the complete knockout of the protein might be lethal for the organism. The idea would be to deplete the protein to a level that is harmful for cancer cells but is tolerated by non-cancerous cells. A disadvantage of targeting mitotic exit in cancers is that it could generate more CIN and cancer heterogeneity. However, the influence of the PRC1 level in combination with a chemotherapeutic drug might enhance the therapeutic effects and highly proliferative cells might be more sensitive towards this combinatorial treatment than slowly dividing cells.

In the future, a drug that directly targets PRC1 should be designed or found. Alternatively, other approaches can also influence the level of PRC1, like p53 or its activation by post-translational modifications, which could be targeted.

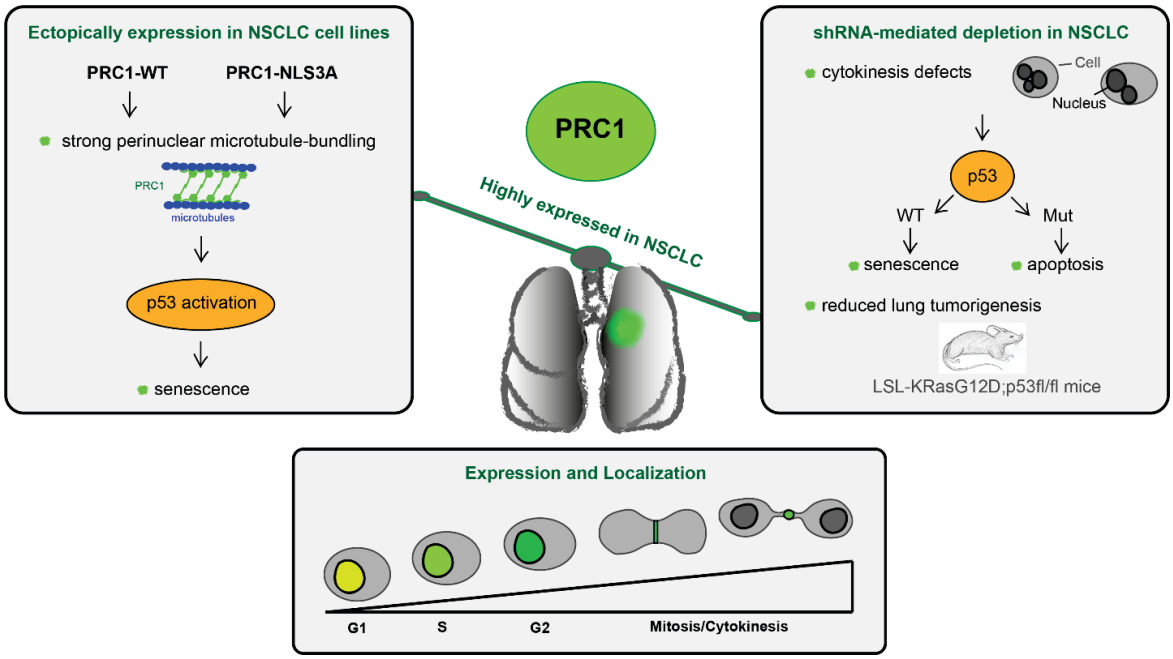

Figure 30: Conclusions and summary.
PRC1 is highly expressed in non-small cell lung cancer (NSCLC). Expression levels are cell cycle regulated with increasing levels from S phase to G2/M phase of the cell cycle. The protein localizes in the nucleus during interphase and then at the central spindle and midbody during mitosis and cytokinesis. Both, ectopically expression of PRC1 wildtype or a nuclear localization mutant (NLS3A) of PRC1, induces strong perinuclear microtubule-bundling in NSCLC cell lines. Finally, the microtubule-bundling phenotype activates a p53-dependent stress response, leading to senescence of the cells. On the other hand, depletion of PRC1 causes cytokinesis defects and multi-nucleation of lung cancer cell lines. Depending on the p53 status, NSCLC cells become senescent (p53-wildtype) or apoptotic (p53-mutated). *In vivo* in mice, KRas/p53-driven lung tumorigenesis is reduced, when PRC1 is depleted, suggesting that is a possible target for therapy for NSCLC.

5 References

Ahrendt, S. A., Hu, Y., Buta, M., McDermott, M. P., Benoit, N., Yang, S. C., … Sidransky, D. (2003). p53 mutations and survival in stage I non-small-cell lung cancer: Results of a prospective study. *Journal of the National Cancer Institute*. https://doi.org/10.1093/jnci/95.13.961

Al-Bassam, J., & Corbett, K. D. (2012). α-Tubulin acetylation from the inside out. *Proceedings of the National Academy of Sciences of the United States of America*. https://doi.org/10.1073/pnas.1217594109

Alvarellos, M. L., Lamba, J., Sangkuhl, K., Thorn, C. F., Wang, L., Klein, D. J., Altman, R. B., & Klein, T. E. (2014). PharmGKB summary: Gemcitabine pathway. Pharmacogenetics and genomics, 24(11), 564-574. https://doi.org/10.1097/FPC.0000000000000086

Álvarez-Fernández, M., Sanz-Flores, M., Sanz-Castillo, B., Salazar-Roa, M., Partida, D., Zapatero-Solana, E., … Malumbres, M. (2018). Therapeutic relevance of the PP2A-B55 inhibitory kinase MASTL/Greatwall in breast cancer. *Cell Death and Differentiation*. https://doi.org/10.1038/s41418-017-0024-0

American Cancer Society. (2021). American Cancer Society. Cancer Facts and Figures 2021. Atlanta: American Cancer Society; 2021.

Amin, M. A., Agarwal, S., & Varma, D. (2019). Mapping the kinetochore MAP functions required for stabilizing microtubule attachments to chromosomes during metaphase. *Cytoskeleton*. https://doi.org/10.1002/cm.21559

Andreassen, P. R., Lohez, O. D., Lacroix, F. B., & Margolis, R. L. (2001). Tetraploid state induces p53-dependent arrest of nontransformed mammalian cells in G1. *Molecular Biology of the Cell*. https://doi.org/10.1091/mbc.12.5.1315

Antonin, W., & Neumann, H. (2016). Chromosome condensation and decondensation during mitosis. *Current Opinion in Cell Biology*. https://doi.org/10.1016/j.ceb.2016.01.013

Barbacid, M. (1987). Ras Genes. *Annual Review of Biochemistry*. https://doi.org/10.1146/annurev.biochem.56.1.779

Bieging, K. T., Mello, S. S., & Attardi, L. D. (2014). Unravelling mechanisms of p53-mediated tumour suppression. *Nature Reviews Cancer*. https://doi.org/10.1038/nrc3711

Bieling, P., Telley, I. A., & Surrey, T. (2010). A Minimal Midzone Protein Module Controls Formation and Length of Antiparallel Microtubule Overlaps. *Cell*, *142*(3), 420–432. https://doi.org/10.1016/j.cell.2010.06.033

Blumenschein, G. R., Saintigny, P., Liu, S., Kim, E. S., Tsao, A. S., Herbst, R. S., … Lippman, S. M. (2013). Comprehensive biomarker analysis and final efficacy results of sorafenib in the BATTLE trial. *Clinical Cancer Research*. https://doi.org/10.1158/1078-0432.CCR-12-1818

Blumenschein, G. R., Smit, E. F., Planchard, D., Kim, D. W., Cadranel, J., De Pas, T., … Jänne, P. A. (2015). A randomized phase II study of the MEK1/MEK2 inhibitor trametinib (GSK1120212) compared with docetaxel in KRAS-mutant advanced non-small-cell lung cancer (NSCLC). *Annals of Oncology*. https://doi.org/10.1093/annonc/mdv072

Bradford, M. M. (1976). A rapid and sensitive method for the quantitation of microgram quantities of protein utilizing the principle of protein-dye binding. *Analytical Biochemistry*. https://doi.org/10.1016/0003-2697(76)90527-3

Brito, D. A., & Rieder, C. L. (2006). Mitotic Checkpoint Slippage in Humans Occurs via Cyclin B Destruction in the Presence of an Active Checkpoint. *Current Biology*. https://doi.org/10.1016/j.cub.2006.04.043

Bu, H., Li, Y., Jin, C., Yu, H., Wang, X., Chen, J., … Kong, B. (2020). Overexpression of PRC1 indicates a poor prognosis in ovarian cancer. *International Journal of Oncology*. https://doi.org/10.3892/ijo.2020.4959

Burgess, J. T., Rose, M., Boucher, D., Plowman, J., Molloy, C., Fisher, M., … Bolderson,

E. (2020). The Therapeutic Potential of DNA Damage Repair Pathways and Genomic Stability in Lung Cancer. Frontiers in Oncology, 10(July), 1–14. https://doi.org/10.3389/fonc.2020.01256

Cancer Genome Atlas Research Network. Integrated genomic analyses of ovarian carcinoma. Nature (2011) 474:609–615. doi:10.1038/nature10166

Carter, S. L., Eklund, A. C., Kohane, I. S., Harris, L. N., & Szallasi, Z. (2006). A signature of chromosomal instability inferred from gene expression profiles predicts clinical outcome in multiple human cancers. *Nature Genetics*. https://doi.org/10.1038/ng1861

Cerami, E., Gao, J., Dogrusoz, U., Gross, B. E., Sumer, S. O., Aksoy, B. A., … Schultz, N. (2012). The cBio Cancer Genomics Portal: An open platform for exploring multidimensional cancer genomics data. *Cancer Discovery*. https://doi.org/10.1158/2159-8290.CD-12-0095

Chen, G., & Deng, X. (2018). Cell Synchronization by Double Thymidine Block. BIO-PROTOCOL. https://doi.org/10.21769/bioprotoc.2994

Chen, J., Rajasekaran, M., Xia, H., Zhang, X., Kong, S. N., Sekar, K., … Hui, K. M. (2016). The microtubule-associated protein PRC1 promotes early recurrence of hepatocellular carcinoma in association with the Wnt/β-catenin signalling pathway. *Gut*, *65*(9), 1522–1534. https://doi.org/10.1136/gutjnl-2015-310625

Chung, V., Heath, E. I., Schelman, W. R., Johnson, B. M., Kirby, L. C., Lynch, K. M., … Holen, K. D. (2012). First-time-in-human study of GSK923295, a novel antimitotic inhibitor of centromere-associated protein e (CENP-E), in patients with refractory cancer. *Cancer Chemotherapy and Pharmacology*. https://doi.org/10.1007/s00280-011-1756-z

Cobrinik, D. (2005). Pocket proteins and cell cycle control. Oncogene, 24(17), 2796–2809. https://doi.org/10.1038/sj.onc.1208619

Cormie, P., Zopf, E. M., Zhang, X., & Schmitz, K. H. (2017). The impact of exercise on cancer mortality, recurrence, and treatment-related adverse effects. *Epidemiologic Reviews*. https://doi.org/10.1093/epirev/mxx007

Cox, A. D., & Der, C. J. (2010). Ras history: The saga continues. *Small GTPases*. https://doi.org/10.4161/sgtp.1.1.12178

Cox, A. D., Fesik, S. W., Kimmelman, A. C., Luo, J., & Der, C. J. (2014). Drugging the undruggable RAS: Mission Possible? *Nature Reviews Drug Discovery*. https://doi.org/10.1038/nrd4389

Cundell, M. J., Bastos, R. N., Zhang, T., Holder, J., Gruneberg, U., Novak, B., & Barr, F. A. (2013). The BEG (PP2A-B55/ENSA/Greatwall) Pathway Ensures Cytokinesis follows Chromosome Separation. *Molecular Cell*. https://doi.org/10.1016/j.molcel.2013.09.005

D'Avino, P. P., Giansanti, M. G., & Petronczki, M. (2015). Cytokinesis in animal cells. *Cold Spring Harbor Perspectives in Biology*. https://doi.org/10.1101/cshperspect.a015834

Dearden, S., Stevens, J., Wu, Y. L., & Blowers, D. (2013). Mutation incidence and coincidence in non small-cell lung cancer: Meta-analyses by ethnicity and histology (mutMap). *Annals of Oncology*. https://doi.org/10.1093/annonc/mdt205

Dimri, G. P., Lee, X., Basile, G., Acosta, M., Scott, G., Roskelley, C., … Campisi, J. (1995). A biomarker that identifies senescent human cells in culture and in aging skin in vivo. *Proceedings of the National Academy of Sciences of the United States of America*. https://doi.org/10.1073/pnas.92.20.9363

Dogan, S., Shen, R., Ang, D. C., Johnson, M. L., D'Angelo, S. P., Paik, P. K., … Ladanyi, M. (2012). Molecular epidemiology of EGFR and KRAS mutations in 3,026 lung adenocarcinomas: Higher susceptibility of women to smoking-related KRAS-mutant cancers. *Clinical Cancer Research*. https://doi.org/10.1158/1078-0432.CCR-11-3265

Dominguez-Brauer, C., Thu, K. L., Mason, J. M., Blaser, H., Bray, M. R., & Mak, T. W. (2015). Targeting Mitosis in Cancer: Emerging Strategies. *Molecular Cell*. https://doi.org/10.1016/j.molcel.2015.11.006

Douglas, M. E., & Mishima, M. (2010). Still entangled: Assembly of the central spindle by multiple microtubule modulators. *Seminars in Cell and Developmental Biology*.

https://doi.org/10.1016/j.semcdb.2010.08.005
DuPage, M., Dooley, A. L., & Jacks, T. (2009). Conditional mouse lung cancer models using adenoviral or lentiviral delivery of Cre recombinase. *Nature Protocols*, *4*(7), 1064–1072. https://doi.org/10.1038/nprot.2009.95
El Osta, B. E., Behera, M., Kim, S., Berry, L. D., Sica, G., Pillai, R. N., … Ramalingam, S. S. (2017). Characteristics and outcomes of patients (pts) with metastatic KRAS mutant lung adenocarcinomas: Lung Cancer Mutation Consortium (LCMC) database. *Journal of Clinical Oncology*. https://doi.org/10.1200/jco.2017.35.15_suppl.9021
Engeland, K. (2018). Cell cycle arrest through indirect transcriptional repression by p53: I have a DREAM. *Cell Death and Differentiation*. https://doi.org/10.1038/cdd.2017.172
Esterlechner, J., Reichert, N., Iltzsche, F., Krause, M., Finkernagel, F., & Gaubatz, S. (2013). LIN9, a Subunit of the DREAM Complex, Regulates Mitotic Gene Expression and Proliferation of Embryonic Stem Cells. *PLoS ONE*. https://doi.org/10.1371/journal.pone.0062882
Fellmann, C., Hoffmann, T., Sridhar, V., Hopfgartner, B., Muhar, M., Roth, M., … Lai, D. Y. (2013). *Resource An Optimized microRNA Backbone for Effective Single-Copy RNAi*. (3), 1704–1713. https://doi.org/10.1016/j.celrep.2013.11.020
Fennell, D. A., Summers, Y., Cadranel, J., Benepal, T., Christoph, D. C., Lal, R., … Ferry, D. (2016). Cisplatin in the modern era: The backbone of first-line chemotherapy for non-small cell lung cancer. *Cancer Treatment Reviews*. https://doi.org/10.1016/j.ctrv.2016.01.003
Ferrer, I., Zugazagoitia, J., Herbertz, S., John, W., Paz-Ares, L., & Schmid-Bindert, G. (2018). KRAS-Mutant non-small cell lung cancer: From biology to therapy. *Lung Cancer*. https://doi.org/10.1016/j.lungcan.2018.07.013
Fischer, M., Grundke, I., Sohr, S., Quaas, M., Hoffmann, S., Kno, A., … Rother, K. (2013). *p53 and Cell Cycle Dependent Transcription of kinesin family member 23 (KIF23) Is Controlled Via a CHR Promoter Element Bound by DREAM and MMB Complexes*. *8*(5). https://doi.org/10.1371/journal.pone.0063187
Fischer, M., & Muller, G.A. (2017). Cell cycle transcription control: DREAM/MuvB and RB-E2F complexes. Critical reviews in biochemistry and molecular biology 52: 638-662. https://doi.org/10.1080/10409238.2017.1360836
Fischer, M., Quaas, M., Nickel, A., & Engeland, K. (2015). Indirect p53-dependent transcriptional repression of Survivin, CDC25C, and PLK1 genes requires the cyclin-dependent kinase inhibitor p21/CDKN1A and CDE/CHR promoter sites binding the DREAM complex. *Oncotarget*. https://doi.org/10.18632/oncotarget.6356
Fischer, M., Quaas, M., Steiner, L., & Engeland, K. (2016). The p53-p21-DREAM-CDE/CHR pathway regulates G2/M cell cycle genes. *Nucleic Acids Research*. https://doi.org/10.1093/nar/gkv927
Forester, C. M., Maddox, J., Louis, J. V., Goris, J., & Virshup, D. M. (2007). Control of mitotic exit by PP2A regulation of Cdc25C and Cdk1. *Proceedings of the National Academy of Sciences of the United States of America*. https://doi.org/10.1073/pnas.0709879104
Fu, C., Yan, F., Wu, F., Wu, Q., Whittaker, J., Hu, H., … Yao, X. (2007). Mitotic phosphorylation of PRC1 at Thr470 is required for PRC1 oligomerization and proper central spindle organization. *Cell Research*. https://doi.org/10.1038/cr.2007.32
Gaillard, J., Neumann, E., Van Damme, D., Stoppin-Mellet, V., Ebel, C., Barbier, E., … Vantard, M. (2008). Two microtubule-associated proteins of Arabidopsis MAP65s promote antiparallel microtubule bundling. *Molecular Biology of the Cell*. https://doi.org/10.1091/mbc.E08-04-0341
Gao, J., Aksoy, B. A., Dogrusoz, U., Dresdner, G., Gross, B., Sumer, S. O., … Schultz, N. (2013). Integrative analysis of complex cancer genomics and clinical profiles using the cBioPortal. *Science Signaling*. https://doi.org/10.1126/scisignal.2004088
Gibbs, J. B., Sigal, I. S., Poe, M., & Scolnick, E. M. (1984). Intrinsic GTPase activity distinguishes normal and oncogenic ras p21 molecules. *Proceedings of the National Academy of Sciences of the United States of America*.

https://doi.org/10.1073/pnas.81.18.5704
Glotzer, M. (2009). The 3Ms of central spindle assembly: Microtubules, motors and MAPs. *Nature Reviews Molecular Cell Biology*. https://doi.org/10.1038/nrm2609
Glotzer, M., Murray, A. W., & Kirschner, M. W. (1991). Cyclin is degraded by the ubiquitin pathway. *Nature*. https://doi.org/10.1038/349132a0
Gourley, C., Balmaña, J., Ledermann, J. A., Serra, V., Dent, R., Loibl, S., … Boulton, S. J. (2019). Moving from poly (ADP-ribose) polymerase inhibition to targeting DNA repair and DNA damage response in cancer therapy. *Journal of Clinical Oncology*, *37*(25), 2257–2269. https://doi.org/10.1200/JCO.18.02050
Green, R. A., Paluch, E., & Oegema, K. (2012). Cytokinesis in Animal Cells. Annual Review of Cell and Developmental Biology. https://doi.org/10.1146/annurev-cellbio-101011-155718
Gründl, M., Walz, S., Hauf, L., Schwab, M., Werner, K. M., Spahr, S., … Gaubatz, S. (2020). Interaction of YAP with the Myb-MuvB (MMB) complex defines a transcriptional program to promote the proliferation of cardiomyocytes. *PLoS Genetics*. https://doi.org/10.1371/journal.pgen.1008818
Gulluni, F., Martini, M., De Santis, M. C., Campa, C. C., Ghigo, A., Margaria, J. P., … Hirsch, E. (2017). Mitotic Spindle Assembly and Genomic Stability in Breast Cancer Require PI3K-C2α Scaffolding Function. *Cancer Cell*. https://doi.org/10.1016/j.ccell.2017.09.002
Gupta, A., Shah, K., Oza, M. J., & Behl, T. (2019). Reactivation of p53 gene by MDM2 inhibitors: A novel therapy for cancer treatment. *Biomedicine and Pharmacotherapy*. https://doi.org/10.1016/j.biopha.2018.10.155
Gupta, S., Ramjaun, A. R., Haiko, P., Wang, Y., Warne, P. H., Nicke, B., … Downward, J. (2007). Binding of Ras to Phosphoinositide 3-Kinase p110α Is Required for Ras-Driven Tumorigenesis in Mice. *Cell*. https://doi.org/10.1016/j.cell.2007.03.051
Gyorffy, B., Surowiak, P., Budczies, J., & Lánczky, A. (2013). Online survival analysis software to assess the prognostic value of biomarkers using transcriptomic data in non-small-cell lung cancer. *PLoS ONE*. https://doi.org/10.1371/journal.pone.0082241
Hanahan, D., & Weinberg, R. A. (2011). Hallmarks of cancer: The next generation. *Cell*. https://doi.org/10.1016/j.cell.2011.02.013
Hannabuss, J., Lera-Ramirez, M., Cade, N. I., Fourniol, F. J., Nédélec, F., & Surrey, T. (2019). Self-Organization of Minimal Anaphase Spindle Midzone Bundles. Current Biology. https://doi.org/10.1016/j.cub.2019.05.049
Haschka, M., Karbon, G., Fava, L. L., & Villunger, A. (2018). Perturbing mitosis for anti-cancer therapy: is cell death the only answer? *EMBO Reports*. https://doi.org/10.15252/embr.201745440
Herbst, R. S., Morgensztern, D., & Boshoff, C. (2018). The biology and management of non-small cell lung cancer. *Nature*. https://doi.org/10.1038/nature25183
Hernández-Ortega, S., Sánchez-Botet, A., Quandt, E., Masip, N., Gasa, L., Verde, G., … Clotet, J. (2019). Phosphoregulation of the oncogenic protein regulator of cytokinesis 1 (PRC1) by the atypical CDK16/CCNY complex. *Experimental and Molecular Medicine*. https://doi.org/10.1038/s12276-019-0242-2
Holland, A. J., & Cleveland, D. W. (2009). Boveri revisited: chromosomal instability, aneuploidy and tumorigenesis. *Nature Reviews Molecular Cell Biology*, *10*(7), 478–487. https://doi.org/10.1038/nrm2718
Hou, G., Dong, C., Dong, Z., Liu, G., Xu, H., Chen, L., & Liu, L. (2017). *Upregulate KIF4A Enhances Proliferation , Invasion of Hepatocellular Carcinoma and Indicates poor prognosis Across Human Cancer Types*. (January), 1–10. https://doi.org/10.1038/s41598-017-04176-9
Hou, J., Aerts, J., den Hamer, B., van IJcken, W., den Bakker, M., Riegman, P., … Philipsen, S. (2010). Gene Expression-Based Classification of Non-Small Cell Lung Carcinomas and Survival Prediction. *PLoS ONE*. https://doi.org/10.1371/journal.pone.0010312
Hu, C. K., Coughlin, M., Field, C. M., Mitchison, T. M. (2011). KIF4 Regulates Midzone

Length during Cytokinesis. Curr Biol. 2011 May 24; 21(10): 815-824. doi: 10.1016/j.cub.2011.04.019

Hu, C. K., Ożlü, N., Coughlin, M., Steen, J. J., & Mitchison, T. J. (2012). Plk1 negatively regulates PRC1 to prevent premature midzone formation before cytokinesis. *Molecular Biology of the Cell*. https://doi.org/10.1091/mbc.E12-01-0058

Iegiani, G., Gai, M., Di Cunto, F., & Pallavicini, G. (2021). Cenpe inhibition leads to mitotic catastrophe and dna damage in medulloblastoma cells. *Cancers*. https://doi.org/10.3390/cancers13051028

Iltzsche, F., Simon, K., Stopp, S., Pattschull, G., Francke, S., Wolter, P., … Gaubatz, S. (2016). An important role for Myb-MuvB and its target gene KIF23 in a mouse model of lung adenocarcinoma. *Oncogene*, *36*(1), 110–121. https://doi.org/10.1038/onc.2016.181

Iness, A. N., Rubinsak, L., Meas, S. J., Chaoul, J., Sayeed, S., Pillappa, R., … Litovchick, L. (2021). Oncogenic B-Myb Is Associated With Deregulation of the DREAM-Mediated Cell Cycle Gene Expression Program in High Grade Serous Ovarian Carcinoma Clinical Tumor Samples. *Frontiers in Oncology*. https://doi.org/10.3389/fonc.2021.637193

Ingham, M., Schwartz, G. K. (2017). Cell-Cycle Therapeutics Come of Age. J Clin Oncol. 2017 Sep 1;35(25):2949-2959. doi: 10.1200/JCO.2016.69.0032. Epub 2017 Jun 3.

Israels, E.D., Israels, L.G. (2001). The cell cycle. Stem cells. https://doi.org/10.1634/stemcells.19-1-88

Jackson, E. L., Olive, K. P., Tuveson, D. A., Bronson, R., Crowley, D., Brown, M., & Jacks, T. (2005). The differential effects of mutant p53 alleles on advanced murine lung cancer. *Cancer Research*. https://doi.org/10.1158/0008-5472.CAN-05-2193

Jackson, E. L., Willis, N., Mercer, K., Bronson, R. T., Crowley, D., Montoya, R., … Tuveson, D. A. (2001). Analysis of lung tumor initiation and progression using conditional expression of oncogenic K-ras. *Genes and Development*. https://doi.org/10.1101/gad.943001

Janssen, A., Kops, G. J. P. L., & Medema, R. H. (2009). Elevating the frequency of chromosome mis-segregation as a strategy to kill tumor cells. *Proceedings of the National Academy of Sciences of the United States of America*. https://doi.org/10.1073/pnas.0904343106

Jeffery, J., Sinha, D., Srihari, S., Kalimutho, M., & Khanna, K. K. (2016). Beyond cytokinesis: The emerging roles of CEP55 in tumorigenesis. *Oncogene*. https://doi.org/10.1038/onc.2015.128

Jiang, W., Jimenez, G., Wells, N. J., Hope, T. J., Wahl, G. M., Hunter, T., & Fukunaga, R. (1998). PRC1: A human mitotic spindle-associated CDK substrate protein required for cytokinesis. *Molecular Cell*. https://doi.org/10.1016/s1097-2765(00)80302-0

Joerger, A. C., & Fersht, A. R. (2016). The p53 Pathway: Origins, Inactivation in Cancer, and Emerging Therapeutic Approaches. *Annual Review of Biochemistry*. https://doi.org/10.1146/annurev-biochem-060815-014710

Johnson, L., Greenbaum, D., Cichowski, K., Mercer, K., Murphy, E., Schmitt, E., … Jacks, T. (1997). K-ras is an essential gene in the mouse with partial functional overlap with N-ras. *Genes and Development*. https://doi.org/10.1101/gad.11.19.2468

Jordan, M. A., Wilson, L. (2004). Microtubules as a target for anticancer drugs. Nat Rev Cancer. 2004 Apr;4(4):253-65. doi: 10.1038/nrc1317.

Juang, Y. L., Huang, J., Peters, J. M., McLaughlin, M. E., Tai, C. Y., & Pellman, D. (1997). APC-mediated proteolysis of Ase1 and the morphogenesis of the mitotic spindle. *Science*. https://doi.org/10.1126/science.275.5304.1311

Kanehira, M., Katagiri, T., Shimo, A., Takata, R., Shuin, T., Miki, T., … Nakamura, Y. (2007). Oncogenic role of MPHOSPH1, a cancer-testis antigen specific to human bladder cancer. *Cancer Research*. https://doi.org/10.1158/0008-5472.CAN-06-3748

Karnoub, A. E., & Weinberg, R. A. (2008). Ras oncogenes: Split personalities. *Nature Reviews Molecular Cell Biology*. https://doi.org/10.1038/nrm2438

Kellogg, E. H., Howes, S., Ti, S. C., Ramírez-Aportela, E., Kapoor, T. M., Chacón, P., &

Nogales, E. (2016). Near-atomic cryo-EM structure of PRC1 bound to the microtubule. *Proceedings of the National Academy of Sciences of the United States of America*. https://doi.org/10.1073/pnas.1609903113

Khosravi-Far, R., Solski, P. A., Clark, G. J., Kinch, M. S., & Der, C. J. (1995). Activation of Rac1, RhoA, and mitogen-activated protein kinases is required for Ras transformation. *Molecular and Cellular Biology*. https://doi.org/10.1128/mcb.15.11.6443

Kieserman, E. K., Glotzer, M., & Wallingford, J. B. B. (2008). Developmental Regulation of Central Spindle Assembly and Cytokinesis during Vertebrate Embryogenesis. *Current Biology*. https://doi.org/10.1016/j.cub.2007.12.028

Kim, D., Langmead, B., & Salzberg, S. L. (2015). HISAT: A fast spliced aligner with low memory requirements. *Nature Methods*. https://doi.org/10.1038/nmeth.3317

Kim, H. C., & Choi, C. M. (2020). Current status of immunotherapy for lung cancer and future perspectives. *Tuberculosis and Respiratory Diseases*, *83*(1), 14–19. https://doi.org/10.4046/trd.2019.0039

Kim, J. M., Kang, D. W., Long, L. Z., Huang, S. M., Yeo, M. K., Yi, E. S., & Kim, K. H. (2011). Differential expression of Yes-associated protein is correlated with expression of cell cycle markers and pathologic TNM staging in non-small-cell lung carcinoma. *Human Pathology*. https://doi.org/10.1016/j.humpath.2010.08.003

Kiraz, Y., Adan, A., Kartal Yandim, M., & Baran, Y. (2016). Major apoptotic mechanisms and genes involved in apoptosis. Tumor Biology. https://doi.org/10.1007/s13277-016-5035-9

Kitagawa, M., & Lee, S. H. (2015). The chromosomal passenger complex (CPC) as a key orchestrator of orderly mitotic exit and cytokinesis. Frontiers in Cell and Developmental Biology. https://doi.org/10.3389/fcell.2015.00014

Knudsen, E. S., Pruitt, S. C., Hershberger, P. A., Agnieszka, K., Goodrich, D. W., & Comprehensive, P. (2019). Cell Cycle and Beyond: Exploiting New RB1 Controlled Mechanisms for Cancer Therapy. 5(5), 308–324. https://doi.org/10.1016/j.trecan.2019.03.005.Cell

Kuffer, C., Kuznetsova, A. Y., & Storchová, Z. (2013). Abnormal mitosis triggers p53-dependent cell cycle arrest in human tetraploid cells. *Chromosoma*. https://doi.org/10.1007/s00412-013-0414-0

Kurasawa, Y., Earnshaw, W. C., Mochizuki, Y., Dohmae, N., & Todokoro, K. (2004). Essential roles of KIF4 and its binding partner PRC1 in organized central spindle midzone formation. *EMBO Journal*. https://doi.org/10.1038/sj.emboj.7600347

Kutner, R. H., Zhang, X. Y., & Reiser, J. (2009). Production, concentration and titration of pseudotyped HIV-1-based lentiviral vectors. *Nature Protocols*, *4*(4), 495–505. https://doi.org/10.1038/nprot.2009.22

Labrière, C., Talapatra, S. K., Thoret, S., Bougeret, C., Kozielski, F., & Guillou, C. (2016). New MKLP-2 inhibitors in the paprotrain series: Design, synthesis and biological evaluations. *Bioorganic and Medicinal Chemistry*. https://doi.org/10.1016/j.bmc.2015.12.042

Laffin, J., Fogleman, D., & Lehman, J. M. (1989). Correlation of DNA content, p53, T antigen, and V antigen in simian virus 40-infected human diploid cells. Cytometry. https://doi.org/10.1002/cyto.990100212

Lakso, M., Sauer, B., Mosinger, B., Lee, E. J., Manning, R. W., Yu, S. H., … Westphal, H. (1992). Targeted oncogene activation by site-specific recombination in transgenic mice. *Proceedings of the National Academy of Sciences of the United States of America*. https://doi.org/10.1073/pnas.89.14.6232

Lane, D., & Levine, A. (2010). p53 Research: the past thirty years and the next thirty years. *Cold Spring Harbor Perspectives in Biology*. https://doi.org/10.1101/cshperspect.a000893

Lanni, J. S., & Jacks, T. (1998). Characterization of the p53-Dependent Postmitotic Checkpoint following Spindle Disruption. *Molecular and Cellular Biology*. https://doi.org/10.1128/mcb.18.2.1055

Lau, A. N., Curtis, S. J., Fillmore, C. M., Rowbotham, S. P., Mohseni, M., Wagner, D. E., … Kim, C. F. (2014). Tumor-propagating cells and Yap/Taz activity contribute to lung tumor progression and metastasis. *EMBO Journal*. https://doi.org/10.1002/embj.201386082

Law, C. W., Chen, Y., Shi, W., & Smyth, G. K. (2014). Voom: Precision weights unlock linear model analysis tools for RNA-seq read counts. *Genome Biology*. https://doi.org/10.1186/gb-2014-15-2-r29

Lee, S. J., Rodriguez-Bravo, V., Kim, H., Datta, S., & Foley, E. A. (2017). The PP2AB56 phosphatase promotes the association of Cdc20 with APC/C in mitosis. *Journal of Cell Science*. https://doi.org/10.1242/jcs.201608

Lee, Y., & Bae, S. (2015). *How do K - RAS -activated cells evade cellular defense mechanisms ? 35*(7), 827–832. https://doi.org/10.1038/onc.2015.153

Leevers, S. J., Paterson, H. F., & Marshall, C. J. (1994). Requirement for Ras in Raf activation is overcome by targeting Raf to the plasma membrane. *Nature*. https://doi.org/10.1038/369411a0

Lengauer, C., Kinzler, K. W., & Vogelstein, B. (1997). Genetic instability in colorectal cancers. *Nature*. https://doi.org/10.1038/386623a0

Lens, S. M. A., & Medema, R. H. (2019). Cytokinesis defects and cancer. *Nature Reviews Cancer*. https://doi.org/10.1038/s41568-018-0084-6

Leroy, B., Anderson, M., & Soussi, T. (2014). TP53 mutations in human cancer: Database reassessment and prospects for the next decade. *Human Mutation*. https://doi.org/10.1002/humu.22552

Li, J., Dallmayer, M., Kirchner, T., Musa, J., & Grünewald, T. G. P. (2018). PRC1 : Linking Cytokinesis , Chromosomal Instability , and Cancer Evolution. *TRENDS in CANCER*, *4*(1), 59–73. https://doi.org/10.1016/j.trecan.2017.11.002

Li, M., Yang, J., Zhou, W., Ren, Y., Wang, X., Chen, H., … Wang, L. (2017). *Activation of an AKT / FOXM1 / STMN1 pathway drives resistance to tyrosine kinase inhibitors in lung cancer*. *117*(7), 974–983. https://doi.org/10.1038/bjc.2017.292

Liao, Y., Smyth, G. K., & Shi, W. (2014). FeatureCounts: An efficient general purpose program for assigning sequence reads to genomic features. *Bioinformatics*. https://doi.org/10.1093/bioinformatics/btt656

Litovchick, L., Sadasivam, S., Florens, L., Zhu, X., Swanson, S. K., Velmurugan, S., … DeCaprio, J. A. (2007). Evolutionarily Conserved Multisubunit RBL2/p130 and E2F4 Protein Complex Represses Human Cell Cycle-Dependent Genes in Quiescence. Molecular Cell. https://doi.org/10.1016/j.molcel.2007.04.015

Liu, M., Liu, H., Chen, J. (2018). Mechanisms of the CDK4/6 inhibitor palbociclib (PD 0332991) and its future application in cancer treatment (Review). Oncology Reports 39: 901-911, 2018. DOI: 10.3892/or.2018.6221

Liu, R., Holik, A. Z., Su, S., Jansz, N., Chen, K., Leong, H. S., … Ritchie, M. E. (2015). Why weight? Modelling sample and observational level variability improves power in RNA-seq analyses. *Nucleic Acids Research*. https://doi.org/10.1093/nar/gkv412

Liu, X., Chen, Y., Li, Y., Petersen, R. B., & Huang, K. (2019). Targeting mitosis exit: A brake for cancer cell proliferation. *Biochimica et Biophysica Acta - Reviews on Cancer*. https://doi.org/10.1016/j.bbcan.2018.12.007

Liu, X., Gong, H., & Huang, K. (2013). Oncogenic role of kinesin proteins and targeting kinesin therapy. *Cancer Science*. https://doi.org/10.1111/cas.12138

Liu, X., Li, Y., Meng, L., Liu, X. Y., Peng, A., Chen, Y., … Huang, K. (2018). Reducing protein regulator of cytokinesis 1 as a prospective therapy for hepatocellular carcinoma article. *Cell Death and Disease*. https://doi.org/10.1038/s41419-018-0555-4

Liu, X., Li, Y., Zhang, X., Liu, X. Y., Peng, A., Chen, Y., … Huang, K. (2018). Inhibition of kinesin family member 20B sensitizes hepatocellular carcinoma cell to microtubule-targeting agents by blocking cytokinesis. *Cancer Science*. https://doi.org/10.1111/cas.13794

Liu, X., Zhou, Y., Liu, X., Peng, A., Gong, H., Huang, L., … Huang, K. (2014).

MPHOSPH1: A potential therapeutic target for hepatocellular carcinoma. *Cancer Research*. https://doi.org/10.1158/0008-5472.CAN-14-1279

Luo, H. W., Chen, Q. B., Wan, Y. P., Chen, G. X., Zhuo, Y. J., Cai, Z. D., … Zhong, W. De. (2016). Protein regulator of cytokinesis 1 overexpression predicts biochemical recurrence in men with prostate cancer. *Biomedicine and Pharmacotherapy*. https://doi.org/10.1016/j.biopha.2016.01.004

Malumbres, M., Barbacid, M. To cycle or not to cycle: a critical decision in cancer. Nat Rev Cancer 1, 222–231 (2001). https://doi.org/10.1038/35106065

Malumbres, M., Barbacid, M. RAS oncogenes: the first 30 years. Nat Rev Cancer 3, 459–465 (2003). https://doi.org/10.1038/nrc1097

Mannefeld, M., Klassen, E., & Gaubatz, S. (2009). B-MYB is required for recovery from the DNA damage-induced G2 checkpoint in p53 mutant cells. *Cancer Research*, *69*(9), 4073–4080. https://doi.org/10.1158/0008-5472.CAN-08-4156

Marino, S., Vooijs, M., Van Der Gulden, H., Jonkers, J., & Berns, A. (2000). Induction of medulloblastomas in p53-null mutant mice by somatic inactivation of Rb in the external granular layer cells of the cerebellum. *Genes and Development*. https://doi.org/10.1101/gad.14.8.994

Martínez-García, D., Manero-Rupérez, N., Quesada, R., Korrodi-Gregório, L., & Soto-Cerrato, V. (2019). Therapeutic strategies involving survivin inhibition in cancer. *Medicinal Research Reviews*. https://doi.org/10.1002/med.21547

Massarelli, E., Varella-Garcia, M., Tang, X., Xavier, A. C., Ozburn, N. C., Liu, D. D., … Wistuba, I. I. (2007). KRAS mutation is an important predictor of resistance to therapy with epidermal growth factor receptor tyrosine kinase inhibitors in non-small cell lung cancer. *Clinical Cancer Research*. https://doi.org/10.1158/1078-0432.CCR-06-3043

Matheson, C. J., Backos, D. S., & Reigan, P. (2016). Targeting WEE1 Kinase in Cancer. Trends in Pharmacological Sciences, 37(10), 872–881. https://doi.org/10.1016/j.tips.2016.06.006

Maton, G., Edwards, F., Lacroix, B., Stefanutti, M., Laband, K., Lieury, T., … Dumont, J. (2015). Kinetochore components are required for central spindle assembly. *Nature Cell Biology*. https://doi.org/10.1038/ncb3150

McGrath, J. P., Capon, D. J., Goeddel, D. V., & Levinson, A. D. (1984). Comparative biochemical properties of normal and activated human ras p21 protein. *Nature*. https://doi.org/10.1038/310644a0

McKenzie, C., & D'Avino, P. P. (2016). Investigating cytokinesis failure as a strategy in cancer therapy. *Oncotarget*. https://doi.org/10.18632/oncotarget.13556

McLemore, T. L., Adelberg, S., Czerwinski, M., Hubbard, W. C., Yu, S. J., Storeng, R., Wood, T.G., Hines, R. N., Boyd, M. R. (1989). Altered Regulation of the Cytochrome P4501A1 Gene: Novel Inducer-Independent Gene Expression in Pulmonary Carcinoma Cell Lines. Journal of the National Cancer Institute, Volume 81, Issue 23, 6 December 1989, Pages 1787–1794, https://doi.org/10.1093/jnci/81.23.1787.

Meek, D. W. (2015). Regulation of the p53 response and its relationship to cancer. *Biochemical Journal*. https://doi.org/10.1042/BJ20150517

Meerbrey, K. L., Hu, G., Kessler, J. D., Roarty, K., Li, M. Z., Fang, J. E., … Elledge, S. J. (2011). The pINDUCER lentiviral toolkit for inducible RNA interference in vitro and in vivo. *Proceedings of the National Academy of Sciences*, *108*(9), 3665–3670. https://doi.org/10.1073/pnas.1019736108

Miller, V. A., Hirsh, V., Cadranel, J., Chen, Y. M., Park, K., Kim, S. W., … Yang, J. C. H. (2012). Afatinib versus placebo for patients with advanced, metastatic non-small-cell lung cancer after failure of erlotinib, gefitinib, or both, and one or two lines of chemotherapy (LUX-Lung 1): A phase 2b/3 randomised trial. *The Lancet Oncology*. https://doi.org/10.1016/S1470-2045(12)70087-6

Mitchison, T. J., & Salmon, E. D. (2001). Mitosis: A history of division. Nature Cell Biology. https://doi.org/10.1038/35050656

Mokhtari, R. B., Homayouni, T. S., Baluch, N., Morgatskaya, E., Kumar, S., Das, B., &

Yeger, H. (2017). Combination therapy in combating cancer. *Oncotarget*. https://doi.org/10.18632/oncotarget.16723

Molinari, M. (2000). Cell cycle checkpoints and their inactivation in human cancer. Cell Prolif. 2000, 33, 261-274. https://doi.org/10.1046/j.1365-2184.2000.00191.x

Mollinari, C., Kleman, J. P., Jiang, W., Schoehn, G., Hunter, T., & Margolis, R. L. (2002). PRC1 is a microtubule binding and bundling protein essential to maintain the mitotic spindle midzone. *Journal of Cell Biology*. https://doi.org/10.1083/jcb.200111052

Morgan, D. O. (2013). The D box meets its match. *Molecular Cell*. https://doi.org/10.1016/j.molcel.2013.05.023

Musa, J., Aynaud, M. M., Mirabeau, O., Delattre, O., & Grünewald, T. G. (2017). MYBL2 (B-Myb): a central regulator of cell proliferation, cell survival and differentiation involved in tumorigenesis. *Cell Death & Disease*. https://doi.org/10.1038/cddis.2017.244

Nagy, Á., Lánczky, A., Menyhárt, O., & Gyorffy, B. (2018). Validation of miRNA prognostic power in hepatocellular carcinoma using expression data of independent datasets. *Scientific Reports*. https://doi.org/10.1038/s41598-018-27521-y

Neef, R., Gruneberg, U., Kopajtich, R., Li, X., Nigg, E. A., Sillje, H., & Barr, F. A. (2007). Choice of Plk1 docking partners during mitosis and cytokinesis is controlled by the activation state of Cdk1. *Nature Cell Biology*. https://doi.org/10.1038/ncb1557

Niederhuber, J. E., Armitage, J. O., Doroshow, J. H., Kastan, M. B., & Tepper, J. E. (2013). Abeloff's Clinical Oncology: Fifth Edition. In *Abeloff's Clinical Oncology: Fifth Edition*. https://doi.org/10.31524/bkkmedj.2015.09.018

Noone AM, Howlader N, Krapcho M, Miller D, Brest A, Yu M, Ruhl J, Tatalovich Z, Mariotto A, Lewis DR, Chen HS, Feuer EJ, Cronin KA (eds), C. K. (2018). SEER Cancer Statistics Review, 1975-2015, National Cancer Institute, Bethesda, MD, https://seer.cancer.gov/csr/1975_2015/, based on November 2017 SEER data submission, posted to the SEER web site, April 2018.

Novak, A., Guo, C., Yang, W., Nagy, A.,and Lobe, C. G. (2000). Z/EG, a Double Reporter Mouse Line That Expresses Enhanced Green Fluorescent Protein Upon Cre-Mediated Excision. genesis 28:147–155 (2000). https://doi.org/10.1002/1526-968X(200011/12)28:3/4<147::AID-GENE90>3.0.CO;2-G

Oriola, D., Needleman, D. J., & Brugués, J. (2018). The Physics of the Metaphase Spindle. *Annual Review of Biophysics*. https://doi.org/10.1146/annurev-biophys-060414-034107

Osterloh, L., Von Eyss, B., Schmit, F., Rein, L., Hübner, D., Samans, B., … Gaubatz, S. (2007). The human synMuv-like protein LIN-9 is required for transcription of G2/M genes and for entry into mitosis. EMBO Journal, 26(1), 144–157. https://doi.org/10.1038/sj.emboj.7601478

Otto, T., Sicinski, P. (2017). Cell cycle proteins as promising targets in cancer therapy. Nat Rev Cancer. 2017 Jan 27;17(2):93-115. doi: 10.1038/nrc.2016.138.

Papadimitrakopoulou, V., Jack Lee, J., Wistuba, I. I., Tsao, A. S., Fossella, F. V., Kalhor, N., … Herbst, R. S. (2016). The BATTLE-2 study: A biomarker-integrated targeted therapy study in previously treated patients with advanced non-small-cell lung cancer. *Journal of Clinical Oncology*. https://doi.org/10.1200/JCO.2015.66.0084

Pattschull, G., Walz, S., Gründl, M., Schwab, M., Rühl, E., Baluapuri, A., … Gaubatz, S. (2019). The Myb-MuvB Complex Is Required for YAP-Dependent Transcription of Mitotic Genes. *Cell Reports*. https://doi.org/10.1016/j.celrep.2019.05.071

PDQ Adult Treatment Editorial Board. PDQ Non-Small Cell Lung Cancer Treatment. Bethesda, MD: National Cancer Institute. Updated <11/19/2020>. Available at: https://www.cancer.gov/types/lung/hp/non-small-cell-lung-treatment-pdq. Accessed <12/12/2020>. [PMID: 26389304]

Pellman, D., Bagget, M., Tu, H., & Fink, G. R. (1995). Two microtubule-associated proteins required for anaphase spindle movement in Saccharomyces cerevisiae. *Journal of Cell Biology*. https://doi.org/10.1083/jcb.130.6.1373

Peng, T., Zhou, W., Guo, F., Wu, H. S., Wang, C. Y., Wang, L., & Yang, Z. Y. (2017).

Centrosomal protein 55 activates NF-κB signalling and promotes pancreatic cancer cells aggressiveness. *Scientific Reports*. https://doi.org/10.1038/s41598-017-06132-z

Perchey, R. T., Serres, M. P., Nowosad, A., Creff, J., Callot, C., Gay, A., … Besson, A. (2018). p27 Kip1 regulates the microtubule bundling activity of PRC1. Biochimica et Biophysica Acta - Molecular Cell Research. https://doi.org/10.1016/j.bbamcr.2018.08.010

Petitjean, A., Mathe, E., Kato, S., Ishioka, C., Tavtigian, S. V., Hainaut, P., & Olivier, M. (2007). Impact of mutant p53 functional properties on TP53 mutation patterns and tumor phenotype: Lessons from recent developments in the IARC TP53 database. *Human Mutation*. https://doi.org/10.1002/humu.20495

Pfleger, C. M., & Kirschner, M. W. (2000). The KEN box: An APC recognition signal distinct from the D box targeted by Cdh1. *Genes and Development*. https://doi.org/10.1101/gad.14.6.655

Potapova, T. A., Zhu, J., & Li, R. (2013). Aneuploidy and chromosomal instability: A vicious cycle driving cellular evolution and cancer genome chaos. *Cancer and Metastasis Reviews*. https://doi.org/10.1007/s10555-013-9436-6

Raab, M., Krämer, A., Hehlgans, S., Sanhaji, M., Kurunci-Csacsko, E., Dötsch, C., … Strebhardt, K. (2015). Mitotic arrest and slippage induced by pharmacological inhibition of Polo-like kinase 1. *Molecular Oncology*, *9*(1), 140–154. https://doi.org/10.1016/j.molonc.2014.07.020

Rale, M. J., Kadzik, R. S., & Petry, S. (2018). Phase Transitioning the Centrosome into a Microtubule Nucleator. *Biochemistry*. https://doi.org/10.1021/acs.biochem.7b01064

Rath, O., & Kozielski, F. (2012). Kinesins and cancer. *Nature Reviews Cancer*, *12*(8), 527–539. https://doi.org/10.1038/nrc3310

Reichert, N., Wurster, S., Ulrich, T., Schmitt, K., Hauser, S., Probst, L., … Gaubatz, S. (2010). Lin9, a Subunit of the Mammalian DREAM Complex, Is Essential for Embryonic Development, for Survival of Adult Mice, and for Tumor Suppression. *Molecular and Cellular Biology*. https://doi.org/10.1128/mcb.00028-10

Rhodes, D. R., Yu, J., Shanker, K., Deshpande, N., Varambally, R., Ghosh, D., … Chinnaiyan, A. M. (2004). ONCOMINE: A Cancer Microarray Database and Integrated Data-Mining Platform. *Neoplasia*. https://doi.org/10.1016/s1476-5586(04)80047-2

Rodriguez-Viciana, P., Warne, P. H., Khwaja, A., Marte, B. M., Pappin, D., Das, P., … Downward, J. (1997). Role of phosphoinositide 3-OH kinase in cell transformation and control of the actin cytoskeleton by Ras. *Cell*. https://doi.org/10.1016/S0092-8674(00)80226-3

Sadasivam, S., & DeCaprio, J. A. (2013). The DREAM complex: master coordinator of cell cycle-dependent gene expression. *Nature Reviews Cancer*, *13*(8), 585–595. https://doi.org/10.1038/nrc3556

Sanjiv, K., Hagenkort, A., Calderón-Montaño, J. M., Koolmeister, T., Reaper, P. M., Mortusewicz, O., … Helleday, T. (2016). Cancer-Specific Synthetic Lethality between ATR and CHK1 Kinase Activities. Cell Reports. https://doi.org/10.1016/j.celrep.2015.12.032

Sansregret, L., Vanhaesebroeck, B., & Swanton, C. (2018). Determinants and clinical implications of chromosomal instability in cancer. Nature Reviews Clinical Oncology. https://doi.org/10.1038/nrclinonc.2017.198

Schafer, K. A. (1998). The Cell Cycle: A Review. Veterinary Pathology 35:461-478 (1998). https://doi.org/10.1177/030098589803500601

Scheffzek, K., Ahmadian, M. R., Kabsch, W., Wiesmüller, L., Lautwein, A., Schmitz, F., & Wittinghofer, A. (1997). The Ras-RasGAP complex: Structural basis for GTPase activation and its loss in oncogenic ras mutants. *Science*. https://doi.org/10.1126/science.277.5324.333

Scheffzek, K., Lautwein, A., Kabscht, W., Ahmadian, M. R., & Wittinghofer, A. (1996). Crystal structure of the GTPase-activating domain of human p120GAP and implications for the interaction with Ras. *Nature*. https://doi.org/10.1038/384591a0

Schmit, F., Cremer, S., & Gaubatz, S. (2009). LIN54 is an essential core subunit of the DREAM/LINC complex that binds to the cdc2 promoter in a sequence-specific manner. FEBS Journal, 276(19), 5703–5716. https://doi.org/10.1111/j.1742-4658.2009.07261.x

Schmit, F., Korenjak, M., Mannefeld, M., Schmitt, K., Franke, C., Von Eyss, B., … Gaubatz, S. (2007). LINC, a human complex that is related to pRB-containing complexes in invertebrates regulates the expression of G2/M genes. Cell Cycle. https://doi.org/10.4161/cc.6.15.4512

Scholey, J. M., Brust-Mascher, I., & Mogilner, A. (2003). Cell division. *Nature*. https://doi.org/10.1038/nature01599

Sergushichev, A. A. (2016). An algorithm for fast preranked gene set enrichment analysis using cumulative statistic calculation. *BioRxiv*. doi: https://doi.org/10.1101/060012

She, Z. Y., Wei, Y. L., Lin, Y., Li, Y. L., & Lu, M. H. (2019). Mechanisms of the Ase1/PRC1/MAP65 family in central spindle assembly. *Biological Reviews*. https://doi.org/10.1111/brv.12547

Shimo, A., Nishidate, T., Ohta, T., Fukuda, M., Nakamura, Y., & Katagiri, T. (2007). Elevated expression of protein regulator of cytokinesis 1, involved in the growth of breast cancer cells. *Cancer Science*. https://doi.org/10.1111/j.1349-7006.2006.00381.x

Shukla, S., Milewski, D., Pradhan, A., Rama, N., Rice, K., Le, T., … Kalin, T. V. (2019). The FOXM1 inhibitor RCM-1 decreases carcinogenesis and nuclear b-catenin. *Molecular Cancer Therapeutics*. https://doi.org/10.1158/1535-7163.MCT-18-0709

Siegel, R. L., Miller, K. D., & Jemal, A. (2017). Cancer statistics, 2017. *CA: A Cancer Journal for Clinicians*. https://doi.org/10.3322/caac.21387

Siegel, R. L., Miller, K. D., & Jemal, A. (2018). Cancer statistics, 2018. *CA: A Cancer Journal for Clinicians*. https://doi.org/10.3322/caac.21442

Siegel, R. L., Miller, K. D., & Jemal, A. (2019). Cancer statistics, 2019. *CA: A Cancer Journal for Clinicians*. https://doi.org/10.3322/caac.21551

Singh, A., Trivedi, P., & Jain, N. K. (2018). Advances in siRNA delivery in cancer therapy. *Artificial Cells, Nanomedicine and Biotechnology*. https://doi.org/10.1080/21691401.2017.1307210

Stewart, S. A., Dykxhoorn, D. M., Palliser, D., Mizuno, H., Yu, E. Y., An, D. S., Sabatini, D. M., Chen, I. S., Hahn, W. C., Sharp, P. A., Weinberg, R. A., Novina, C. D. (2003). Lentivirus-delivered stable gene silencing by RNAi in primary cells. RNA 2003 Apr;9(4):493-501. doi: 10.1261/rna.2192803.

Stokoe, D., Macdonald, S. G., Cadwallader, K., Symons, M., & Hancock, J. F. (1994). Activation of Raf as a result of recruitment to the plasma membrane. *Science*. https://doi.org/10.1126/science.7811320

Su, L. L., Ma, W. X., Yuan, J. F., Shao, Y., Xiao, W., & Jiang, S. J. (2012). Expression of yes-associated protein in non-small cell lung cancer and its relationship with clinical pathological factors. *Chinese Medical Journal*. https://doi.org/10.3760/cma.j.issn.0366-6999.2012.22.017

Subramanian, A., Tamayo, P., Mootha, V. K., Mukherjee, S., Ebert, B. L., Gillette, M. A., … Mesirov, J. P. (2005). Gene set enrichment analysis: A knowledge-based approach for interpreting genome-wide expression profiles. *Proceedings of the National Academy of Sciences of the United States of America*. https://doi.org/10.1073/pnas.0506580102

Subramanian, R., Ti, S., Tan, L., Darst, S. A., & Kapoor, T. M. (2013). Marking and Measuring Single Microtubules by PRC1 and Kinesin-4. *Cell*, *154*(2), 377–390. https://doi.org/10.1016/j.cell.2013.06.021

Subramanian, R., Wilson-kubalek, E. M., Arthur, C. P., Bick, M. J., Campbell, E. A., Darst, S. A., … Kapoor, T. M. (2010). Insights into Antiparallel Microtubule Crosslinking by PRC1 , a Conserved Nonmotor Microtubule Binding Protein. *Cell*, *142*(3), 433–443. https://doi.org/10.1016/j.cell.2010.07.012

Sun, C. Y., Zhang, Q. Y., Zheng, G. J., & Feng, B. (2019). Phytochemicals: Current

strategy to sensitize cancer cells to cisplatin. Biomedicine and Pharmacotherapy, 110(August 2018), 518–527. https://doi.org/10.1016/j.biopha.2018.12.010

Takahashi, Y., Rayman, J. B., & Dynlacht, B. D. (2000). Analysis of promoter binding by the E2F and pRB families in vivo: Distinct E2F proteins mediate activation and repression. *Genes and Development*. https://doi.org/10.1101/gad.14.7.804

Tanaka, Y., Patestos, N. P., Maekawa, T., & Ishii, S. (1999). B-myb is required for inner cell mass formation at an early stage of development. *Journal of Biological Chemistry*. https://doi.org/10.1074/jbc.274.40.28067

Tang, J. C., Wu, K., Zheng, X., Xu, M., Dai, Y., Wei, S. S., & Cai, X. J. (2019). GSK923295 as a potential antihepatocellular carcinoma agent causing delay on liver regeneration after partial hepatectomy. *Chinese Medical Journal*. https://doi.org/10.1097/CM9.0000000000000053

Taniwaki, M., Takano, A., Ishikawa, N., Yasui, W., Inai, K., Nishimura, H., … Daigo, Y. (2007). Activation of KIF4A as a prognostic biomarker and therapeutic target for lung cancer. *Clinical Cancer Research*. https://doi.org/10.1158/1078-0432.CCR-07-1328

Tao, Z., Le Blanc, J. M., Wang, C., Zhan, T., Zhuang, H., Wang, P., … Lu, B. (2016). Coadministration of trametinib and palbociclib radiosensitizes KRAS-mutant non-small cell lung cancers in vitro and in vivo. Clinical Cancer Research. https://doi.org/10.1158/1078-0432.CCR-15-0589

Tessema, M., Lehmann, U., & Kreipe, H. (2004). Cell cycle and no end. *Virchows Archiv*. https://doi.org/10.1007/s00428-003-0971-3

Tovar, C., Rosinski, J., Filipovic, Z., Higgins, B., Kolinsky, K., Hilton, H., … Vassilev, L. T. (2006). Small-molecule MDM2 antagonists reveal aberrant p53 signaling in cancer: Implications for therapy. *Proceedings of the National Academy of Sciences of the United States of America*. https://doi.org/10.1073/pnas.0507493103

Vanarsdale, T., Boshoff, C., Arndt, K. T., & Abraham, R. T. (2015). Molecular Pathways : Targeting the Cyclin D – CDK4 / 6 Axis for Cancer Treatment. 2905–2911. https://doi.org/10.1158/1078-0432.CCR-14-0816

Voets, E., Marsman, J., Demmers, J., Beijersbergen, R., & Wolthuis, R. (2015). The lethal response to Cdk1 inhibition depends on sister chromatid alignment errors generated by KIF4 and isoform 1 of PRC1. *Nature Publishing Group*, (August), 1–12. https://doi.org/10.1038/srep14798

Vousden, K. H., & Prives, C. (2009). Blinded by the Light: The Growing Complexity of p53. *Cell*. https://doi.org/10.1016/j.cell.2009.04.037

Wang, Yang, Dong, Q., Zhang, Q., Li, Z., Wang, E., & Qiu, X. (2010). Overexpression of yes-associated protein contributes to progression and poor prognosis of non-small-cell lung cancer. *Cancer Science*. https://doi.org/10.1111/j.1349-7006.2010.01511.x

Wang, Yu, Shi, F., Xing, G. H., Xie, P., Zhao, N., Yin, Y. F., … Xuan, S. Y. (2017). Protein regulator of cytokinesis PRC1 confers chemoresistance and predicts an unfavorable postoperative survival of hepatocellular carcinoma patients. *Journal of Cancer*. https://doi.org/10.7150/jca.17640

Weaver, B. A. (2014). How Taxol/paclitaxel kills cancer cells. *Molecular Biology of the Cell*. https://doi.org/10.1091/mbc.E14-04-0916

Weinberg, R. A. (2014). Biology of the Cancer. In Garland Science. https://doi.org/10.1007/s13398-014-0173-7.2

Weinstock, G., & Gaubatz, S. (2019). One way to rule them all: G2/M gene regulation by oncogenic YAP1 and B-MYB. *Molecular and Cellular Oncology*. https://doi.org/10.1080/23723556.2019.1648026

Wilhelm, S. M., Carter, C., Tang, L. Y., Wilkie, D., McNabola, A., Rong, H., … Trail, P. A. (2004). BAY 43-9006 exhibits broad spectrum oral antitumor activity and targets the RAF/MEK/ERK pathway and receptor tyrosine kinases involved in tumor progression and angiogenesis. *Cancer Research*. https://doi.org/10.1158/0008-5472.CAN-04-1443

Wolter, P., Hanselmann, S., Pattschull, G., Schruf, E., & Gaubatz, S. (2017). Central spindle proteins and mitotic kinesins are direct transcriptional targets of MuvB, B-

MYB and FOXM1 in breast cancer cell lines and are potential targets for therapy. *Oncotarget*. https://doi.org/10.18632/oncotarget.14466

Wood, K. W., Lad, L., Luo, L., Qian, X., Knight, S. D., Nevins, N., … Jackson, J. R. (2010). Antitumor activity of an allosteric inhibitor of centromere-associated protein-E. *Proceedings of the National Academy of Sciences of the United States of America*. https://doi.org/10.1073/pnas.0915068107

Wu, F., Shi, X., Zhang, R., Tian, Y., Wang, X., Wei, C., … Kong, X. (2018). Regulation of proliferation and cell cycle by protein regulator of cytokinesis 1 in oral squamous cell carcinoma. *Cell Death and Disease*. https://doi.org/10.1038/s41419-018-0618-6

Yamano, H. (2019). APC/C: current understanding and future perspectives. *F1000Research*. https://doi.org/10.12688/f1000research.18582.1

Yang, Z., Kenny, A. E., Brito, D. A., & Rieder, C. L. (2009). Cells satisfy the mitotic checkpoint in Taxol, and do so faster in concentrations that stabilize syntelic attachments. *Journal of Cell Biology*. https://doi.org/10.1083/jcb.200906150

Yeung, B., Yu, J., & Yang, X. (2016). Roles of the Hippo pathway in lung development and tumorigenesis. *International Journal of Cancer*. https://doi.org/10.1002/ijc.29457

Yuan, M., Huang, L.-L., Chen, J.-H., Wu, J., & Xu, Q. (2019). The emerging treatment landscape of targeted therapy in non-small-cell lung cancer. *Signal Transduction and Targeted Therapy*. https://doi.org/10.1038/s41392-019-0099-9

Zhan, P., Xi, G. M., Liu, H. B., Liu, Y. F., Xu, W. J., Zhu, Q., … Song, Y. (2017). Protein regulator of cytokinesis-1 expression: Prognostic value in lung squamous cell carcinoma patients. *Journal of Thoracic Disease*. https://doi.org/10.21037/jtd.2017.06.91

Zhan, P., Zhang, B., Xi, G. min, Wu, Y., Liu, H. bing, Liu, Y. fang, … Song, Y. (2017). PRC1 contributes to tumorigenesis of lung adenocarcinoma in association with the Wnt/β-catenin signaling pathway. *Molecular Cancer*. https://doi.org/10.1186/s12943-017-0682-z

Zhang, B., Shi, X., Xu, G., Kang, W., Zhang, W., Zhang, S., … Zou, X. (2017). Elevated PRC1 in gastric carcinoma exerts oncogenic function and is targeted by piperlongumine in a p53-dependent manner. *Journal of Cellular and Molecular Medicine*. https://doi.org/10.1111/jcmm.13063

Zhou, Y., Zhou, B., Pache, L., Chang, M., Khodabakhshi, A. H., Tanaseichuk, O., … Chanda, S. K. (2019). Metascape provides a biologist-oriented resource for the analysis of systems-level datasets. *Nature Communications*. https://doi.org/10.1038/s41467-019-09234-6

Zhu, C., & Jiang, W. (2005). Cell cycle-dependent translocation of PRC1 on the spindle by Kif4 is essential for midzone formation and cytokinesis. *Proceedings of the National Academy of Sciences of the United States of America*. https://doi.org/10.1073/pnas.0408438102

Zhu, C., Lau, E., Schwarzenbacher, R., Bossy-Wetzel, E., & Jiang, W. (2006). Spatiotemporal control of spindle midzone formation by PRC1 in human cells. *Proceedings of the National Academy of Sciences of the United States of America*. https://doi.org/10.1073/pnas.0506926103

6 Appendix

6.1 Supervised bachelor thesis

Shin, Woojin. (2018). Charakterisierung des Mikrotubuli-bindenden Proteins PRC1 in Krebszellen und nicht-transformierten Zellen.

6.2 Lung tumor area

Table 41: Analysis of tumor area of shLuc infected mice (1)

Mouse number	#2738		#2740		#2741		#2744		#2746	
Section	13	23	13	23	13	23	13	23	13	23
Lobe 1 total [µm²]	898289503 1	114684946 94	199538019 03	181223638 50	278755394 54	272166969 08	197674493 48	180463219 44	105912652 00	855520893 4
Lobe 1 tumor [µm²]	103897206 8	853468293	213660467 4	122669414 6	787841654	880254973	386582584	515754848	586948109	416463138
Lobe 2 total [µm²]	280411055 06	216115207 98	232412488 68	221797397 02	203176876 800	219627920 52	272204614 00	333864878 88	106609894 90	459967017 95
Lobe 2 tumor [µm²]	220111959 47	132792975 6	154659279 86	694485442	462653171	559256370	464384602 6	477348242 0	357255632	153694499
Lobe 3 total [µm²]	157039868 60	165365257 44	177531263 72	109079759 37	207268349 50	184454455 01	211107529 61	259621067 90	214186842 99	242457701 01
Lobe 3 tumor [µm²]	961399874	286636467	917262800	502658645	498801137 1	654954368 5	555855987	471565221	240132231	350415922
Lobe 4 total [µm²]	237827801 16	293596979 06	120291955 46	228378331 57	155024841 16	152988441 42	124866329 02	628350260 5	265128396 38	251881795 91
Lobe 4 tumor [µm²]	142378389 9	452014751 3	971697123	187119890 3	625011654	784817135	104986116 0	120709998 1	609696324	803070498
Lobe 5 total [µm²]	290078186 40	323926154 84	318840183 01	251149086 94	939021357 5	126764078 41	157552550 07	137531334 17	199348550 65	139648139 86
Lobe 5 tumor [µm²]	480365491 3	209558314 2	164886151 6	387548782	484550707	891518738	278848266 6	270632881 6	220235294	717421870
Total lung [µm²]	1.08444E+11		1.02012E+11		94706473170		96886052131		82836138250	
Total tumor [µm²]	11046211836		5951802409		8506729729		9549429855		2227666759	
Relative tumor area [%]	10.18612401		5.834407927		8.98220517		9.856351502		2.689245063	

Table 42: Analysis of tumor area of shLuc infected mice (2)

Mouse number	#2751		#2755		#2757		#2758		#2759	
Section	13	23	13	23	13	23	13	24	13	23
Lobe 1 total [µm²]	211771445 57	144065324 51	125738276 25	884385880 5	324542643 50	338795492 70	148232519 20	336116807 28	140896037 53	327891830 95
Lobe 1 tumor [µm²]	476041641 8	306895580 6	215555422	372049630	120231817 25	164499945 71	188916778 9	688246338 0	426591281 8	514645214 0
Lobe 2 total [µm²]	217934585 39	188214573 78	230408546 43	204654235 48	273209802 90	357263170 64	256354521 95	338942840 20	217124834 32	372304079 62
Lobe 2 tumor [µm²]	112135223 97	121683481 21	145521855 3	105950985 7	211019021 1	134003524 9	500601551 3	528242647 2	238266094 7	301273002 2
Lobe 3 total [µm²]	239313762 06	259802562 49	212434866 00	172535404 65	215307391 60	161904003 37	102110048 39	106281000 52	256561814 76	290204861 58
Lobe 3 tumor [µm²]	544216527 3	412591892 5	806691885 6	389924169 3	603953691	390427510 6	679891878	108421430 6	449444234 4	537394368 5
Lobe 4 total [µm²]	362901775 10	356705913 69	257803055 54	305366523 60	208143231 065	225591488 41	186619912 00	253625245 73	177293068 19	146282337 96
Lobe 4 tumor [µm²]	101384381 11	165241342 55	225155507	125150214 5	136085193 2	144845663 9	112982452 9	561753364	240970270 4	347190553 8
Lobe 5 total [µm²]	103000256 70	253335137 76	226014783 26	192441712 84	105510764 48	143084566 10	162746013 01	120107446 05	172628798 89	125405910 80
Lobe 5 tumor [µm²]	107530395	142733070	553825664	499076638	240977747 96	315111262 5	714192012	208654094	118791981 4	120896696 27
Total lung [µm²]	1.16852E+11		1.00792E+11		1.17668E+11		1.00557E+11		1.1133E+11	
Total tumor [µm²]	33846081386		8799026983		25118704923		12658245119		16477318470	
Relative tumor area [%]	28.964847 92		8.72990364		21.347166 94		12.588152 06		14.800472 45	

Table 43: Analysis of tumor area of shPRC1 infected mice (1)

Mouse number	#2654		#2656		#2657		#2737		#2743	
Section	13	23	13	23	13	23	13	23	13	23
Lobe 1 total [µm²]	185847455 56	739735978 9	189102243 06	133548227 47	205979232 58	286667377 06	191856592 74	196518601 42	112177337 742	770661181 1
Lobe 1 tumor [µm²]	175543016 9	177868801	496147903 4	303136568 0	582695564	123075283	211150023	216101799 8	144849760 5	612916998
Lobe 2 total [µm²]	188335632 91	126733651 27	212506313 71	320403559 05	133818352 68	974474978 7	281122894 24	292076296 02	261452481 38	264172429 75

Lobe 2 tumor [µm²]	26034376 7	18308048 3	29067685 67	15531902 30	12835522 7	74651061	67352497 8	11071980 39	76572956 9	22664462 9
Lobe 3 total [µm²]	18888018 248	27324033 058	23407320 582	19304618 517	15072637 075	19880163 625	19718258 832	29011829 579	18332037 633	17843724 740
Lobe 3 tumor [µm²]	84470682 9	12892033 05	18664819 65	28131252 82	16814861 3	32883816 2	89589216 2	17626838 06	53907741 5	37185269 7
Lobe 4 total [µm²]	31503409 858	32986414 491	23081428 294	12131370 577	31669086 404	35907743 426	22412597 189	22283043 099	14858199 108	10525932 093
Lobe 4 tumor [µm²]	57269627 4	56739477 9	27401901 83	95691119 4	26868415 1	30343929 7	12988084 55	57012159 3	58080729 6	77973399 7
Lobe 5 total [µm²]	25270229 989	20846850 153	11520408 065	66492848 69	13026169 141	14136347 415	72404859 40	16015728 261	21621183 867	20760095 898
Lobe 5 tumor [µm²]	32734406 3	26759924	85881000 4	95031923 9	11851576 3	77572196	19072755 2	26337129 34	60232297 9	29882791 7
Total lung [µm²]	1.07154E+11		90825232617		1.01042E+11		1.0642E+11		87713807003	
Total tumor [µm²]	3002414197		11319320689		10869876599		6702593870		3113205551	
Relative tumor area [%]	2.801961983		12.46274891		1.075781282		6.298264755		3.549276513	

Table 44: Analysis of tumor area of shPRC1 infected mice (2)

Mouse number	#2749		#2760		#2786		#2836		#2826	
Section	13	23	14	23	13	24	14	23	13	23
Lobe 1 total [µm²]	30049973 362	29209324 466	18217731 569	11279069 520	13562759 558	11466217 219	14179117 545	11207494 101	12608969 401	10682941 061
Lobe 1 tumor [µm²]	56771443 8	70026049	24603024 5	50164047 3	28022511	57764223	33927190 2	23626439	87724182	22023131 8
Lobe 2 total [µm²]	30279404 267	31771456 648	43354944 51	15139054 820	21594374 338	20295821 921	25739076 425	21850030 489	20181132 537	14803404 828
Lobe 2 tumor [µm²]	21902589 6	10322278 92	51904962	19815500 95	85538034	49682002 3	13796219	23410404 7	10480517 35	26675387 14
Lobe 3 total [µm²]	27195408 986	21569428 080	19563890 849	18321709 415	18596102 466	12547614 507	25726219 282	16878562 995	28337078 319	25883279 703
Lobe 3 tumor [µm²]	46560706 6	41218540 8	12462195 61	14749976 8	73744792 9	39927920 4	96120037 81	50332827 35	49289100 6	53277435 1
Lobe 4 total [µm²]	18604153 070	11807244 810	24850335 063	30289681 506	25441751 913	29670453 687	25102321 921	30370727 822	17275723 164	20493223 078

Lobe 4 tumor [µm²]	1143945550	449260380	621043047	651660519	816273139	135765596	589006953	894113238	124268065	293921150
Lobe 5 total [µm²]	1355737879 6	957424465 8	237306805 30	277918231 92	273009237 48	299555588 04	267893030 49	254315214 66	220757880 63	310737652 50
Lobe 5 tumor [µm²]	1333830581	163207342	512495275	191235865 1	27712432	37775643	0	0	736345420	468708736
Total lung [µm²]	1.11809E+11		96759735458		1.05216E+11		1.11637E+11		1.01708E+11	
Total tumor [µm²]	2928515301		3936201298		1411199367		8369602657		3336227339	
Relative tumor area [%]	2.619212296		4.068015771		1.341242963		7.497145746		3.280212698	

6.3 Number of lung tumors and tumor grade

Table 45: Number of lung tumors and tumor grade of shLuc infected mice

Mouse number-section	Grade1	Grade 2	Grade 3	Grade 4	Number of lung tumors
2738-23	18	15	11	1	
2738-13	12	14	3	0	
Mean	15	14.5	7	0.5	37
2740-23	13	7	2	0	
2740-13	16	6	4	0	
Mean	14.5	6.5	3	0	24
2741-23	8	8	1	1	
2741-13	12	7	1	1	
Mean	10	7.5	1	1	19.5
2744-23	12	7	4	0	
2744-13	18	8	2	1	
Mean	15	7.5	3	0.5	26
2746-23	2	0	0	0	
2746-13	2	0	0	0	
Mean	2	0	0	0	2
2751-23	19	12	10	2	
2751-13	21	8	2	2	
Mean	20	10	6	2	38
2755-23	7	6	1	2	
2755-13	8	4	1	2	
Mean	7.5	5	1	2	15.5
2757-23	18	6	4	1	
2757-13	15	8	6	4	
Mean	16.5	7	5	2.5	31
2758-23	11	10	3	3	
2758-13	13	5	0	2	
Mean	12	7.5	1.5	2.5	23.5
2759-23	14	16	5	1	
2759-13	15	18	5	2	
Mean	14.5	17	5	1.5	38

Total number	127	82.5	32.5	12.5	254.5
Percentage	49.9	32.4	12.8	4.9	100

Table 46: Number of lung tumors and tumor grade of shPRC1 infected mice

Mouse number-section	Grade1	Grade 2	Grade 3	Grade 4	Number of lung tumors
2654-23	7	4	0	0	
22654-13	6	5	0	0	
Mean	6.5	4.5	0	0	11
2656-23	16	12	2	0	
2656-13	18	14	2	0	
Mean	17	13	2	0	32
2657-23	4	2	0	0	
2657-13	1	2	1	0	
Mean	2.5	2	0.5	0	5
2737-23	21	6	4	0	
2737-13	9	2	1	0	
Mean	15	4	2.5	0	21.5
2743-23	3	10	1	0	
2743-13	2	7	2	0	
Mean	2.5	8.5	1.5	0	12.5
2749-23	4	9	1	0	
2749-13	7	6	2	0	
Mean	5.5	7.5	1.5	0	14.5
2760-23	5	9	2	0	
2760-14	10	6	1	0	
Mean	7.5	7.5	1.5	0	16.5
2786-24	4	4	0	0	
2786-13	1	2	1	0	
Mean	2.5	3	0.5	0	6
2836-23	2	1	1	1	
2836-14	1	2	1	1	
Mean	1.5	1.5	1	1	5
2826-23	5	3	0	1	
2826-13	5	3	1	0	
Mean	5	3	0.5	0.5	9
Total number	65.5	54.5	11.5	1.5	133
Percentage	49.3	41.0	8.6	1.1	100

6.4 Gene set enrichment analysis of the RNA-seq data with FGSEA by using the hallmark gene sets

Table 47: Top 10 upregulated and downregulated hallmark gene sets by FGSEA in comparison of PRC1-WT and PRC1-NLS3A expression

	PRC1-WT		PRC1-NLS3A	
Hallmark	NES	p-value	NES	p-value
P53_PATHWAY	2.86	1.82e-3	2.93	1.86e-3
INTERFERON_ALPHA_RESPONSE	2.26	1.96e-3	2.13	2.00e-3
APICAL_JUNCTION	2.02	1.82e-3	1.52	1.87e-3
COAGULATION	1.97	1.84e-3	1.98	1.86e-3
INTERFERON_GAMMA_RESPONSE	1.97	1.85e-3	1.73	1.86e-3

BILE_ACID_METABOLISM	1.86	1.95e-3	1.80	1.99e-3
MYOGENESIS	1.81	1.88e-3	1.59	3.85e-3
HEME_METABOLISM	1.76	1.84e-3	1.41	1.32e-2
INFLAMMATORY_RESPONSE	1.69	1.88e-3	1.18	1.63e-1
HYPOXIA	1.68	1.82e-3	1.29	3.16e-2
OXIDATIVE_PHOSPHORYLATION	-1.72	2.24e-3	0.87	8.07e-1
DNA_REPAIR	-1.81	2.19e-3	-1.37	2.57e-2
SPERMATOGENESIS	-1.90	2.07e-3	-1.79	2.02e-3
MTORC1_SIGNALING	-1.97	2.25e-3	-1.93	2.17e-3
MITOTIC_SPINDLE	-2.04	2.24e-3	-2.38	2.21e-3
UNFOLDED_PROTEIN_RESPONSE	-2.24	2.09e-3	-2.09	2.06e-3
MYC_TARGETS_V2	-2.86	1.99e-3	-2.76	1.94e-3
MYC_TARGETS_V1	-3.35	2.26e-3	-3.02	2.19e-3
G2M_CHECKPOINT	-3.50	2.27e-3	-3.44	2.20e-3
E2F_TARGETS	-3.79	2.27e-3	-3.75	2.20e-3

NES: normalized enrichment score

6.5 Fold changes and statistical significance of top regulated genes by PRC1 overexpression

Additional data to results part 3.8 and Figure 28. In Table 48 the top 20 upregulated genes upon PRC1 expression are shown. Table 48 shows the comparison of PRC1-WT and PRC1-NLS3A expression in logFC, adjusted p-value (adj. p-val.) and t-statistics (t).

Table 48: Statistics of top regulated genes in comparison to PRC1-WT and PRC1-NLS3A expression

	PRC1-WT expression			**PRC1-NLS3A expression**		
Genes	logFC	adj. p-val.	t	logFC	adj. p-val.	t
PRC1	2.04	1.38E-11	26.72	1.92	3.76E-11	25.21
BTG2	1.53	1.78E-09	19.33	1.44	9.13E-09	17.54
CDKN1A	1.42	2.02E-09	18.73	1.12	7.86E-08	14.78
ACTA2	1.79	2.37E-08	15.90	1.40	9.41 E-07	12.49
CYFIP2	1.05	7.36E-08	14.64	0.83	3.06E-06	11.37
TP53I3	1.16	8.83E-08	14.32	1.01	9.41E-07	12.37
TRIML2	1.46	9.89E-08	14.09	1.65	6.10E-08	15.28
SULF2	1.26	3.94E-07	12.83	1.12	3.94E-06	11.09
MDM2	1.05	3.94E-07	12.73	0.76	4.88E-05	9.13
ADAMTS7	1.60	4.83E-07	12.42	1.13	8.40E-05	8.57
TP53INP1	1.76	4.83E-07	12.38	1.25	7.03E-05	8.76
MR1	1.32	4.83E-07	12.35	0.97	7.03E-05	8.75
ZMAT3	1.10	6.57E-07	12.05	0.72	7.27E-07	7.46
SESN1	1.17	7.39E-07	11.91	0.99	2.87 E-05	9.60
FAS	1.04	1.32E-06	11.43	0.86	5.50E-05	8.98
EPS8L2	0.75	2.19E-06	11.02	0.63	3.82E-05	9.36
FAM210B	0.94	2.56E-06	10.87	0.77	7.73E-05	8.66
NDRG4	0.97	2.73E-06	10.78	0.71	1.99E-04	7.87
SLC52A1	2.09	2.76E-06	10.73	2.14	2.14E-05	9.86
SPATA18	1.44	2.81E-06	10.65	1.08	2.78E-04	7.49

6.5 Supplementary figures

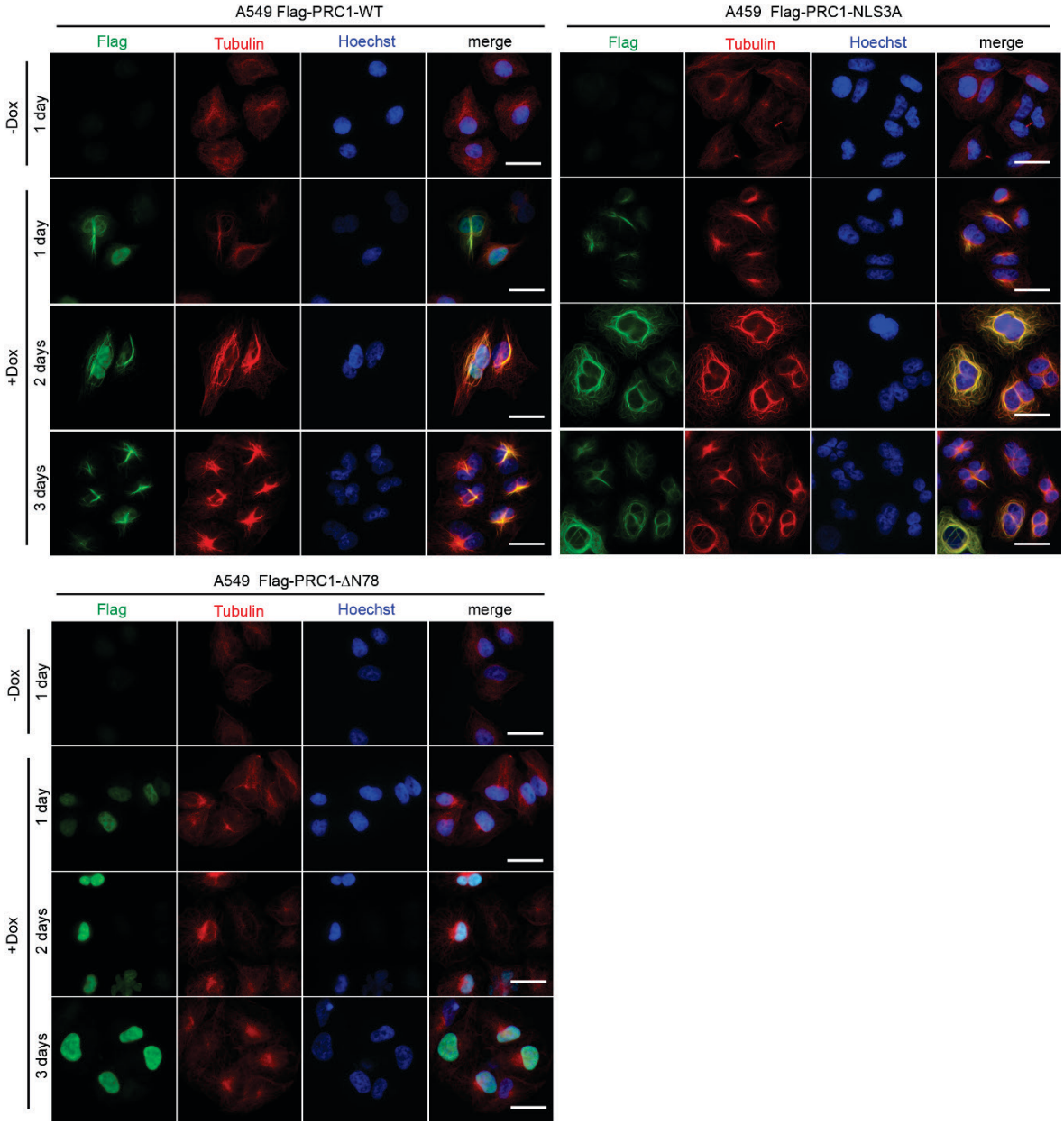

Supplementary Figure 1: PRC1-WT and PRC1-NLS3A expression leads to microtubule-bundling after 1-, 2-, and 3 days.
A549 cells either expressing PRC1-WT, PRC1-NLS3A or PRC1-ΔN78 were treated with (+) or without (-) 0.25 µg/ml doxycycline (Dox) for 1-, 2-, 3-, and 4 days. Subsequently, cells were fixed and immunostained for flag (green), tubulin (red), and Hoechst (blue) and investigated by fluorescence microscopy. An example image of 1-, 2-, and 3 days after induction of the different constructs and non-induced cells is shown. An example image after 4 days of induction of the different constructs is shown in Figure 21. Bar: 25 µm.

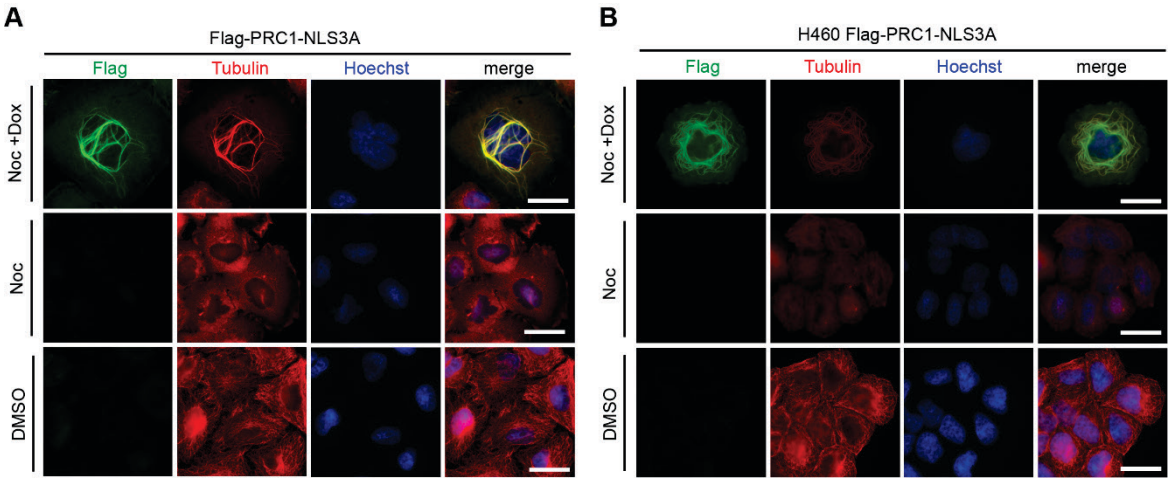

Supplementary Figure 2: Microtubules are protected from degradation by PRC1 overexpression.
(A,B) A549 or H460 lung cancer cells were cultured for two days in the presence of 0.5 µg/ml doxycycline to induce the PRC1-NLS3A construct. Subsequently cells were treated with 1 µg/ml nocodazole for 1.5 hours. Afterwards cells were fixed and immunostained for flag (green), tubulin (red) and Hoechst (blue) and investigated by fluorescence microscopy. The experiment was performed by Shin, 2018. Nocodazole interferes with the structure and function of microtubules and is here used for degradation of the filamentous structures which is protected by PRC1-NLS3A overexpression. Bar: 25 µm.

6.6 List of figures

6.7 List of tables

6.8 Abbrevations

ACTA2	Actin, alpha 2, smooth muscle, aorta
ADAMTS7	ADAM metallopeptidase with thrombospondin type 1 motif 7
AKT	Protein kinase B
APC	Adenomatous polyposis coli
APC/C	Anaphase-promoting complex/cyclosome
APS	Amonium persulfate
ATP	Adenosine triphosphate
BIRC5	Baculoviral IAP repeat-containing protein 5
Blasti	Blasticidin
Bp	Base pairs
BRCA2	Breast cancer 2
BSA	Bovine serum albumin
BSL2	Biosafety level 2
BTG2	BTG anti-proliferation factor 2
CCNY	Cyclin Y
CDC	Cell division cycle
cDNA	Complementary deoxyribonucleic acid
CDKs	Cyclin-dependent kinases
CDKN1A	Cyclin dependent kinase inhibitor 1A
CEP55	Centrosomal protein of 55

CHR	Cell cycle genes homology region
CIN	Chromosomal instability
CKI	Cyclin-dependent kinase inhibitors
CLASP	Cytoplasmic linker-associated protein
CMV-VSVg	Cytomegalovirus-vesicular stomatitis virus g
CNA	Somatic copy alteration
CPC	Chromosome passenger complex
CTLA-4	Cytotoxic T lymphocyte-associated antigen-4
CYFIP2	Cytoplasmic FMR1 interacting protein 2
DBD	Deoxyribonucleic acid binding domain
ddH_2O	Double-distilled/purified water
DEPC	Diethyl pyrocarbonate
DMEM	Dulbecco's Modified Eagle Medium
DMSO	Dimethyl sulfoxide
DNA	Deoxyribonucleic acid
Dox/Doxy	Doxycycline
dNTPs	Deoxynucleotide triphosphates
DREAM	DP, RB-like, E2F and multi-vulval class B complex
DTT	Dithiothreitol
E2F	Adenovirus early gene 2 binding factor
ECL	Enhanced chemiluminescence solution
EDTA	Ethylenediaminetetraacetic acid
EGFR	Epidermal growth factor receptor
EPS8L2	EPS8 like 2 or Epidermal Growth Factor Receptor Kinase Substrate 8-Like Protein 2
ERK	Extracellular signal-regulated kinase
EtOH	Ethanol
FAM210B	Family with sequence similarity 210 member B
FAS	Fas cell surface death receptor
FBS	Fetal Bovine Serum
FGSEA	Fast preranked gene set enrichment analysis
Fig.	Figure
Fl	Flanked

FOXM1	Forkhead box protein M1
FOXO	Forkhead box O
Fw	Forward
FZD1	Frizzled class receptor 1
G0 phase	Gap 0 phase
G1 phase	Gap 1 phase
G2 phase	Gap 2 phase
GAP	Guanosintriphosphatase activating protein
GDP	Guanosindiphosphat
GEF	Guanine nucleotide exchange factor
GFP	Green fluorescent protein
GISTIC	Genomic Identification of Significant Targets in Cancer
GTP	Guanosintriphosphat
HBS	HEPES buffered saline
HCC	Hepatocellular carcinoma
H/E	Hematoxylin and Eosin
HRP	Horseradish peroxidase
hTERT	Human telomerase reverse transcriptase
INCENP	Inner centrosome protein
KIF	Kinesin family member
K-RAS	Kirsten rat sarcoma viral oncogene homolog
LB	Luria Bertani
LSL	LoxP-Stop-LoxP
LTR	Long terminal repeat
Luc	Luciferase
M phase	Mitosis phase
MAPK	Mitogen-activated protein kinase
MAPs	Microtubule-associated proteins
MDM2	Murine double-minute 2 or MDM2 proto-oncogene
MEK	Mitogen-activated protein kinase kinase
MKLP1	Mitotic kinesin-like protein 1
MMB	Myb-MuvB complex
MPP1	M-phase phosphoprotein 1

MR1	Major histocompatibility complex, class I-related
MuvB	Multi-vulval class B
MTA	Microtubule-targeting agents
MTB	Microtubule binding
mTOR	Mammalian target of rapamycin
MSigDB	Molecular signatures database
MYC	MYC proto-oncogene, bHLH transcription factor
N	Number
N/A	Not applicable
NDRG4	NDRG family member 4
Neo	Neomycin
NF-κB	Nuclear factor kappa-light-chain-enhancer of activated B cells
NIH	National Institutes of Health
NLS	Nuclear localization signal
Ns	not significant
NSCLC	Non-small cell lung cancer
NTRK	Neurotrophic tyrosine receptor kinase
O/N	Over night
PARP	Poly [ADP-ribose] polymerase
PBS	Phosphate buffered saline
PBS-T	Triton-X in Phosphate buffered saline
PCR	Polymerase chain reaction
PD-1/PD-L1	Programmed cell death-1/ programmed cell death ligand
PDK1	Phosphoinositide-dependent kinase 1
PEG	Polyethylene glycol
Pen-Strep	Penicillin-Streptomycin
PFA	Paraformaldehyde
PGK	3-Phosphoglycerate kinase
PI	Propidium iodide
PIC	Protease inhibitor cocktail
PI3K	Phosphatidylinositol 3-kinase
PIP2	Phosphatidylinositol 4,5-bisphosphate
PIP3	Phosphatidylinositol (3,4,5)-trisphosphate

PLK1	Polo-like kinase 1
PMSF	Phenylmethylsulfonyl fluoride
pRB	Retinoblastoma protein
PRC1	Protein regulator of cytokinesis 1
PVDF	Polyvinylidene fluoride
qPCR	Quantitative polymerase chain reaction
qRT-PCR	Quantitative real-time polymerase chain reaction
RAF	Rapidly accelerated fibrosarcoma
RNA	Ribonucleic acid
RNAi	Ribonucleic acid interference
RNA-seq	Ribonucleic acid sequencing
R-point	Restriction point
RPMI	Roswell Park Memorial Institute
RI	RNase inhibitor
RT	Room temperature or Reverse transcriptase
rtTA3	Reverse tetracycline-controlled transactivator 3
Rv	Reverse
S-phase	Synthesis phase
SAC	Spindle assembly checkpoint
SCLC	Small cell lung cancer
SD	Standard deviation
SDS	Sodium dodecyl sulfate
SDS-PAGE	Sodium dodecyl sulfate polyacrylamide gel electrophoresis
SEM	Standard error of the mean
SESN1	Sestrin 1
shRNA	Small hairpin ribonucleic acid
siRNA	Small interfering ribonucleic acid
SLC52A1	Solute carrier family 52 member 1
SPATA18	Spermatogenesis associated 18
SULF2	Sulfatase 2
Suppl.	Supplementary
TBS	Tris buffered saline
TBS-T	Tris buffered saline with Tween 20

TEMED	Tetramethylethylenediamine
TKI	Tyrosine kinase inhibitor
TP53I3	Tumor protein p53 inducible protein 3
TP53INP1	Tumor protein p53 inducible nuclear protein 1
TRE2	Tetracycline-responsive element 2
TRIML2	Tripartite motif family like 2
tRFP	turbo red fluorescence protein
TU	Transducing units
Ubc	Ubiquitin C
UV	Ultraviolet
Wnt	Wingless and Int-1
WT	Wildtype
YAP	Yes-associated protein
ZMAT3	Zinc finger matrin-type 3

6.9 Curriculum vitae

6 Appendix

6.10 Publication list and conference contributions

6.10.1 Publication list

Steffen Hanselmann, Patrick Wolter, Jonas Malkmus and Stefan Gaubatz (2017): **The microtubule-associated protein PRC1 is a potential therapeutic target for lung cancer.** Oncotarget. 2017 Dec 22;9(4):4985-4997. doi: 10.18632/oncotarget.23577. eCollection 2018 Jan 12.

Patrick Wolter*, **Steffen Hanselmann***, Grit Pattschull, Eva Schruf, Stefan Gaubatz (2017): **Central spindle proteins and mitotic kinesins are direct transcriptional targets of MuvB, B-MYB and FOXM1 in breast cancer cell lines and are potential targets for therapy.** Oncotarget. 2017 Feb 14;8(7):11160-11172. doi: 10.18632/oncotarget.14466.

and

Zdenka Cicova, Mario Dejung, Tomas Skalicky, Nicole Eisenhuth, **Steffen Hanselmann**, Brooke Morriswood, Luisa M. Figueiredo, Falk Butter, and Christian J. Janzen (2016): **Two flagellar BAR domain proteins in Trypanosoma brucei with stage-specific regulation.** Scientific Reports 2016 Oct 25;6:35826. doi: 10.1038/srep35826.

* These authors contributed equally to this work.

6.10.2 Conference contributions

10/2019 **Poster at the 14th International GSLS Students' Symposium Eureka!** at the Rudolf Virchow Center, Würzburg, Germany
Poster "Cytokinesis defects and p53 pathway activation upon PRC1 overexpression leading to senescence in A549 cells" by Steffen Hanselmann, Woo Jin Shin, Carsten P. Ade and Stefan Gaubatz

10/2018 **Poster at the 13th International GSLS Students' Symposium Eureka!** at the Rudolf Virchow Center, Würzburg, Germany
Poster "The microtubule-associated protein PRC1 is required for lung tumorigenesis *in vivo*" by Steffen Hanselmann, Patrick Wolter and Stefan Gaubatz
1st Place of the image contest: A curly cancer cell

10/2016 **Poster at the 11th International GSLS Students' Symposium Eureka!** at the Rudolf Virchow Center, Würzburg, Germany
Poster "The mitotic protein PRC1 is required for proliferation of lung cancer cell lines" by Steffen Hanselmann, Jonas Malkmus and Stefan Gaubatz

6.11 Acknowledgement

Zu aller erst möchte ich mich ganz herzlich bei Prof. Dr. Stefan Gaubatz bedanken, dass er mir die Möglichkeit gegeben hat, in seiner Arbeitsgruppe und an einem sehr interessanten Projekt arbeiten zu dürfen. Man konnte jederzeit mit Fragen, Problemen oder auch neuen Ergebnissen vorbeikommen und über dies sprechen. Die Arbeitsatmosphäre war sehr gut und ich habe mich immer wohl gefühlt. Es war eine sehr lehrreiche Zeit für die ich mich bedanken möchte.

Ich möchte mich ebenfalls bei meinen Thesis-Komitee, bestehend aus Prof. Dr. Svenja Meierjohann und Dr. Markus Diefenbacher, für die Hilfsbereitschaft und den Input für mein Projekt ganz herzlich bedanken. Außerdem möchte ich mich bei Prof. Dr. Alexander Buchberger bedanken, dass er den Prüfungsvorsitz übernimmt.

Ich bin ebenfalls sehr dankbar, dass ich über die GSLS promovieren durfte. Neben vielen wissenschaftlichen Kursen, Seminaren, Retreats oder Symposien, wurde auch viel Wert auf soziale Aktivitäten gelegt. Ich bin sehr dankbar für die vielen internationalen Kontakte, die dort geknüpft wurden und die ganzen Erfahrungen, die man dort gesammelt hat.

Außerdem möchte ich mich bei Dr. Carsten Ade bedanken, der mich bei meinem RNA-Seq Experiment unterstützt hat.

Für die tolle Arbeitsatmosphäre und Unterstützung jeden Tag im Labor möchte ich mich auch bei meinen ehemaligen Kollegen und Kolleginnen bedanken: Susanne Spahr, Adelgunde Wolpert, Sabine Stopp, Grit Weinstock, Marco Gründl, Katja Simon und Camila Fetiva. Außerdem möchte ich mich noch bei meinen Studenten, die ich während meiner Promotion betreuen durfte, für die schöne Zeit und Unterstützung bedanken: Marcela Werner und Woo Jin Shin.

Zu guter Letzt möchte ich mich noch bei meiner Familie und Eva, die mir stets zur Seite stehen, Zuspruch geben und motivieren, von ganzen Herzen bedanken.

6.12 Affidavit

6.12.1 Affidavit

I hereby confirm that my thesis entitled “PRC1 serves as a microtubule-bundling protein and is a potential therapeutic target for lung cancer” is the result of my own work. I did not receive any help or support from commercial consultants. All sources and/or materials applied are listed and specified in the thesis.

Furthermore, I confirm that this thesis has not yet been submitted as part of another examination process neither in identical nor in similar form.

_____

Place, Date Signature

6.12.2 Eidesstattliche Erklärung

Hiermit erkläre ich an Eides statt, die Dissertation „PRC1 dient als ein Mikrotubuli-bündelndes Protein und ist ein potenzielles therapeutisches Target für Lungenkrebs“ eigenständig, d.h. insbesondere selbstständig und ohne Hilfe eines kommerziellen Promotionsberaters, angefertigt und keine anderen als die von mir angegebenen Quellen und Hilfsmittel verwendet zu haben.

Ich erkläre außerdem, dass die Dissertation weder in gleicher noch in ähnlicher Form bereits in einem anderen Prüfungsverfahren vorgelegen hat.

_____

Place, Date Signature